WORLD METEOROLOGICAL ORGANIZATION

INSTRUMENTS AND OBSERVING METHODS

REPORT No. 107

WMO INTERCOMPARISON OF HIGH QUALITY RADIOSONDE SYSTEMS

Yangjiang, China, 12 July – 3 August 2010

J. Nash (United Kingdom)
T. Oakley (United Kingdom)
H. Vömel (Germany)
LI Wei (China)

WMO/TD-No. 1580

2011

Chairperson, Publications Board
World Meteorological Organization (WMO)
7 bis, avenue de la Paix
P.O. Box 2300
CH-1211 Geneva 2, Switzerland

Tel.: +41 (0) 22 730 84 03
Fax: +41 (0) 22 730 80 40
E-mail: Publications@wmo.int

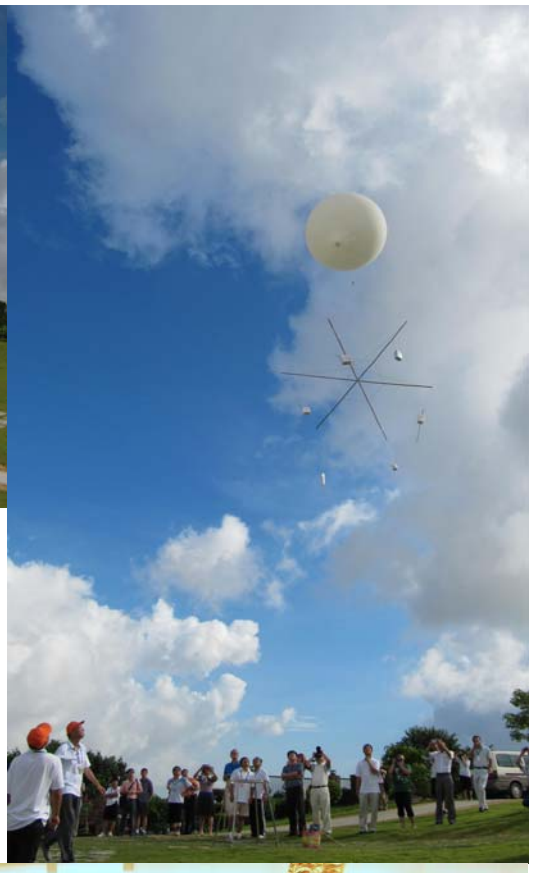

WMO INTERCOMPARISON OF HIGH QUALITY RADIOSONDE SYSTEMS
YANGJIANG, CHINA,
12th July to 3rd August 2010

FOREWORD

In the World Meteorological Organization (WMO) strategic plan, the Organization recognizes that its Members and the Organization as a whole must take a number of fundamental actions in particular by providing more timely, accurate and cost-effective weather observations that meet the requirements of governmental and business sector decision makers. The Commission for Instruments and Methods of Observation (CIMO) as one of the eight Technical Commissions of WMO focuses its work on accurate weather observation by promoting and facilitating international standardization and compatibility of meteorological observing systems used by Members within the WMO Global Observing System to improve quality of products and services of Members.

The CIMO mission is achieved by supporting initiatives, which by coordinating collective actions by Members with respect to observing systems produce results that exceed what each Member could produce unilaterally to meet their critical needs. CIMO supports development of new observing equipment critical to Members' needs, collaborates with meteorological instrument manufacturers, the scientific community and other developers to facilitate a production of reliable instruments that are adequately tested before use, and supports capacity building in developing and least developed countries to close the gap between them and the developed countries.

The WMO Intercomparison of Radiosonde Systems conducted in Yangjang, China, July 2010, is one essential component of the work of CIMO experts. It aims at improving the quality and cost-effectiveness of upper air observing systems by providing recommendations on system performances, improvements of instruments and methods of observation, suitable working references to WMO Members and instrument manufacturers.

This work has a long history. The accuracy of radiosondes and the homogeneity of the world upper air network was a matter of concern already more than 50 years ago, at the time of the first international intercomparisons. More recently, radiosonde intercomparisons conducted under the auspices of CIMO took place in UK 1984, USA 1985, the former USSR 1989, Japan 1993, USA/Russian Federation 1995-7, Brazil 2001, Mauritius Island 2005, and China 2010.

The China 2010 Intercomparison faced two emerging challenges: on one hand, there was never in the history of radiosonde intercomparisons such a high number of radiosonde manufacturers (11 manufacturers) participating in the intercomparison, including for the first time three manufacturers from China. The need for this global intercomparison was in turn driven by the changes made in the designs of the operational Quality Radiosonde Systems (QRS) and the tests were conducted under tropical/subtropical moist conditions. On the other hand there was also a need to advise GCOS on radiosondes suitable for use in the GCOS Reference Upper Air Network (GRUAN) and the evaluation of the best quality Scientific Sounding Instruments (SSI) to supplement the operational radiosondes in the GRUAN network.

The present report includes a detailed analysis of the QRS intercomparisons, a specific analysis of the SSI group, and draws conclusions and recommendations that are key information for the manufacturers, the NMHS as well as the scientific and climate community. Results show that unprecedented performances have been achieved with QRS while the expected performances to be reached with respect to the GRUAN specifications still require more research. This work is an essential contribution to the WMO Integrated Global Observing Systems (WIGOS) to improve services to society by increasing the data quality and consequently availability to improve outputs from models and provide information and products to support decision making at all levels.

Finally I wish to express my sincere appreciation to all the major players involved in the preparation of the China 2010 experiment, in the field campaign, and in the analysis of the results and preparation of the final report of this campaign: Mr Tim Oakley the Project Leader, Dr John Nash the radiosonde test expert and former CIMO President, Dr Holger Voemel for leading the SSI experiment, and the other members of the project team: Mr LI Wei, Mr Sergey Kurnosenko, Mr Mark Smees and Mr Gonzague Romanens.

The success of this Intercomparison is directly linked to the excellent and significant support provided by the China Meteorological Administration (CMA) and in particular Mr LI Wei the China Focal Point, as well as the numerous CMA staff who provided support either during the comparison or for its preparation. This full commitment of CMA must be gratefully acknowledged. Finally, the support and the contribution from the manufacturers made this WMO China 2010 Intercomparison of Radiosonde Systems clearly the most successful to date.

(Prof. B. Calpini)
President
Commission for Instruments and
Methods of Observation

EXECUTIVE SUMMARY

The 8th WMO Intercomparison of High Quality Radiosonde Systems held in China in July 2010 has produced a large data set on the performance of new operational radiosonde designs, backed up by measurements from Scientific Sounding Instrumentation. This was the result of China supporting this test very actively, and very good collaboration with the various manufacturers.

This allows recommendations as to the radiosonde designs that are potentially suitable for the GRUAN network operations and those which are suitable for routine operations, together with recommendations to improve systems without excessive development expenditure.

At night, most radiosonde systems can provide temperature measurements of suitable quality for both weather and climate work. In the day, many designs need improvement to the sensor exposure to improve the reproducibility of measurements near 10 hPa, and some further testing are needed to reduce the systematic bias between the various radiosondes at these upper levels. With more documentation, several systems have potential for use in GRUAN operations.

The relative humidity sensors tested in Yangjiang had good reproducibility, but several types had large systematic errors at all heights in the troposphere, and the origin of these needs to be identified and rectified as soon as possible. Several systems showed potential for observing relative humidity in the upper troposphere in the tropics, and the new correction schemes seem to have good potential for future observations. It was possible to check the measurements in cloud, using cloud radar (up to 15 km) and ceilometer observations (up to 12 km) to identify some of the clouds. Thus, with more documentation several systems have potential for use in GRUAN operations.

GPS height measurements are very reproducible, and are clearly suitable for all radiosonde operations, given that the equipment is initiated correctly. On the other hand, cheaper radiosondes may be used by exploiting systems such as the Chinese secondary radar for good quality operational results.

Thus, where GPS radiosondes are set up correctly, pressure can be deduced from the geopotential heights and the radiosonde measurements of temperature and relative humidity profile.

As a result of the test, many errors in the various quality radiosonde systems were identified and subsequently rectified ensuring improved accuracy for future radiosondes.

The Radiosonde Comparison was performed as a first collaboration between CIMO and a range of climate scientists associated with GCOS and GRUAN, as part of a WIGOS Pilot Project.

TABLE OF CONTENTS

WMO INTECOMPARISON OF RADIOSONDE SYSTEMS
YANGJIANG, CHINA, 12th July to 3rd August 2010

1 Introduction

1.1 Objectives

The objectives for the intercomparison were agreed by the third session of the Joint meeting of the CIMO Expert Team and International Organizing Committee on Upper-Air Systems Intercomparisons (ET/IOC), Payerne, Switzerland, 2-6 June 2008.

The main objective of this intercomparison was to test in the tropical / subtropical moist conditions the relative performances of operational Quality Radiosonde Systems (QRS) in conjunction with the Scientific Sounding Systems (SSI). The results would be used to advise Members on a selection of QRS suitable for RBSN/RBCN and its GUAN sub-network as well as advise GCOS on a selection of systems suitable for GCOS Reference Upper-Air Network (GRUAN).

The ET/IOC agreed on further objectives as follows:

- To improve the accuracy of daytime operational QRS measurements and the associated correction procedures to provide temperature and relative humidity accuracies currently possible with night time measurements.
- To assess the accuracy and availability of the GPS wind measuring systems.
- To evaluate the performance of geometric and geopotential height values obtained from GPS radiosondes (with a possibility to check the associated algorithms).
- To evaluate the quality and reliability of SSI, and to use this information to evaluate the quality of the working references for the radiosonde test.
- To evaluate the day-night differences of temperature, relative humidity of operational QRS and SSI against available remote sensing observations; and to identify, as far as possible, the origins of differences.
- To recommend suitable QRS systems to be used in the RBSN/RBCN and GUAN.
- To assess the magnitude of changes introduced by new radiosonde designs.
- To identify the best practices used in the preparation of operational QRS radiosondes for launch.
- To evaluate the added value of using remote sensing equipment in radiosonde systems intercomparisons as recommended by ET-RSUT&T experts (following test-bed evaluations).
- To publish the Executive Summary within three months, the draft Final Report within six months and the approved Final Report within nine months after the Intercomparison in the *WMO Instruments and Observing Methods Report* (IOM) series.

1.2 Relevance of the test for weather forecast and climate monitoring operations

Radiosonde equipment gains vast benefits from progress in technology, so that most of the radiosonde manufacturers are developing their products and introducing new ideas, e.g. corrections for time constants of response, and daytime corrections for relative humidity errors. The test exercises the equipment in challenging conditions, over a large number of flights so that the way the radiosondes cope with various conditions, e.g. rain or the presence of thick high clouds, or the cold temperatures at the tropical tropopause, is checked. The reliability of the new features is also checked, and policy is made about how these features should be managed in future, to ensure traceability of measurements is not lost.

The results allow users to choose equipment for the future, with knowledge of the performance that can be expected, and for a network like GRUAN, it is essential to have more than one good quality radiosonde type to form the backbone of future operations.

Identification of the limits of the radiosonde measurements helps users to optimise their use of the data. For instance, one of the results of the previous radiosonde comparison in Mauritius was the recognition that many radiosonde humidity sensors worked differently between night and day, and this factor was then introduced into the way the measurements were used in Numerical Weather Prediction.

Knowledge of the relative performances of the scientific sounding instruments and the quality radiosondes systems is needed to ensure successful planning of future GRUAN operations.

1.3 Relationships with previous intercomparisons

The first four WMO Radiosonde Comparisons compared most of the radiosonde types in operational use between 1984 and 1993. However, advances in computing and electronics suitable for use on the radiosondes, plus an understanding of sensor errors that could be avoided without excessive expense have radically changed the performance of the better quality radiosondes.

The 5th Radiosonde Comparison of relative humidity sensors hastened the change from the carbon hygristor and goldbeaters skin to thin film capacitative humidity sensors, which now prevail in modern radiosonde systems.

The 6th Radiosonde Comparison in Brazil saw the introduction of new GPS radiosonde designs, that had much better radiofrequency electronics than was generally used until that time. This solved the problems of measuring winds with GPS in tropical conditions, which was the major issue with radiosonde systems at the time.

By the time of the 7th Comparison in Mauritius, the new designs had matured and it was possible for the first time to see the high reproducibility of GPS geopotential height measurements. The basic GPS geometric heights were readily converted into geopotential heights using the variation of gravity with height at the given latitude. The results suggested that it might no longer be necessary to use pressure sensors on the radiosondes, since the pressure could be computed from the geopotential height plus the temperature and relative humidity profile to that height. The test also showed that some operational radiosonde systems were starting to measure relative humidity in the upper troposphere without excessive errors. Day-night differences in relative humidity were quantified for many types of operational radiosonde.

The test in Yangjiang allows testing of the new correction schemes for relative humidity in the upper troposphere, testing a new generation of very fast response temperature sensors and a wider range of GPS radiosondes. It allows manufacturers in Region II to compare with the European and American/African designs, helping to inform the meteorological services in Region II as to the suitable methods for future radiosonde operations.

1.4 Relationships with the scientific community

The Comparison in Yangjiang was the first time that the experts in operational radiosonde testing have worked directly together with the scientific community associated with GCOS. This is the start of a process that needs to continue in the future, given the requirements to run GRUAN and GUAN as long-term observing networks. Certainly, looking at the performance of the systems together has led to many hard but fruitful discussions and this is to the benefit of both communities for the future

Some of the manufacturers have implemented correction schemes in the upper troposphere as advocated in Miloshevich, et. al, 2009 for the Vaisala RS92, and this test gives the opportunity to test the results on an extensive database of both daytime and nighttime soundings.

2. Organisation of the Intercomparison

The 8th WMO Intercomparison of High Quality Systems was organised by the CIMO Expert Team on Upper-Air Systems Intercomparisons, chaired by Mr T. Oakley. The intercomparison consisted of 72 successful multiple radiosonde soundings (60 QRS and 12 SSI), performed between the 13th July and 1st August 2010 at the Chinese Meteorological Administration (CMA) Yangjiang Station, Guangdong Province, China. Details of all the soundings are contained within Annex F.

In order to ensure that all the necessary planning and organisation was agreed well in advance of the intercomparison, two International Organisation Committee (IOC) meetings were held in Payerne, Switzerland (June 08) and Yangjiang, China (September 09). These meetings were fundamental in not only agreeing on the participants at the intercomparison, but also focusing on the infrastructure and the responsibility for CMA in hosting a campaign of this size. The reports of these meetings are available from the WMO website (www.wmo.int).

It was agreed that the number of comparison flights attempted should be about 15 at night and 15 in the day for each radiosonde type, and because of limitations in balloon payload and available radiofrequency reception, that all quality QRS would be flown two times per day on 4 test flights, with SSI systems tested separately on their own flights. This large number of ascents is essential to give a reliable evaluation of operational performance, given that the results of the test will be used in making decisions about system procurement for future radiosonde operations worldwide.

The test was designed to benefit Quality Radiosonde Systems, i.e new/modified radiosonde designs in operational use for 2 years, that have undergone qualifying testing at a CIMO Lead centre. These must have small random errors in measurements to generate representative statistics with relatively small samples of 15 night and 15 day comparisons. For a quality radiosonde to justify all this work, it should be capable of performing above the minimum standards set for operational use, and therefore be suitable for use at least at GUAN observing network sites. The Scientific Sounding Instruments (SSI) are specialised scientific instruments, which have not been used as often as the QRS, sometimes only used in specialised scientific tests. The two systems that were used as working references in the previous WMO Radiosonde Comparison, LMS Multithermistor and Snow White hygrometer, fall somewhere between SSI and QRS in status in Yangjiang, and were certainly acting as working references on many QRS test flights. The CFH can be used to cross reference measurements of water vapour in the lower stratosphere from the QRS test flights even without being on the QRS flights, since water vapour at these heights shows minimal variation with time of day in the tropics.

As an outcome of the first IOC meeting and with respect to the requirements from WMO, CMA was selected to be responsible for hosting the intercomparison and the Yangjiang station was selected as the location (see Annex B). To ensure the success of the intercomparison significant effort was made by CMA (before, during and after) in the areas as follows:

- Reconstruction of the balloon launch area (extending available land).
- Operating staff training, and logistics.
- Work service to the accommodation (for instrumentation and operators, WMO office, data centre, local organisers, meeting room, rest area, smoking area). See Annex C for a detailed map of the Yangjiang station.
- Backup power supply plus UPS offered to every individual manufacturer.
- Hydrogen and balloon supply plus permission to launch non-standard balloons.
- Hotel reservation.
- Access to the internet.
- Transportation (transfer from/to airport and local travel).
- Food at site.
- Electromagnetic environment.
- Import and export procedures.
- Technical Support (on-site).

Over the 4 weeks of the intercomparison a total of 102 people were involved, 45 International visitors, 14 Chinese manufacturers and 43 CMA staff (see Annex A). In addition, there were a significant number of visitors to the site either from the local town or CMA staff from elsewhere.

Annex H provides a table of estimated costs (hours, travel and accommodation, equipment) which were encured for this Intercomparison.

3 Contribution of GRUAN

3.1 GRUAN background

The reliable detection of the vertical structure of changes in climate variables in the atmosphere requires very high quality atmospheric observations with well characterized measurement uncertainties. The need for a reference upper-air network to better meet the needs of the international climate research community has long been recognized. This was formalized between 2005 and 2007 when a reference upper-air network was planned, which was conceived as the GCOS Reference Upper-Air Network (GRUAN; GCOS-112, GCOS-134) in 2008. GRUAN is specifically designed for climate research and will provide reference observations of upper-air essential climate variables (ECV), through a combination of in situ measurements made from balloon-borne instruments and from ground-based remote sensing observations. GRUAN is driven by the requirements of long-term climate trend detection and measurements need to be made in a stable way over decadal time scales to achieve data homogeneity both in time and between measurement stations. In this sense GRUAN will operate like a long-term operational network for the detection of climate change. Thus, it needs strong links to the operational community as well as its scientific community. On the other hand the GRUAN network is a research network constantly striving to improve measurement techniques, quantify and reduce measurement uncertainties, and improve precision and accuracy. These two aspects of GRUAN operations are not mutually exclusive, but do need to be carefully balanced.

The primary goals of GRUAN are to:

i) Provide vertical profiles of reference measurements suitable for reliably detecting changes in global and regional climate on decadal time scales. The uniformity and coherence of standard operating procedures at GRUAN stations and the resultant homogeneity of GRUAN data products will lead to improved detection of changes in the climate of the troposphere and stratosphere.

ii) Provide a calibrated reference standard for global satellite-based measurements of atmospheric ECVs. This facilitates the creation of seamless, stable, and long-term databases of satellite-based measurements suitable for detection of trends in climate in the upper troposphere and stratosphere.

iii) Fully characterize the properties of the atmospheric column. This is necessary for the understanding of processes and for radiative transfer modelling.

As denoted by its name, GRUAN will provide reference quality measurements for a range of upper-air climate variables, in particular of the vertical profiles of water vapor and temperature. Reference quality atmospheric observations are based on key concepts in metrology, in particular traceability. Metrological traceability is the process whereby a measurement result, i.e. a measurement and its uncertainty, can be related to a reference through a documented, unbroken chain of calibrations, each of which contributes to the measurement uncertainty.

A reference measurement does not refer to a measurement that is perfect, nor to a measurement that will never change. Rather it refers to the current best estimate of the value for some atmospheric parameter, as well as a best estimate for the level of confidence that is associated with this value, recognizing that future improvements in measurement techniques and/or reprocessing following new knowledge may lead to refinements in that reference value. A reference measurement may not necessarily be the outcome of a measurement by a single instrument but may be an average of measurements from one instrument or an average of results from multiple instruments.

The estimate for the level of confidence is expressed as measurement uncertainty and is a property of the measurement that combines instrumental as well as operational uncertainties. The measurement uncertainty describes the current best knowledge of instrument performance under the conditions encountered during an observation, it describes the factors impacting a measurement as a result of operational procedures, and it makes all factors that contribute to a measurement traceable. An important point is that within GRUAN this uncertainty will be vertically resolved and each measurement in a profile will be treated as a single measurement result requiring both the measurement and its uncertainty. To provide the best estimate for the instrumental uncertainty, a detailed understanding of the instrumentation is required for the conditions under which it is used. Specific requirements that an observation must fulfill to serve as a reference for calibrating or validating other systems, have been defined in Immler et al. (2010).

A reference measurement typically results from a measurement procedure that provides sufficient confidence in its results by relating to well-founded physical or chemical principles, or a measurement standard that is calibrated to a recognized standard, in general a standard provided by a National Metrological Institute (NMI). For GRUAN a reference measurement is one where the uncertainty of the calibration and the measurement itself is carefully assessed. This includes the requirement that all known systematic errors have been identified and corrected, and that the uncertainty of these corrections has also been determined and reported. An additional requirement for a reference measurement is that the measurement method and associated uncertainties should be accepted by the user community as being appropriate for the application.

Another important requirement is that the methods by which the measurements are obtained and the data products derived must be reproducible by any end-user at any time in the future. It should be kept in mind that these end-users are likely to use GRUAN data for decades to come. They should be able to reproduce how measurements were made, which corrections were applied, and be informed as to what changes occurred during the observation and post-observation periods to the instruments and the algorithms.

In brief, *reference* within GRUAN means that, at a minimum, the observations are tied to a traceable standard, that the uncertainty of the measurement (including corrections) has been determined, and that the entire measurement procedure and set of processing algorithms are properly documented and accessible.

3.2 GRUAN analysis

The GRUAN contribution to the CIMO intercomparison aims at identifying and quantifying known sources of measurement uncertainty on a select set of instruments, which were labeled as Scientific Sounding Instruments (SSI). This terminology expresses that these instruments have a strong scientific background and that they are well documented. The analysis routines for SSI instruments should be open and documented and factors contributing to measurement uncertainty should be well understood. This traceability is required to support the needs for GRUAN and is essential for the detection of long term changes in upper air essential climate variables, most importantly water vapor and temperature.

The analysis approach that is the basis of GRUAN uses the measurement uncertainty to quantify, whether two redundant measurements are consistent or not. This analysis approach has been described in detail by Immler et al. (2010). Given two independent measurements m_1 and m_2 and their respective uncertainties u_1 and u_2, these two measurements can be considered consistent if $|m_1 - m_2| < k\sqrt{u_1^2 + u_2^2}$. Here k is the statistical significance factor.
Following the approach by Immler et al. (2010) this condition can be translated into the statements:

$\lvert m_1 - m_2 \rvert < k\sqrt{u_1^2 + u_2^2}$	**True**	**False**	**Significance level**
k=1	consistent	suspicious	32%
k=2	in agreement	significantly different	4.5%
k=3	-	inconsistent	0.27%

Thus, if an uncertainty estimate has been performed, this analysis can be obtained. This condition implies, that for k=1, 68% of pairs of observations need to satisfy this condition to be able to state that these observations are '*consistent*'. This also means that 32% of the observational pairs may violate this condition. At a higher statistical significance, i.e. k=2 only 4.5% of the observational pairs may violate the consistency condition if these observations are to be called '*in agreement*'. Some of the analysis below will be based on this approach. For instruments, for which no uncertainty has been established, this comparison can still be done assuming that the uncertainty for these instruments is zero. In this case, the uncertainty for the other measurements must be known.

4 Description of the systems tested

4.1 QRS

The ET/IOC chose 13 radiosonde types to participate in the intercomparison (11 operational systems and 2 working references) and their system specifications are given in Table 4.1.1 below. Prior to the intercomparison the IOC received a request from Roshydromet (Russia) to participate in the intercomparison with their radiosonde system but owing to radio-frequency incompatibilities with the Chinese L-Band system it proved not possible to include them in the test. Subsequently it was agreed that two observers from Russia would attend for part of the intercomparison. Figures 4.1.1 to 4.1.11 shows the pictures of each systems (where available) as follows; (a) temperature sensor; (b) humidity sensor; (c) ground system and (d) radiosonde.

Company	Ground System	Radiosonde	Temp. sensor	Humidity sensor	Digital Frequency Specification
InterMet Africa	iMet-3200	iMet-2	Bead thermistor	Thin film Capacitor(E+E)	Range: 400 to 406 MHz Tuning:250 kHz steps Stability: +/- 6.5 KHz R/S Power: 125 mW
Modem	SR2K2	M2K2DC	Bead thermistor	Capacitive polymer	Range: 400 to 406 MHz Tuning:200 kHz steps Stability: +/- 2 KHz R/S Power: 200mW
Graw Radiosondes	GS-E	DFM-09	Thermistor	Thin film Capacitor(E+E)	Range: 400 to 406 MHz Tuning:20 kHz steps Stability: +/- 3 KHz R/S Power: 100mW
Meteolabor (2 Systems)	ARGUS 37	SRS-C34	Thermocouple	Hygroclip Rotronic +*Snow White hygrometer	Range: 400 to 406 MHz Tuning:Any in range Stability: +/- 2 KHz R/S Power: 100mW
Nanjing Da Qiao Machine Co Ltd	L-Band GFE1 type	GTS1-2 digital	Cylindrical thermistor	Thin film Capacitor (China made HS02)	Range: 1675 +/-3MHz Tuning: n/a Stability: +/- 3 MHz R/S Power: 500mW
Jinyang	GL-5000P	RSG-20A	NTC Thermistor	Thin film Capacitor(E+E)	Range: 400 to 406 MHz Tuning: 10kHz Stability: +/- 3 KHz R/S Power: 100mW
Meisei Co. LTD	RD-06G + Temp .Ref	RS-06G	Thermistor Tungsten helix	Capacitance polymer	Range: 400 to 406 MHz Tuning: 100kHz Stability: +/- 5 KHz R/S Power: 100mW
Vaisala Oyj	DigiCora, MW31 +DryCap Ref	RS92-SGP	Capacitive wire	Thin film capacitor, heated twin sensor Polymer for low R.H.	Range: 400 to 406 MHz Tuning: 10kHz Stability: +/- 2 KHz R/S Power: 60mW
Beijing Chang Feng Surface Acoustic wave Co.	GPS Radiosounding System	CF-06-A	Bead resistance	Thin film Capacitor (Sweden XC06)	Range: 400 to 406 MHz Tuning:Any in range Stability: +/- 10 KHz R/S Power: 100mW
China Huayun	HY-GTS(U)	GTS(U)1-1	Bead thermistor	Thin film Capacitor(E+E)	Range: 400 to 406 MHz Tuning: 50kHz Stability: +/- 5 KHz R/S Power: 200mW
Lockheed Martin Sippican INC	LMG6	GPS LMS6 Radiosonde + Multi-thermistor	Chip thermistor	Thin film Capacitor(E+E)	Range: 400 to 406 MHz Tuning: 50kHz Stability: +/- 5 KHz R/S Power: 63 mW

Table 4.1.1: QRS and working reference radiosonde systems participating in the 8th WMO Radiosonde Intercomparison

Fig. 4.1.1 (a) InterMet Temperature sensor

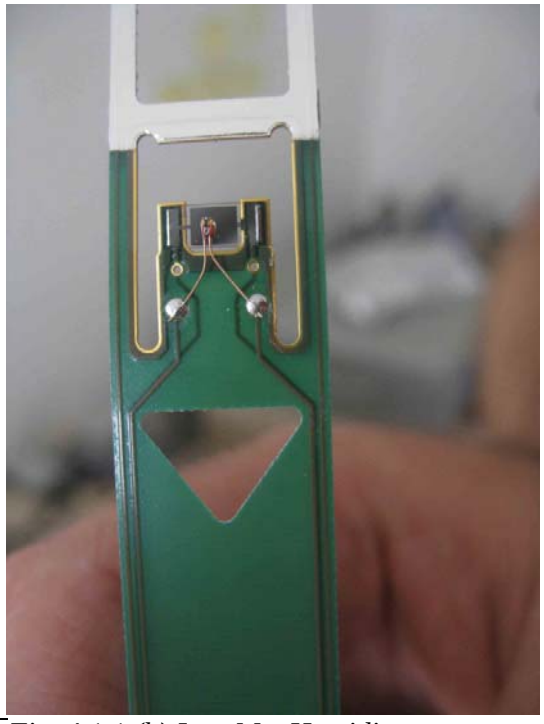

Fig. 4.1.1 (b) InterMet Humidity sensor

Fig. 4.1.1 (c) InterMet Ground System

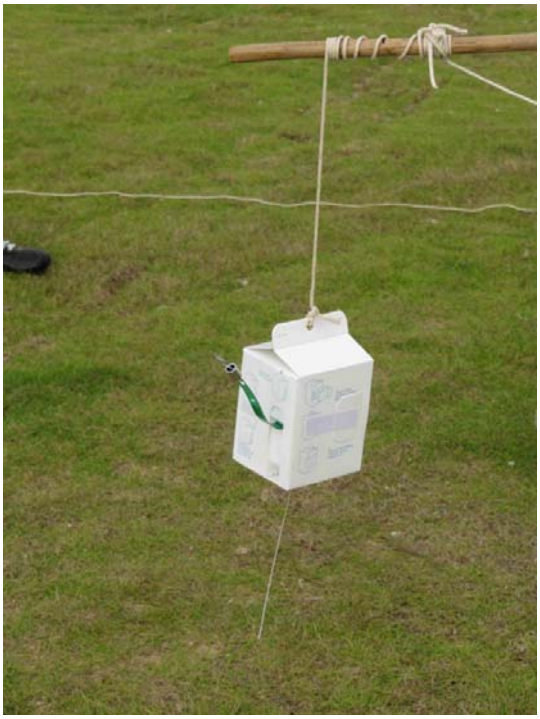

Fig. 4.1.1 (d) InterMet iMet-2 radiosonde

Modem

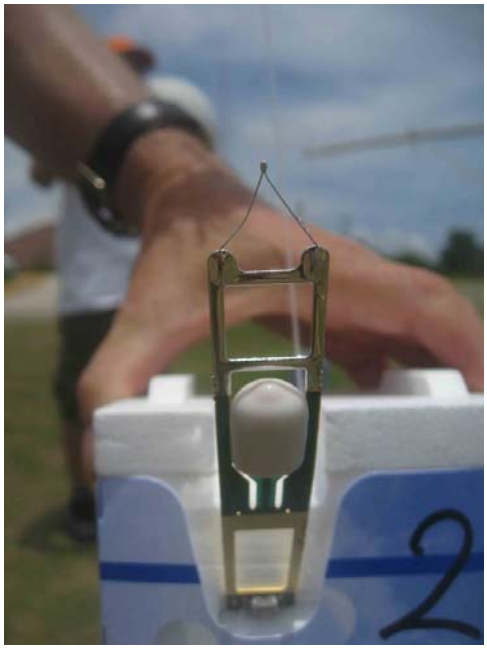

Fig. 4.1.2 (a) Modem Temperature Sensor

Fig. 4.1.2 (b) Modem Humidity Sensor

Fig. 4.1.2 (c) Modem team & SR2K2 Ground System

Fig. 4.1.2 (d) Modem M2K2DC R/S

Graw GS-E

Fig. 4.1.3 (a) Graw Temperature sensor

Fig. 4.1.3 (b) Graw Humidity sensor

Fig.4.1.3 (c) Graw team and Ground System

Fig. 4.1.3 (d) Graw DFM-09 R/S

Meteolabor SRS

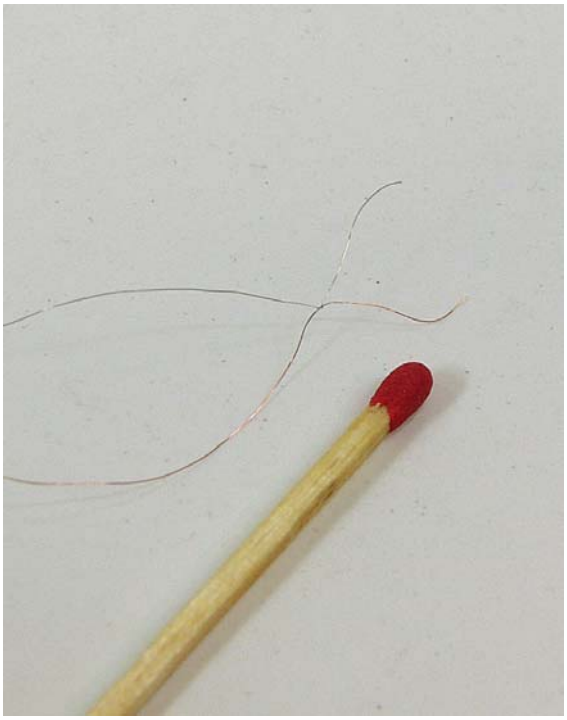

Fig. 4.1.4 (a) Meteolabor Temperature sensor

Fig. 4.1.4 (b) Meteolabor Humidity sensor

Fig. 4.1.4(c) Meteolabor Team

Fig. 4.1.4 (d) Meteolabor SRS radiosonde

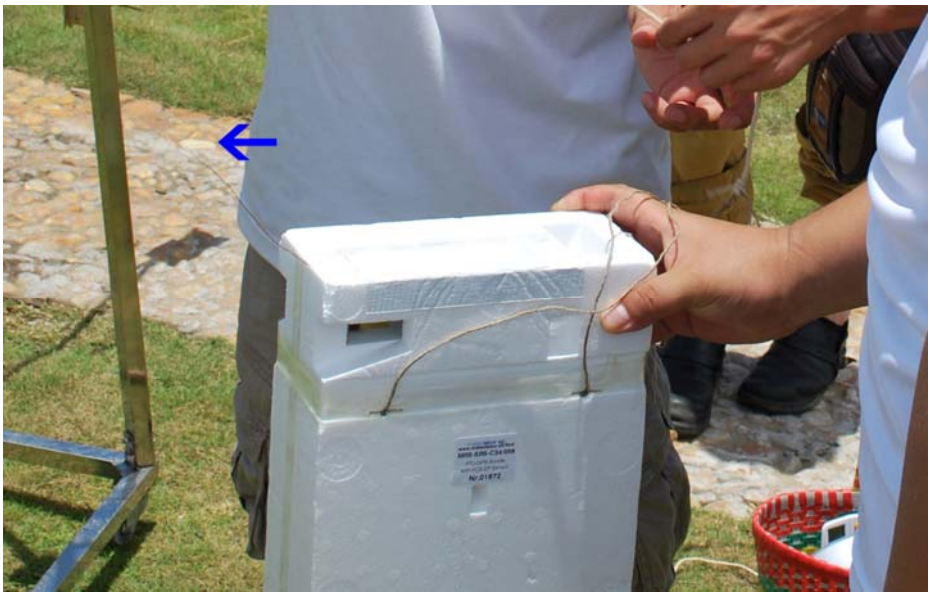

Fig. 4.1.4 (e) Thermocouple located above Meteolabor C-34 body during flight

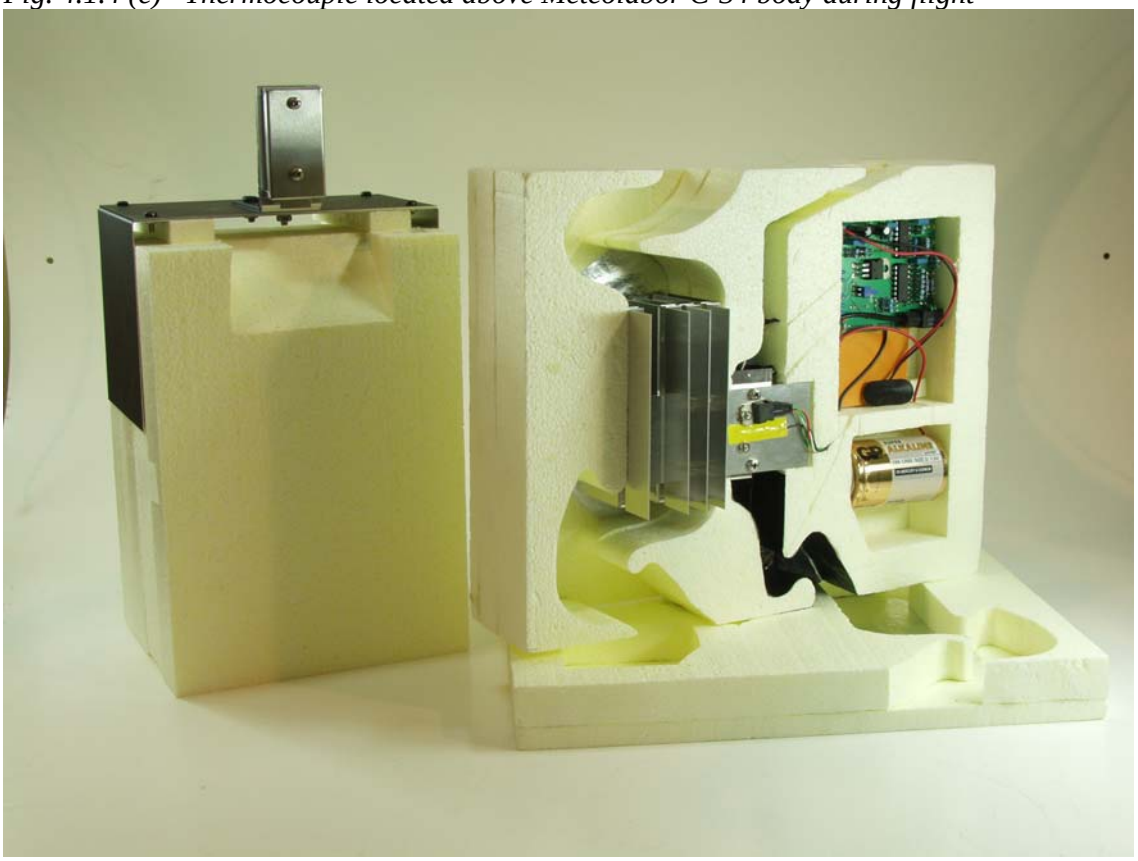

Fig. 4.1.4 (f) Nightime (left) and Daytime Snow White. At night, the Snow White cooled mirror is located above the top of the Snow White body, therefore sensor ventilation is much better than in the daytime.

Nanjing Da Qiao L-Band

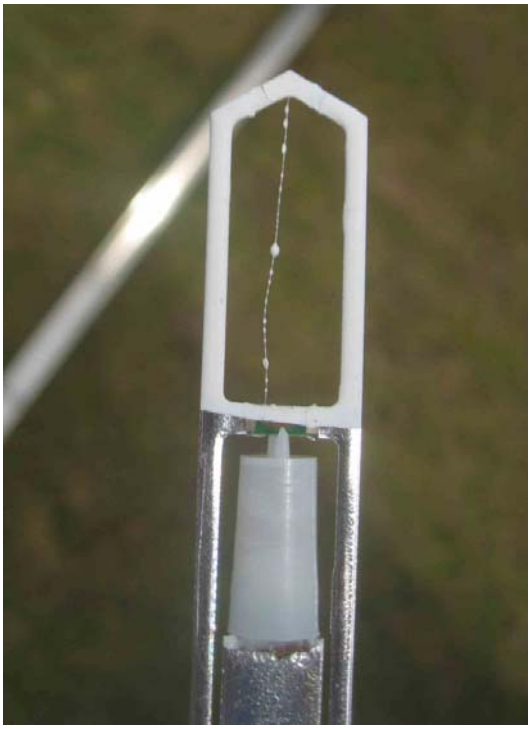

Fig. 4.1.5 (a) Da Qiao Temperature sensor

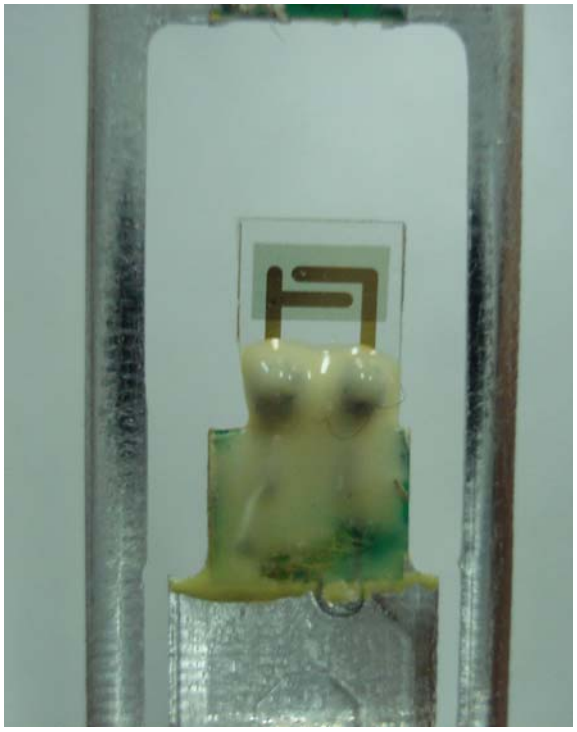

Fig. 4.1.5 (b) Da Qiao Humidity Sensor

Fig. 4.1.5 (c) Da Qiao team and Ground System (above), Da Qiao GTS1-2 Radiosonde (right-top) and Secondary Radar (right-bottom)

Jinyang GL-5000P

Fig. 4.1.6 (a) Jinyang Temperature sensor

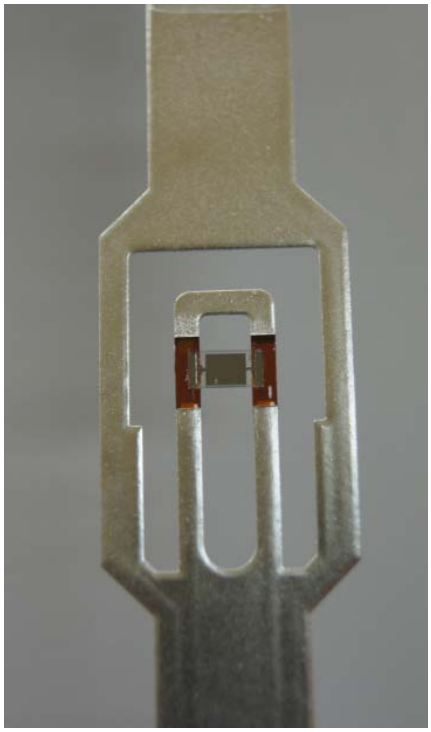

Fig. 4.1.6 (b) Jinyang Humidity sensor

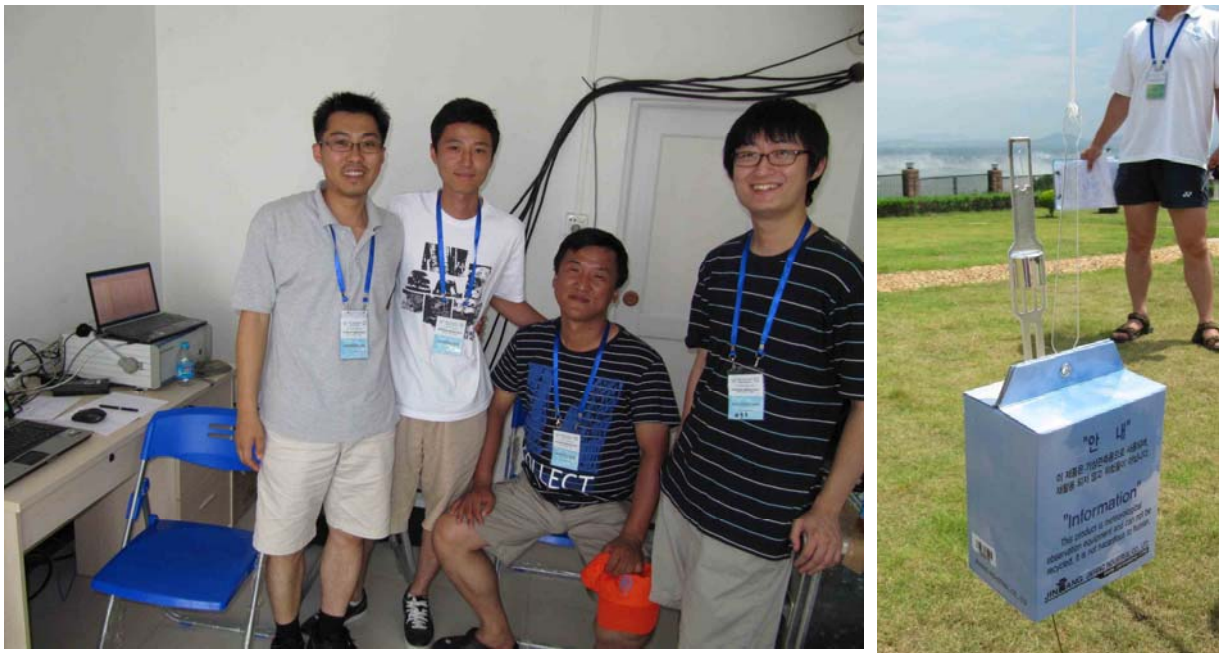

Fig. 4.1.6 (c) Jinyang GL-5000P Ground System and team (left) and Jinyang RSG-20A Radiosonde (right)

Meisei RD-06G

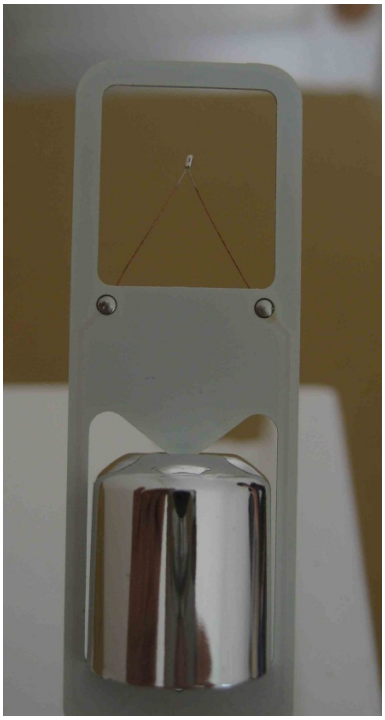

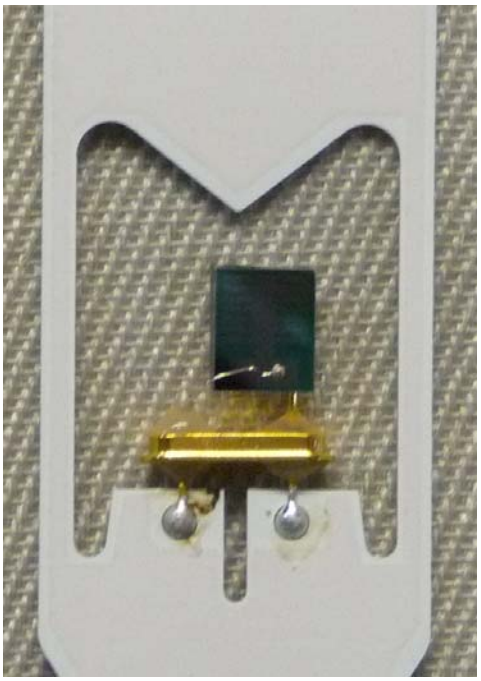

Fig. 4.1.7 (a) Meisei Temperature sensor Fig. 4.1.7 (b) Meisei Humidity sensor

Fig. 4.1.7 (c) Meisei RD-06G Ground System and team Fig. 4.1.7 (d) Meisei RS-06G R/S

Vaisala Oyj DigiCora MW31

Fig. 4.1.8 (a) Vaisala Temperature + Humidity sensor *Fig. 4.1.8 (b) Vaisala Humidity sensor (close-up)*

Fig. 4.1.8 (c) Vaisala DigiCora Ground System *Fig. 4.1.8 (d) Vaisala RS92-SGP R/S*

Beijing Changfeng

Fig. 4.1.9 (a) Changfeng Temperature sensor

Fig. 4.1.9 (b) Changfeng Humidity sensor

Fig. 4.1.9 (c) Changfeng Ground System

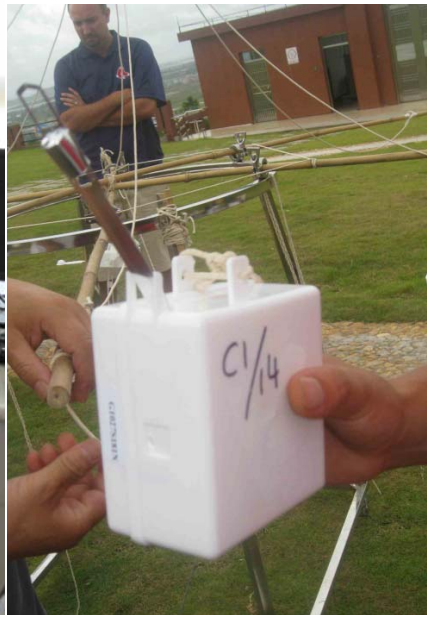

Fig. 4.1.9 (d) Changfeng CF-06-A R/S

Huayun HY-GTS(U)

Fig. 4.1.10 (a) Huayun Temperature sensor

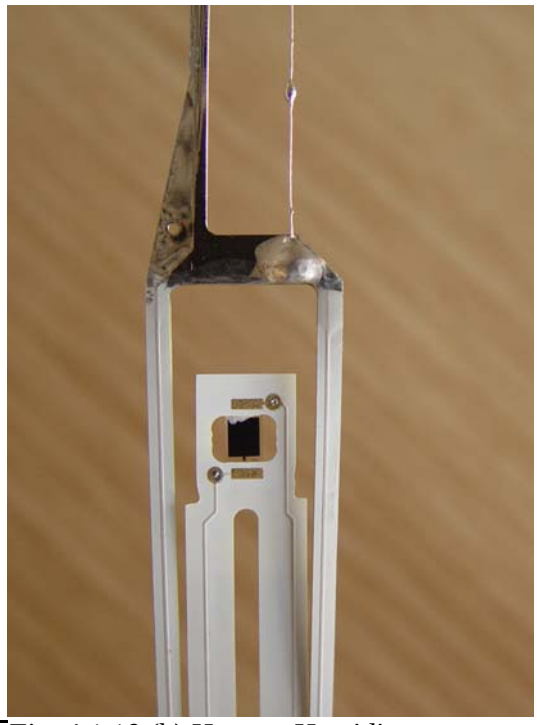

Fig. 4.1.10 (b) Huayun Humidity sensor

Fig. 4.1.10 (c) Huayun HY-GTS(U) Ground System

Fig. 4.1.10 (d) Huayun GTS(U)1-1 R/S

Fig. 4.1.11 (a) LMS Temperature sensor

Fig. 4.1.11 (b) LMS Humidity sensor

Fig. 4.1.11 (c) LMS ground system

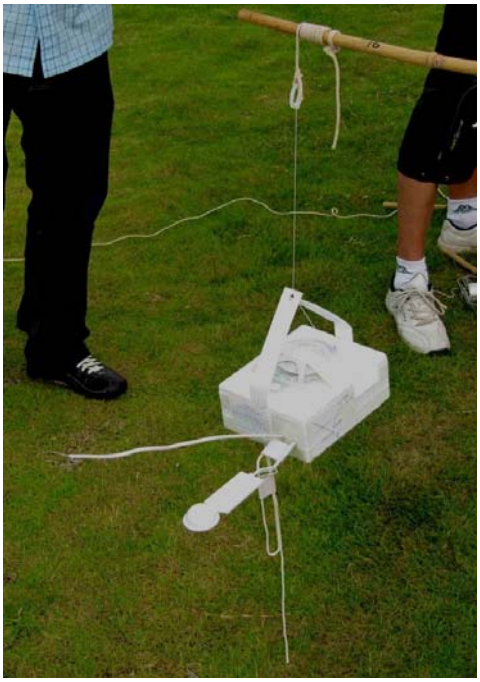

Fig. 4.1.11 (d) GPS LMS6

4.1.1 Snow White hygrometer

The Snow White hygrometer was flown in the previous WMO Radiosonde Comparison as a working reference for water vapour measurements, of similar status to the LMS Multithermistor for temperature measurements.

To fly the system with the SSI instrumentation would have made the SSI payload too heavy. Whilst in the past Snow White was flown on a variety of host radiosondes, the Snow White's in Yangjiang were flown with the Meteolabor system, one of the QRS radiosondes. MeteoSwiss flies Snow White regularly with this radiosonde system, and they have invested a lot of effort within the last year in improving the reliability of the system.

The Snow White chilled mirror measures dew point or frost point directly (depending on whether the film on the mirror is water or ice), see Fig. 4.1.12. Note the CFH SSI instrument, (see SSI group) also has a chilled mirror but cooled by a different method. Thus, relative humidity from Snow White requires a temperature and a pressure from the radiosonde system and reference to the following sections shows that these errors are small in the Meteolabor system.

Thus, in Yangjiang, the temperature of the Meteolabor radiosondes was used for the conversion. It is necessary to estimate when the film on the mirror turns from water to ice. The change in phase does not normally occur at a mirror temperature near 0°C, but usually in the range -20°C to -30°C. The identification is made by comparing with the conventional relative humidity on Snow White. Sometimes the change in phase of water on the mirror takes more than several minutes and these data were flagged out by the operators.

Two variants of Snow White were deployed in Yangjiang:

(1) The 'day-time' Snow White system has the chilled mirror mounted in an internal duct to protect the sensor from daylight. The circulation through the duct system was improved to some extent by adding stainless steel tubing above the inlet to try to minimise contamination within the duct, as originally designed by Masatomo Fujiwara. At low temperatures, with relatively wet conditions in the lower atmosphere, contamination can build up in the duct, and although humidity structure can be seen, the absolute values are biased high and were flagged out in the data editing process.

(2) The 'night-time' Snow White eliminates the internal duct and the chilled mirror sensor is exposed directly in the atmosphere. In Yangjiang, the night-time Snow Whites were not flown if there was a chance of rain during the ascent and it was fortunate there were fewer flights where rain was experienced during the ascent than in Mauritius. A lot of development had been done on the reception and data processing of the Meteolabor radiosonde, so relatively little Snow White data had to be flagged out because of instability in the feedback control loop for the mirror. It is possible that on occasions, the mirror film is lost in high humidity near the tropopause and some observations have been flagged out where the dew-points reported seem unrealistically low.

In order to understand the reliability of Snow White, it is necessary to check whether the batteries have sufficient power left in the stratosphere to drive the Peltier cooler to a low enough temperature to measure frostpoints as low as -90 deg C. In Yangjiang, because the depth of very dry layers in the troposphere was limited, the batteries always had sufficient

power to deliver the necessary cooling. Further housekeeping, gives a measure of the state of the film on the mirror, and on the three flights where the film seem to be lost near the tropopause, a difference in the state of this monitor has now been seen. Other measurements were reliable in terms of the functioning of the chilled mirror, but not necessarily free of contamination.

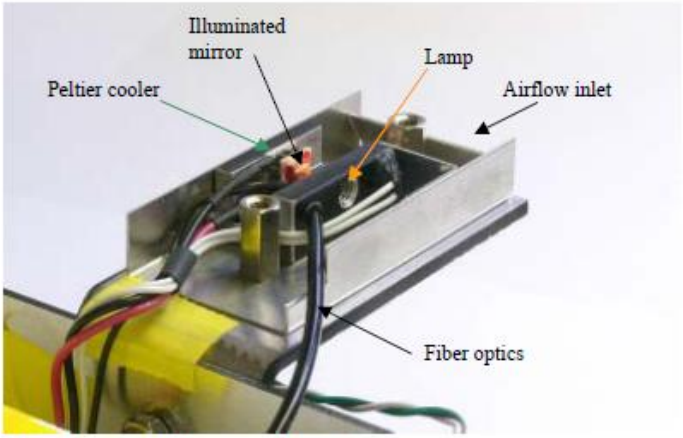

(1) *Inside a nighttime Snow White sensor*

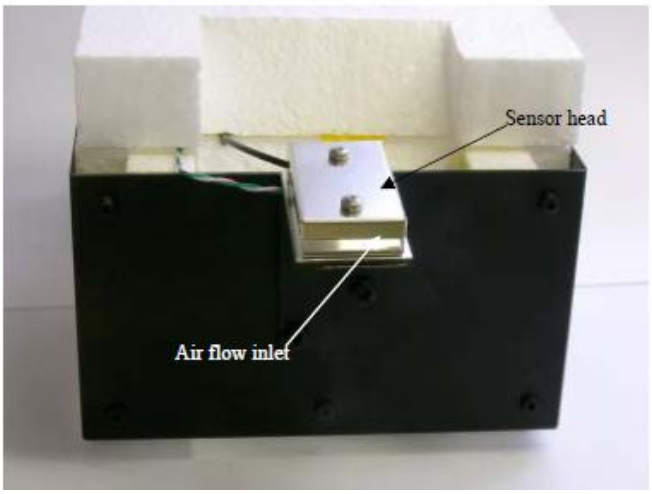

Fig. 4.1.12 Views of Night time Snow White sensing system.

4.1.2 Calibration at cold temperatures

A brief survey, conducted by the GRUAN Lead Center, of the lowest temperatures at which the relative humidity (RH) sensor and the temperature sensor are calibrated shows that there is a significant range between manufacturers, see table 4.1.2.

In particular for RH, but for temperature as well, accurate measurements can only be taken if the temperature range at which a measurement is being taken lies within the temperature range of the calibration. Once ambient conditions fall outside the temperature range of the calibration, some fits to the calibration data may create increasingly large errors, which should be avoided.

Observations in the tropics and in the polar stratosphere frequently reach temperatures of -90°C and it would be wise that this temperature should be covered in the calibration procedure of the temperature and the humidity sensor.

Manufacturer	Model	RH formula	Lowest Temp for RH Cal	Lowest Temp for Temp Cal
Vaisala	RS92-SGP	Wexler	-90	-90
Graw	DFM-09	Hyland Wexler	-80	-85
Modem	M2K2DC	Goff Gratch	-60	-90
Sippican	LMS 6	Wexler	-55	-70
Meteolabor	SRS C34	Sonntag	-40	-100
Meteolabor	Snow-White	Sonntag	-100	-100
Meisei	RD-06G	Buck (1981)	room temp	-85
InterMet	InterMet 2-AA	Bolton (Goff Gratch)	room temp	-70
Jinyang	RSG-20A	Goff Gratch	Room temp	-80
Nanjing Da Qiao	GTS 1-2	Goff (1957)	-40	-90
Huayun	GTS(U)1-1	Goff Gratch	-30	-90
Changfeng	CF-06-A	Goff Gratch	-60	-90

Table 4.1.2: Review of the formula used for water vapour of ice at low temperatures and the ranges of calibration of temperature and relative humidity sensors.

4.2 SSI

The sensors used as part of the scientific sounding instruments are separated by sensor and not by manufacturer. These sensors were expected to provide additional measurements not achievable through operational radiosondes. Each SSI sensor was used in combination with a particular radiosonde, which provided the other atmospheric parameters, which will be discussed in the respective sections.

Table 4.2.1 lists the instruments that were flown on the SSI payload. Two scientific humidity sensors were used on the SSI payload, as well as two scientific temperature sensors, all of which are, at this stage, not considered operational sensors, but rather scientific instruments. Each of these sensors will be described in greater details in the following sections.

In addition up to five operational radiosondes were used on the SSI payloads, most of which also served as transmitter of the data from the respective SSI sensors. The operational radiosondes used on the SSI payload were the Vaisala RS92-SGP, which also carried the data of the RD100 humidity sensor, the Meisei RS06G, which also transmitted the data of the MTR temperature sensor, the LMS6 Multithermistor, in which the operational temperature sensor is just part of the Multithermistor sensor, and the GRAW DFM-09, which was willing to fly as a sonde of opportunity. The InterMet (US) iMet-1 radiosonde was used as data transmitter for the CFH data and did not participate in the formal intercomparison. It was therefore not considered in the analysis presented below. The data from the temperature and humidity sensors of these operational radiosondes were compared to the output of the respective SSI sensors in the analysis presented below. These comparisons may be used to expand the lessons learned from the SSI sensors to the operational sensors.

SSI Sensor	Company	Radiosonde	Temperature Sensor	Humidity sensor	Comments
CFH	EnSci Corp.	InterMet iMet-1	-	Frost-point hygrometer	PTU from RS92
RD100	Vaisala Oyj	Vaisala RS92	-	Thin film Drycap	Data could not be used because of operational problem
MTR	MEISEI Co. LTD	Meisei RS-06G	Ultra-thin Tungsten wire	-	
Multithermistor	L. M. Sippican INC	LMS-6	Multi chip thermistors	Thin film (E+E)	Also flown with daytime QRS test flights
	Graw GmbH	DFM-09	Thermistor	Thin film (E+E)	QRS radiosonde

Table 4.2.1: Sensors and radiosondes in SSI group.

4.2.1 Cryogenic Frostpoint Hygrometer

The Cryogenic Frostpoint Hygrometer (CFH, *Vömel et al., 2007a*) is a balloon borne frostpoint hygrometer capable of measuring water vapor in the troposphere and lower stratosphere. This instrument has a rich history and is currently considered to be one of the very few instruments capable of measuring stratospheric water vapor. It was hoped that this instrument can provide information about the absolute water vapor content of the upper troposphere and lower stratosphere and thus serve as reference to the other humidity sensors. The CFH is a chilled mirror hygrometer, which has been built at the University of Colorado (Vömel et al., 2007a). Like many chilled mirror instruments, the CFH (Figure 4.2.1) does not require calibration in a relative humidity chamber to measure water vapour and so can be considered an absolute reference for water vapor measurements, as long as water vapour contamination is not present during the ascent. The CFH uses a feedback loop that actively regulates the temperature of a small mirror, which is coated with ice (or dew in the lower troposphere). In this feedback loop an optical detector senses the amount of ice covering the mirror and the feedback controller regulates the temperature of the mirror such that the amount of ice remains constant. If the feedback controller is operating properly, then the frost layer remains constant (by definition) and the mirror temperature is equal to the frost point temperature.

The cryogenic frostpoint hygrometer uses a cold liquid as coolant of the mirror during flight. Preparation and handling of this liquid before flight requires training and special handling procedures to avoid personal injury.

The water vapor mixing ratio and relative humidity can be calculated through a variation of the Clausius Clapeyron equation using the measured mirror temperature, air temperature and pressure.

The instrument measures the mirror reflectivity using a phase sensitive detector, which by design is insensitive to sunlight. Therefore condensate detection and frost point control are not influenced by daylight and the performance is the same for measurements during day or night time.

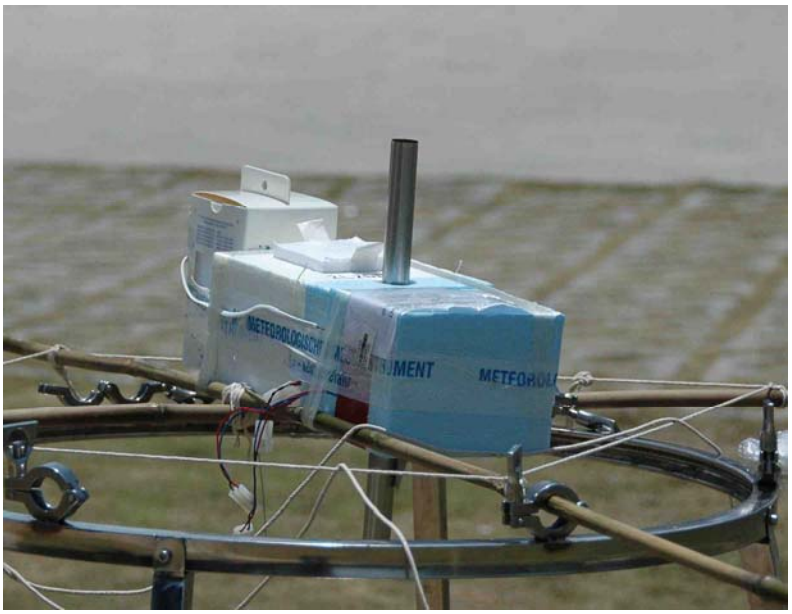

Figure 4.2.1 Cryogenic Frostpoint Hygrometer being prepared for a nighttime launch.

The largest source of measurement uncertainty in a frostpoint hygrometer is the stability and the drift of the feedback controller. For the CFH the total measurement uncertainty is estimated to be about 0.5°C in dew point or frost point temperature. This translates to roughly 9% of the RH percentage value at the tropical tropopause (Vömel et al., 2007a) and about 4% near the surface. Electronic noise and the presence of cloud particles in very dense cirrus clouds may increase the uncertainty.

The time response of the instrument is a function of the amount of water vapor and the accuracy and stability of the feedback controller. For the CFH, the time response varies from a few seconds in the lower troposphere to a few 10 seconds in the stratosphere.

Contamination through outgassing of water vapor from any surface is an issue in the lower stratosphere and is flagged out manually in the data processing. The amount of contamination is strongly influenced by the amount of clouds that the balloon payload has to pass and is generally higher in cloudy conditions. Contamination through outgassing limits the vertical range that the instrument can probe. To achieve the necessary airflow across the mirror, the detector is installed inside a straight vertical tube segment, which is extended beyond the actual instrument box before flight, by installing inlet tubes. These inlet tubes significantly reduce self-contamination by the sensor housing.

The CFH instruments launched in Yangjiang have been modified from the earlier version using the Vaisala RS80 as data transmitters. The version used in Yangjiang transmitted its data through an InterMet iMet-1 radiosonde.

4.2.2 Vaisala RD100

The Vaisala RR01 is the Vaisala reference radiosonde, which has been under development since 2007. This radiosonde incorporates the RD100 Drycap sensor, which is a capacitive thin film technology sensor specifically developed for low water vapor conditions in the upper troposphere and lower stratosphere (Fig. 4.2.2).

The Drycap sensor has been tested in campaigns at Sodankylä between 2007 and 2010 and at Lindenberg in November 2008. At both locations the sensor has shown sensitivity to water vapor at these conditions, although some work was still required to improve the absolute calibration. The campaigns at Lindenberg and at Sodankylä were characterized by dry fall and winter conditions, low tropopause heights and low cloud top heights.

The first two test soundings in Yangjiang showed extremely high frostpoint temperatures in the stratosphere, possibly due to liquid water contamination during the passage through clouds. To avoid wetting of the sensor during cloud penetration in subsequent soundings, a weather shield was employed, which had not been used in the previous campaigns. This rain shield covers the sensor during launch and in the lower troposphere. The shield was supposed to open at an altitude of about 8 km, allowing the sensor to have sufficient time to equilibrate to ambient conditions and to allow the auto calibration cycle to complete. However, the weather shield did not open as expected. Rather it opened near the tropopause, which did not give the sensor enough time to equilibrate sufficiently to ambient conditions and did not give the auto calibration cycle sufficient time to adjust the sensor calibration.

Thus the values that have been reported cannot be considered as representative measurements by the RD100 sensor, but rather as artifacts due to the malfunction of the weather shield. These measurements were, therefore, excluded in its entirety from the analysis.

The RR01, however, also contains the regular RS92 temperature and humidity sensors. The output from these sensors was used in the subsequent analysis. In particular the RS92 PTU data were used for the CFH frostpoint measurements to derive relative humidity and mixing ratio.

Figure 4.2.2 Vaisala RR01 radiosonde with RD100 Drycap sensor. Note, that the Drycap sensor is still covered by its rain shield

4.2.3 MTR

The MTR temperature sensor (Shimizu and Hasebe, 2010) is based on the temperature dependency of the electric resistance of an ultra thin tungsten wire, 10 μm in diameter, with the total length of 44 cm (which is then wound up in a helical coil with the diameter of 200 μm and the pitch of 100 μm). The wire is coated with aluminum to improve reflectivity and reduce solar heating. The response time is estimated to be between 9 ms at 5 km altitude and 40 ms at 30 km. The short wave radiation error is expected to be less than 0.43 K at 30 km and long wave heating and cooling of the sensor may be negligible. The self heating of the sensor due to the measuring current is expected to be less than 0.05 K. The maximum value of the systematic errors estimated in laboratory measurements does not exceed 0.14 K. The sensor characteristics are described in greater detail by Shimizu and Hasebe (2010).

The MTR is attached to the Meisei's operational radiosonde RS06G (Fig. 4.2.3). The sensor output is lowpass-filtered within the radiosonde at 3 Hz and transmitted to the ground at 6 Hz, corresponding to an effective vertical resolution of about 2 m. The PTU and GPS data from RS06G are obtained every second. Using data from several MTR soundings in Japan and Indonesia, Shimizu and Hasebe (2010) described contamination issues due to the radiosonde package box (for an older sensor-mount version of the MTR), balloon wake, solar eclipse effect by the overhead balloon, and the variation of insolation associated with the solid angle change of the solar illumination against the sensor body. Note the special flight configuration for the WMO Intercomparison with a bamboo rig and in some case, with a 700 mm suspension line from the rig (Fig. 4.2.5), in which contamination due to the rig may have occurred. In the analysis of this report, 10s averaged MTR data will be used for the basic intercomparison. The original 6 Hz data will be used for the investigation of contamination.

Figure 4.2.3 Combination of the Meisei MTR and RS06G radiosonde. Note, that the picture shows the sensor with the protective support structure, which is removed just before launch.

4.2.4 LMS Multithermistor radiosonde

The Multithermistor measures the radiative effects and the air temperature at the same time during the flight by using five temperature sensors with different radiative properties, instead of estimating the short/long-wave radiative errors based on laboratory measurements. Of the five temperature sensors three are aluminum-metalized (small emissivity and moderate solar absorptivity), one is coated white (large emissivity and small solar absorptivity), and one is coated black (large emissivity and large solar absorptivity). Theoretically, the measured temperature can be expressed with a sum of the actual air temperature term, long-wave radiative term, and short-wave radiative term (self heating term and systematic errors arising from, e.g., imperfect sensor calibration are neglected here). Thus, the three unknowns, i.e. the actual air temperature, the long-wave net radiative heating, and the short-wave radiative heating, can be solved from the set of heat energy equations for three differently coated temperature sensors. The basic principle of the Multithermistor method is explained by Schmidlin et al. (1986).

The LMS Multithermistor radiosonde is an independent and improved instrument and based on the NASA Accurate Temperature Measuring (ATM) Multithermistor radiosonde developed by Schmidlin et al. (1986) (Fig. 4.2.4). There are three aluminum-metalized thermistors, one white and one black coated thermistor. The thermistors on the LMS Multithermistor radiosonde are mounted in a relatively large frame, which allows nearly unobstructed air flow around the sensors and minimizes potential contamination from the radiosonde body. It should be noted that many Multithermistor radiosondes were flown within QRS groups as well, and the results have been analyzed within the QRS sections.

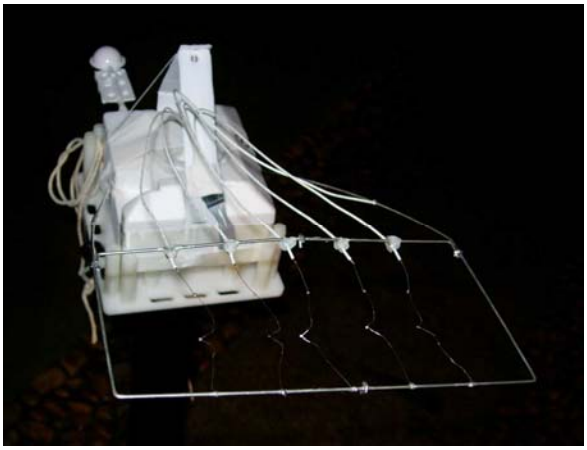

Figure 4.2.4 LMS Multithermistor radiosonde. The picture shows the thermistor frame with five thermistors (from left to right: aluminium-metalized, black coated, white coated, and two aluminium-metalized thermistors.)

The aluminum-metalized temperature sensor is the LMS chip thermistor, which uses a reflective coating, which minimizes errors due to solar and infrared radiation effects. This sensor is used as operational temperature sensor and is also part of the Multithermistor sensor. The manufacturer claims that infrared radiation effects are negligible and solar radiation effects are significantly reduced (e.g., 0.95 ºC at 10 hPa at 90 degree solar elevation angle). The manufacturers also states that time lag effects are negligible (<0.05 ºC) and that the coating behavior appears stable throughout flight. Furthermore, electronic and connecting wire effects are presumed to be negligible. The accuracy of the sensors is stated as +/-0.2 ºC (rms) with a resolution of 0.1 ºC in the range of +60 ºC to -90 ºC (Sippican, 2003).

The sounding system provides data of the standard sensor temperature, which includes the solar radiation correction; the Multithermistor "solution" temperature; and three standard sensor temperatures without solar radiation correction applied. In the analysis of this report, both the standard sensor temperature which is regarded as an operational sensor temperature (labeled as LMS6 temperature) and the Multithermistor "solution" temperature (labeled as Multithermistor temperature) are analyzed.

4.2.5 SSI Soundings

Figure 4.2.5 shows an example of the SSI payload (flight number 002). For all soundings but one, the CFH was mounted in the center of the bamboo cross. The other instruments were usually hung on the ends of the bamboo rods using 70 cm of string. To balance the payload a counterweight was used on the remaining empty rod end, which was replaced by the Graw radiosondes in the second half of the campaign. Table 4.2.2 lists all payloads and their respective launch configurations.

Figure 4.2.5 Preparation for the flight number 002. The CFH has been fixed in the centre of the crossed bamboo rig. The Meisei MTR/RS06G, the LMS Multithermistor radiosonde, and the Vaisala RR01/RS92-SGP were hung on ends of the bamboo rods using 70 cm of rope. The light blue carton hung on the front-side of the rig is a counter weight to balance the whole payload. For this flight, 30 m of string were used instead of an unwinder.

Flight #	Date	Time (LST)	P	U	G	Comments
02 (1)	7/14/10	12:58:00	y	n	n	
10 (2)	7/16/10	02:59:28	y	y	n	
15 (3)	7/17/10	02:56:49	n	y	n	No MTR/Meisei GPS/P data
20 (4)	7/18/10	03:06:25	y	n	n	
26 (5)	7/20/10	12:51:23	y	n	n	
32 (6)	7/21/10	14:45:02	y	y	y	MTR broke at launch; no Multithermistor data
43 (7)	7/25/10	03:01:24	y	n	y	RR01&MTR tied to bamboo rig
48 (8)	7/26/10	02:49:51	y	n	y	RR01 tied to bamboo rig,
53 (9)	7/27/10	02:55:47	y	y	n	RR01 tied to bamboo rig; No MTR (shortage of radiosondes); CFH suspended on side. CFH data excluded due to unexplained high bias.
56 (10)	7/28/10	15:05:31	y	y	y	RR01&MTR tied to bamboo rig
61 (11)	7/29/10	14:48:34	y	y	y	RR01&MTR tied to bamboo rig
66 (12)	7/30/10	14:53:00	y	y	y	RR01&MTR tied to bamboo rig

Table 4.2.2: Summary of 12 SSI launch configurations. Column P: Parachute present (yes or no), Column U: Unwinder present (yes or no); Column G: Graw DFM-09 radiosonde part of the payload (yes or no)

4.3 Remote sensing

This section describes the remote sensing systems instruments deployed in and around Yangjiang for the duration of the intercomparison and the data obtained.

Equipment	Provided by
GPS/MET water vapour network	CMA
S band Doppler Weather Radar	CMA
All-sky imager	CMA
Mobile Whole coherent Millimetre-wave Cloud-detection Radar	CMA
Mobile Boundary Layer Wind Profiler Radar	CMA
CL51 Ceilometer	Vaisala
Microwave Radiometer	CMA

Table 4.3.1: Remote Sensing Systems deployed in and around Yangjiang test site.

- **Global Positioning System (GPS)/MET water vapour network**

A Leica GPS/MET sensor is installed at the Yangjiang observing station (Latitude 21^{o} 50' North, Longitude 111^{o} 58' East, and 89.9m amsl).

Figure 4.3.1 GPS/MET Leica sensor at Yangjiang station.

As well as the sensor at Yangjiang data was provided for 5 other sensors around Yangjiang, their Latitude, Longitude and height are provided in table 4.3.2 below, and a map of their locations can be found in Figure 4.3.2 below.

Station Name	Latitude	Longitude	Height (m)
Yangjiang (yj)	21.833 N	111.967 E	89.9
Enping (ep)	22.177 N	112.296 E	28.596
Luoding (ld)	22.713 N	111.593 E	53.139
Tai Shan (ts)	22.247 N	112.785 E	30.437
Xin Xi (xx)	22.714 N	112.219 E	12.306
Yang Chun (yc)	22.164 N	111.787 E	32.815

Table 4.3.2: GPS/MET sensor locations

Figure 4.3.2 GPS/MET sensor locations

The data provided was date, time, sensor location, and the Integrated Water Vapour (IWV) in spreadsheets for each of the locations. Data was primarily from 12th to 31st July, with hourly values from Yangjiang, and half-hourly data from the other stations, there was some missing data, all times are UTC. At Yangjiang, the surface pressure data were adjusted to antenna height (correction of 0.3hPa).

- **S Band Doppler Weather Radar**

This radar is at the Yangjiang observing station, which is on a small hill above the city of Yangjiang; see Figure 4.3.3 and 4.3.4 below. It has a vertical scanning mode, and can obtain vertical structure property of the upper air above the observed region. Gif's of the radar plot were supplied for selected hours from the 14th to 30th July, please note the radar was normally only switched on when there was precipitation. The gif's have ranging circles from 50 km to 230 km, and the time stamps are in UTC.

Figure 4.3.3 S Band radar location

Figure 4.3.4 S Band Doppler Weather Radar

- **All-Sky imager**

The all-sky imager is a passive infrared detector for the whole sky, and is used to detect the height, and amount of the cloud. The instrument was deployed on the roof of Yangjiang observing station, as seen in Figure 4.3.5 below. Images (jpg) were provided for dates from 11th to 30thJuly; however, there was no data for the 22nd. Three types of files were provided, a ZC folder with pictures of the sky, a GFS folder with infrared images and an YZ folder. For both the latter, dark blue is clear sky, cyan is cloud, and red is ground clutter. All the dates and times are in UTC and the cloud amount is in tenths.

Figure 4.3.5 All-Sky Imager

- **Mobile fully coherent Millimetre-Wave Cloud-detection Radar**

The radar can obtain the vertical structure of the cloud above the area. It works at the K_a frequency (35 GHz ± 10M Hz), and can detect non-precipitating clouds and weak precipitating clouds up to a range of 30 km. It obtains data on the reflectivity, velocity, spectrum width and lineal depolarization ratio of the target. It can also provide secondary products such as, cloud distribution, size as well as the phase of the particles in the cloud. The radar, see Figure 4.3.6 below, was located approximately 1.6 km NE of the observing station, by a lake. At latitude 21° 51' 26" North, longitude 111° 59' 17" East, and a height of approximately 10 m, see Figure 4.3.7 for location of the radar.

Figure 4.3.6 Mobile Cloud Radar

Figure 4.3.7 Mobile Cloud Radar and Yangjiang observing station location

Detection range	Range	0.15 to 30 km
	Position	0 to 360°
	Elevation	0 to +90°
	Reflectivity	-50 to +30 dBz
	Velocity	-8.5 to 8.5 m/s
	Spectrum width	0 to 4 m/s
	Depolarization ratio	-30 to -5 dB

Table 4.3.3: Technical Specifications of the Observed Elements

Antenna type	Cassegrain Antenna
Diameter	1.5 m
Wave Width	<=0.4°
Antenna Gain	>= 51 dB
First Side Lobe	<=23 dB
Cross-polarization Isolation	<=30 dB
Transmitting Tube	Travelling Wave Tube (TWT)
Transmitting Pulse Power	0.6 kW
Pulse Width	0.5μs 20μs 40μs
Repetition Frequency	1000 2000 4000 Hz
Noise Figure	<= 4.5 dB
Intermediate Frequency	50 MHz
Range Bin	75 m
Reflectivity Processing	Linear Average
Velocity Processing	Fast Fourier Transform (FFT), Pulse Pair Processing (PPP)
Accumulation	32/64/128/256/512/1024/
Reflectivity Z	-50 to -30 dB. Accuracy <=0.5 dB
Lineal Depolarization Ratio (LDR)	-10 to -30 dB. Accuracy <= 0.5 dB
Power Consumption	<= 3 kW

Table 4.3.4: Technical Specifications of Hardware

The radar tracked the flight of the balloon, the position of the balloon was provided by various radiosonde manufactures. Images (jpg) of the radar plot were supplied, Plan Position Indicator (PPI) for selected times between the 20th and 22nd July. Range Height Indicator (RHI) plots were supplied for the times of each launch from 14th to 30 July, the RHI plots tracked the position of the radiosondes. The files are named with the local date and time, and an intensity scale 'bmp' file is included with the dataset, as the scale is hard to read on some plots.

- **Mobile Boundary Layer Wind Profiler Radar**

The wind profiler is used for all-weather detection of air wind field, and providing boundary layer wind field information with high spatial and time resolution, and operates on a point-frequency between 1270-1375 MHz. The wind profiler was located at the Yangjiang observing station, see Figure 4.3.8, below. The time resolution of the wind profiler is: for 3 beam, less than or equal to 3 min; for 5 beam, less than or equal to 5 min.	
Max. Height	>= 2 km
Min. Height	<= 100 m
Range	Velocity 0 to 60 m/s Direction 0 to 360° Virtual Temperature 223~323 K
Root mean sq error	Velocity <=1.5 m/s Direction <=10° Virtual Temperature <= 1 K
Resolution	Velocity 0.2 m/s. Direction 0.5°. Altitude 60 m 120 m.

Table 4.3.5: Technical Specification of Observed Elements

Figure 4.3.8 Wind Profiler at Yangjiang

Beam Pointing	5 beam, a vertical beam and 4 mutually orthogonal direction beams, the elevation beams with the same angle.
Beam Width	<= 9^o
Antenna Gain	>= 24 db
Max Side lobe Level	<= -20 dB Scanning and non-scanning surfaces
Far-zone side lobe	<= -25dB
Voltage Standing Wave Ratio (VSWR)	<= 1.3
Polarization	Linear polarization
Lobe forms	Pen-shaped beam
Peak output power	>= 1 kW
Pulse width	0.4μs and 0.4 μs multiples
Pulse repetition cycle	40~80μs
Max duty cycle	>= 8%

Table 4.3.6: Hardware Technical Specification

- **Vaisala CL51 Ceilometer**

The CL51 is a 910 nm ceilometer designed to measure high-range cirrus cloud height without surpassing the low and middle-layer clouds, or vertical visibility in harsh conditions. Advanced single-lens design provides excellent performance also at low altitudes. The CL51 employs a pulsed diode laser LIDAR (Light Detection And Ranging) technology, where short, powerful laser pulses are sent out in a vertical or near-vertical direction. The reflection of light (backscatter) caused by the clouds, precipitation or other obscuration is analyzed and used to determine the cloud base height.

Figure 4.3.9 Vaisala CL51 Ceilometer

Cloud reporting range	0… 13 km
Backscatter profiling range	0… 15 km
Reporting cycle	Programmable 6… 120 seconds or polling
Reporting resolution	10 m, units selectable
Distance measurement accuracy against a hard target	Greater of ± 1% or ± 5 m
Laser	InGaAs diode, 910 nm

Table 4.3.7: CL51 Performance details

The data available for the CL51 are 6 hourly .DAT files from 11th July to 1st August.

- **Microwave Radiometer**

The microwave radiometer can produce vertical profiles from the surface to 10 km in height including temperature and water vapour profiles, and low-resolution liquid profiles. It includes two radio frequency (RF) subsystems in the same cabinet that share the same antenna and antenna pointing system. The temperature profiling (TP) subsystem utilizes sky observations at selected frequencies between 51 and 59 GHz. The water vapour profiling (WVP) subsystem receives at selected frequencies between 22 and 30 GHz. Passive technology is used to prevent any detectable emitting radiation. Surface meteorological sensors (Met Sensors) measure air temperature, relative humidity and barometric pressure. It could be helpful to evaluate humidity measurement together with GPS/MET vapour sensing system and other cloud detection instruments.

Calibrated Brightness Temperature Accuracy	0.2 + 0.002*|TkBB-Tsky|
Long Term Stability	<1.0 K / yr typical
Resolution (depends on integration time)	0.1 to 1 K
Brightness Temperature Range	0-400 K
Antenna System Optical Resolution and Side Lobes 22-30 GHz 51-59 GHz	 4.9 - 6.3° -24 dB 2.4 - 2.5° -27 dB
Integration Time (user selectable in 10 msec increments)	0.01 to 2.5 seconds
Frequency Agile Tuning Range Water Vapour Band Oxygen Band Minimum Frequency step size	 22-30 GHz 51-59 GHz 4.0 MHz
Standard channels used for profiles	12
Spectrum Analyzer Mode10 (brightness temperatures only)	Up to 40 channels
Pre-detection channel bandwidth (effective double-sided)	300 MHz
Surface Sensor Accuracy Temperature (-50° to +50° C) Relative Humidity (0-100%) Barometric pressure (800 to 1060 hPa) IRT (Note: ΔT = Tambient - Tcloud)	 0.5°C @ 25°C 2 % 0.3 hPa (0.5 + .007*ΔT)°, C
Brightness Temperature algorithm for level1 products	4 point nonlinear model
Retrieval algorithms for level2 products	Neural Networks
Calibration Systems Primary standards Operational standards	 LN2 and TIP methods Noise Diodes + ambient Black Body Target
Environmental Operating Range Temperature Relative Humidity Altitude Wind (operational/survival)	 -40° to +40° C 0-100 % -300 to 3000 m 100 km/hr / 200 km/hr

Physical Properties Size (H X W X L) Mass	 50 X 28 X 76 cm (add 17 cm to height for IRT) 29 kg
Power requirements Radiometer (100 to 250 VAC / 50 – 60 Hz) Superblower (100 to 125 VAC / 50 – 60 Hz)12	 200 watts max 100 watts max
Data Interface Primary computer port Auxiliary port Standard cable length13	 RS232 38.4 Kbaud RS232 1.2 to 38.4 Kbaud 30 m
Data File Formats	ASCII CSV (comma separated variables)

Table 4.3.8: Hardware Technical Specification

Figure 4.3.10 Microwave Radiometer.

5 Procedures

5.1 Radio-Frequency

Most participants arrived a few days before the official opening of the Comparison, and this time was used to test out the radiofrequency allocations for the different radiosonde types. Each system was assigned a set frequency, although when a given QRS switched between the two main groups these had to be adjusted slightly. Satisfactory flights were obtained in the trial flights with some small adjustments to the original radiofrequency plan, and the frequencies were then kept the same throughout the test.

The site at Yangjiang was mostly free from interference, although on occasions some interference from a source in the town was experienced by some systems. It was found that it was necessary to prepare the SSI instruments for flight after a QRS test flight, rather than before, because this avoided interference with the QRS systems in flight, even if the SSI systems were on different frequencies to the QRS.

This type of experiment can only work well if all radiosondes have very good radiofrequency stability, and this was the case for all the QRS systems at Yangjiang.

5.2 Balloon preparation and launch

In order to achieve this task CMA has selected some experienced staff from nationwide upper-air sites, and carried out launching training in Beijing (April 10). This training included the creation of a detailed launching plan and specific support platform design for releasing frame (see Fig. 5.2.1 below). Two experts from the UK Met Office, who had participated in previous intercomparison, arrived in Yangjiang four days prior to the start of the intercomparison to do additional training for the releasing group and check preparation jobs. In addition, the project team organized frequency group tests, and finalized the radiosonde-grouping plan.

Considering the day and night shifts, three releasing teams were established, with four staff members for each team, as well as three shift team leader appointed. The tasks for the releasing group included producing the rig frame, attaching the radiosonde to the rig, surface observation recording, hydrogen filling and balloon releasing. Manufacturers were responsible for the radiosonde preparation and assisting in the balloon releasing. China focal point (LI Wei from CMA) took charge of the overall releasing task, and the three releasing team leaders were responsible for the fieldwork. In case of emergency, the team leader, the China focal point and the project team members had discussions and found proper solutions in time.

Fig. 5.2.1 Types of support platform (round and square available to rig frame design differently for 4, 5, 6 or 7 radiosonde attaching and balance adjustment)

In order to get efficient communication between manufacturers and releasing team, every type of radiosonde was assigned a numerical code from 1 to 17; in particular note that "13" was not used for certain western world taboo (see Table 5.2.1 below). In addition, the releasing group had prepared sand bags corresponding to the weight of each type of radiosonde, which could be used as alternative of corresponding radiosonde for keeping releasing frame balance if needed.

Radiosonde				**Radiosonde**			
Name	**Designated simplified name by WMO**	**Designated numerical code by releasing group**	**Weight (on launch)**	**Name**	**Designated simplified name by WMO**	**Designated numerical code by releasing group**	**Weight (on launch)**
InterMet	I	1	225g	**Modem**	M	2	210g
Graw	G	3	90g	**Meteolabor + Snow White**	S	3	1050g
Meteolabor	ML	5	620g	**China Daqiao**	C	6	370g
Jinyang	Y	7	250g	**Multi-thermistor**	MT	8	265g
CFH	F	9	1000g	**Meisei**	J	10	150g
Meisei Referance	J*	11	200g	**Vaisala**	V	12	290g
China Changfeng	C1	14	260g	**China Huayun**	C2	15	360g
Sippican	P	16	230g	**Vaisala Reference**	V*	17	300g

Table 5.2.1: Detail information for radiosonde launches

All staff and manufacturers were at the intercomparison field (Yangjiang site) at least 45 minutes in advance of the planed balloon launching time. The manufacturers went to designated working room for their preparation and kept communication always available with the releasing team leader (walkie-talkies). The releasing team leader informed manufacturers to read the surface observation data from the board in front of the data centre (also electronic sheet was filled after launching by the releasing team, see Annex F) and to start attaching radiosondes to the flight rig when 15 minutes were left, and special check notification when 5 minutes were left. Note that some delay was allowed in case of emergency (strong wind, rain, manufacturers not ready), but the capacity of radiosonde battery was carefully considered and make sure sounding data acquisition, as well as agreement of intercomparison project team.

To ensure the smooth intercomparison, daily weather forecasting was provided by Yangjiang meteorological bureau, especially for rain and wind. During the intercomparison, to the surprise of many, two typhoons passed close to the site (only one at most in normal July conditions). The launch program was adjusted accordingly and special preventive measures were taken for outside antennas. Thanks to all efforts made no damage or casualties occurred.

5.3 Balloon performance

The adequate sounding height for enough data sample and reasonable balloon ascent rate for sensor ventilation were key factors for the radiosonde intercomparison. The 2000g meteorological balloons used in Yangjiang intercomparison were provided by Zhuzhou Research & Design Institute, Chemchina Rubber Corp (detail information can be found at www.hwoyee.com), a specialized research institute and the largest manufacturer of meteorological balloons in China.

Appropriate high quality, cold resistant plasticizer was applied to the 2000g balloon for promoting its stretching performance under low temperature along with a new type of anti-ozone and anti-UV aging agent for strengthening its anti-aging capability.

Fig. 5.3.1 - The initial balloon launching after the opening ceremony by Tim Oakley

During the campaign a total 72 balloons were launched (see Fig. 5.3.1). No complete balloon failures occurred, with 52 balloons achieving a burst height of over 30000 m (near 10hPa). The average burst height was 30578 m and maximum burst height was near 40 km (39295 m and 3.1 hPa) for 28th flight at 20:00 on July 20th (see Fig. 5.3.2 to 5.3.4).

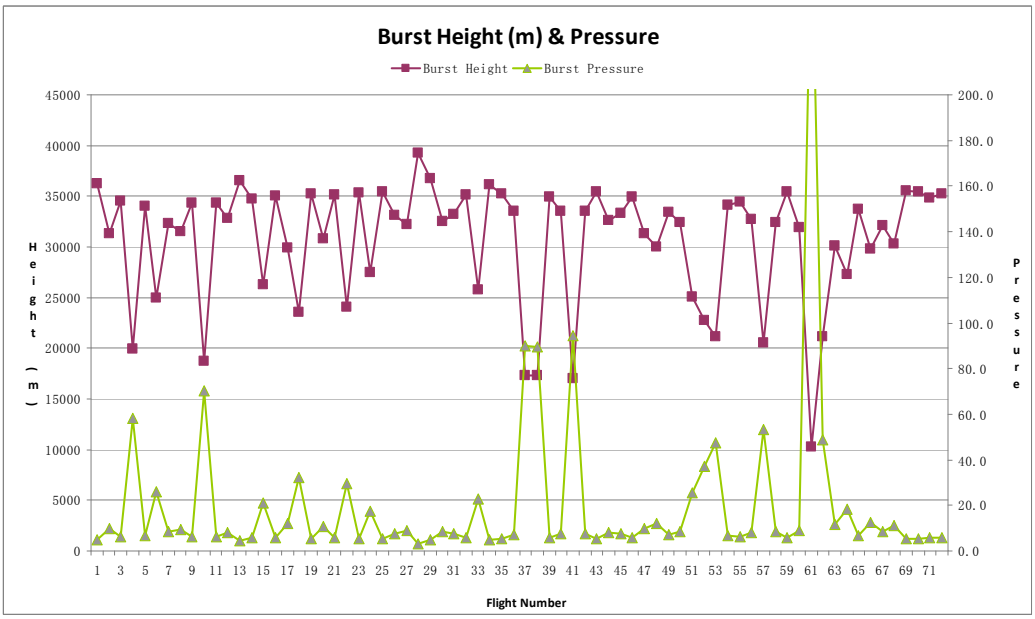

Fig. 5.3.2 Burst height and pressure

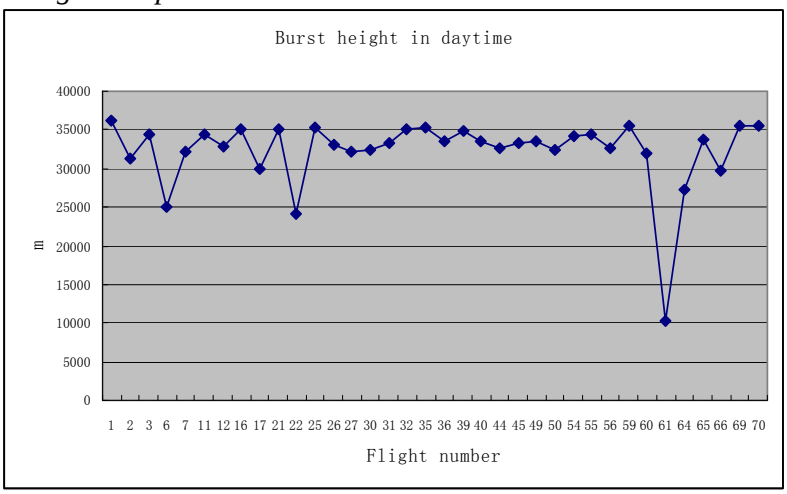

Fig. 5.3.3 Burst height in daytime

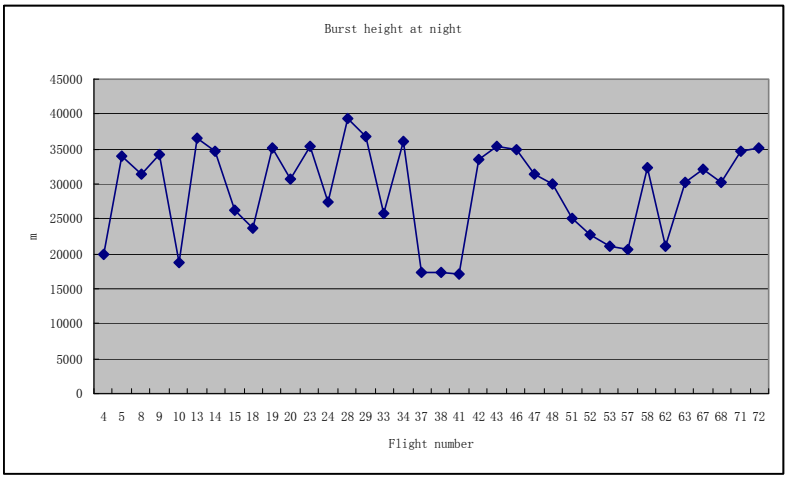

Fig. 5.3.4 Burst height at night

Comparing day and night flight height, the burst height in daytime was significantly higher than at night: the average height for day flight was 32269 m and for night flight 29136 m. The balloon has better performance in daytime than at night.

From Fig. 5.3.2, note that the burst heights of Flight 4,10, 37, 38 and 41 in daytime and Flight 61 at night are obviously low (below 20000 m). Therefore, we should look at these typical examples. (Figs. 5.3.5 to 5.3.10 show the conditions during flight on these occasions.)

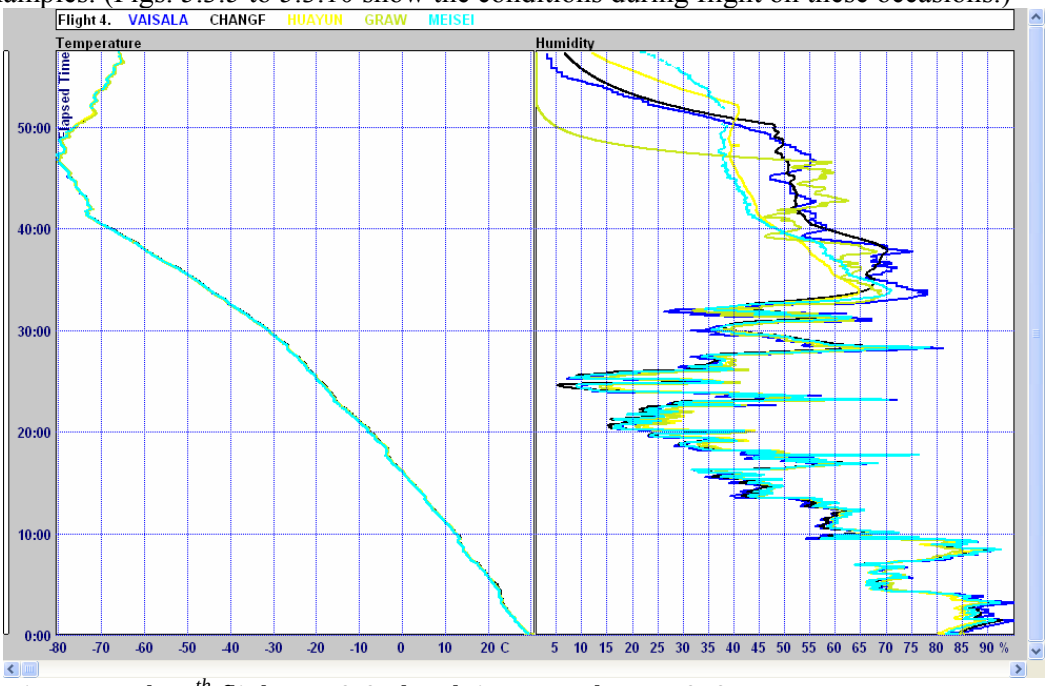

Fig. 5.3.5 The 4th flight at 20:01 local time on July 14, 2010

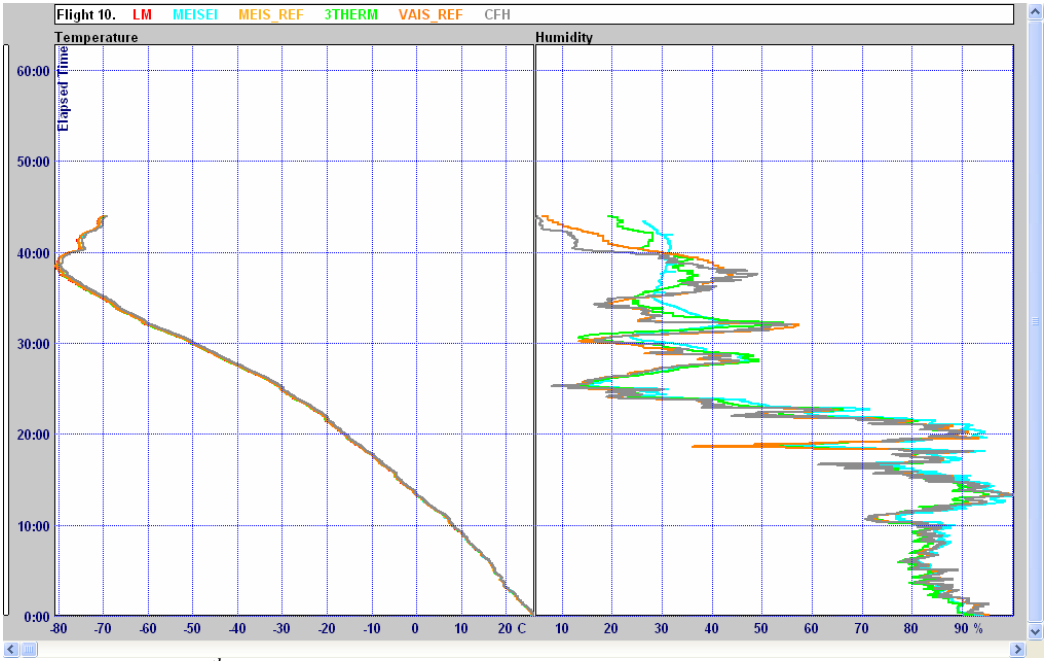

Fig. 5.3.6 The 10th flight at 03:00 local time on July 16, 2010

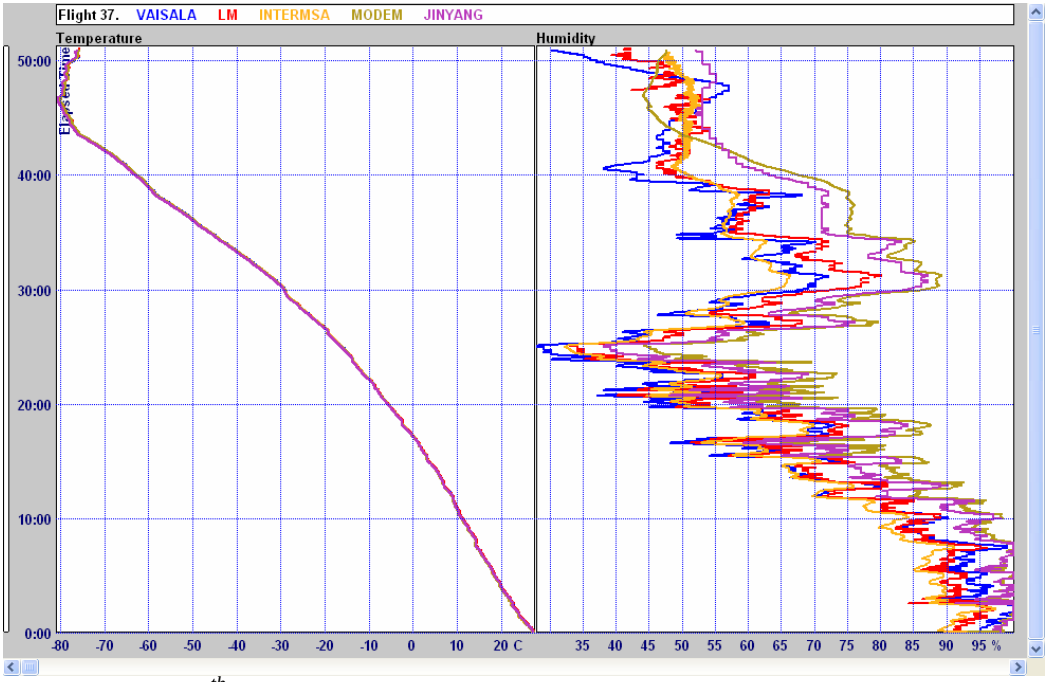

Fig. 5.3.7 The 37th flight at 20:07 local time on July 23, 2010

Fig. 5.3.8 The 38th flight at 00:45 local time on July 24, 2010

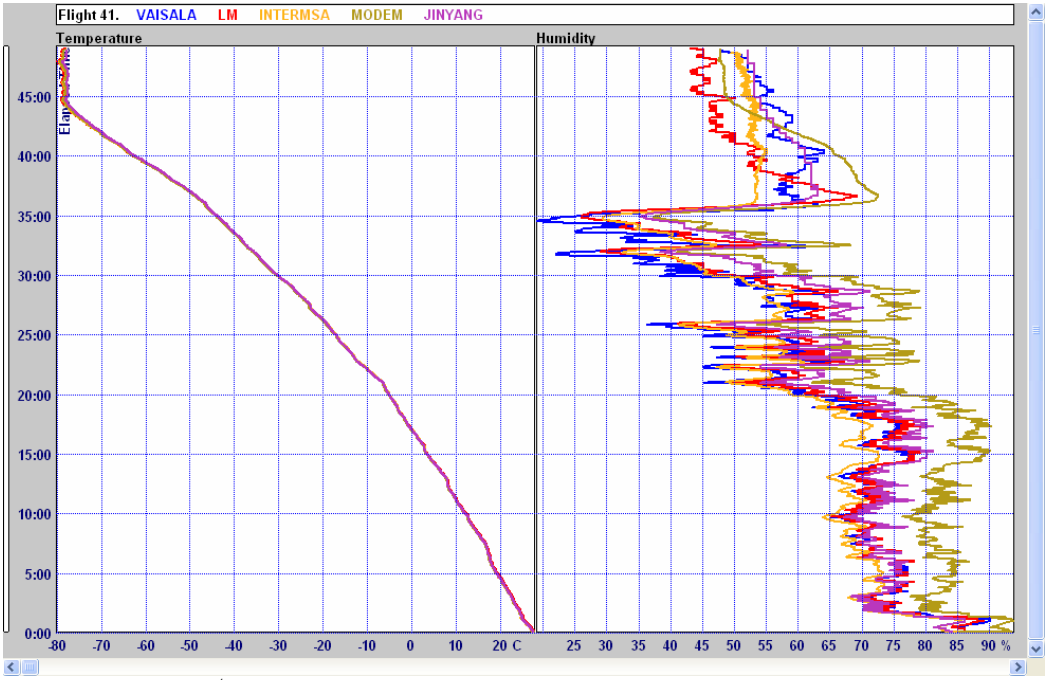

Fig. 5.3.9 The 41st flight at 20:00 local time on July 24, 2010

Fig. 5.3.10 The 61st flight at 14:49 local time on July 29, 2010, struck by electrical discharge

Flights 4, 10, 37, 38 and 41 show similar characteristics:

(1) night flight,
(2) lower than -80 °C for minimal temperature at tropopause,
(3) high humidity near surface (over 80% RH) and keeping high humidity under troposphere (over 50% RH) and
(4) upper cloud is clearly present.

According to the balloon manufacturer's specification, the vitrification temperature for 2000g balloon is about -70°C. Due to high humidity and cloud, the balloon experienced water contamination on the surface at initial ascent stage and then freeze to hasten the vitrification process. If the vitrification phenomenon occurs in daytime, the sun's radiation counters the vitrification process, the balloon will resume elastic character after passing through the tropopause, and temperature will rise again. However, at night, due to ice frozen induced by water contamination and low temperature, the balloon will burst early below the expected height. It is also the reasons why burst height in daytime was higher than at night.

For Flight 61, the balloon skin may have been covered with ice from an intense thunderstorm anvil; see Fig. 8.3.1, but there was also some electrical discharge since all the radiosondes stopped working.

In order to prevent balloon from water contamination and reach higher burst heights the balloon manufacturer used a special (double balloon) technology, as shown below.

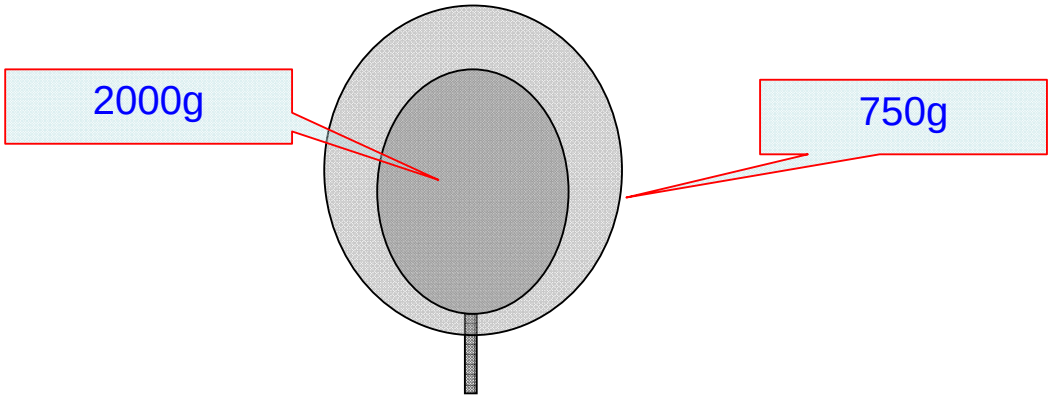

The 2000g balloon was inside a 750g balloon. A suitable amount of gas was filled both in the 2000g balloon and between the two balloon skins to ensure the net lift would be the same as for a single 2000g balloon, as used before. Due to water contamination and low temperature, the 750g balloon would burst early near the tropopause, and then the 2000g balloon would continue ascending as a fully new balloon, i.e. the outside 750g balloon offers protection for the inside 2000g balloon. The final burst height proved the good effect of the double balloon, particularly in rainstorm.

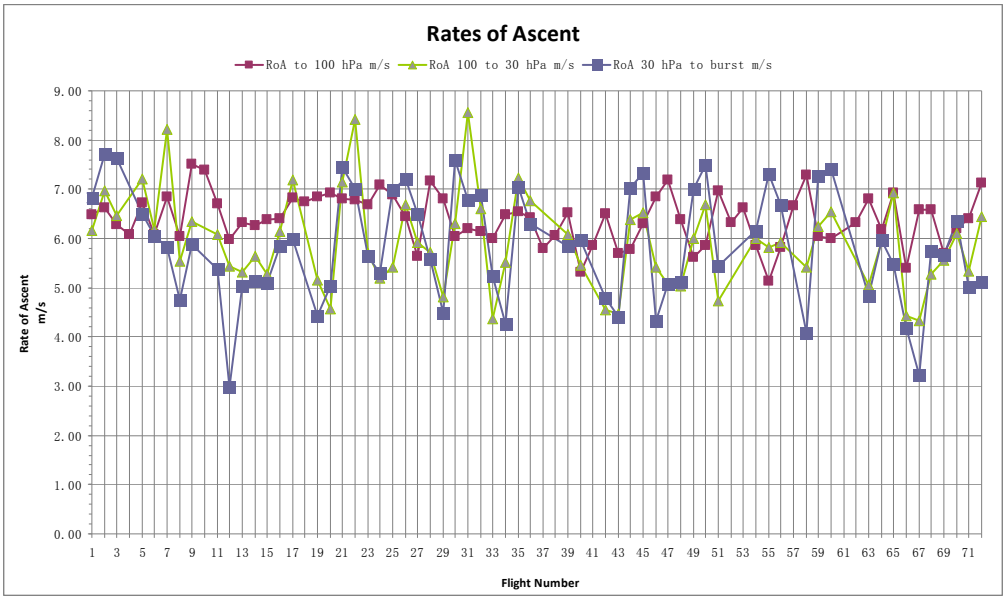

Fig. 5.3.11 Rates of ascent for balloons

From Fig. 5.3.11, it can be seen that the average rate of ascent was 373 m/min (6.22 m/s) from surface to burst height along with 428 m/min (7.13 m/s) from surface to 100 hPa, 387 m/min (6.45 m/s) from 100 hPa to 30 hPa, and 307 m/min (5.12 m/s) from 30 hPa to burst height. Therefore, the average rate of ascent can be satisfied, also note that fluctuation of rate of ascent increases with height, caused by gravity waves.

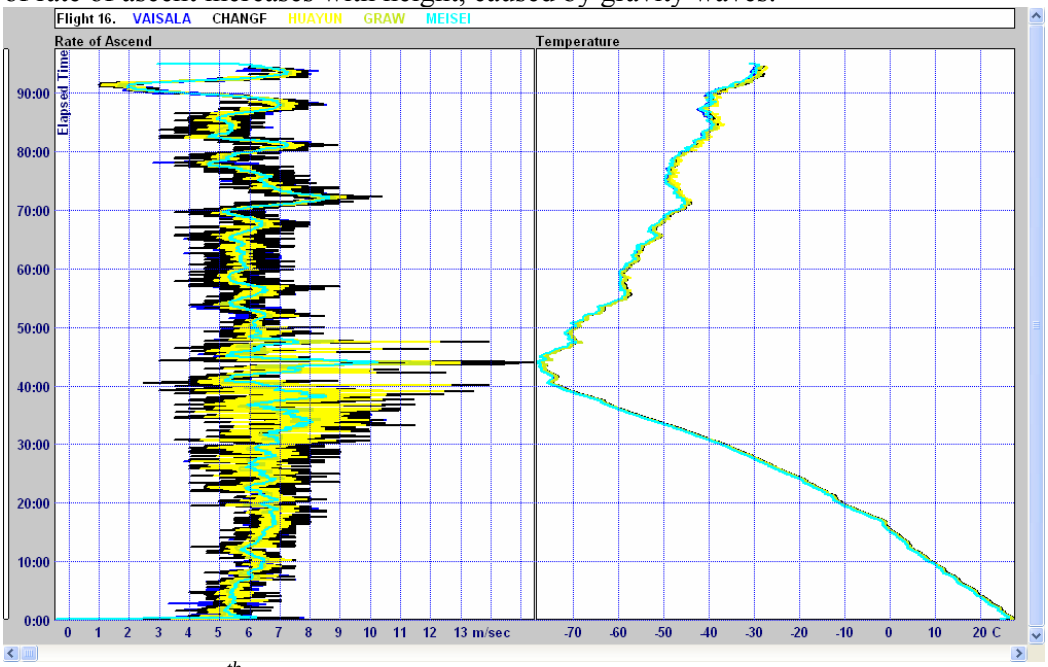

Fig. 5.3.12 The 16th flight at 08:3 local time on July 17, 2010

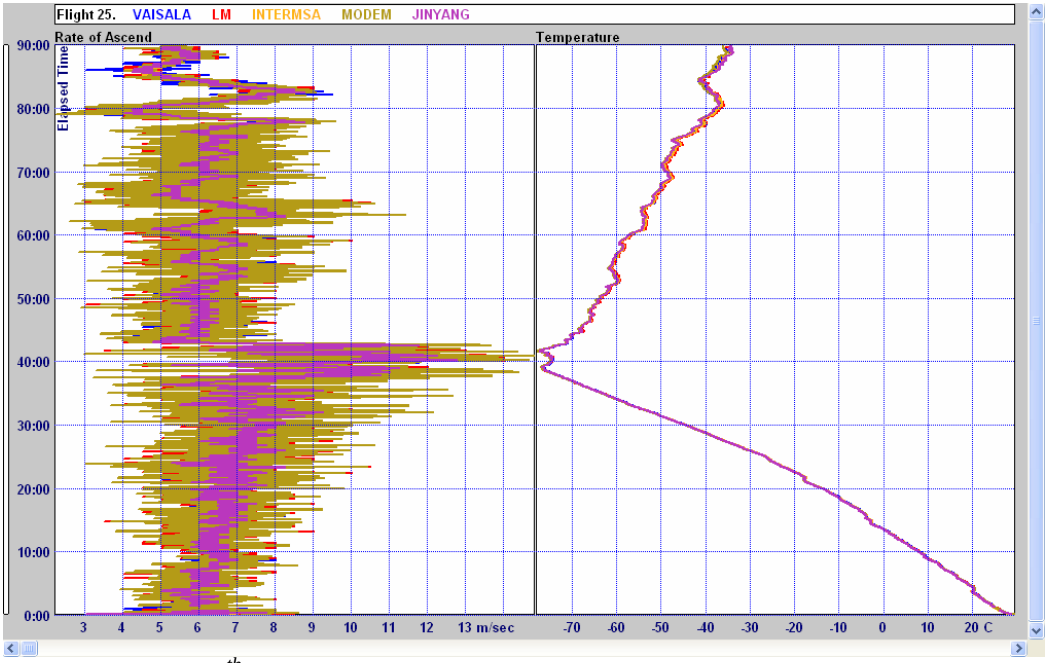

Fig. 5.3.13 The 25th flight at 08:32 on July 20, 2010

According to the above examples, note that the rate of ascent always becomes larger near the tropopause. Maybe it is due to double-balloon method, early burst of 750g balloon at tropopause cause discontinuity as lift changes to the 2000g balloon alone. Figures 5.3.12 and 5.3.13 illustrate the change in rate of ascent that occurred with the double balloon system.

In conclusion, the good quality of 2000g balloon, as well as double-balloon method, which can provide high burst height and suitable ascent rate, has ensured the success of Yangjiang intercomparison.

6 Data Collection, processing and editing (QRS)

6.1 Software used

The processing software used for this intercomparison was again kindly provided by Mr Kurnosenko. This was a new updated version of the RSKOMP software used to analyze results from Phases III and IV of earlier WMO Radiosonde Intercomparisons (see Kurnosenko and Oakley, 1996) and in Mauritius (see Annex G).

6.2 Intercomparison procedures

Sergey Kurnosenko was the data manager at the intercomparison in Yangjiang supervising the input of data into the Comparison database, with the assistance of Gonzague Romanens from MeteoSwiss.

CMA ran a data centre where the data were collected from the participants and from the remote sensing systems. All the manufacturers had to send their data using specific memory disks (offered by releasing group) to data centre after balloon burst. Firstly, the staff of data centre checked for viruses, secondly copied the data file to specific computer, then opened the data file and checked the file data again. Both staff and manufacturers signed the data receiving record sheet after the confirmation. The WMO project team got the data from the data centre. Note that permission was obtained from the project team leader in case any manufacturers wanted data files to be changed for some special reasons (i.e. wrong data copy or data reprocess) in the data centre, or anyone wanted data copy from data centre. All the data had to be destroyed after the end of the intercomparison under the inspection of the project team.

Most of the participants had coordinated with Mr Kurnosenko before the start of the field phase of the intercomparison, so data handed in was readily added to the WMO database. Data for each radiosonde type were handed into the CMA Data Collection Office, usually within 1 hour of balloon burst, but for the last flight at night, it was handed in as soon as possible in the morning. Data were then transferred from CMA into the WMO database managed by Mr. Kurnosenko. The WVIEW software was then used to check for errors in system set up. As a result, Graw were advised to modify the Graw software set up to improve data sampling for input to the comparison database. Meisei and Jinyang revised or initiated solar temperature correction schemes, as there were clear problems with what they were using in the first few flights. Daqiao changed the ground check procedures for the relative humidity, and a few flights were reprocessed in agreement with the WMO Project Team. Individual data review meetings were held with all the manufacturers, as requested.

Software had to be modified to sample CFH and MTR (SSI systems) not previously involved in WMO Radiosonde Comparisons. This ensured that SSI data were made available for initial comparisons in the main Comparison database. Thus, the SSI systems were subject to a similar discipline as the QRS systems of submitting data into the comparison database before the test was completed in Yangjiang.

No serious revision of the SSI data occurred after the completion of the comparison, but CFH data have been further processed as indicated in the section concerning the SSI results. Similarly, no QRS data were revised apart from Graw geopotential heights and pressure. This was the result of an error in the computation of geopotential heights, where the conversions

from GPS geometric height had become mixed with the generation of a geopotential height from a radiosonde with pressure, temperature and humidity. The effects of the error were relatively small and could only be detected by comparison with the other GPS geopotential height measurements. With this error removed, the Graw heights parallel all the other GPS systems in terms of differences with height. This problem showed that the WMO Guide to Meteorological Instruments and Methods of Observations (WMO-No. 8, 2008, hereafter called CIMO Guide) was not sufficiently specific in defining the algorithm for conversion from geometric height to geopotential height, stressing that once the geometric height is measured, you only need to know the variation of gravity in the vertical at that latitude to generate the geopotential height. This will have to be rectified.

The timing of data samples in terms of time since launch was checked using the WVIEW software to match structures in temperature and relative humidity in the lower troposphere. Timing discrepancies in the data submitted were smaller than in Mauritius and only Jinyang required an adjustment of at least -5 s in all data. Otherwise, adjustments greater than 3 s were rare. The adjustment procedure should synchronise the data to an uncertainty of 1 s.

The early results comparing systems together were reviewed towards the end of the first week by all the participants. The team leaders agreed that intercomparison procedures were satisfactory.

6.3 Principles of data editing

Data from the database were edited by the WMO Radiosonde expert before the statistics were processed. Editing is the process of hiding measurements in the database, where the origin of the error is understood and not relevant to the aims of the intercomparison. Hiding means that the poor data are not destroyed but can be recovered at will by the data processing staff. This was performed manually, aided by the histogram function in the statistical processing as described below. Lists of discarded data can readily be generated, if required, but sometimes the problems are produced in the conversion from the flight data into that inserted into the database. Thus, if for one radiosonde type there is one 1 s temperature sample with a difference of 10 K and all the other 6000 differences are within 0.3 K, the 10 K difference will be hidden as it clearly does not represent the typical performance from the radiosonde required in the intercomparison.

For most radiosonde types, data reception was very good and there was no need to eliminate outliers in many flights. For all data types, the RSKOMP software has a histogram display function, so the distribution of the individual errors was checked to identify where the large anomalies had occurred. For, instance if the data from one flight were quite different to all the other measurements of that radiosonde type, then this flight would be eliminated. On Flight 55, the radiosondes were damaged by an electrical discharge from a cloud associated with a nearby thunderstorm, three continued to observe after the discharge event but none of these data have been used in comparison statistics.

Thus, the reader can assume that in the following result plots standard deviations and random error estimates are computed for difference distributions with no significant outliers. If the standard deviations are higher than acceptable for operational or GRUAN use, these have been checked several times to assure that the standard deviations are a true representation of the performance observed, and could not be

significantly reduced by eliminating one or two spurious flights out the group processing.

Standard deviations are computed by two different methods in RSKOMP software. In the first, all the difference samples within the chosen band (whether delineated by height or pressure) for all the relevant flights (e.g. all night or all day flights) are used to calculate the standard deviation. This type of standard deviation computation is used for all the comparisons apart from wind measurements.

In the second method, an average difference for the height band chosen is computed for each individual flight in the category, and then the standard deviation of these differences is computed, this is termed flight-by-flight standard deviation in RSKOMP output, and in the following sections is only widely used in the comparisons of wind measurements. The two values will be the same if the standard deviation is primarily caused by difference in sensor performance flight to flight. If the random errors in the individual comparison samples within a given test flight are larger than those found in flight-to-flight, then the flight-by-flight standard deviations will be smaller than the basic standard deviation.

In most of the results processed here, the two methods of computing the standard deviation of the differences give very similar results, i.e. the differences in sensor performance are primarily flight-by-flight. However, with GPS winds, flight-by-flight standard deviations are generally much smaller. Thus, random differences in the detailed structure within a test flight were larger than the averaged differences flight to flight, see chapter 11.

6.4 Statistical processing, group working references, linking radiosondes, working reference systems, references used for results

The flight schedule divided the Quality Radiosonde Systems into two main groups LMS, Modem, InterMet, and Jinyang, and Changfeng, Huayun, Graw and Meisei, referred to respectively as the LMIJ or CHGM group in the rest of the document.

Statistical processing was based on the WSTAT program supplied by S. Kurnosenko. This software has a wide range of options for data processing, so that vertical resolution of the statistics can be selected as required by the operator. Within each group, one of the radiosonde types had to be chosen as the group working reference, for use in processing the comparison data with the WSTAT software. The group working reference had to function reliably, i.e. have data on nearly all group comparison flights and to have relatively small random errors and systematic bias. The group working reference was not the same for all the meteorological variables, and thus will be specified near the beginning of the relevant chapter later.

Some radiosonde types flew on approximately half of the LMIJ flights and half the CHGM flights. This can be seen on examples of the number of flights processed for the two groups in Figure 6.4.1 from the basic WSTAT processing. Comparisons with these radiosondes could be used to link the performance of the two group references, where the data were of sufficient reproducibility. These radiosonde types were, Daqiao, Meteolabor, Meteolabor Snow White [relative humidity only], LMS Multithermistor [day-time temperature only] and Vaisala. These radiosondes have been designated link radiosondes for the purpose of this test.

Number of flights (common with reference)

Layer	LM	VAISAL	DAQIAC	CHANG	HUAYUI	INTERM	MODEN	GRAW	MEISEI	ML	JINYAN	ML_SW	MEIS_R	3THERM	VAIS_REF
500	22	14	8	4	4	15	15	4	6	9	15	8	3	3	3
1500	22	14	8	4	4	15	15	4	6	9	15	8	3	3	3
2500	22	14	8	4	4	15	15	4	6	9	15	8	3	3	3
3500	22	14	8	4	4	15	15	4	6	9	15	8	3	3	3
4500	22	14	8	4	4	15	15	4	6	9	15	8	3	3	3
5500	22	14	8	4	4	15	15	4	6	9	15	8	3	3	3
6500	22	14	8	4	4	15	15	4	6	9	15	8	3	3	3
7500	22	14	8	4	4	15	15	4	6	9	15	8	3	3	3
8500	22	14	8	4	4	15	15	4	6	9	15	8	3	3	3
9500	22	14	8	4	4	15	15	4	6	9	15	8	3	3	3
10500	22	14	8	4	4	15	15	4	6	9	15	8	3	3	3
11500	22	14	8	4	4	15	15	4	6	9	15	8	3	3	3
12500	22	14	8	4	4	15	15	4	6	9	15	8	3	3	3
13500	22	14	8	4	4	15	15	4	6	9	15	8	3	3	3
14500	22	14	8	4	4	15	15	4	6	9	15	8	3	3	3
15500	22	14	8	4	4	15	15	4	6	9	15	8	3	3	3
16500	21	13	8	4	4	14	14	4	6	9	14	8	3	3	3
17500	21	13	8	4	4	14	14	4	6	9	14	8	3	3	3
18500	20	12	8	4	4	13	13	4	6	9	13	7	3	3	3
19500	19	11	8	4	4	13	13	4	5	9	13	8	2	2	2
20500	19	11	8	4	4	13	13	4	5	9	13	8	2	2	2
21500	18	10	8	3	3	13	13	3	4	9	13	8	2	2	2
22500	17	9	8	2	2	13	13	2	3	9	13	8	2	2	2
23500	17	9	8	2	2	13	13	2	3	9	13	8	2	2	2
24500	17	9	8	2	2	13	12	2	3	9	13	8	2	2	2
25500	16	8	8	2	2	11	11	2	3	8	12	7	2	2	2
26500	14	6	8	2	2	10	9	2	3	8	9	7	2	2	2
27500	13	6	8	2	2	10	9	2	3	8	9	7	1	1	1
28500	12	6	7	2	2	9	8	2	3	7	8	6	1	1	1
29500	12	6	7	2	2	8	8	2	3	6	7	5	1	1	1
30500	10	5	5	2	2	5	7	2	2	5	6	5	1	1	1
31500	8	4	5	1	1	5	7	1	1	5	6	5	0	0	0
32500	8	4	4	1	1	5	7	1	0	5	6	5	0	0	0
33500	7	3	4	1	1	5	6	1	0	4	6	4	0	0	0
34500	8	4	4	1	1	4	6	1	1	5	6	4	0	0	0
35500	3	1	1	1	1	1	2	1	0	1	2	1	0	0	0

(a) LMIJ group, number of flights comparisons with group reference, LMS.

Number of flights (common with reference)

Layer	MEISEI	VAISAL	DAQIAC	CHANG	HUAYUI	LM	INTERM	MODEN	GRAW	ML	JINYAN	ML_SW	MEIS_R	3THERM	VAIS_RI	CFH
500	17	9	6	11	11	6	0	2	13	6	2	5	4	4	4	4
1500	19	9	8	13	13	6	0	2	14	8	2	7	4	4	4	4
2500	19	9	8	13	13	6	0	2	14	8	2	7	4	4	4	4
3500	19	9	8	12	12	6	0	2	15	8	2	7	4	4	4	4
4500	19	9	8	12	12	6	0	2	15	8	2	7	4	4	4	4
5500	19	9	8	12	12	6	0	2	15	8	2	7	4	4	4	4
6500	19	9	8	12	12	6	0	2	15	8	2	7	4	4	4	4
7500	19	9	8	12	13	6	0	2	15	8	2	7	4	4	4	4
8500	19	9	8	12	13	6	0	2	15	8	2	7	4	4	4	4
9500	19	9	8	12	13	6	0	2	15	8	2	7	4	4	4	4
10500	19	9	8	12	13	6	0	2	15	8	2	7	4	4	4	4
11500	19	9	8	12	13	6	0	2	15	8	2	7	4	4	4	4
12500	19	9	8	12	13	6	0	2	15	8	2	7	4	4	4	4
13500	19	9	8	12	13	6	0	2	15	8	2	7	4	4	4	4
14500	19	9	8	12	13	6	0	2	15	8	2	7	4	4	4	4
15500	19	9	8	12	13	6	0	2	15	8	2	7	4	4	4	4
16500	19	9	8	12	13	6	0	2	15	8	2	7	4	4	4	4
17500	19	9	8	12	13	6	0	2	15	8	2	7	4	4	4	4
18500	18	9	7	11	12	6	0	2	14	7	2	6	4	4	4	4
19500	17	9	7	11	12	5	0	2	14	7	2	6	3	3	3	3
20500	16	8	7	10	11	5	0	2	13	7	2	6	3	3	3	3
21500	15	7	7	9	10	4	0	2	12	7	2	6	3	3	3	3
22500	13	6	6	7	8	3	0	2	10	6	2	5	3	3	3	3
23500	13	5	6	7	8	3	0	2	10	5	2	4	3	3	3	3
24500	12	4	6	6	7	3	0	1	9	6	2	5	3	3	3	3
25500	11	4	5	5	6	3	0	1	8	5	2	4	3	3	3	3
26500	12	4	6	6	7	3	0	1	9	5	1	4	3	3	3	3
27500	12	4	6	6	6	3	0	1	9	5	1	4	3	3	3	3
28500	12	4	6	6	6	3	0	1	9	5	1	4	3	3	3	3
29500	12	4	6	6	6	3	0	1	9	5	1	4	3	3	3	3
30500	10	3	6	5	6	2	0	1	7	5	1	4	2	2	2	2
31500	9	3	6	5	6	1	0	1	7	5	1	5	1	1	1	1
32500	6	2	4	4	4	0	0	0	5	3	1	3	1	1	1	1
33500	5	1	4	4	4	0	0	0	4	3	1	3	0	0	0	0
34500	4	1	2	3	3	1	0	0	3	2	1	2	0	0	0	0
35500	4	0	2	3	3	0	0	0	3	1	0	2	0	0	0	0

(b) CHGM group, number of flights compared with group reference Meisei

Fig. 6.4.1 Examples of number of flights available to be processed in the two comparison groups using the group references for night-time temperature.

Figure 6.4.2 shows the individual values of linking the two group references for night-time temperature, some values being obtained with link radiosondes and some measured directly. The worksheet also shows the best estimate obtained for Meisei –LMS night temperature and the uncertainty associated with the best estimate [k=1] derived from the standard deviation of the average of the linking estimates from the different sources. The random errors associated with linking the group references are then indicated later in the chapters relevant to the meteorological variable under evaluation. This method assumes that the conditions in all the flights are similar so that the performance of the link radiosondes in each group was similar. In some cases, this does not hold, especially if the random errors in the measurements are much larger than best performance, e.g. in daytime temperature and some of the linking values can be seen to be unreliable and are edited out. In Fig. 6.4.2, the number of flights through cloud affects the number of flights with evaporative cooling errors, and this affects the linking so that the link referencing above 10 km has lower uncertainty than in the lower troposphere.

	Link	Link	Link	Direct	Direct			
	VAIS	ML	DAQ	qrs	sci		best estimate	
Layer	MEI-LM	MEI-LM	MEI-LM	MEI-LM	MEI-LM		Meisei -LMS	error
500	-0.06	-0.06	-0.03	0.12	0.14		-0.02	0.04
1500	-0.09	-0.1	-0.03	0.15	0.14		-0.04	0.05
2500	-0.22	-0.11	-0.01	0.15	0.11		-0.07	0.07
3500	-0.39	-0.11	0.00	0.17	0.12		-0.10	0.10
4500	-0.26	-0.11	0.01	0.19	0.15		-0.08	0.08
5500	-0.17	-0.14	0.02	0.25	0.1		-0.08	0.08
6500	-0.18	-0.09	0.02	0.3	0.14		-0.05	0.08
7500	-0.20	-0.16	0.01	0.35	0.15		-0.06	0.10
8500	-0.21	-0.19	0.01	0.38	0.13		-0.08	0.11
9500	-0.18	-0.17	0.02	0.37	0.18		-0.06	0.11
10500	-0.07	-0.02	0.04	0.26	0.21		0.00	0.07
11500	0.17	0.17	0.06	0.19	0.24		0.11	0.03
12500	0.26	0.25	0.08	0.14	0.16		0.14	0.03
13500	0.15	0.18	0.10	0.22	0.16		0.11	0.02
14500	0.08	0.13	0.12	0.33	0.21		0.09	0.04
15500	0.21	0.26	0.14	0.27	0.19		0.14	0.02
16500	0.30	0.28	0.16	0.26	0.19		0.15	0.03
17500	0.20	0.24	0.15	0.21	0.21		0.12	0.01
18500	0.02	0.1	0.16	0.29	0.13		0.05	0.04
19500	-0.02	0.06	0.15	0.33	0.1		0.04	0.06
20500	-0.03	0	0.15	0.38	0.14		0.02	0.07
21500	-0.04	0.05	0.16	0.25	0.17		0.04	0.05
22500	0.07	0.06	0.17	0.19	0.19		0.07	0.03
23500	0.09	0.08	0.19	0.17	0.13		0.07	0.02
24500	0.11	0.15	0.22	0.19	0.09		0.08	0.02
25500	0.17	0.09	0.24	0.19	0.11		0.09	0.03
26500	0.15	0.19	0.18	0.16	0.14		0.10	0.01
27500	0.13	0.25	0.22	0.16	0.17		0.11	0.02
28500	0.09	0.09	0.22	0.22	0.24		0.07	0.03
29500	0.01	-0.08	0.24	0.34	0.27		0.01	0.08
30500	-0.28	-0.28	0.30	0.46	0.15		-0.09	0.15
31500	0.08	-0.26	0.40	0.24	0.14		-0.02	0.11
32500	0.12	-0.26	0.32		0.18		-0.02	0.11

Fig. 6.4.2 Worksheet showing the values obtained for the difference between the group references, Meisei-LMS for night-time temperature, using link radiosondes and direct measurements, and the resultant best estimate and associated uncertainty.

Once the link between the two group references is established then this can be used to generate a value of the systematic bias against one of the two group references, and this is usually LMS from the LMIJ group. Fig. 6.4.3 shows how information from the two groups is combined together for a linking radiosonde, in this case Daqiao, then resulting in a satisfactory total number of flights used.

		Number			number	link		Number
Layer	DAQ-LMS			DAQ-MEI		MEI-LMS	DAQ-LMS	
500	-0.06	8		0.02	6	-0.02	-0.04	14
1500	-0.08	8		0.04	8	-0.04	-0.04	16
2500	-0.09	8		0.01	8	-0.07	-0.07	16
3500	-0.08	8		0.01	8	-0.10	-0.09	16
4500	-0.06	8		0.02	8	-0.08	-0.06	16
5500	-0.05	8		0.04	8	-0.08	-0.04	16
6500	-0.02	8		0.07	8	-0.05	0.00	16
7500	-0.01	8		0.13	8	-0.06	0.03	16
8500	0	8		0.19	8	-0.08	0.06	16
9500	0.03	8		0.19	8	-0.06	0.08	16
10500	0.05	8		0.08	8	0.00	0.07	16
11500	0.08	8		-0.08	8	0.11	0.06	16
12500	0.07	8		-0.17	8	0.14	0.02	16
13500	0.08	8		-0.13	8	0.11	0.03	16
14500	0.08	8		-0.1	8	0.09	0.03	16
15500	0.01	8		-0.31	8	0.14	-0.08	16
16500	-0.07	8		-0.5	8	0.15	-0.21	16
17500	-0.01	8		-0.33	8	0.12	-0.11	16
18500	0.04	8		-0.12	7	0.05	-0.01	15
19500	0.02	8		-0.08	7	0.04	-0.01	15
20500	-0.02	8		-0.08	7	0.02	-0.04	15
21500	0.02	8		-0.13	7	0.04	-0.03	15
22500	0	8		-0.2	6	0.07	-0.06	14
23500	-0.03	8		-0.28	6	0.07	-0.11	14
24500	-0.04	8		-0.3	6	0.08	-0.12	14
25500	-0.06	8		-0.34	5	0.09	-0.13	13
26500	-0.06	8		-0.36	6	0.10	-0.15	14
27500	-0.07	8		-0.34	6	0.11	-0.14	14
28500	-0.15	7		-0.31	6	0.07	-0.19	13
29500	-0.29	7		-0.28	6	0.01	-0.28	13
30500	-0.43	5		-0.1	6	-0.09	-0.30	11
31500	-0.45	5		-0.12	6	-0.02	-0.28	11
32500	-0.31	4		-0.04	4	-0.02	-0.19	8

Figure 6.4.3 Example of how the final values relative to LMS are calculated for Daqiao, which participated in both groups of flights.

Reference back to Fig. 6.4.1 shows that Daqiao measurements are available to at least 34.5 km in acceptable numbers, but there is no reliable method of linking them together, so in the final analysis results are not presented above 32.5 km.

In the final plots of systematic bias, the LMIJ group values are the direct values from WSTAT processing, the CHGM values use the Meisei-LMS link with the associated uncertainty shown, although the bias between the group members is that from direct WSTAT processing, and the link radiosondes are partially direct and partially linked as shown in Fig. 6.4.3. However, the zero reference in the final analysis is not a single radiosonde type but a group. For night-time temperature the group was Changfeng, LMS, Modem and Vaisala. Fig. 6.4.4. shows the final results and the average value which has been used to adjust from the differences relative to LMS which were computed through the processes above.

Average ofLMS,Vaisala,ChangFeng,Modem	Height	LMS	meisei	Vaisala	MODEM	meteola	Graw	INTERM	Daqiao	Chang fe	Huayun	Jinyang
-0.03	0.5	0.03	0.01	0.01	-0.22	0.15	0.05	-0.26	0.00	0.14	0.12	-0.06
-0.02	1.5	0.02	-0.02	0.01	-0.21	0.15	0.06	-0.20	-0.02	0.16	0.13	-0.07
-0.01	2.5	0.01	-0.05	0.05	-0.19	0.15	0.05	-0.16	-0.06	0.11	0.10	-0.07
0.00	3.5	0.00	-0.10	0.10	-0.17	0.14	0.09	-0.12	-0.08	0.06	0.07	-0.08
0.00	4.5	0.00	-0.08	0.06	-0.14	0.15	0.08	-0.06	-0.06	0.08	0.07	-0.07
0.01	5.5	-0.01	-0.09	0.04	-0.11	0.17	0.01	-0.03	-0.05	0.09	-0.03	-0.08
0.03	6.5	-0.03	-0.08	0.02	-0.08	0.20	0.03	-0.01	-0.03	0.12	0.03	-0.07
0.03	7.5	-0.03	-0.09	0.02	-0.05	0.19	0.02	0.03	0.00	0.09	0.02	-0.06
0.02	8.5	-0.02	-0.09	0.04	-0.08	0.21	0.02	0.09	0.04	0.08	0.02	-0.04
0.03	9.5	-0.03	-0.09	0.03	-0.08	0.18	0.03	0.11	0.05	0.10	0.04	-0.03
0.03	10.5	-0.03	-0.03	0.03	-0.09	0.13	0.02	0.14	0.03	0.12	0.07	-0.06
0.03	11.5	-0.03	0.08	0.01	-0.07	0.07	0.00	0.17	0.02	0.14	0.06	-0.07
0.04	12.5	-0.04	0.10	0.00	-0.05	0.03	-0.03	0.19	-0.02	0.13	0.04	-0.02
0.07	13.5	-0.07	0.04	0.02	0.00	0.00	0.01	0.19	-0.04	0.12	0.06	0.00
0.11	14.5	-0.11	-0.02	0.02	0.07	-0.01	0.06	0.16	-0.07	0.13	0.06	0.06
0.13	15.5	-0.13	0.01	-0.01	0.11	-0.05	0.13	0.17	-0.21	0.16	0.00	0.07
0.14	16.5	-0.14	0.01	-0.03	0.08	-0.04	0.32	0.24	-0.35	0.24	-0.11	0.00
0.12	17.5	-0.12	0.00	0.00	0.03	-0.04	0.31	0.24	-0.23	0.21	-0.09	0.01
0.12	18.5	-0.12	-0.07	0.05	0.01	-0.03	0.26	0.19	-0.13	0.17	-0.08	0.04
0.11	19.5	-0.11	-0.07	0.06	-0.03	-0.11	0.23	0.20	-0.12	0.19	0.02	0.02
0.09	20.5	-0.09	-0.07	0.07	-0.05	-0.11	0.22	0.22	-0.13	0.16	0.05	-0.02
0.10	21.5	-0.10	-0.06	0.09	-0.05	-0.09	0.20	0.18	-0.13	0.16	0.09	-0.03
0.09	22.5	-0.09	-0.02	0.08	-0.08	-0.10	0.20	0.20	-0.15	0.19	0.03	-0.05
0.08	23.5	-0.08	-0.01	0.11	-0.09	-0.11	0.13	0.22	-0.19	0.15	0.02	-0.08
0.08	24.5	-0.08	0.00	0.13	-0.10	-0.11	0.11	0.23	-0.20	0.14	-0.03	-0.12
0.09	25.5	-0.09	0.00	0.14	-0.10	-0.12	0.07	0.26	-0.22	0.14	0.04	-0.14
0.07	26.5	-0.07	0.03	0.09	-0.11	-0.07	0.10	0.30	-0.22	0.16	0.06	-0.11
0.09	27.5	-0.09	0.02	0.12	-0.12	-0.06	0.16	0.28	-0.23	0.18	0.13	-0.18
0.09	28.5	-0.09	-0.02	0.12	-0.14	-0.13	0.20	0.29	-0.28	0.20	0.06	-0.22
0.09	29.5	-0.09	-0.09	0.14	-0.16	-0.12	0.17	0.35	-0.38	0.21	0.02	-0.17
0.12	30.5	-0.12	-0.21	0.23	-0.10	-0.04	0.03	0.46	-0.42	0.12	0.12	-0.17
0.15	31.5	-0.15	-0.17	0.21	-0.18	-0.04	0.18	0.36	-0.43	0.26	0.08	-0.25
0.12	32.5	-0.12	-0.14	0.16	-0.32	-0.02	0.39	0.38	-0.30	0.40	0.03	-0.33

Figure 6.4.4 Adjustment from biases relative to LMS to the final reference for the systematic bias plot using a group reference, with the average values shown on the left

In Mauritius, Snow white and Multithermistor measurements were used as working references for relative humidity, and daytime temperature respectively, but both had reliability problems, requiring a lot of extra work by the WMO Team.

In this test, the LMS Multithermistor submitted its data, and apart from removing a few spurious spikes in the temperature, little more effort was required by the WMO Project Team. Thus, this system functioned much more reliably in terms of operational reliability than in Mauritius. Now that it is working in a reproducible fashion, the results obtained probably need checking to optimise the accuracy and reduce the spread of daytime temperature measurements at around 10 hPa.

Snow White reliability was also much improved since the Mauritius test. Identifiable failure modes that still remain and needed to be flagged out were:

• Contamination in the day-time Snow White design, with the sensor mounted in a duct. The contamination probably builds up on some of the cold surfaces near the sensor where ventilation may be poor. This contamination resulted in dewpoints that were much too high compared to the values established by scientific experiments in the tropics, e.g. see CFH data in this test. In the night-time Snow White design, the chilled mirror is exposed directly in the atmosphere and this contamination problem is not so common.

• Loss of the ice film on the chilled mirror. In Yangjiang, this seemed to happen in a few flights (3) in humid layers just under the tropopause. When the condensation on the mirror disappears, the Peltier cooler drives the mirror temperature down to an unreasonably low value. Therefore, Snow White data with unreasonably low dew/frost points near the tropopause has been flagged out in Yangjiang.

Individual radiosonde types were not used as references for the results (apart from in the wind processing), but an average of the performance of several radiosonde types. The references are detailed in the relevant chapters later in the report.

For temperature, the references used were an average of four systems that had reliable sensors with measurements in the day found to be of good quality, and relatively small day-night difference. Please do not use the choice of a system in these references as the guide to choosing a system, as this should be based on the overall performance evaluation presented later.

Similarly, the references for relative humidity comparisons were systems that have been shown to have small day-night differences in the lower and middle troposphere.

With geopotential height and pressure, only the systems with poor reproducibility were not used in the reference for the results.

6.5 Estimating random errors using the standard deviations of the differences between two radiosonde types

The standard deviations of the differences between the other radiosonde types and Group references were computed using WSTAT. The standard deviations have been used in sections 7 to 10 to estimate the random error in the radiosonde measurements as a function of height. For instance, the estimates of random error in Temperature measurements in Fig. 7.2 were derived from the standard deviations of the differences between measurements by the different systems on the assumption that the errors were not correlated between the different systems.

Then,

$$[\text{Standard deviation (type1-Group ref.)}]^{2} = \varepsilon_1^{2} + \varepsilon_{GREF}^{2}$$

where ε_1 and ε_{GREF} are the random errors for the measurements of type 1 and the group reference respectively.

The choice of the value of ε_{GREF} for the computation is largely arbitrary, with the values normally chosen so the values of ε_1 and ε_{GREF} were similar for the radiosonde type that agreed most closely with the group reference. Thus, in the plots of estimated random error, such as Fig. 7.2, the radiosonde types with largest errors are usually clearly identified, but it is not possible to discriminate between the measurement accuracy of the best radiosonde measurements.

The random error values of the better radiosonde measurements indicate a typical error value for these radiosondes, but the plots do not identify which was the best radiosonde measurement during the test. Conditions varied within the comparison flights, and the situations which caused the larger errors were not evenly distributed between the different categories and groups, e.g. evaporative cooling on emerging from cloud.

7. Comparison of simultaneous temperature measurements

7.1 QRS test results

7.1.1 Introduction

All the temperature sensors used in the Yangjiang test were very much smaller than those in operational use before 2000. Pictures of the temperature sensors and the position of the sensor relative to the radiosonde body can be found in the system descriptions in Chapter 4.

Of these sensors, only those used in the LMS radiosonde, the LMS Multithermistor and the Meteolabor are the same as those used in the previous WMO Radiosonde Comparison in Mauritius in 2005. The thickness of the Vaisala sensor was increased slightly in 2007-8, with the support frame reduced slightly in size.

The five thermistors in the Sippican multi-thermistor radiosonde were flown with thermistors held in the plane of the support framework, as decided by the manufacturer. This was not the same as in the Mauritius test where the Met Office had decided that the thermistors should be located above the level of the supporting wires and frame (see Fig. 9.1, Nash et al., 2005). Subsequent testing by LMS suggests that this may not have been critical for the results.

7.1.2 Results of statistical processing

7.1.2.1 Processing details

Temperature comparison statistics were computed for simultaneous samples, banded into layers 1 km thick from the surface to 33 km using WSTAT software. There were measurements at higher levels on some flights but there is insufficient data at higher levels to enable satisfactory linking between the two groups of quality radiosonde systems.

Group working references had to be on most flights in a group, and have good measurement quality, see Table 7.1.1. In the CHGM group, Meisei was the preferred reference for systematic bias estimates, but Graw also had to be used to crosscheck the uncertainty estimates in the day. The uncertainty plots should not be used to discriminate between the radiosondes of good performance, but can be used to identify those problem with large uncertainties. LMS was used as the group working reference in the LMIJ group.

The linking radiosondes are just those, which flew in enough numbers in each QRS group to contribute to the link. The most useful are those with high measurement quality. The higher uncertainty in linking Meisei to LMS between 0 and 8 km was the results of errors introduced by evaporative cooling of wet sensors on some flights emerging from cloud. At night, the references for the systematic difference plots in Fig. 7.1.1 were four independent sensor types with good time constants of response at all heights and the same systems were used as the reference group for Fig. 7.1.3. Time series of geopotential height measurements at 100 hPa, (30-100) hPa, and 10-30 hPa will be used to check day-night consistency, see later section.

Height range, [km]	Group working references	Linking radiosondes	Typical uncertainty in LMS-Meisei link, [K]	Reference for systematic difference plot	Category
0 to 8	LMS, Meisei	Vaisala, Meteolabor, Daqiao	<0.1	LMS, Vaisala, Modem, Changfeng,	night
0 to 8	LMS, Meisei, [Graw for uncertainty estimates in CHGM group]	Vaisala, Meteolabor, Multithermistor, Daqiao	<0.1	LMS, Vaisala, Changfeng, Modem	day
8 to 16	LMS, Meisei	Vaisala, Meteolabor, Daqiao	<0.05	LMS, Vaisala, Modem, Changfeng,	night
8 to 16	LMS, Meisei, [Graw for uncertainty estimates in CHGM group]	Vaisala, Meteolabor, Multithermistor, Daqiao	<0.05	LMS, Vaisala, Changfeng, Modem	day
16 to 32	LMS, Meisei	Vaisala, Meteolabor, Daqiao	<0.05, 0.1 above 29 km	LMS, Vaisala, Modem, Changfeng,	night
16 to 32	LMS, Meisei, [Graw for uncertainty estimates in CHGM group]	Vaisala, Meteolabor, Multithermistor,	<0.05	LMS, Vaisala, Changfeng, Modem [adjusted with results of day –night analysis in 7.1.6]	day

Table 7.1.1: References used in the processing of the statistics and the resultant error in linking the results from the LMIJ and CHGM groups.

Once the two sets of WSTAT statistics were merged using the difference between LMS and Meisei, the final temperature differences were presented against an arbitrary reference, see Table 7.1.1. The random errors were deduced from the standard deviations between the different radiosonde types in the WSTAT processing. Here, the effects of the wet bulb errors can lead to spurious interpretations if not taken into account, especially if they were not evenly distributed between the test flights of both groups. If most of the radiosonde types in one group suffer similar evaporative cooling errors, the radiosonde type, which does not suffer the error, will show larger standard deviations in differences with the others, than when systems with similar errors are compared together. Therefore, where this was happening, the initial results have been overturned and values adjusted to give a reasonable estimate of random error when the systems are working with only few evaporative cooling events in a sample. All the temperature sensors in Yangjiang were different apart from LMS and LMS Multithermistor, so it is unlikely that correlations between the sensors performance give rise to over optimistic estimates of random error.

7.1.2.2 Night time results

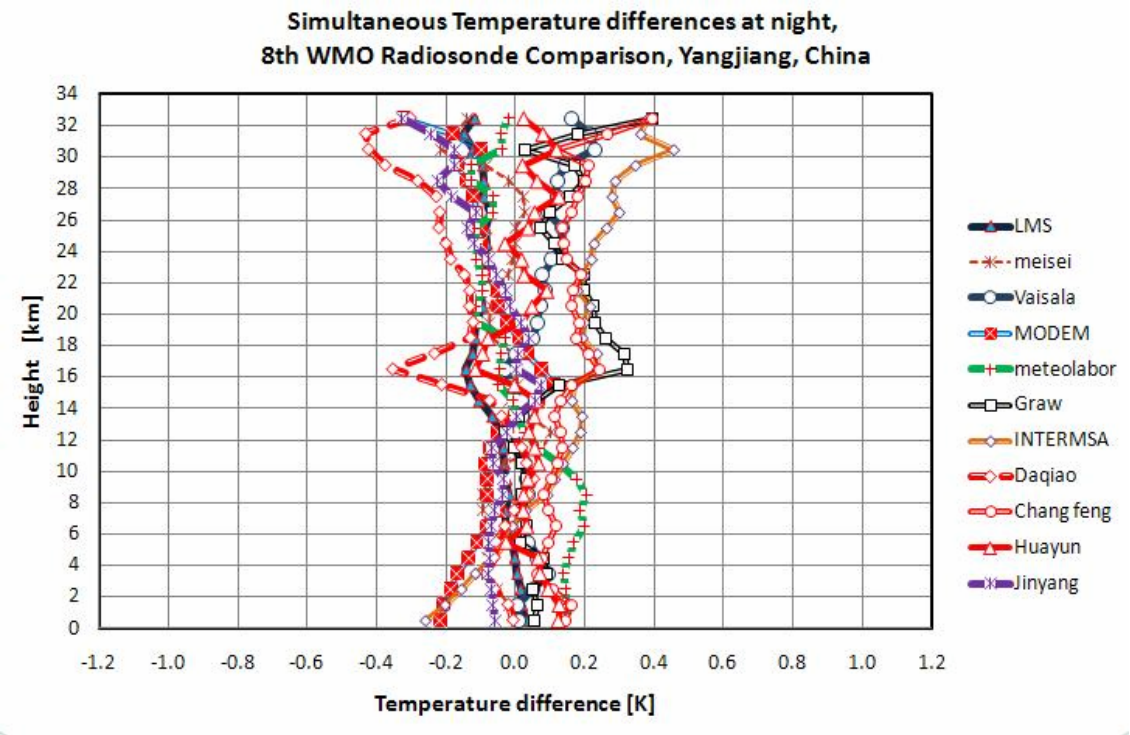

Fig. 7.1.1 Systematic bias between simultaneous temperatures (K) at night, positive bias means the radiosonde reported higher values than the reference

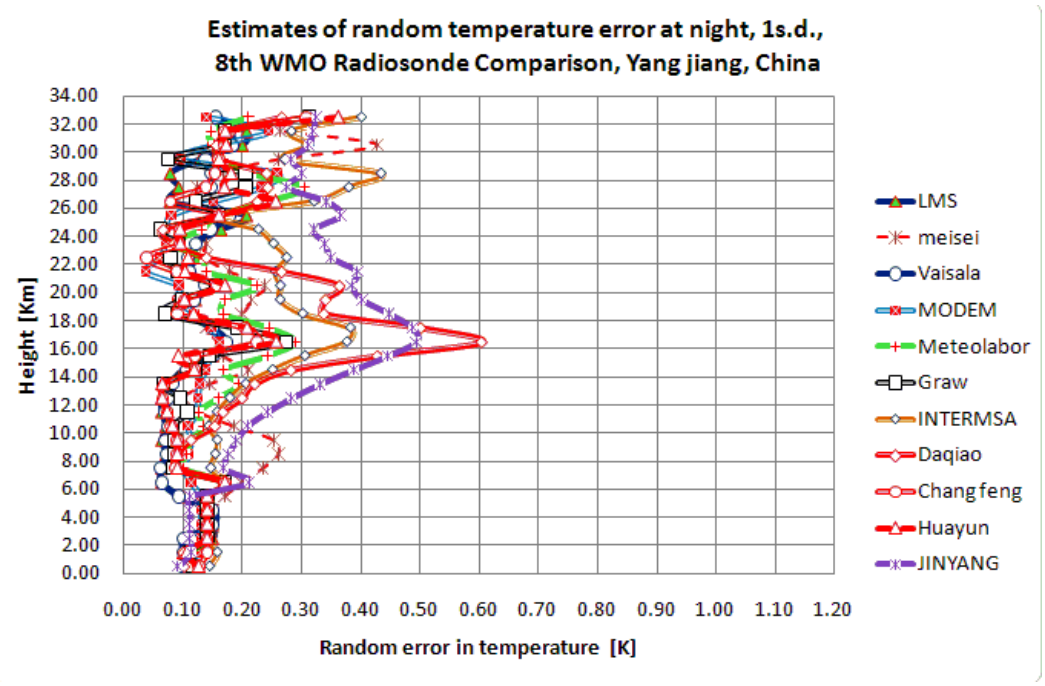

Fig. 7.1.2 Estimated random error in temperature measurements at night.

The estimates of the systematic bias and random errors in the temperature measurements at night are shown in Figs. 7.1.1 and 7.1.2 respectively. The results are for at least 15 successful comparison flights of each type to 26 km, 8 to 29km and 5 to 33 km.

At night, in the previous comparison in Mauritius (Nash et al., 2005), LMS was about 0.1 K warmer than Meteolabor at 10 hPa, and Vaisala was about 0.3 K warmer than LMS at 10 hPa. The results for these three radiosonde types in Yangjiang are almost identical, i.e. Vaisala warmer than LMS by 0.4 K and Meteolabor warmer than LMS by 0.1 K. It is encouraging that in the tropics, the differences seem to have remained constant within the known uncertainties of the test results. Modem is also now very close to Meteolabor and LMS. Previous tests in Europe at night, included in the Mauritius report showed Vaisala much closer to LMS than in Mauritius. A recent comparison in 2010, in the UK of 30 Vaisala against Modem night flights also shows Modem at most 0.1 K colder than Vaisala at 10 hPa, whereas in Yangjiang Vaisala was 0.3 K warmer than Modem at 10 hPa. In an extensive test at Camborne in the UK in 2009 (Smees et al., 2010), Vaisala was higher than LMS by about 0.1 K at 10 hPa and 0.2 K higher than Modem. Thus, the two tropical test show Vaisala 0.35 K higher than LMS, whereas the two UK tests of similar radiosondes show Vaisala higher than LMS by only 0.1 K.

Three radiosonde types agree closely with Vaisala in the stratosphere, InterMet, Graw and Changfeng. Graw biases show a positive shift in temperature of about 0.3K relative to all the other systems on passing the tropopause and Changfeng measurements show a similar positive shift of about half this amplitude between 8 and 18 km. These shifts also occurs in daytime measurements, see Fig. 7.1.3. Even if some InterMet flights with positive biases much higher than 0.5 K relative to the other radiosondes in the stratosphere were removed InterMet was still about 0.2 K higher than the zero value. All the other radiosondes were relatively close to LMS.

Huayun measurements in the upper stratosphere have had a software correction of about 0.4 K applied, and if this were removed, the Huayun measurements would be slightly lower than LMS and Meteolabor. The white paint on the Daqiao temperature is a close approximation to black in the infrared. The effects of the radiation errors caused by this are studied in more detail in a later section of this chapter. Upper cloud has a large influence on the infrared environment above the cloud so when upper cloud is present the Daqiao measurements can shift rapidly to colder values. Thus, the large negative bias in Daqiao just above the tropopause and the colder measurements at upper levels are the result of interaction with upper cloud and infrared cooling and not a fault in the calibration of the temperature sensors. We would request manufacturers to pay attention to the CIMO Guide (WMO-No.8) where it states quite plainly, that white paint should not be used if systems are to have high reproducibility of temperature measurements.

Two radiosonde types, InterMet and Modem show a positive bias in the lower troposphere. Modem was not applying a ground check. When a ground check was applied, their values have been shown to agree more closely with Vaisala and LMS measurements in recent UK tests. Ground checks performed carefully do improve reproducibility of these measurements in the lower troposphere.

The tendency for many of the radiosonde types to have larger random errors near the tropopause, see Fig. 7.1.2, is probably linked to the effects of icing on the sensors when they leave dense upper cloud. This is most pronounced for Daqiao, as will be seen later. Temperature and relative humidity sensors were contaminated with ice when emerging through the tropopause on several occasions.

The random errors in the measurements are such that all systems apart from Daqiao and Jinyang could be expected to provide highest quality temperature measurements, in tropical conditions at night and all systems could provide an acceptable standard of routine operational measurement.

From these results and those in mid-latitudes, it is unwise to assume that any of the current radiosonde temperature measurements can be reproduced consistently to within 0.1 K whether in the tropics or high latitudes, as might be desirable for climate science. The origins of the uncertainty are probably not in the calibration of the sensors, but in the stability of the radiosonde sensor under different conditions during flight or in the stability of radiosonde signal electronics and processing during flight.

7.1.2.3 Daytime results

The processing of the QRS groups and the link between the two group references, LMS and Meisei were performed with same procedures used at night, see Table 7.1.1.

The systematic biases and uncertainty estimates for daytime temperature measurements are presented in Fig. 7.1.3 and 7.1.4 respectively. These data are produced from a data set with at least 12 successful comparison flights for each radiosonde type to 26 km, 12 to 32km and 10 to 33 km. The larger number of flights achieving high burst heights in the day explains why the linking between the groups is better defined at upper levels in the day, rather than at night, see Table 7.1.1.

The estimated uncertainties in Fig. 7.1.2 and 7.1.4 were not derived by averaging the temperatures from each flight over 1 km and then looking at the standard deviations of the differences between the different types, as was used in Mauritius, but were standard deviations derived using all the temperature differences for each second without applying any averaging per flight. When most of the standard deviation comes from flight to flight differences, this makes little difference to the values, but if there is a lot of second by second noise the values will be larger. Usually there is not a lot of short-term noise, see the temperature difference plots from individual flights later in this chapter.

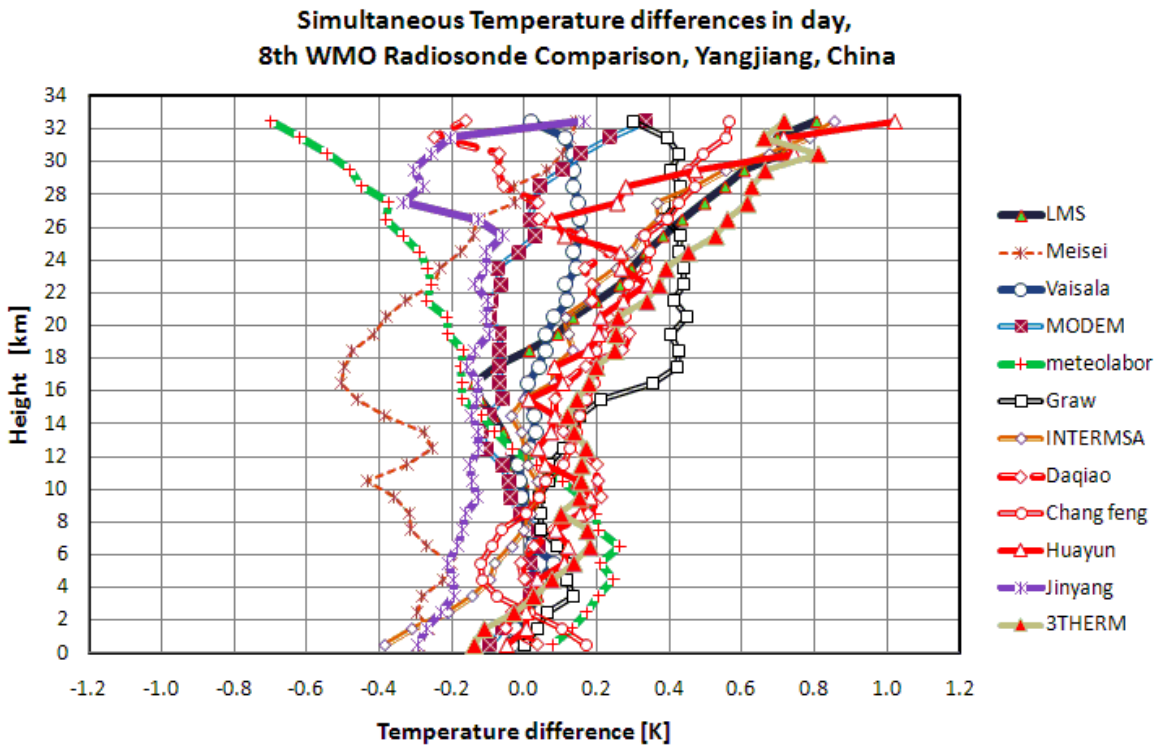

Fig. 7.1.3 Systematic bias between simultaneous temperatures (K) in the day, with reference adjusted above 16 km to take into account estimate of day-night differences in geopotential height analysis in section 7.1.6.

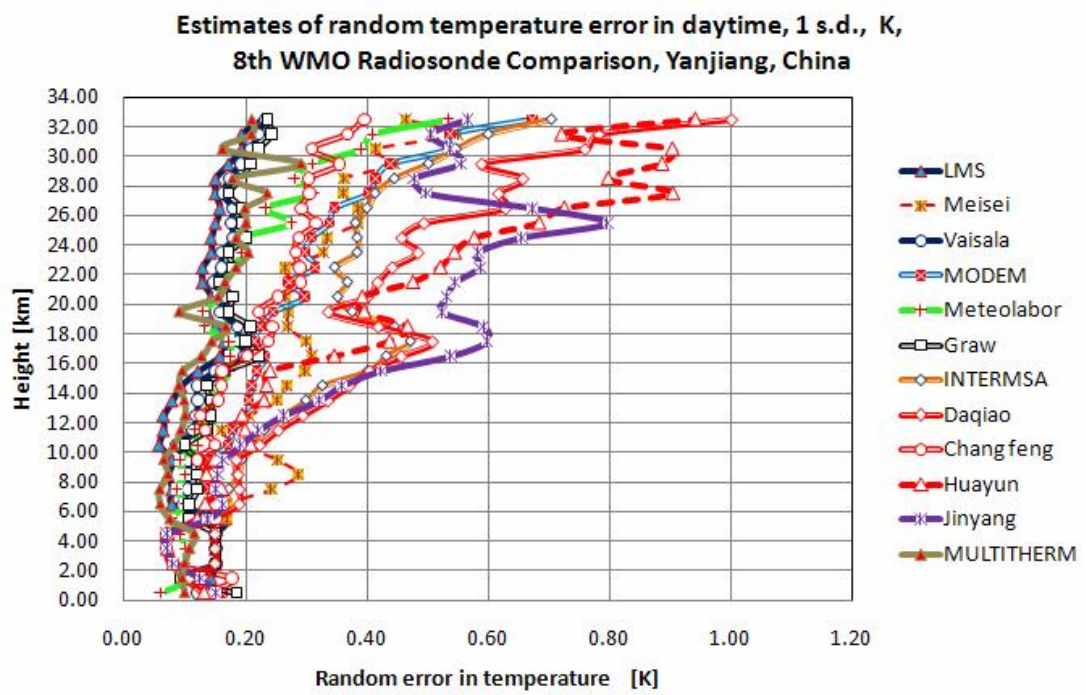

Fig. 7.1.4 Estimated random errors in temperature measurements in the day

All day-time temperature measurements have had a correction applied for solar heating and usually some type of filtering to remove spurious heating pulses shed from the radiosonde body or the sensor supports. These are illustrated in a later section. The Multithermistor system is intended to move to a more active correction scheme for heating errors, so it does not make an assumption about typical solar backscattered albedo. The assumption that heating errors are always the same, even if solar albedo conditions are quite different from normal, e.g. low over the sea with little cloud, or high over plentiful upper cloud is not valid. The heating corrections applied at 10 hPa by the other systems are shown in Table 7.1.2.

Radiosonde Type	Typical correction at 10 hPa K
LMS	0.95
Modem	1.5
InterMet	1.1
Jinyang	2.1
Changfeng	0.6
Huayun	2.3
Graw	1.0
Meisei	1.8
Daqiao	0.9
Vaisala	0.7
Meteolabor	1.8
Multithermistor	Active correction

Table 7.1.2: Software radiation corrections applied at 10 hPa daytime.

In Mauritius, the systematic biases at 10 hPa relative to Vaisala were Meteolabor -0.3 K, LMS+0.4 K, Multithermistor +0.2 K. In Fig. 7.1.3 LMS has a similar bias relative to Vaisala of +0.5 K, Meteolabor is more negative -0.7 K and LMS Multithermistor is much more positive +0.6 K. In tropical conditions, it is possible that the LMS temperature may be under corrected. As Vaisala is warmer than LMS at night and colder in the day, it seems possible that there may be some instability in one or both radiosondes day to night to lead to these results. As well as the solar heating correction, many of the manufacturers apply filtering to daytime measurements to take out positive heating pulses [from sensor supports or radiosonde body]. This filtering creates additional uncertainty in the reported values in the daytime, and introduced an uncertainty into the systematic bias of about 0.2 K (possible reference to Annex showing examples), depending on the precise nature of the fluctuations observed. As far as the author is aware, the Vaisala filtering algorithm was not changed between Mauritius and Yangjiang, although the change in the temperature support structure did lead to smaller amplitude pulses when checked in the UK. When the support structure of the Vaisala temperature and relative humidity sensor was changed, it changed the temperatures at 10 hPa by about +0.2 K. (J. Nash, personal communication of results from Bureau of Meteorology and UK Met Office, independent tests for 15 daytime comparisons each.) With the new design 0.2 K warmer than the old design, probably because the diameter of the new temperature sensor was larger. The filtering algorithm had the effects described above. The geopotential height time series analyses presented later, suggest that between 100 and 30 hPa, LMS daytime temperatures were under corrected.

The increased positive bias in Graw measurements relative to the other systems on passing through the tropopause can be seen, as was seen at night.

Daqiao measurements in the day are also influenced by infrared errors and the negative bias in Daqiao measurements increases with height in the stratosphere.

Throughout the test in Yangjiang, Meisei's radiation correction was queried. This was because in daytime the temperatures were clearly lower than all the other radiosondes in the troposphere. Some problems were identified in differences in filtering between day and night temperatures, but the low bias in the day has remained.

Jinyang implemented a radiation correction scheme at Yangjiang.

In Fig. 7.1.4 the error estimates show that the systems which give most reproducible measurements above 100 hPa were LMS Multithermistor, Vaisala, LMS, Graw, Meteolabor, Changfeng and Modem, and these would be the systems best suitable for the highest quality measurements in GCOS observing sites to the highest levels.

Three systems have very large random errors in the day, which were not seen at night. These were Huayun, Jinyang and Daqiao throughout most of the stratosphere. Modem, InterMet and Meteolabor, only showed large random errors at pressures lower than 15 hPa.

It is suggested the following is checked to rectify this problem:

- Is the radiosonde sensor mounted high enough above the radiosonde body that as it swings around, air heated by flowing over the top of the radiosonde cannot flow over the sensor. Radiosondes swing around a lot in flight, and this needs to be taken into account. Look at the mountings of the systems that do not have big problems in day-time measurements.
- Does the sensor have unobstructed exposure to the air, i.e. there are not unnecessary guards or supports above the sensor. If a support above the sensor is essential, orient the sensor so that heat contamination /conduction from the supports is minimised. If the temperature sensor on the Huayun sensor was facing upwards rather than sideways, with the support structure to each side of the sensor, the random errors in the daytime would be reduced.
- Is the temperature sensor mounting fixed in the same position throughout the flight, so for instance, it cannot move relative to the radiosonde body if it gets iced up for part of the flight.
- Has the sensor assembly been designed so that when the radiosonde rotates it presents similar cross-section of illumination to the sun, to minimise short-term fluctuations.
- Have the radiation characteristics of the sensor changed with time because of changes in manufacturing methods or coatings?

Obtaining high consistency between the radiosonde temperatures in the day at pressures lower than 50 hPa is more difficult than at night. The consistency that can realistically be expected from site to site in daytime measurements at pressures lower than 50 hPa is clearly lower than at night, but the systems with the smallest daytime random errors show what can be achieved.

7.1.3 Measuring temperature fine structure at night

7.1.3.1 Checking the consistency of high temporal resolution measurements

At night infrared cooling has little effect on differences between the small temperature sensors of most modern radiosondes, because of the aluminised sensor coatings. Even at pressures as low as 20 hPa, in Fig. 7.1.5 (a) it is difficult to discern any differences in the response of Vaisala, Graw, Meisei, LMS Multithermistor and the Meisei reference (MTR), whilst the MTR should have the fastest time constant of response. Thus, at night when data are compared second by second, small fluctuations in temperature difference of peak to peak amplitude less than 0.2 K are found if the radiosondes are functioning correctly.

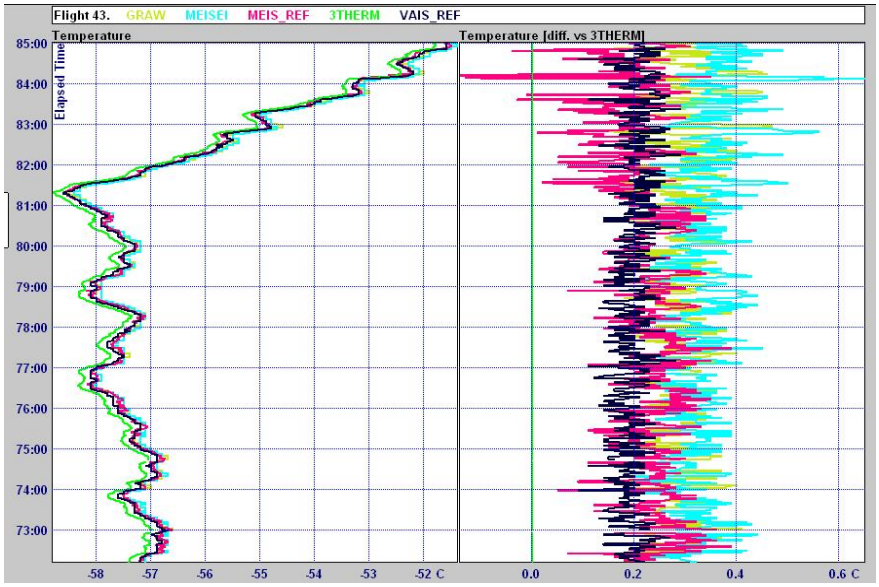

Fig. 7.1.5 (a) Sample of basic data samples and temperature differences between night time temperature measurements from a science systems flight with the LMS Multithermistor measurement (designated 3 Therm) for the pressure range of about 35 hPa (minute 73) to a pressure of about 20 hPa (minute 85). It is expected that the MEIS_REF (MTR) has the fastest time constant of response. Positive bias means values are higher than the Multithermistor reference.

By the end of the same flight, Fig. 7.1.5 (b), the Meisei reference (MTR) slightly drifts negative relative to the LMS Multithermistor and Vaisala. All the temperature difference measurements after minute 105 show larger short term fluctuations with time than in Fig. 7.1.5 (a) some of this resulting from variation in the Multithermistor temperature measurements, not observed by the other systems.

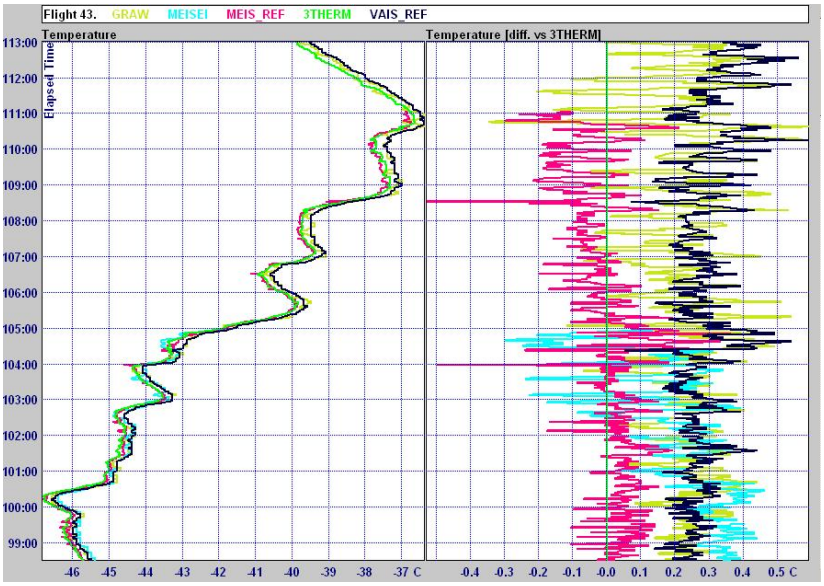

Fig. 7.1.5 (b) Sample of basic data samples and temperature differences between night time temperature measurements from a science systems flight with the LMS Multithermistor measurement (designated 3 Therm) for the pressure range of about 10.6 hPa (minute 99) to a pressure of about 6.5 hPa (minute 113). It is expected that MEIS_REF (MTR) has the fastest time constant of response. Positive bias means values are higher than the Multithermistor reference.

7.1.3.2 Examples of fine structure data from Quality Radiosonde Comparison flights, showing differences in time constants of response at upper levels

Temperature comparison data at night are shown for an LMIJ quality radiosonde test flight in the lower stratosphere see Fig. 7.1.6 (a). Here, the Meteolabor temperature sensor, which has a very fast time constant of response, is used as the working reference for the temperature differences. The peak-to-peak amplitude of the second by second comparisons with the QRS radiosondes can be as large as 0.4 K.

In Figure 7.1.6 (a), there are no significant timing differences between the different radiosonde measurements. Thus, when looking at the end of this flight in Fig. 7.1.6 (b), the separation between the different temperature sensors now depends on whether the temperature is falling or increasing with time. A complicating factor is that, these differences were observed at a time when rates of ascent were changing rapidly with height because of a large amplitude gravity wave (see Figure 7.1.6 (c)) which shows the changes in the balloon rate of ascent and the fluctuation in the N-S wind occurring at the same time.

In Fig. 7.1.6 (b) the temperatures were on average lower than Meteolabor when there was positive lapse rate and on average warmer than Meteolabor when there was a negative positive lapse rate Table 7.1.3 contains a summary of the changes in bias relative to Meteolabor that were found in this flight and the two other flights shown after this. This processing does not assume that the absolute value of the Meteolabor measurements is without error, only that the bias does not change with time over the shallow layer considered.

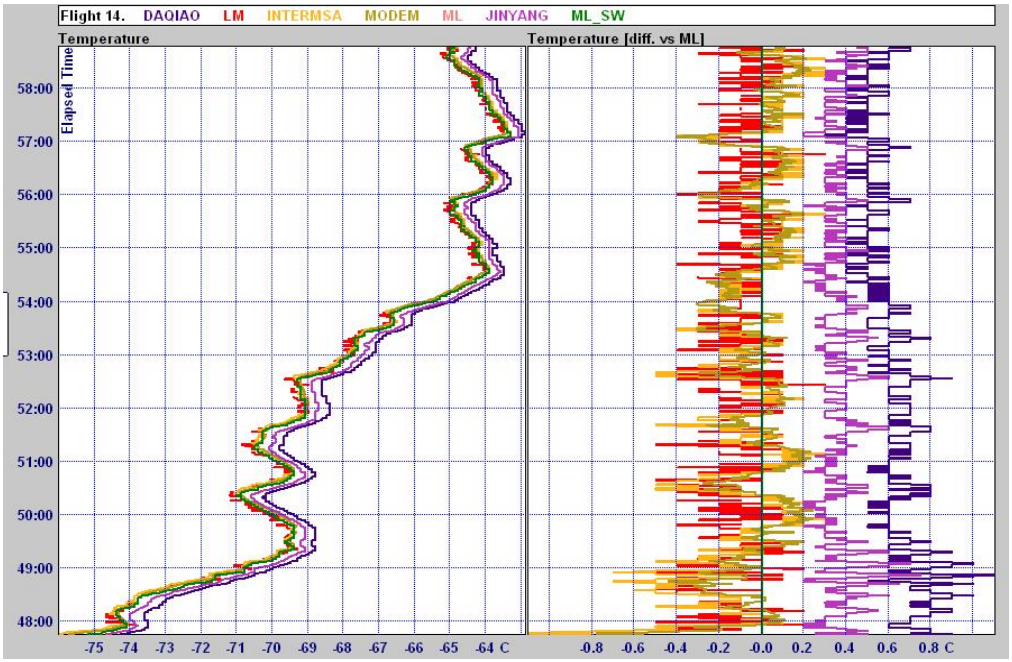

Fig. 7.1.6 (a) Sample of basic data samples and temperature differences between night time temperature measurements from the LMIJ group measurement using Meteolabor as the reference for the temperature differences for the pressure range of about 78 hPa (minute 48) to a pressure of about 46 hPa (minute 58). Positive bias means values are higher than the Meteolabor reference.

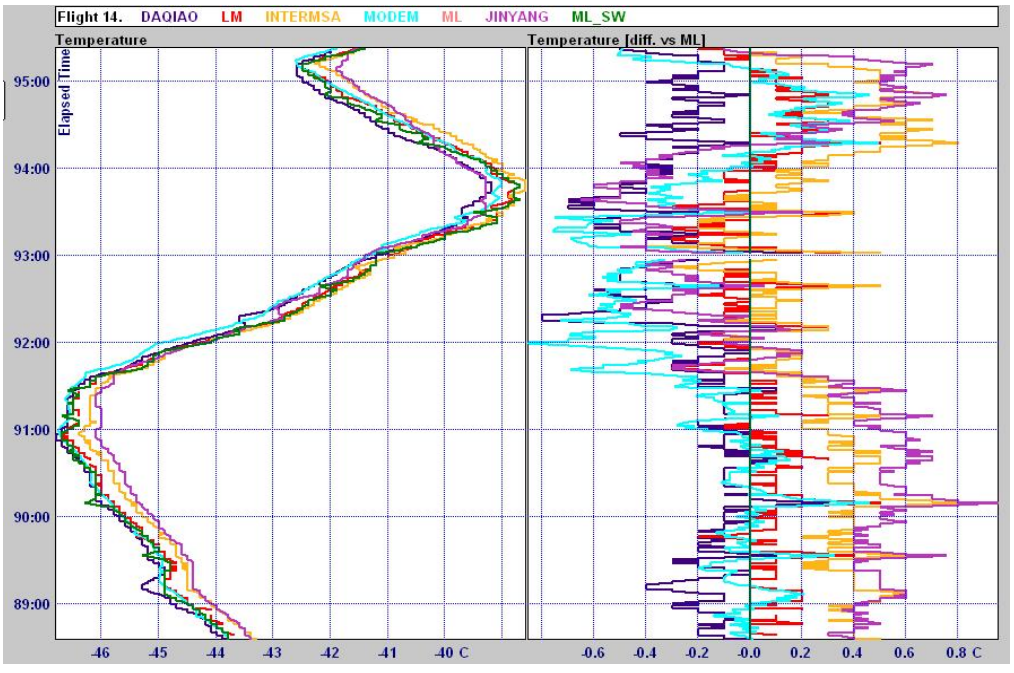

Fig. 7.1.6 (b) Second by second data samples and temperature differences between night time temperature measurements using Meteolabor as the reference for the temperature differences for the pressure range of about 9.4 hPa (minute 89) to a pressure of about 7.6 hPa (minute 95). Meteolabor has the fastest time constant of response. Positive bias means values are higher than the Meteolabor reference.

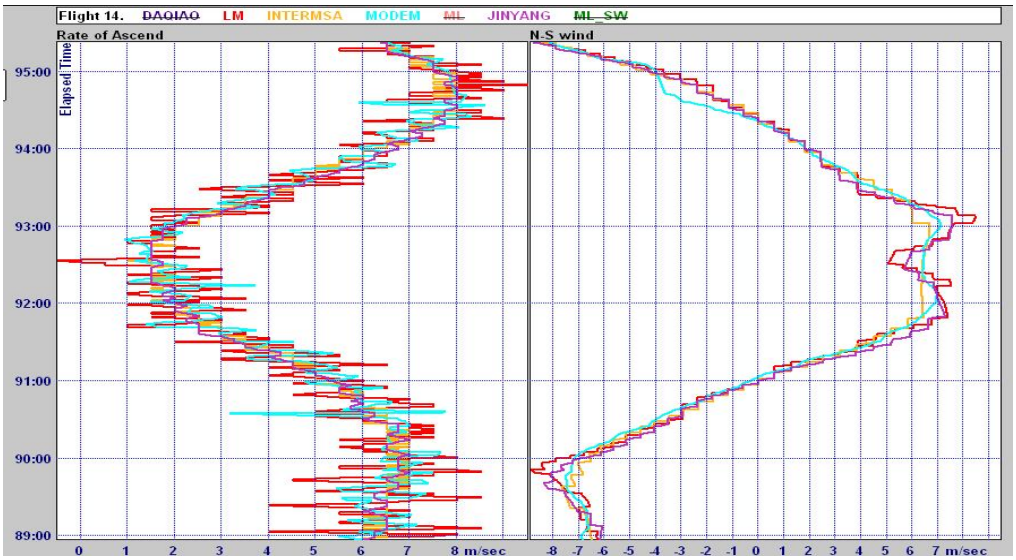

Fig. 7.1.6 (c) Sample of rate ascent with the simultaneous temperature differences between night time temperature measurements from the LMIJ group measurement using Meteolabor as the reference for the temperature differences for the pressure range of about 11.5 hPa (minute 86) to a pressure of about 7 hPa (minute 97).

A similar analysis can be applied to the CHGM group as shown in Figs. 7.1.7 (a)-(c). In Fig. 7.1.7 (a), the radiosonde temperatures follow each other closely, so timing errors between the different systems are small. In Fig. 7.1.7 (b) the Huayun system is responding more slowly than the other sensors and is not able to follow the temperature structure measured by the other systems. This also happened when the rate of ascent has fallen to a low value because of gravity wave activity (Fig. 7.1.7 (c)) and in this case the east-west wind is modulated in association with this gravity wave.

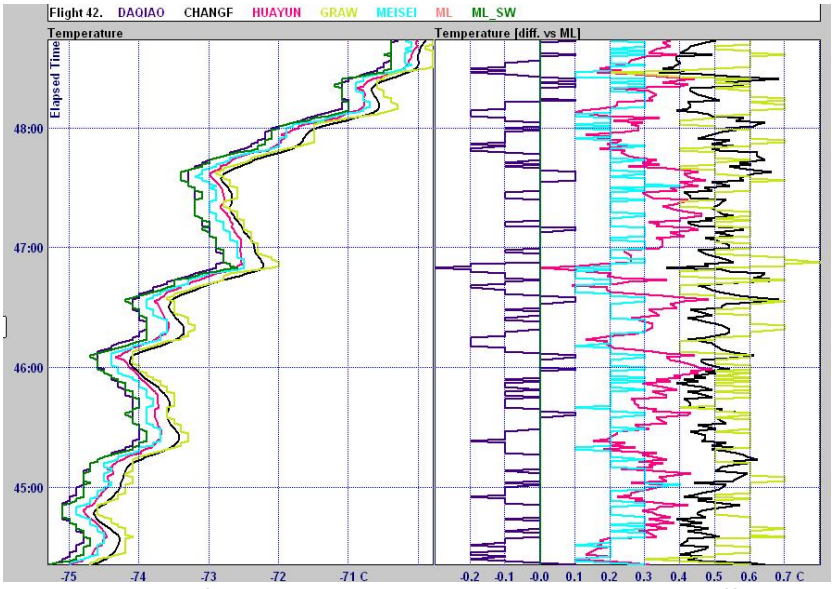

Fig. 7.1.7 (a) Sample of basic data samples and temperature differences between night time temperature measurements from the CHGM group measurement using Meteolabor as the reference for the temperature differences for the pressure range of

about 94 hPa (minute 44) to 74 hPa (minute 50). Positive bias means values are higher than the Meteolabor reference.

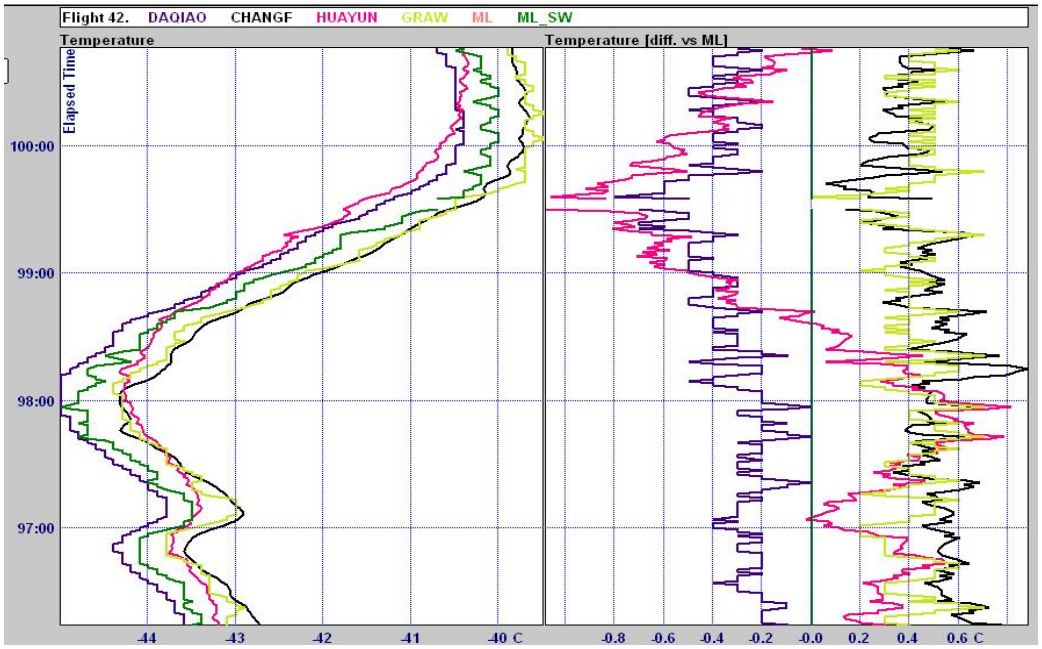

Fig. 7.1.7 (b) Sample of basic data samples and temperature differences between night time temperature measurements from the CHGM group measurement using Meteolabor as the reference for the temperature differences for the pressure range of about 9 hPa (minute 97) to a pressure of about 8.1 hPa (minute 100). Positive bias means values are higher than the Meteolabor reference.

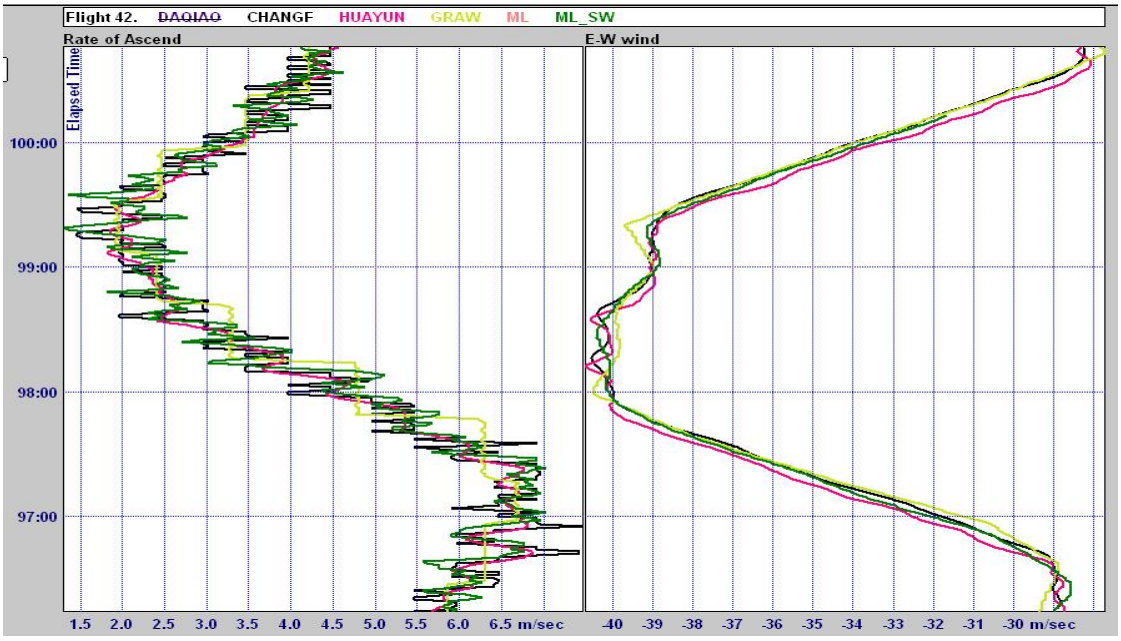

Fig. 7.1.7 (c) Sample of rate ascent with the simultaneous E-W wind measurements from the CHGM group measurement for the pressure range of about 9.0 hPa (minute 97) to a pressure of about 8.1 hPa (minute 100).

Neither Flight 14 nor Flight 42 included Vaisala temperature measurements, but an equivalent analysis can be applied to Fight 67 to assess Vaisala response errors.

The response time of the sensing system relative to Meteolabor has been estimated approximately in Table 7.1.3 using the systematic bias divided by (-) the lapse rate. Theoretically the time constant is also proportional to (rate of ascent)$^{-0.4}$, so this can be used to normalise the time constant to normal ascent rates.

Thus results in Table 7.1.3 show that most of the temperature sensing systems probably had time constants of response between 4 and 5 s at 10 hPa at rates of ascent of 6 m.s^{-1}. This would be consistent with information on time constants published in the CIMO Guide (WMO-No.8, 2008) for small bead thermistors. Jinyang and Huayun sensing systems are not as fast as the others. The Graw biases relative to Meteolabor are very low, but Graw has applied a correction for slow time constant of response, assuming a time constant of response of about 10 s at 10 hPa. The evidence on which this correction is based will need to be documented for future users.

Radiosonde	Systematic bias relative to Meteolabor compared to the bias in zero lapse rate. [deg K]	Rates of ascent, At time of measurement[1] [m/s]	Lapse rate [K/min]	Flight Number	Time Constant versus Meteolabor [s]
Meteolabor	0				
Daqiao	0.1	6.5	-1.3	14	
	-0.4	2.5	+3.5	14	7
	-0.4	2.5	+3	42	8
	-0.25	3	+2	67	
LMS	0.05	6.5	-1.3	14	
	-0.3	2.5	+3.5	14	5
	-0.2	3	+2	67	6
Modem	0.1	6.5	-1.3	14	
	-0.4	2.5	+3.5	14	7
	-0.25	3	+2	67	5
InterMet	0.1	6.5	-1.3	14	
	-0.4	2.5	+3.5	14	7
Jinyang	0.25	6.5	-1.3	14	
	-0.8	2.5	+3.5	14	14
Changfeng	-0.2	2.5	+3	42	4
Huayun	-1.3	2.5	+3	42	About 30
Graw	-0.1	2.5	+3	42	
Meisei	-0.6	2.5	+3	42	12
Vaisala	-0.3	3	+2	67	9

Table 7.1.3: Changes in systematic bias associated with differences in response times of the sensing systems relative to the Meteolabor sensor.

7.1.4 Examples of effects of infrared radiation linked to upper cloud

Comparing Fig. 7.1.6 (a) and (b) shows that Meteolabor, LMS and InterMet had similar systematic differences at both heights. However, the Daqiao bias shifted from a strong positive bias to the most negative as height increased, i.e. decreasing by around 0.9 K from near the tropopause to 10 hPa. On the other hand, when comparing Fig. 7.1.7 (a) and Fig. 7.1.7 (b), the Daqiao measurements are always the coldest, and only decreased with height by about 0.3 K from bottom to top. In Fig. 7.1.6 there was no high cloud, so any cloud had cloud top temperature of -10 deg C at lowest. In Fig. 7.1.7 there was definitely cloud with cloud top temperature lower than -60 deg C, so the infrared environment in the lower stratosphere was quite different. When there is no upper cloud, the infrared radiation warms the white (black in the infrared) temperature sensor up when it is at the lowest temperatures, giving a positive bias near the tropopause and only causing cooling when temperatures are higher in the upper levels.

Fig. 7.1.8 (a) shows an example of the Daqiao temperature measurements when emerging from a cloud which has a cloud top temperature as low as -78 deg C, see the Snow white measurement of relative humidity in Fig. 7.1.8(b). The negative temperature bias of Daqiao is very large immediately above the cloud, and then reduces after 2 minutes to a value more like that shown in Fig. 7.1.6 (a). What happens to the Daqiao sensor if it is coated with ice?

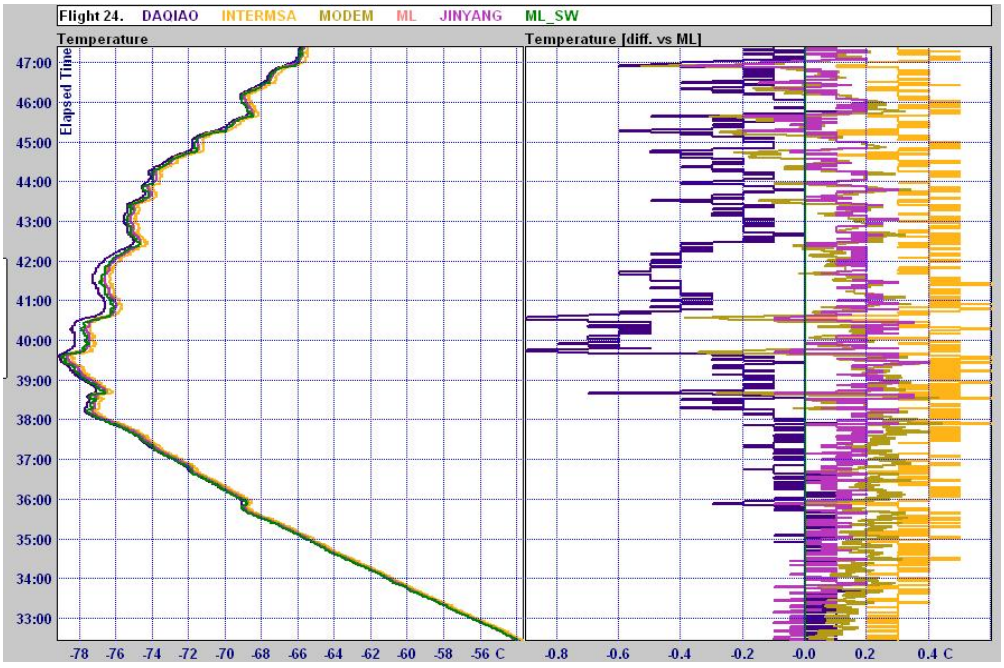

Fig. 7.1.8 (a) Sample of basic data samples and temperature differences between night-time temperature measurements from the LMIJ group using Meteolabor as the reference for the temperature differences centred on the tropopause. The Cloud top temperature is around -78 deg C.

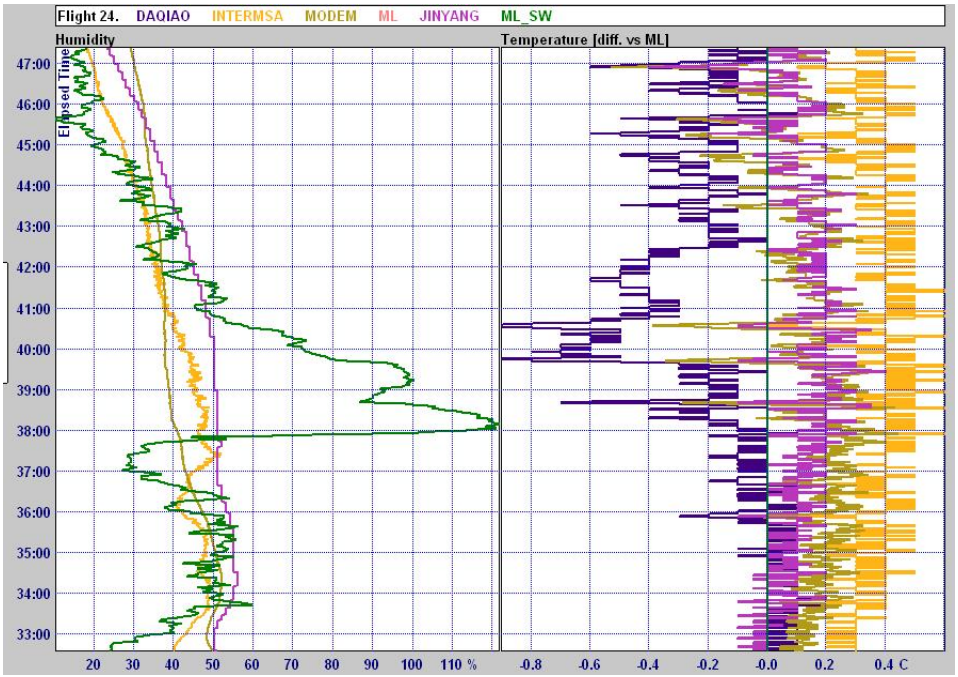

Fig. 7.1.8 (b) Sample of relative humidity samples and temperature differences between night-time temperature measurements from the LMIJ group using Meteolabor as the reference for the temperature differences centred on the tropopause. Cloud top temperature around -78 deg C. Snow White has positive bias from contamination from the cloud, but is able to indicate the cloud top near minute 40.

One way of trying to find out how much cooling is caused by infrared cooling is to look at the cooling of black coated sensors relative to the three aluminised sensors on night-time LMS Multithermistor flights. Nighttimes Multithermistor flights were only on the science flights and Fig. 7.1.9 includes data from five flights, as kindly supplied by LMS. The measurements from the black thermistor have been differenced from the average of the three aluminised thermistors on the radiosonde. Three flights, 15, 43, and 48 were on nights when the cloud radar did not observe cloud higher than 10 km, i.e. with cloud top temperature lower than -40 deg C. On these occasions, the black sensor is clearly warmed up at the low temperatures around the tropopause. On Flight 20 the cloud radar shows a weak cloud of limited extent at 13 km, with cloud top temperature around-55 deg C, see Fig. 7.1.10 (a) and in Flight 53 the ascent goes through thick upper cloud, see the cloud radar in Fig. 7.1.10 (b). On this occasion, instead of warming near the tropopause there was cooling of about 0.2 K. These measurements show that IR cooling of at least 0.5 K can be expected at 32 km whatever the cloud conditions.

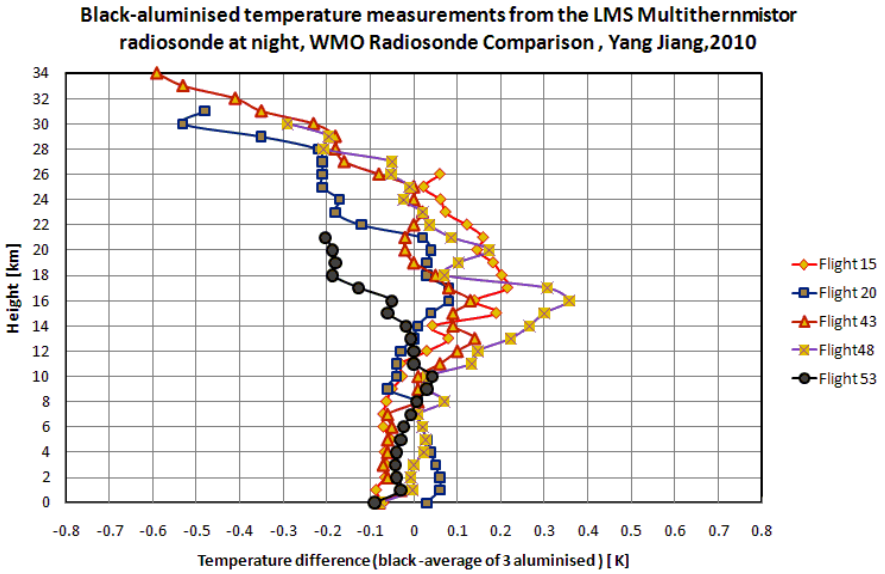

Fig. 7.1.9 Variation of the temperature of a black coated thermistor caused by the infrared radiation fields at Yangjiang (Data supplied by LMS)

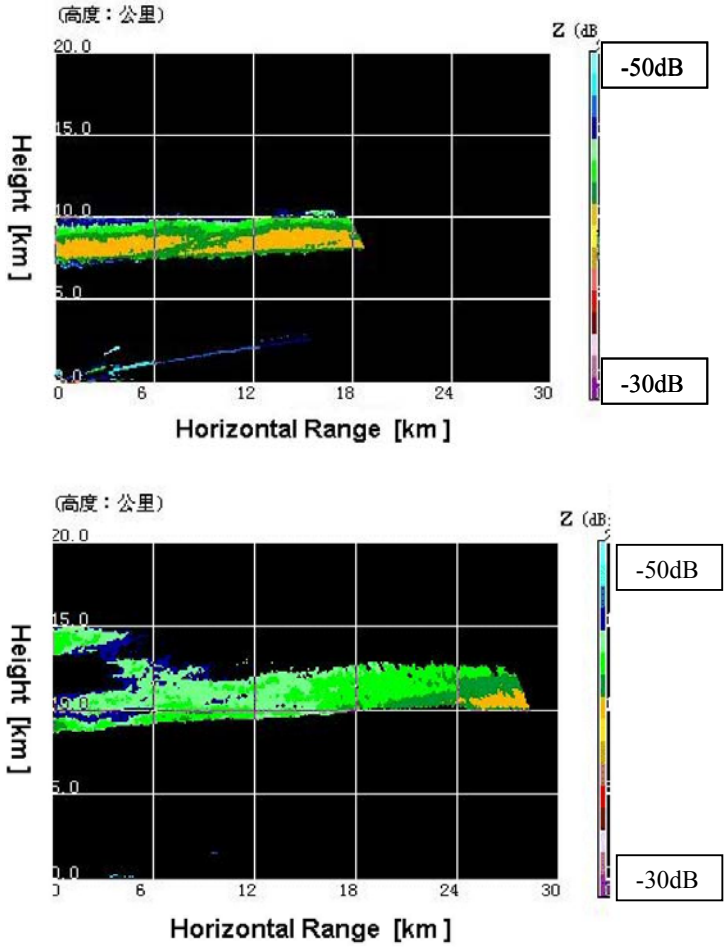

Fig. 7.1.10 Cloud radar measurements in association with Flight 20 (top) and Flight 53 (bottom) Multithermistor measurements, showing the power returns, light blue is weakest signal, yellow is strongest range normalised signals.

To confirm the effect of the upper cloud on infrared conditions in a wider range of flights at night, the WSTAT program was used to compute the average difference of Daqiao from Meteolabor when there was no upper cloud and when there was upper cloud. Meteolabor was on all the Daqiao night-time flights. The resultant differences are shown in Fig. 7.1.11, where the values have been referenced to the zero on the plots in Fig. 7.1.1 (night) and Fig. 7.1.3 (day) respectively. This shows that the typical impact of infrared heat exchange in the stratosphere caused by thick upper cloud was to produce cooling of -0.2 K, relative to the clearer conditions at upper levels, both day and night. However cooling was larger than this near the tropopause, and this was probably not only caused by infrared heat exchange. Above 28 km the infrared errors increase, so that at 32 km the measurements of Daqiao were between 0.4 and 0.6 K lower than the values at 12 km, with the temperatures similar at both heights, as was also seen in the Multithermistor measurements.

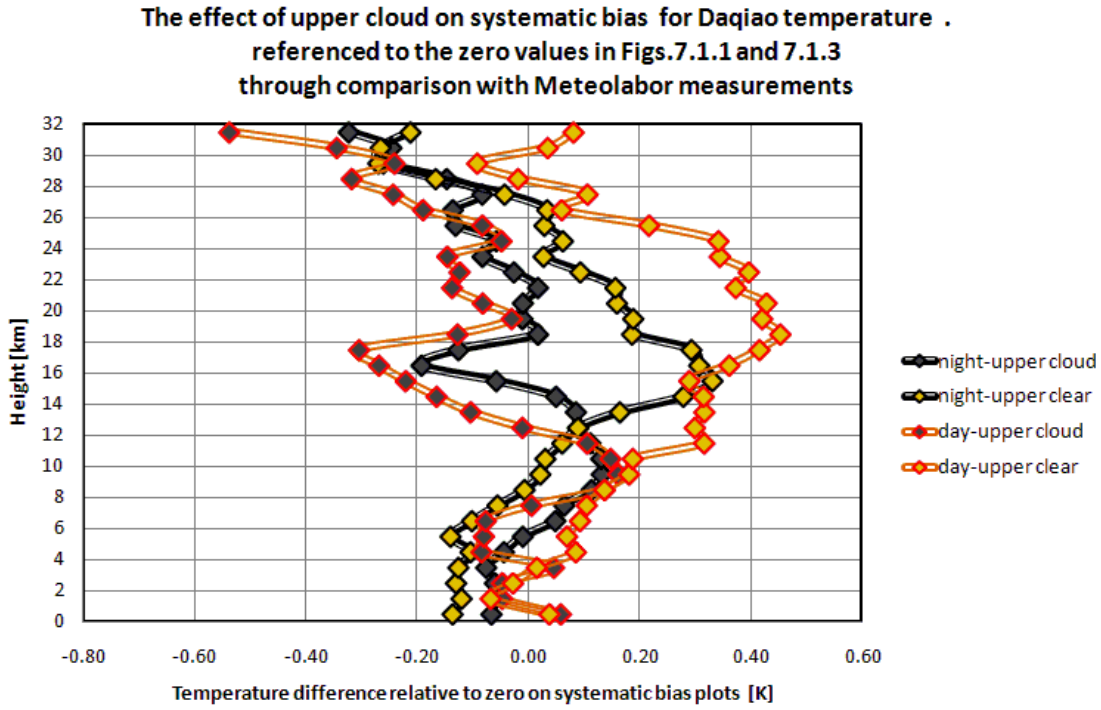

Fig. 7.1.11 Comparison of average differences between Daqiao and Meteolabor, day and night, for times without thick cloud above 11 km and those with thick cloud above 11 km.

The use of white paint even with a very fast sensor, undermines the reproducibility of temperature measurements from location to location is affected by variation in cloud cover and so is clearly unsuitable for use where the observations are to be used for climate studies in future.

It is recommended that white paint is not used on radiosonde temperature sensors for both operational and climate purposes (*ref in CIMO guide*).

7.1.5 Detailed temperature intercomparisons in daytime conditions

In the day, the multi thermistor reference was flown on some but not all of both groups of quality radiosonde flights, but was not flown with Daqiao or Meteolabor, for logistical reasons. Examples of some of the filtering techniques applied to the basic daytime temperature observations at upper levels can be seen in Annex D.

Multithermistor temperatures on flight 35 are compared with the LMIJ group in the lower stratosphere, in Fig. 7.1.12 (a) and in the upper stratosphere in Fig. 7.1.12 (b). The fluctuations in temperature relative to the Multithermistor measurements are larger than found in night time flights, with peak to peak amplitude typically about 0.4 K at 41 hPa and 0.8 K at 7 hPa. In Fig. 7.1.12 (b) the fluctuations in InterMet and Modem measurements appear to be of similar period to the rotation of the radiosonde under the balloon, suggesting that the orientation of the radiosonde relative to the sensor is having some influence on the magnitude of the radiative heating in the sun.

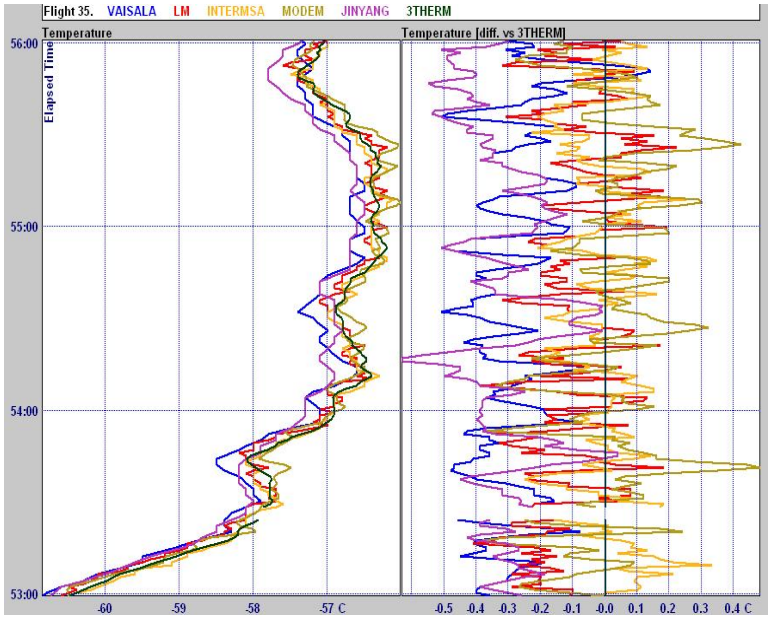

Fig. 7.1.12 (a) Sample of basic data samples and temperature differences between daytime temperature measurements from LMIJ QRS group with the LMS Multithermistor measurement [designated 3 Therm] centred at a pressure of 41 hPa.

For Vaisala measurements, a filter in the data processing removes most, but not those where the pulse is longer than normal, of the positive pulses, correlated with the rotation of the radiosonde under the balloon. At 10 hPa, these pulses were as large as 1 K peak to peak on some flights. Heated air from the sensor support structure can be shed on to the sensor at particular times as the radiosonde rotates. Changfeng has similar support structure and has similar pulses in raw data, the other systems with aluminised sensors without the support frame extending above and around the sensor do not show this problem, see Annex D.

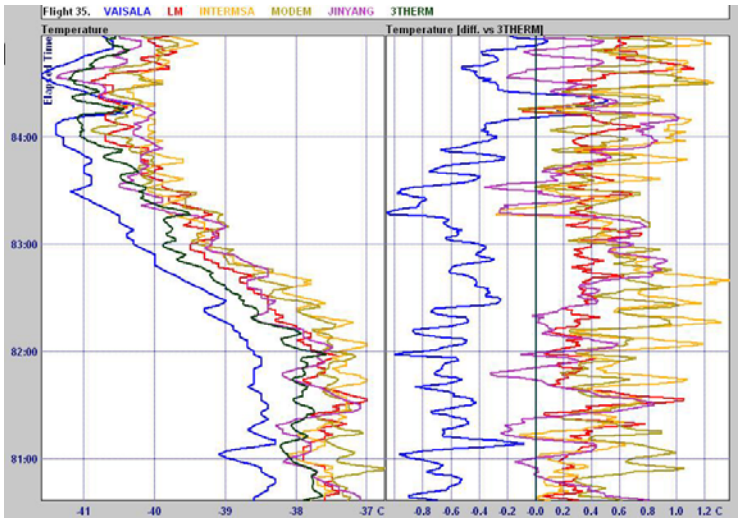

Fig. 7.1.12 (b) Sample of basic data samples and temperature differences between day-time temperature measurements from LMIJ quality radiosonde group with the LMS Multithermistor measurement (designated 3 Therm) centred at a pressure of 7 hPa.

Fig. 7.1.13 presents a similar plot in the lower stratosphere for the CHGM group. Changfeng, and Graw have similar peak-to-peak amplitude relative to the Multithermistor as the LMIJ group in Fig. 7.1.12 (a) pressure, but Meisei and Huayun have larger peak-to-peak amplitude of about 0.6 K relative to the Multithermistor. Huayun and Meisei continued to show larger peak-to-peak amplitudes in fluctuations compared to Changfeng and Graw at lower pressures. Graw daytime temperatures have a time constant of response correction. The Graw measurements have low uncertainties, because of the location well above the radiosonde body and with the sensor well exposed to the air, see Fig. 7.1.4 to confirm that this is generally true.

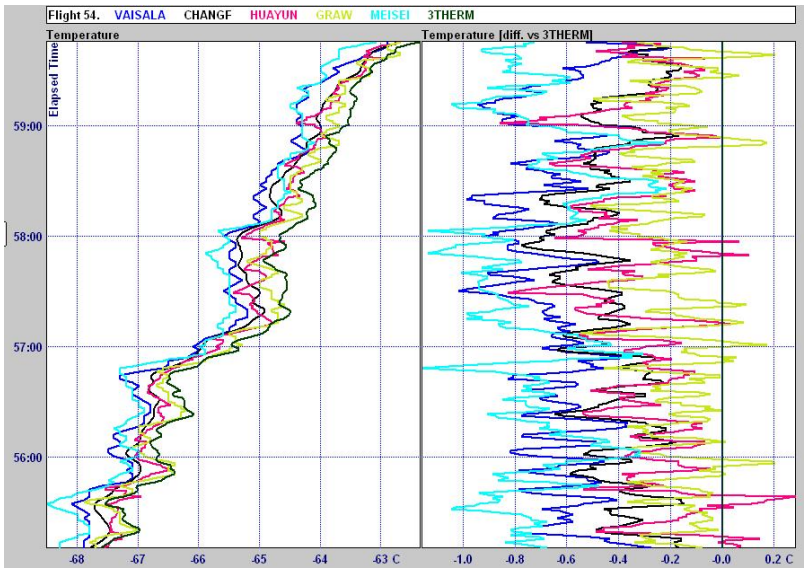

Fig. 7.1.13 Sample of basic data samples and temperature differences between day-time temperature measurements from CHGM quality radiosonde group with the LMS Multithermistor measurement [designated 3 Therm] centred at a pressure of 56 hPa.

The support structure above the Huayun sensor is one sided, so heating pulses from heated air shed from the support, have lower frequency than for Vaisala or Changfeng. These pulses in the Huayun temperatures have not been filtered out in processing, and the structure can most easily be seen at low pressure in Fig. 7.1.14. This shows the quality of Daqiao and Meteolabor measurements in the day, with the Changfeng measurements used as a reference. Both Daqiao and Meteolabor may have slightly larger peak-to-peak fluctuations than the better daytime sensors in the lower stratosphere. Near 10 hPa, Huayun measurements have very large peak-to-peak fluctuations of about 2 K; Daqiao has peak-to-peak fluctuations of about 1 to 1.2 K and Meteolabor of about 0.8 K, similar to the best systems. Raw Huayun shows much larger fluctuations with time suggesting it has a significant heat contamination problem in the daytime. With Daqiao, daytime errors some of the positive peaks have been removed from both the processed and raw data file.

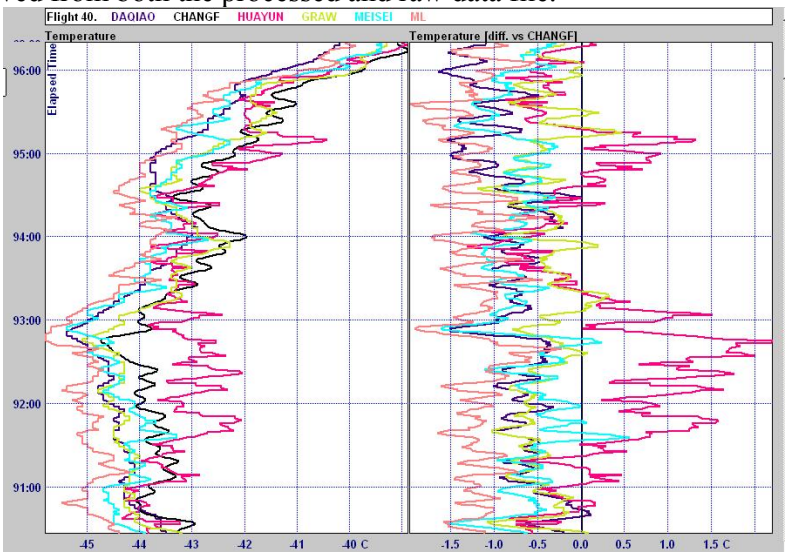

Fig. 7.1.14 Sample of basic data samples and temperature differences between daytime temperature measurements from CHGM quality radiosonde group with the Changfeng measurement [used as reference] centred at a pressure of 11 hPa.

7.1.6 Results of time series analyses of geopotential height measurements

The geopotential height difference between two specified pressures levels is a good approximation proportional to the mean layer temperature between the pressure levels, see CIMO Guide (WMO-No.8).

Thus, if there is a time series of height observations spaced twelve hours apart, one observation time in the dark and one in the day, if there is little atmospheric variation in the geopotential height difference then it is possible to interpolate between the daytime measurements and find the difference of the night time observations from the interpolation. Then the average found over many readings gives an estimate of the systematic difference day-night and the standard deviation of the difference can be used to estimate a maximum value for the random error in the mean layer thickness and hence the mean layer temperature measurements. Only the radiosondes giving correct geopotential heights against pressure were used, hence Graw data are not used in this analysis. In all the rest of the radiosonde the effects of pressure differences between systems, see chapter 10, has a negligible impact on the mean layer temperatures.

Day-night differences also include the effects of local diurnal temperature tides as well as the radiosonde errors. If height observations are 6 hours apart, then the semidiurnal; temperature tide also has some influence on the result.

In Yangjiang, only one radiosonde type had observations at all four times possible in the day. This was Vaisala, and the results from this radiosonde have been used to quantify the difference between observations at 02.00 and 20.00 at night, using 6 hourly interpolations between daytime observations at 08.00.

Two radiosonde types only flew on ascents at 02 and 14 hrs local time, Meteolabor and Daqiao. So the day-night difference from these measurements was input into the plots assuming the night-time offset given by Vaisala. All the other radiosonde types flew partly in a cycle with observations at 02 and 14, but also for another part of the test with observations between 08.00 and 20.00. The day night differences for each 12-hour difference were computed and then related to the night-time differences generated from Vaisala measurements. This allows the reader to see whether the day-night differences look consistent with a reasonable atmospheric variation or whether some radiosonde types have a clear anomaly in day-night difference.

The results for the 300 hPa geopotential, the (100-300) geopotential height difference, and the (30-10) geopotential height difference are shown in Fig. 7.1.15 (a) - (c). There were insufficient continuous series of measurements at 10 hPa, to allow the technique to be reliably applied, and at 30 hPa, many of the systems in the CHGM group did not have enough continuous time series at 30 hPa, because of the pattern of early balloon bursts and occasional radiosonde failure.

The results for the reference group in the final plots are consistent at 300 hPa and (100-300) hPa. These seem to show a small atmospheric diurnal variation in antiphase to the solar heating from the surface to 300 hPa (between daytime measurements at 08.00 and 16.00 given semidiurnal tides are small), and a small diurnal variation in phase with the solar heating between 100 and 300 hPa. All the other radiosonde types give measurements relatively consistent with this picture, apart from Meisei which has a daytime negative bias. Most of the Meisei radiosondes causing the problem were flown at 0800 local time, as can be seen in Fig. 7.1.3.

The continuity of the time series of measurements was poorer at 30 hPa but there were enough to provide useful estimates for the radiosonde types shown

Both Vaisala and Modem indicate little diurnal tidal variation between 30 and 100 hPa. The daytime measurements by LMS also show little difference 14-08 hours. Thus, it seems that the LMS temperature measurements probably had a positive bias day-night near 15m, corresponding to a day-night difference in mean layer temperature of between 0.3 and 0.4 K. Random errors [k=1] in the day-night difference in (c) are about 3 gpm for Vaisala and LMS. The equivalent errors in (a) and (b) were mostly near 2 gpm. A similar analysis for the layer between 30 and 10 hPa, has much less data because of the pattern of balloon bursts, but shows that in this layer there was at least a positive bias of LMS day to night of at least 20 to 25 m.

Based on these results the zero axis of Fig. 7.1.3 was adjusted at heights above 100 hPa to reflect these results.

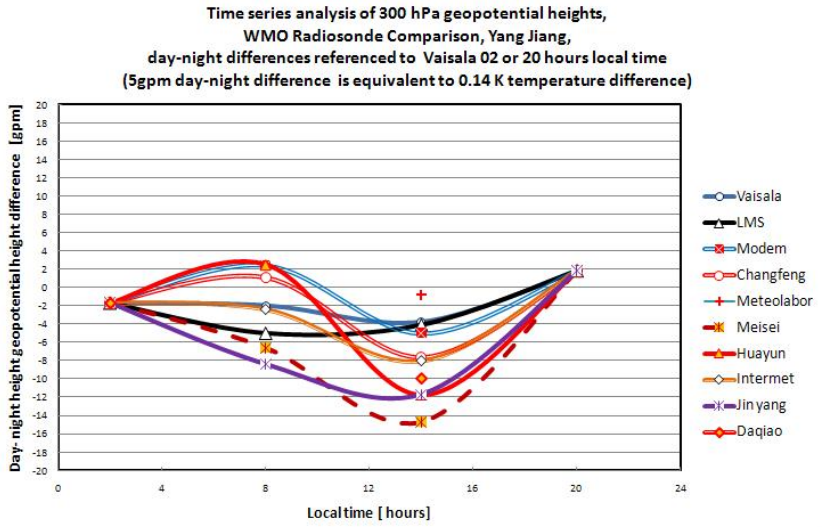

(a)

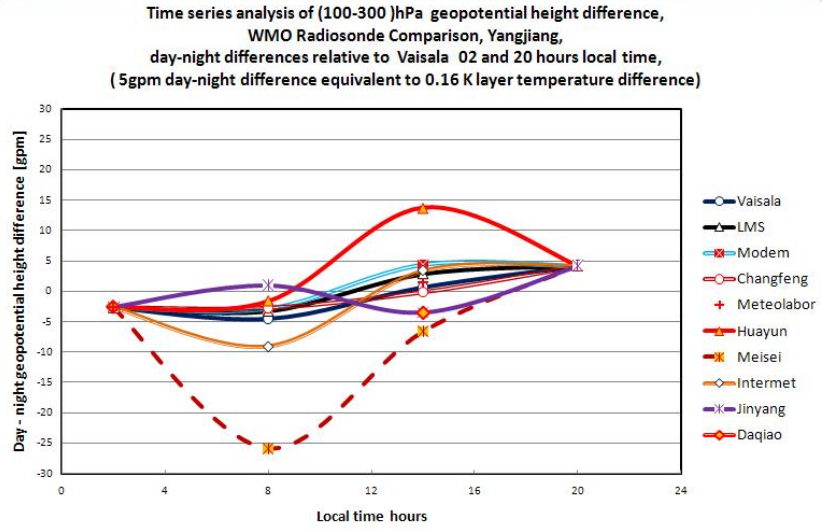

(b)

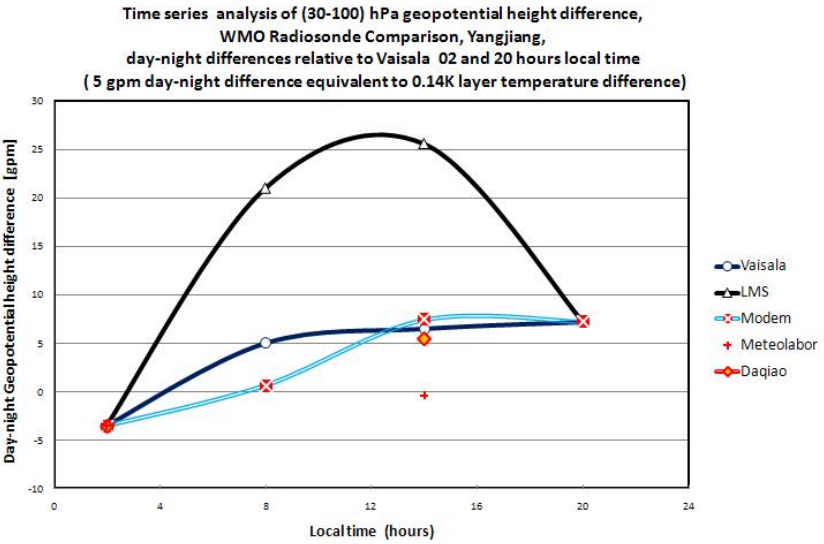

(c)

Fig. 7.1.15 Results of time series analysis of day-night bias in geopotential heights for pressure levels of (a) 300 hPa, (b) (100-300) hPa, (c) (30-100) hPa.

7.1.7 Evaporative cooling errors

As stated earlier, evaporative cooling errors have not been flagged out of the comparison data set. When the radiosondes emerge from a cloud layer, the sensors will be cooled by evaporation, if the sensor is coated with water or ice. Fig. 7.1.16 (a) and (b) contains examples for each of the QRS groups of test flights emerging from cloud, and most of the sensors experiencing evaporative cooling as the water/ice evaporates from the sensor surface.

Fig. 7.1.16 (a) is for the LMIJ group with Meteolabor and Daqiao. All the sensors experience evaporative cooling from shortly after minute 17, when the first decrease in RH above the clouds occur, with Meteolabor and Jinyang recovering first and the others less rapidly. Also, note the very large discrepancies in relative humidity measurements above the cloud, with some radiosonde types clearly contaminated by the water/ice for at least four minutes. It suggests that there were problems with the design of the humidity caps of the worst affected sensors, Daqiao and Modem.

Fig. 7.1.16 (b) is for the CHMG group with Vaisala. The Vaisala temperature sensor has a hydrophobic coating, which minimises the water retained on the sensors and it can be seen how this temperature sensor recovers more quickly from wetting than the sensors of the other radiosonde types. Note – Temperature increase at minute 19.26 corresponds to the time at which rapid decrease in RH occurs, as we would expect.

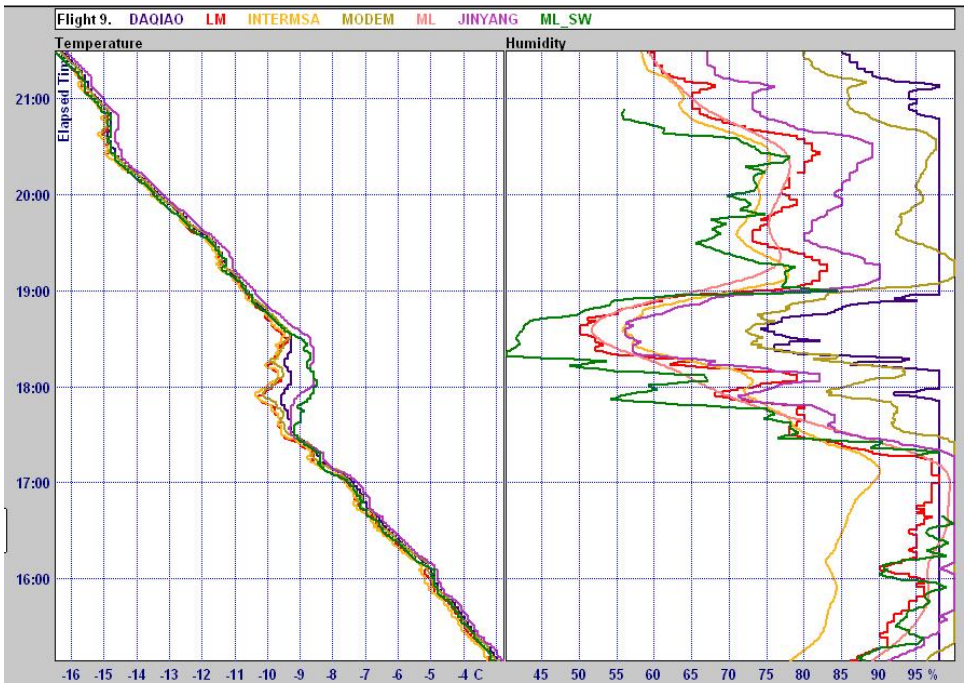

Fig.7.1.16 (a) Simultaneous temperature and relative humidity measurements made by the LMIJ group on emerging from a cloud, the top of the cloud being just after minute 17 into flight, see the relative humidity measurements

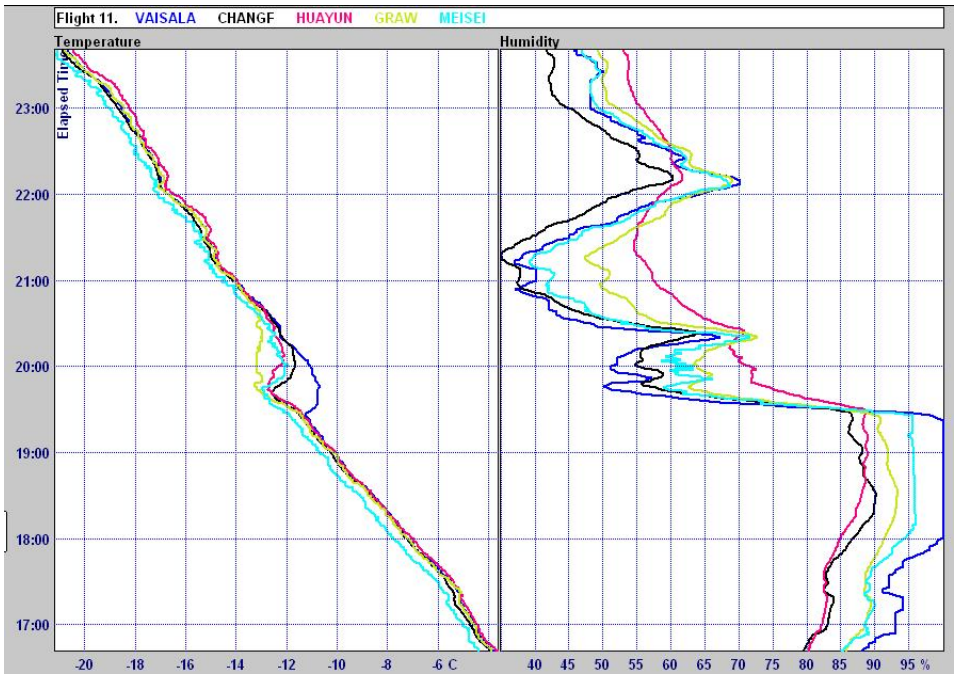

Fig. 7.1.16 (b) Simultaneous temperature and relative humidity measurements made by the CHMG group on emerging from a cloud, the top of the cloud being just after 19 minutes 20 seconds into flight , see the relative humidity measurements

In Yangjiang, evaporative cooling was not as frequent as in Mauritius. In many countries, evaporative cooling is an operational problem, because it corrupts the temperature structure above low cloud, and the numerical forecasters will not accept long-term operational use of a radiosonde, which does not have a hydrophobic coating or other measure to minimise the magnitude of evaporative cooling.

7.2 SSI

7.2.1 Basic intercomparison

Here, the statistical comparison of the temperature measurements on the SSI payload is based on the approach outlined in section 3.2, using the analysis proposed for GRUAN. The GRUAN Lead Centre has developed an uncertainty analysis for the Vaisala temperature sensor so here this is used for the Vaisala RS92 to compare with the other temperature observations.

For this analysis, we separate the vertical profiles into 4 altitude regions: lower troposphere (0 to about 8 km), upper troposphere (about 8 to tropopause), lower stratosphere (tropopause to about 22 km), and middle stratosphere (above roughly 22 km). Within each altitude region, all temperature measurements are compared to the corresponding Vaisala temperature measurement. For a statistical significance of k=2, it is expected that at least 95 % of all pairs fall within the uncertainty estimate that we have assumed for the Vaisala RS92 temperature sensor. Figure 7.2.1 shows the relative fraction of all nighttime observations, where the difference to Vaisala is less than the uncertainty assumed for Vaisala for night time measurements. For all sensors, except for the Meisei RS06G all differences can be explained with the current understanding of the uncertainties and there is no indication for any systematic error in the temperature observations with this data sample, which has not been identified or properly quantified.

Figure 7.2.2 shows the relative fraction of all daytime observations, where the difference to Vaisala is less than the uncertainty assumed for Vaisala for daytime measurements. Here most sensors are consistent with the Vaisala measurements within the uncertainties that were derived for the Vaisala sensor and a standard uncertainty for the other sensor of 0.25 K.

It is important to point out that this consistency test is only possible, if the uncertainty of at least one sensor has been described. It was hoped that the Multithermistor radiosonde could be used as reference instrument, especially since it does not require a solar radiation correction, but rather provides a solution temperature during the day and night, where the radiative heating and cooling of the sensors is explicitly derived from the observations. However, due to the lack of detailed understanding of the method and the algorithms that are required to determine the solution temperature, GRUAN were not able to assign any meaningful uncertainty estimate to each data point.

The same is currently true for the MTR sensor, and thus although it is a very fast sensor, the details of the measurement, in particular the radiation correction are not well enough understood to assign a meaningful uncertainty estimate to that sensor. Therefore, both sensors could not serve as reference in the statistical analysis presented here.

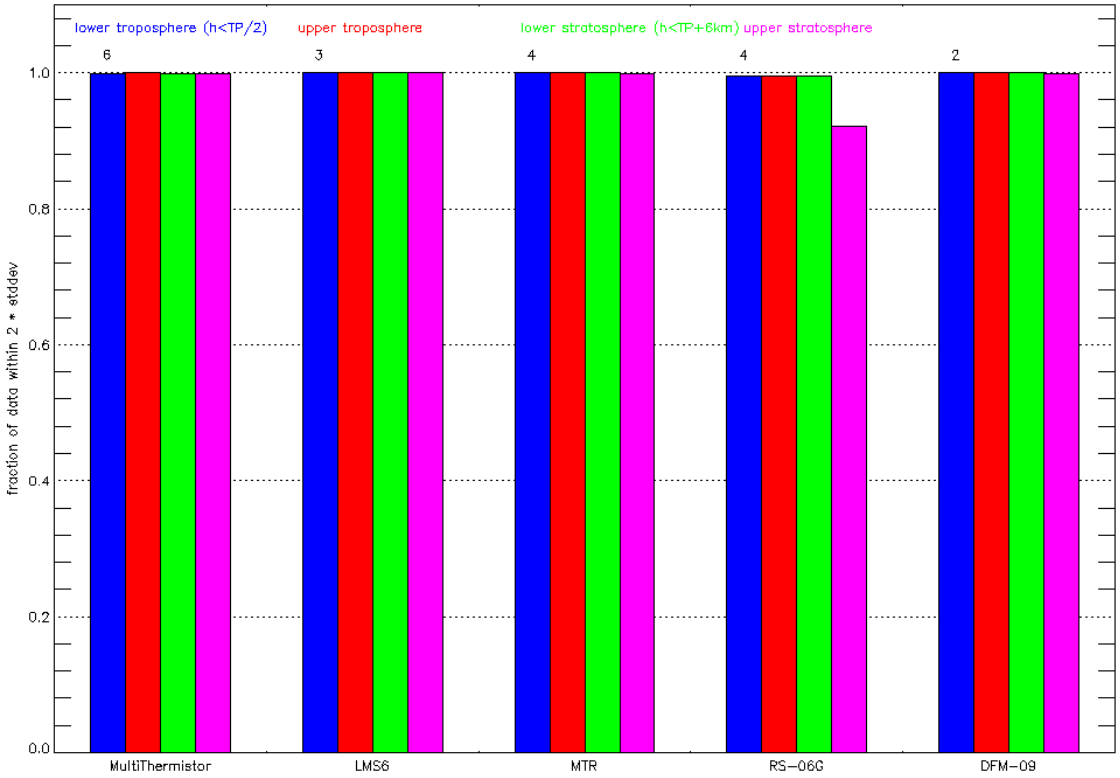

Figure 7.2.1 GRUAN Consistency test for all night-time temperatures.

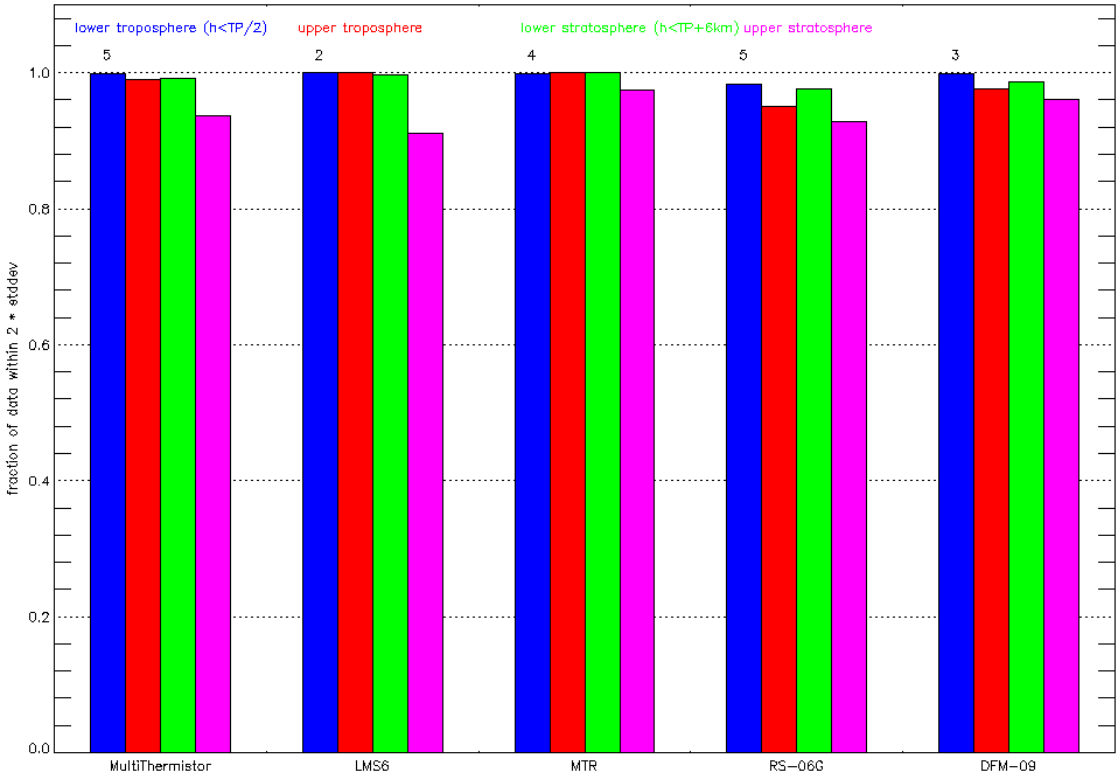

Figure 7.2.2 GRUAN Consistency test for all day-time temperature measurements

7.2.2 Profile intercomparison

The vertical profile of the differences of MTR and Multithermistor to Vaisala RS92 is shown in Figure 7.2.3 for MTR and Figure 7.2.4 for Multithermistor. Vaisala was chosen as reference for the same reason as outlined above. Note: the Vaisala measurements used in these plots were not the data submitted to the WMO data base, but values derived from the Vaisala raw data, as provided to the GRUAN Lead Centre and then corrected using the correction scheme devised by the GRUAN Lead Centre.

Figure 7.2.3 shows that for most altitudes the differences between the MTR and Vaisala are less than 0.5 K. While this difference is not significant in the stratosphere, i.e. it can be explained by the uncertainty of the Vaisala measurements combined with an assumed uncertainty of 0.25 K for the MTR, this difference cannot be fully explained for daytime measurements in the upper troposphere and lower stratosphere. This is the reason for the lower consistency value for MTR in the upper troposphere and lower stratosphere shown in Figure 7.2.2.

Figure 7.2.4 shows the same comparison for Multithermistor relative to Vaisala RS92 as in Figure 7.2.3 for MTR. For night time observations shown in blue colors, the differences are less than 0.3 K on average throughout the entire profile and can be fully explained by the uncertainties assumed. Although the differences in daytime measurements are suggestive of an insufficiently characterized altitude dependent systematic error, the current understanding of the uncertainties of the Vaisala radiation correction combined with a assumed uncertainty of 0.25 K for the Multithermistor are sufficient to explain this behavior of the daytime comparison. To make this difference statistically significant would require a more detailed understanding of the systematic errors in the radiation correction applied for Vaisala and in particular a much better understanding of the uncertainties in the Multithermistor observations. Without additional information that would help quantifying measurement uncertainties, in particular the systematic errors of the radiation correction, no further conclusion can be drawn from this comparison. Thus this information is essential in improving the observations.

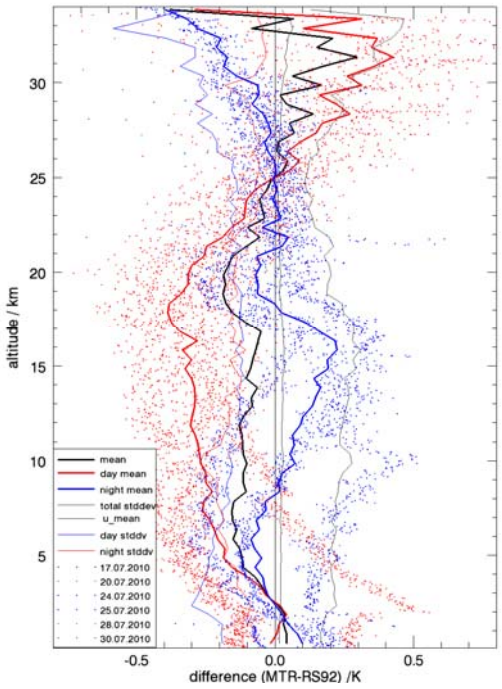

Figure 7.2.3 Vertical profiles of the temperature difference between MTR and Vaisala. Day-time comparisons in red and night-time comparisons in blue.

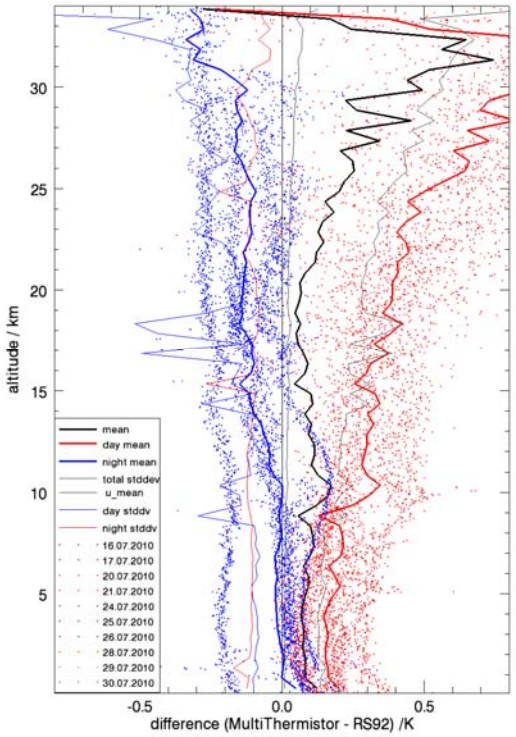

Figure 7.2.4 Vertical profiles of the temperature difference between Multithermistor and Vaisala. Colours are the same as in Figure 7.2.3.

7.2.3 MTR 6 Hz data analysis

The MTR sensor has the advantage of being a very fast sensor and being able to resolve fine structure in the temperature seen by the sensor. This is particularly useful in the evaluation of transient effects that may contaminate the temperature measurements, which have been identified in the past. *Shimizu and Hasebe* (*2010*) discussed the several possible sources of temperature contamination: Contamination through the radiosonde package itself and the rig just above the payload; balloon "wake"; solar eclipse due to the shading of the sun by the overhead balloon during low zenith angle daytime measurements; and several others.

Shimizu and Hasebe (*2010*) suggested that accurate and contamination-free temperature profiles may be obtained from the nighttime soundings using long suspension lines (e.g., 120 m) and descending data would minimize balloon wake effects.

Figures 7.2.5 and 7.2.6 show all four successful, daytime and nighttime, respectively, MTR 6 Hz results together with RS92, Graw, and LMS.

In general, daytime MTR results in the stratosphere show positive pulses, and nighttime MTR results show negative pulses with respect to RS92 (and RS06G) results (see Figure 7.2.3).

Soundings using a 700 mm rope to suspend the instrument from the rig (flight number 020 and 026 shown in Figure 7.2.5) show consistently much greater pulses compared to the soundings in which MTR-RS06G and RS92 are attached directly on the bamboo rig (flight number 043 and 056 shown in Figure 7.2.6). During the latter soundings temperature spikes were significantly reduced on generally less than 0.3 K. This result strongly suggests that contamination of the temperature measurement occurred due to the bamboo rig itself. Individual temperature spikes may reach up to 1 K above their background temperature.

Note that *Shimizu and Hasebe* (*2010*) reported for a sounding of the same sensor and a flight configuration with a 120-m suspension line that some pulses of up to 0.4 K were observed, which the authors attributed to the variation of insolation associated with the solid angle. An effect of this magnitude was not confirmed in Yangjiang, when the sensor was taped directly to the rig.

For the nighttime soundings (Figure 7.2.5), negative pulses up to 1.0 K were observed. Shimizu and Hasebe (2010) show that their nighttime flights showed negative pulses of 0.5 K in magnitude.

It has to be pointed out that these results apply to the sensor configuration used on the MTR. For sensors that are being mounted closer to the instrument package, self contamination may be more visible. There was no clear indication of self contamination in the configuration used on the MTR.

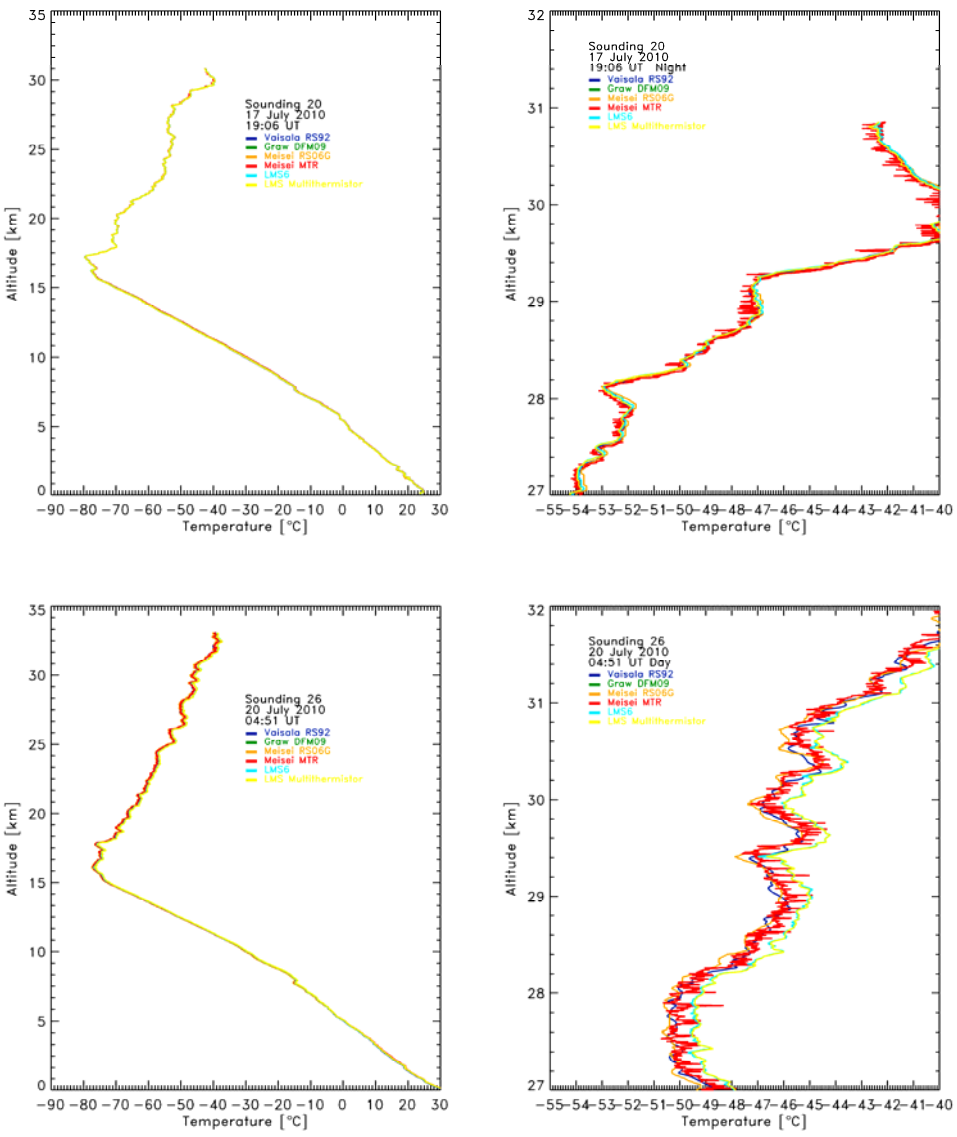

Figure 7.2.5 Temperature profile details for soundings 20 (night time) and 26 (day time). Strong temperature spikes can be detected in the MTR data, with night time observations giving cold excursions, and daytime observations giving warm excursions. In these soundings the MTR was suspended below the bamboo rigging using 70 cm of string.

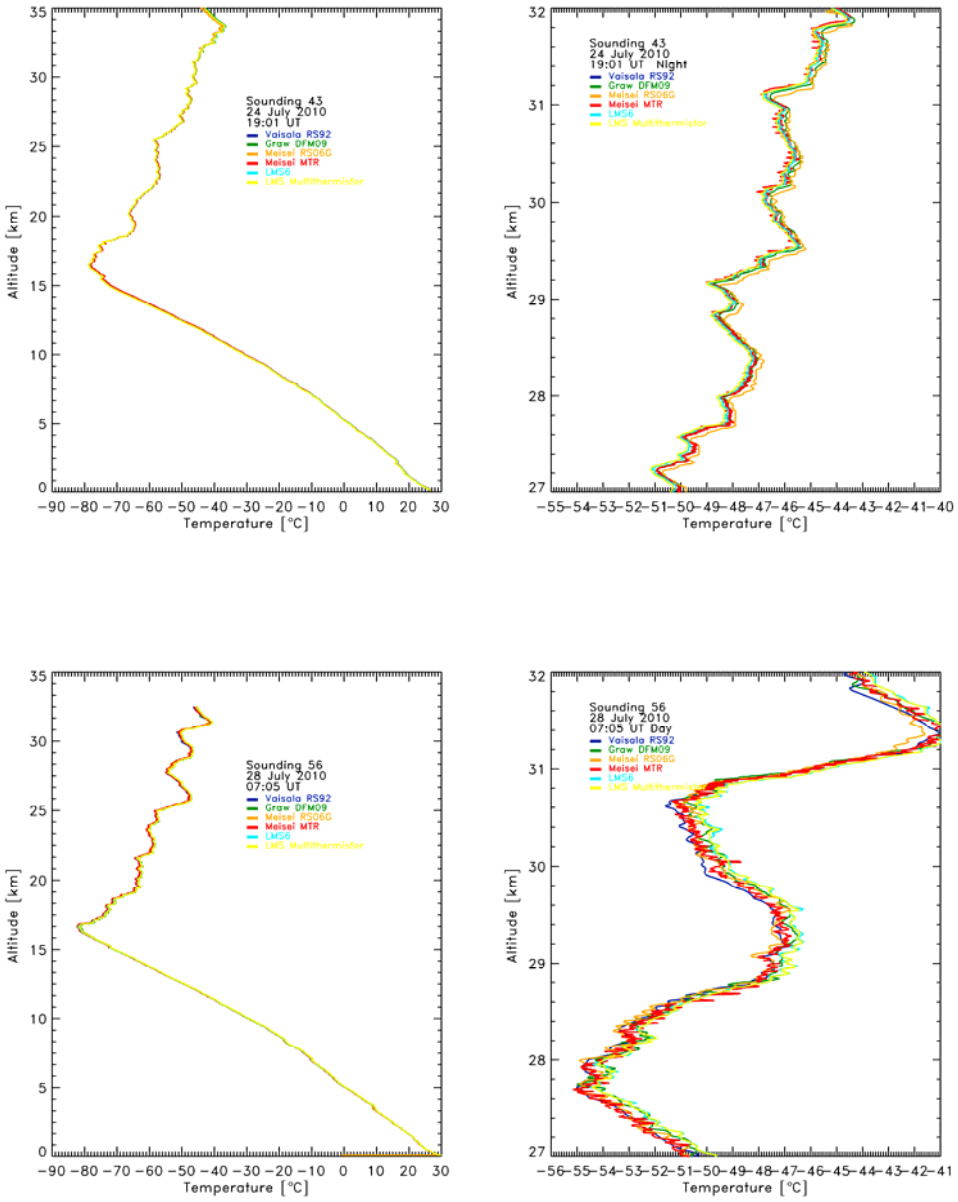

Figure 7.2.6 Temperature profile details for soundings 43 (night time) and 56 (day time). In these soundings the MTR was mounted directly onto the bamboo rigging, i.e. no rigging part was located above the temperature sensor. The temperature spikes detected in the MTR data are reduced compared to the configuration, where the MTR was suspended below the bamboo.

The lessons learned from the MTR observations are the following:

- There was no clear indication of temperature contamination by the balloon itself. Thus balloon wake signals did not appear to play a significant role for the configuration used in Yangjiang, and in particular the length of the string to the balloon appeared to have been sufficient.

- Temperature spikes were observed during the day and night time; however, the direct cause of these spikes is not fully understood.

- These spikes were very much shorter than the problems that poorly exposed QRS temperature sensors have at these heights, see Annex D.

- Filtering of spikes should be performed; however, the clear identification of spikes in software is an important factor to document, as improper spike filtering may introduce artificial systematic errors, either by incorrectly fitting real temperature structure, or omitting or smoothing over true contamination spikes, which should have been removed. To evaluate measurement uncertainty it is essential to have detailed information how contamination spikes are being removed.

- Temperature contamination on the larger payload was detectable by the MTR and created positive temperature anomalies of up to 1 K during daytime and negative anomalies of similar magnitude during nighttime at the highest levels observed, above 27 km. There was some discussion as to whether these anomalies originated from the bamboo supports or were picked up from the support structure of the MTR temperature sensor itself, and further work is required to reach a full conclusion of the issue. [Note: When the MTR data were sampled onto a 1second interval in the main comparison database, these differences were barely noticeable.]

- Temperature anomalies were much reduced when the radiosonde was taped directly onto the bamboo rig, but whether this was because the sensors were above the bamboo or because the radiosonde was held rigidly to the bamboo rig was not clear

8 Comparison of simultaneous humidity measurements

8.1 QRS

8.1.1 Operational sensors used

Most of the relative humidity sensors tested in Yangjiang were of a similar type, thin film capacitance sensors. Pictures of these are shown in section 4.1. Graw, LMS, InterMet, Huayun, Jinyang used a sensor from the same manufacturer, E+E, but as will be seen these did not all have the same performance. There are several sensors on offer from E+E, so this adds further complications when attempting to assess why the measurements from a similar sensor differ quite a lot for the different radiosonde type. The basic principle of the Vaisala capacitive sensor in Yangjiang was similar to that in the Mauritius comparison. In the Vaisala system, two sensors are exposed directly to the air, and are heated in turn to drive off water and ice picked up in cloud and rain. This happens down to -60 deg C, but when the pulse heating ceases only one of the two sensors reports for the remainder of the flight. In recent years, the humidity sensor supports were fully aluminised. The supporting structure around the Vaisala temperature sensors, which influences the temperature of the Vaisala relative humidity sensor, was reduced in size compared to Mauritius. Thus, the day-night differences in Vaisala relative humidity could be expected to be smaller than in Mauritius, because the sensor would not be heated as much above atmospheric temperature by the support structure. The humidity sensor measures the relative humidity at its own temperature and not that indicated for the atmosphere by the main temperature sensor. However, some other radiosonde systems measure the humidity sensor temperature independently (see Annex D).

In addition, in Yangjiang, Vaisala were using new software (issued subsequently in December 2010) to adjust for slow sensor response at very low temperatures and for correcting for this daytime heating of the humidity sensor relative to the air temperature. At high humidity in the layer immediately under the tropopause, the overall daytime correction was about 20% and that due to the solar heating correction about 16 per cent whilst at relative humidity near 25 per cent, the time constant correction had reduced the value by at least 6 per cent on average relative to the raw values.

In the LMS-6 radiosonde the humidity sensor is mounted on an outrigger under a canopy, unlike its position in an internal duct used in Mauritius. Thus, the performance should not have been the same as in Mauritius, especially in the upper troposphere. LMS also uses an independent temperature sensor located close to the humidity sensor.

Modem, Changfeng and Daqiao used thin film capacitors from other manufacturers.

Thin film capacitance sensors may differ in flight performance because of:

- Differences in the properties of the polymer film used
- Chemical contamination changing sensor performance
- Method of estimating the temperature of the relative humidity sensor, and exposure of the sensor to minimise misleading fluctuations in humidity sensor temperature
- Errors in interfacing and referencing in the radiosonde electronics
- Differences in methods of exposure
- Method of eliminating water vapour/ice contamination during the ascent
- Effects of hygroscopic surfaces near the sensor e.g. if there is a protective cap over the sensor, is it non-hygroscopic?

8.1.2 Results of statistical processing

Relative humidity comparison statistics have been computed in temperature bands in the troposphere from 30 to 0 deg C, 0 to -20 deg C, -20 to -40 deg C, -40 to -60 deg C, -60 to -70 deg C, and -70 to -80 deg C for day and night. The results were originally computed using the WSTAT program as a function of relative humidity observed by the group working reference, but here the results are presented as a function of temperature for relative humidity bands 20 per cent wide, so that the reader can see the extent to which the sensor performance varies with temperature. Temperature at a given height does not vary much from flight to flight in Yangjiang, so the temperature bands are centred approximately at the heights given in Table 8.1.1.

When processing using WSTAT, pressure must be higher than 80 hPa for the humidity data to be used in the computations. This was intended to only process observations from the troposphere in a given temperature band. Observations in the lower stratosphere will be considered in a later part of this chapter.

Group working references had to be on most flights in a group, and have good measurement quality. For relative humidity, both Graw and LMS use a similar humidity sensor, so the standard deviations against other radiosonde systems will appear higher if the sensor observes more or less vertical structure than the E+E sensor, so it is essential to check if this is happening against the data from individual flights shown later in this section. The uncertainty plots should not be used to discriminate between the radiosondes of good performance, but can be used to identify those systems that have problems, producing large uncertainties. The linking radiosondes are just those that flew in enough numbers in each QRS group to contribute to the link. The most useful are those with high measurement quality. The references for the systematic difference plots were three independent sensor types that showed very little day night difference in comparison with the GPS integrated water vapour measurements (see later section). Thus, certainly at low levels, day-night difference in the systematic bias plots references should be small, and what happens at higher levels will have to be checked by comparing measurements in cloud, both day and night (see later section).

Temperature Range , [deg C]	Group working references	Linking radiosondes	Typical uncertainty in LMS-Graw link, [% RH]	Reference for systematic difference plot	Approximate Central height [km]
> 0	LMS, Graw	Vaisala, Meteolabor, Snow-White, Multithermistor, Daqiao	<0.1	LMS, Vaisala, Snow white	3
0 to -20	LMS, Graw	Vaisala, Meteolabor, Snow-White, Multithermistor, Daqiao	1	LMS, Vaisala, Snow white	7
-20 to -40	LMS, Graw	Vaisala, Meteolabor, Snow-White, Multithermistor, Daqiao	1.5	LMS, Vaisala, Snow white	10
-40 to -60	LMS, Graw	Vaisala, S-W, Multithermistor,	2.5	LMS, Vaisala, Snow white	12.5
-60 to -70	LMS, Graw	Vaisala, Multithermistor,	3	LMS, Vaisala, Snow white	14.5
-70 to -80	LMS, Graw	Vaisala, Multithermistor,	3	LMS, Vaisala, Snow white	16

Table 8.1.1: References used in the processing of the statistics and the resultant error in linking the results from the LMIJ and CHGM groups.

The processed results are separated into humidity bands, because the errors in some systems vary with relative humidity and for instance in the first two WMO Radiosonde Comparisons none of the sensors had uniform performance across the whole relative humidity range. Thus, just performing an average difference for all humidity can be quite misleading, since positive errors in one humidity range would cancel negative errors in other humidity ranges. The range of relative humidity values that were sampled in the Yangjiang test is illustrated in Figs. 8.1.1(a) and (b). Flights 12 to 24 were in a mixture of conditions in terms of cloud at the uppermost levels in the troposphere, with one Vaisala flight showing very low humidity in the upper troposphere, whereas in Flights 33 to 48 the two flights showed relatively low humidity were both measured by Snow White.

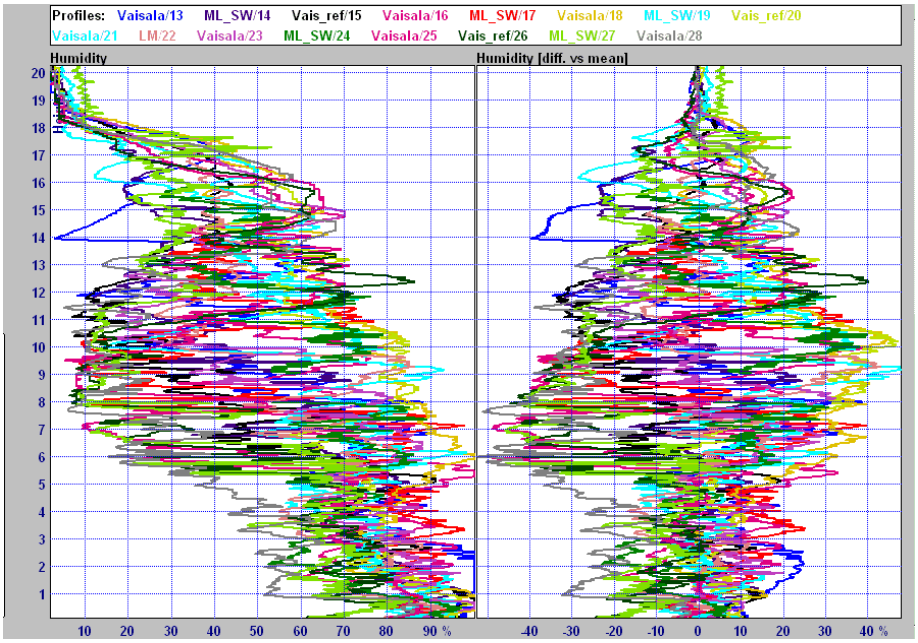

Fig. 8.1.1 (a) Summary of relative humidity measurements from 12 consecutive flights early in the test.

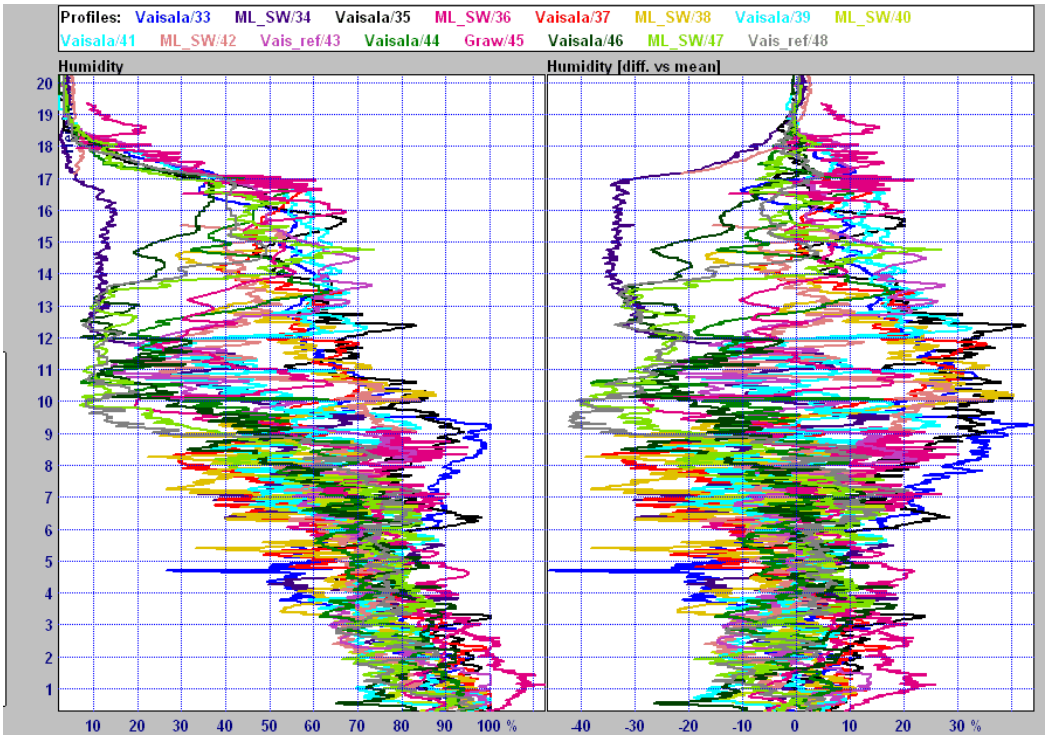

Fig. 8.1.1 (b) Summary of relative humidity measurements from 12 consecutive flights just before and following typhoon Chanthu.

The quality of these lower than usual Snow White Vaisala humidity measurements in the upper troposphere will be discussed when looking at the detail of flights, in section 8.1.3.

Fig. 8.1.2 shows the systematic biases for the relative humidity band 80 to 100 per cent, separated into day and night, and the results should be considered in conjunction with the random errors shown in Fig. 8.1.3. In this humidity band, InterMet and Jinyang had significant differences in performance from the other E+E sensors, Huayun, Graw and LMS. It is noted that there is more than one model of the E+E sensor and more than one way of interfacing and calibrating the sensor (see section 3.3 and Table 4.1.1). Hence, the methods and type of sensor used clearly matter, and the E+E sensor can give poorer results if the radiosonde manufacturer has not paid attention to every detail in the sounding system of sensor plus mount plus protective cap and to the calibration at low temperatures. The InterMet measurements were clearly too low in Fig. 8.1.2, as can be seen when the measurements in cloud in section 8.3 are considered, but the error is likely to be in the calibration/software because the negative bias seems similar both day and night at these higher temperatures.

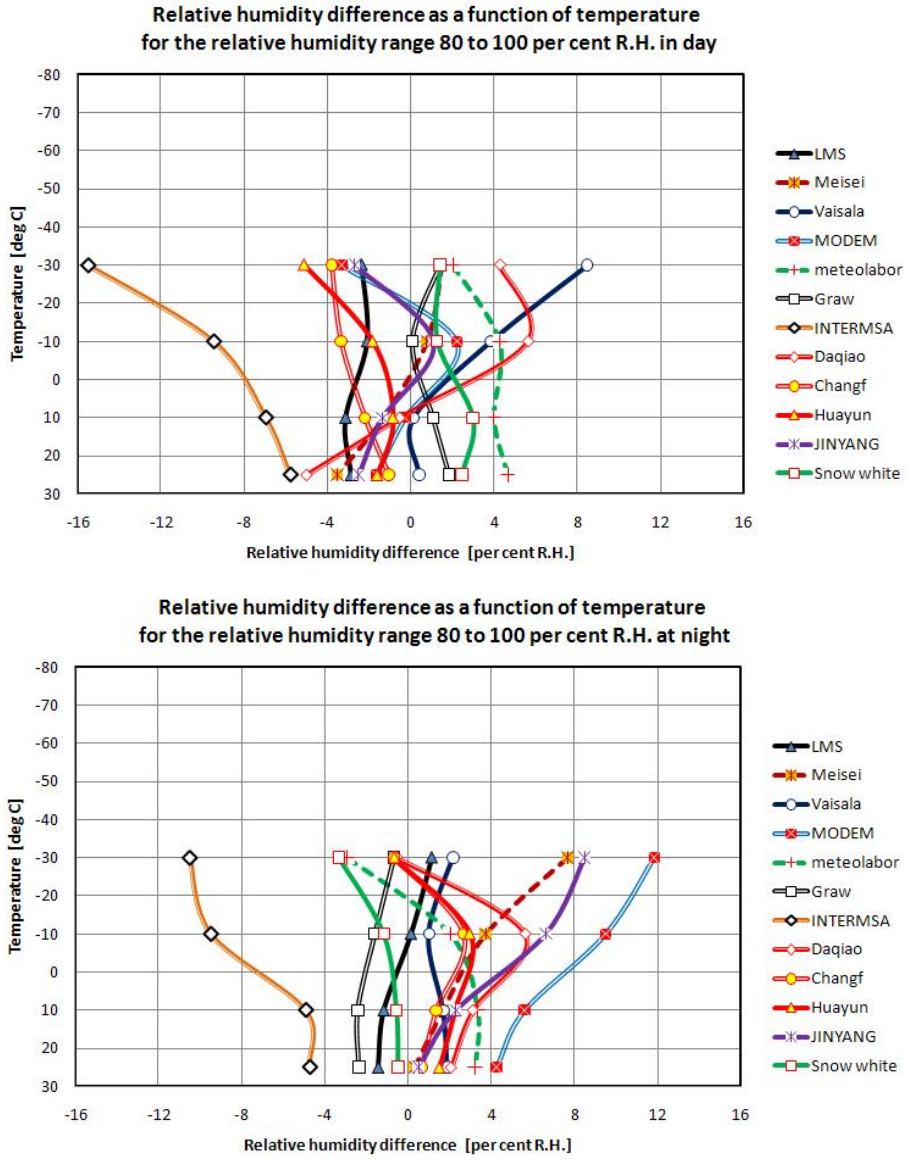

Fig. 8.1.2 Systematic bias (%) of relative humdity sensors from all QRS flights for the relative humdity band 80 to 100 per cent R.H. (Day-time top and Night-time bottom)

In Fig. 8.1.2 the Vaisala systematic bias at night does not vary with height and is essentially parallel in performance to LMS and Snow White, the other two sensor measurements used to reference the bias plot. However, in day-time the positive bias of the Vaisala measurements increased as the temperature fell/as height increased. For a systematic bias to be reported in the plots there have to be around 80 samples differenced to give the value. The sample for Vaisala at -30 deg C is on this limit. These measurements would have been in cloud. Hence, it is concluded that the day-time heating correction applied by Vaisala to the day-time humidity measurements is sometimes too big when there is cloud around.

Fig. 8.1.3 (a) and (b) shows the random errors, k=1, that were deduced from the standard deviations of the differences relative to the group working reference. Daqiao measurements were not as reproducible as the other systems.

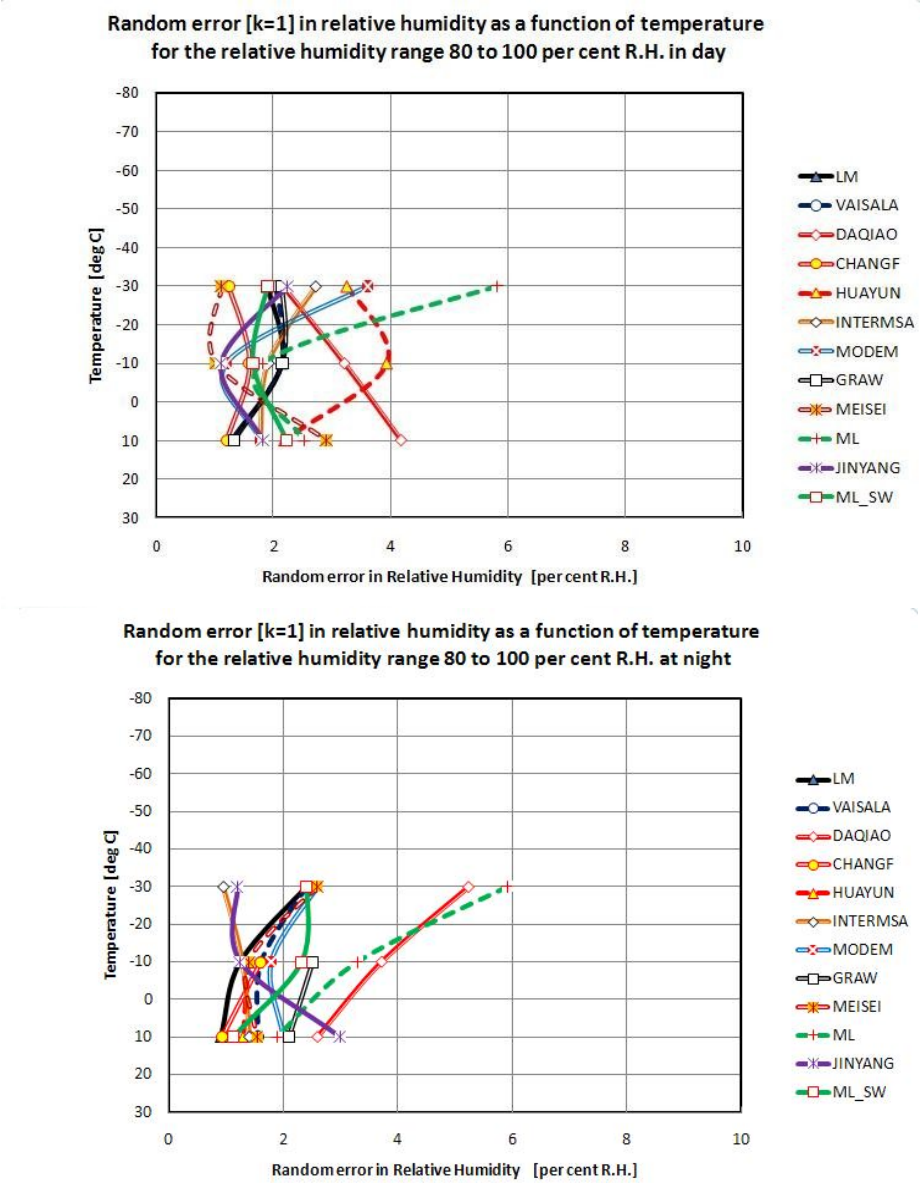

Fig. 8.1.3 Estimates of uncertainty in relative humidity measurements for measurements from 80 to 100 per cent R.H. (Day-time top and Night-time bottom)

The systematic biases for the relative humidity band from 60 to 80 per cent R.H. are shown in Fig. 8.1.4, and the associated uncertainty estimates in Fig. 8.1.5. Many of the observations at the lowest temperatures will be in cloud. Modem, Jinyang and Daqiao have significant positive biases at night, but not in the day.

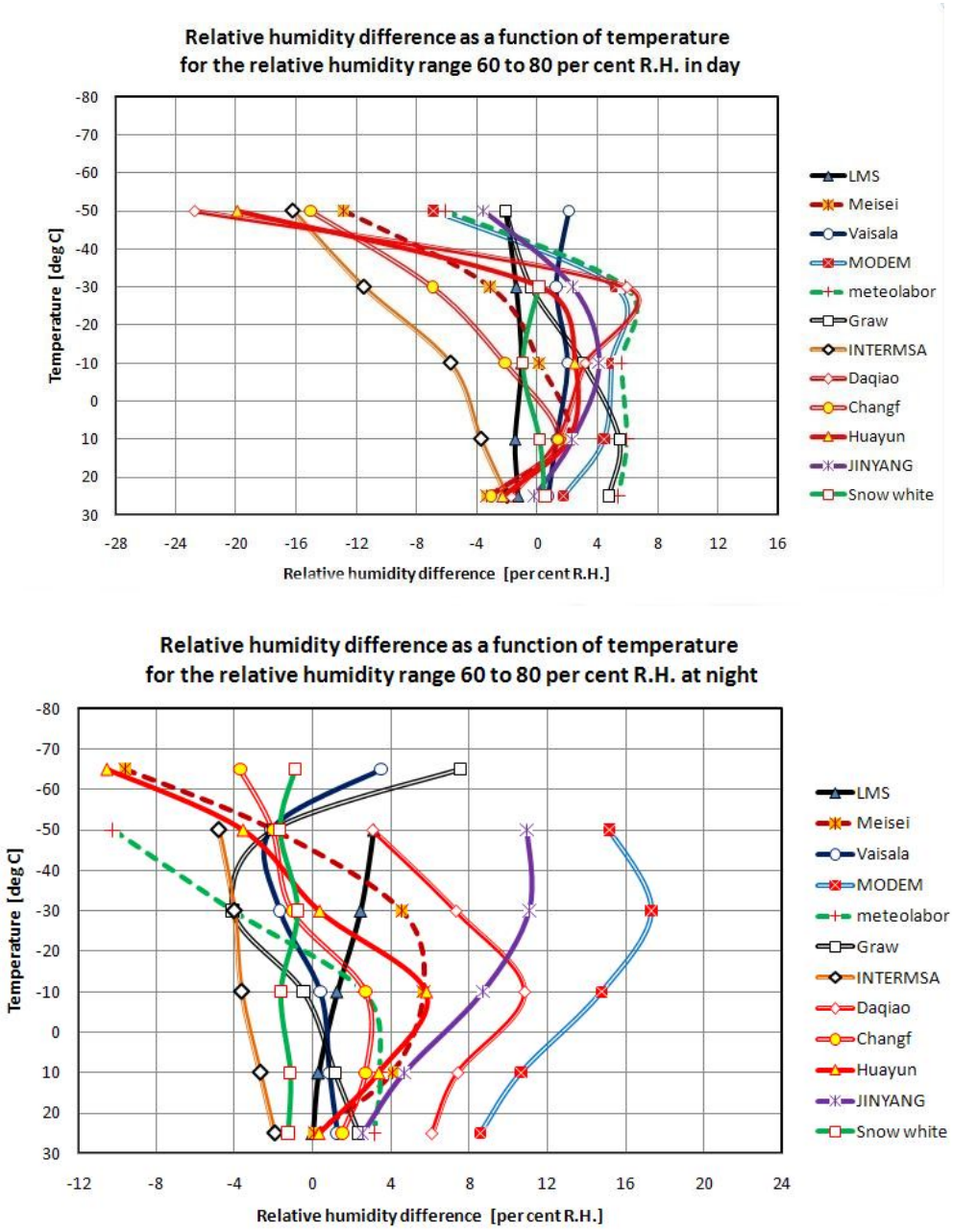

Fig. 8.1.4 Systematic bias (%) of relative humidity sensors from all QRS flights for the relative humidity band 60 to 80 per cent R.H. (Day-time top and Night-time bottom)

In Fig. 8.1.4, the day-time Vaisala measurements have been adjusted to compensate solar heating and in this relative humidity band, the correction scheme seems reasonable down to -60 deg C. This correction is not yet applied to operational Vaisala measurements

The random error estimates of the various humidity sensors associated with the systematic bias plots are shown in Fig. 8.1.5. The uncertainty in Daqiao measurements is again higher than the others are and increases rapidly as the temperature drops.

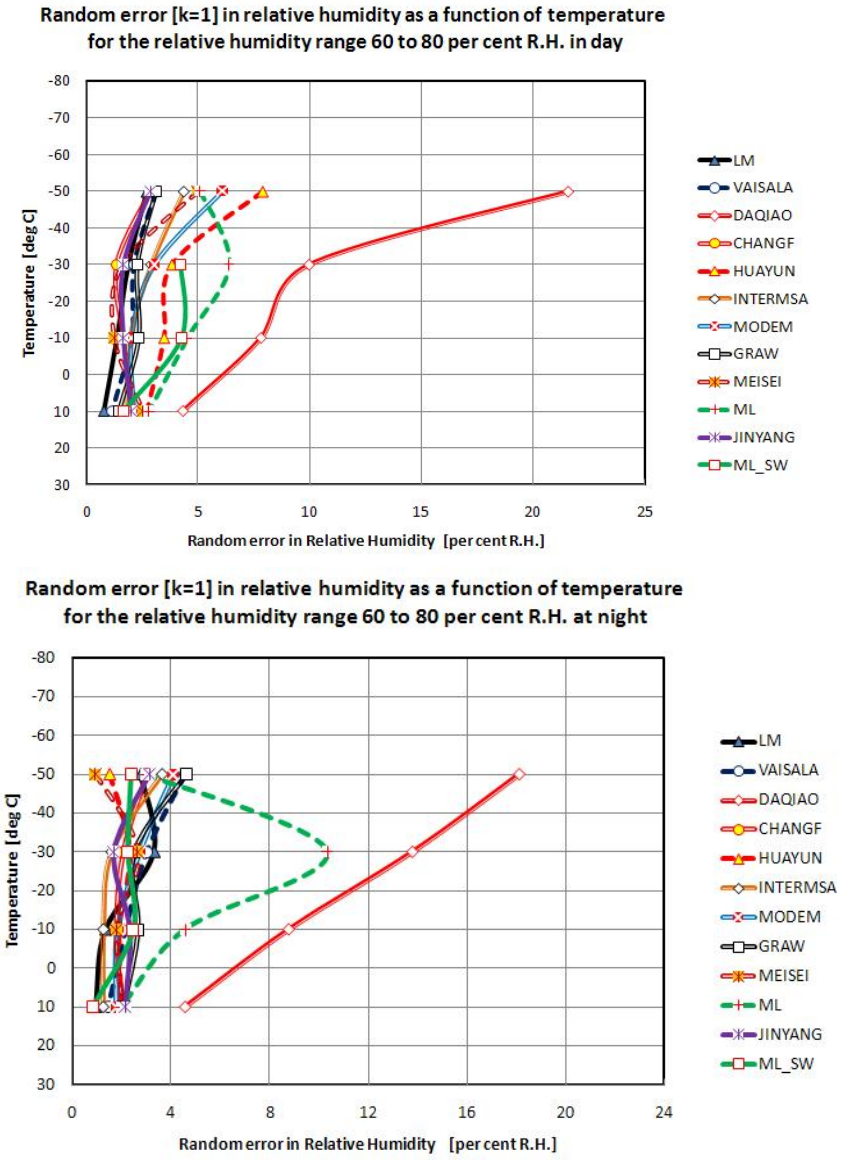

Fig. 8.1.5 Estimates of random error in relative humidity measurements for measurements from 60 to 80 per cent R.H. (Day-time top and Night-time bottom)

A similar group of plots for the relative humidity band 40 to 60 per cent R. H. is found in Figs. 8.1.6 and 8.1.7. At night, the average of Vaisala, Snow White and LMS is used as the zero reference, but Snow White is not available at the coldest temperatures in the day, so the referencing at the coldest temperatures reflects that the average Vaisala values during the day were 3 per cent higher than at night.

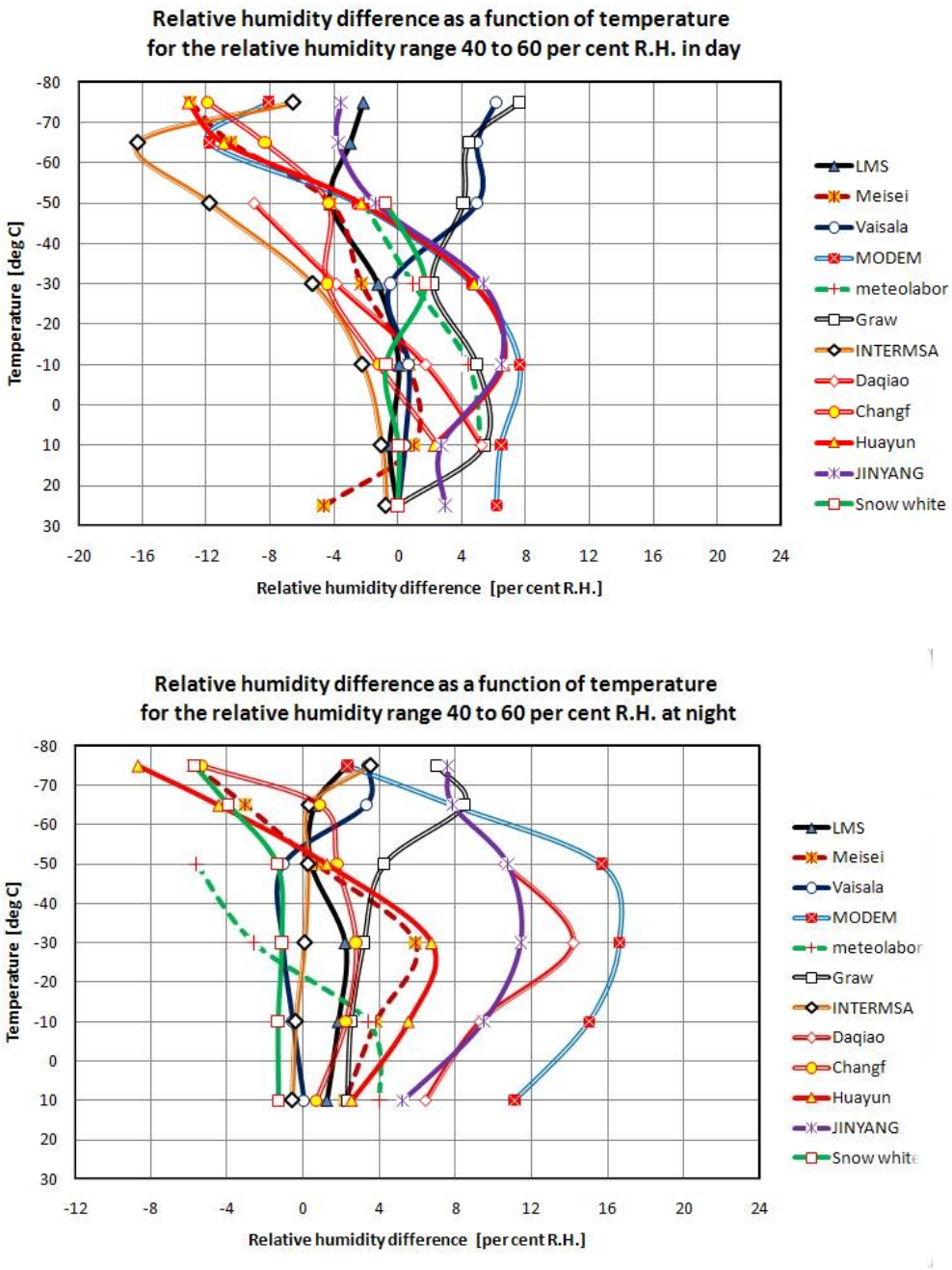

Fig. 8.1.6 Systematic bias [%] of relative humidity sensors from all QRS flights for the relative humidity band 40 to 60 per cent R.H. (Day-time top and Night-time bottom)

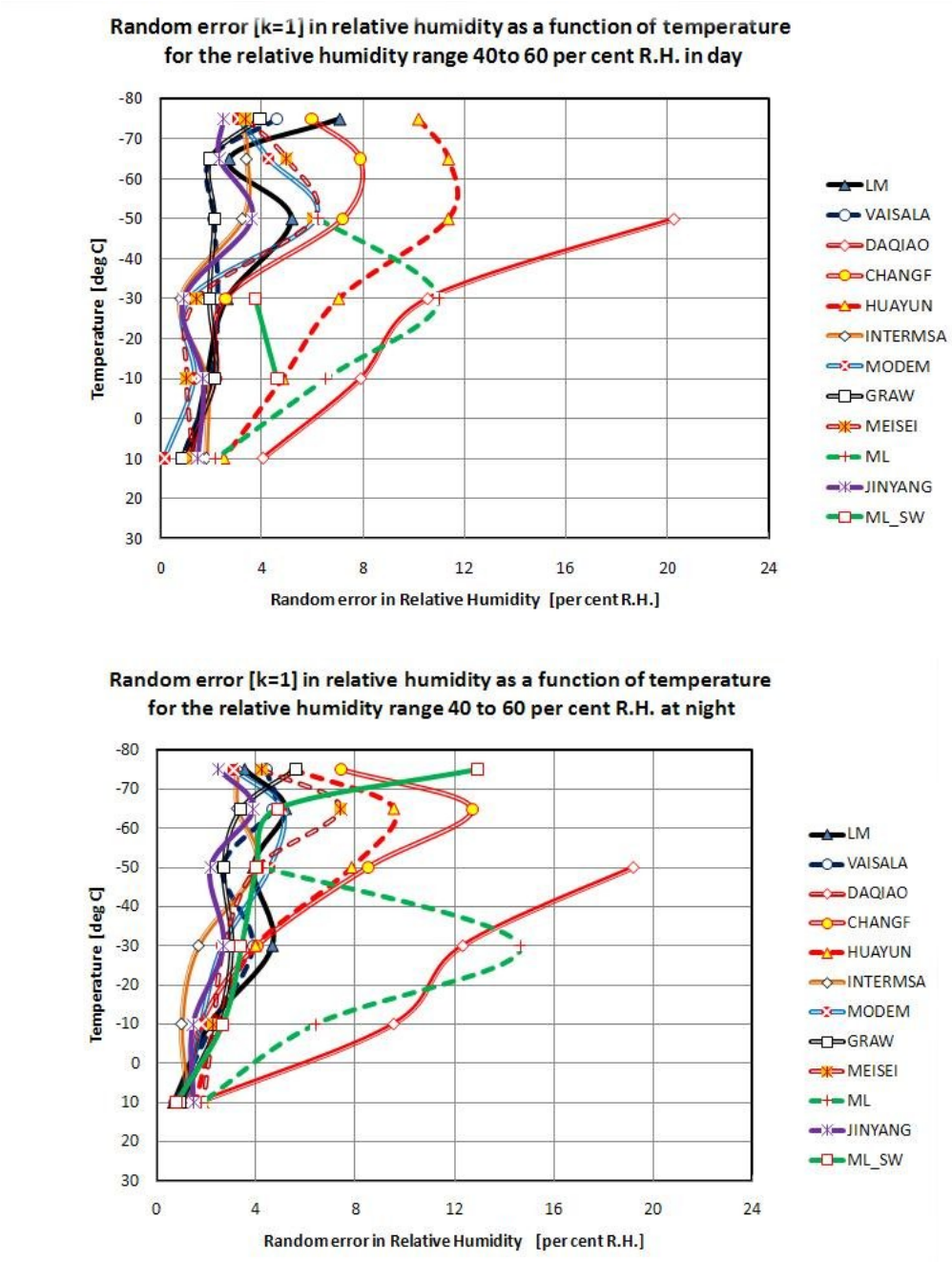

Fig. 8.1.7 Estimates of random error in relative humidity measurements for measurements from 40 to 60 per cent R.H. (Day-time top and Night-time bottom)

At the lowest temperatures in Figs. 8.1.6 and 8.1.7, the results correspond to situations when there was cloud in the upper troposphere. If systems report much lower values than the average of Snow White and LMS both day and night at low temperatures in these conditions, it implies some problem with the sensor calibration. If only day-time measurements are low, then the sensor is probably not well protected against heat contamination, and the sensor is much warmer than the value being observed by the external temperature sensor.

To assist in interpreting what is happening with the cloud, the SSI results have been processed in similar fashion, using CFH as the reference between day and night in Fig. 8.1.8 with results from the LMS Multithermistor and Vaisala. Here there are about 4 flights in day and 4 flights at night, compared to the 15 for Fig. 8.1.6. Therefore, the sample sizes in Fig. 8.1.8 are not large enough to distinguish between day-time and night-time performance. At -75 deg C, the SSI results show Vaisala about 8 per cent higher on average than LMS for high humidity compared to about 5 per cent higher in Fig. 8.1.6. CFH was higher than Vaisala at -75 deg C and about 2 per cent higher than Vaisala at the other temperatures.

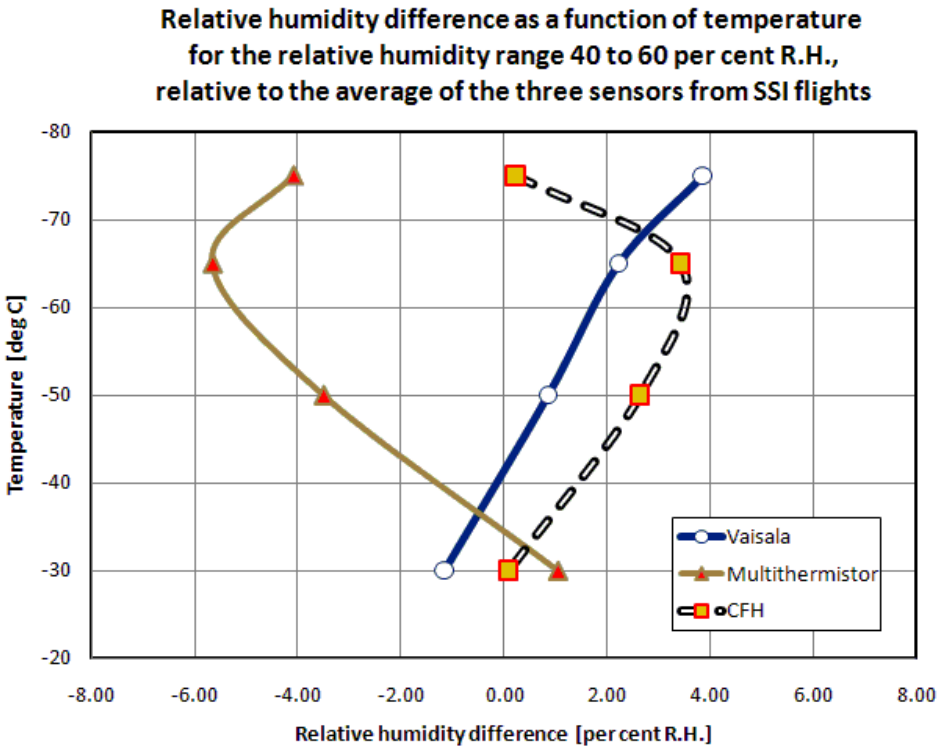

Fig. 8.1.8 Results from the SSI flights showing the differences between CHF and Vaisala and LMS relative humidity measurements in the upper troposphere, with CFH flights with contamination discarded.

How these measurements relate to conditions where high cloud was identified and the level of supersaturation with respect to ice implied by the measurements is discussed further in section 8.3. At the lowest temperatures, the Vaisala measurements are not completely independent of the CFH measurements, since the development of the Vaisala corrections has involved testing with the CFH. When compared with saturation with respect to ice the LMS observations are a little low in the day.

The group of plots for relatively dry conditions at all heights, 20 to 40 per cent R.H., are shown in Figs. 8.1.9 and 8.1.10.

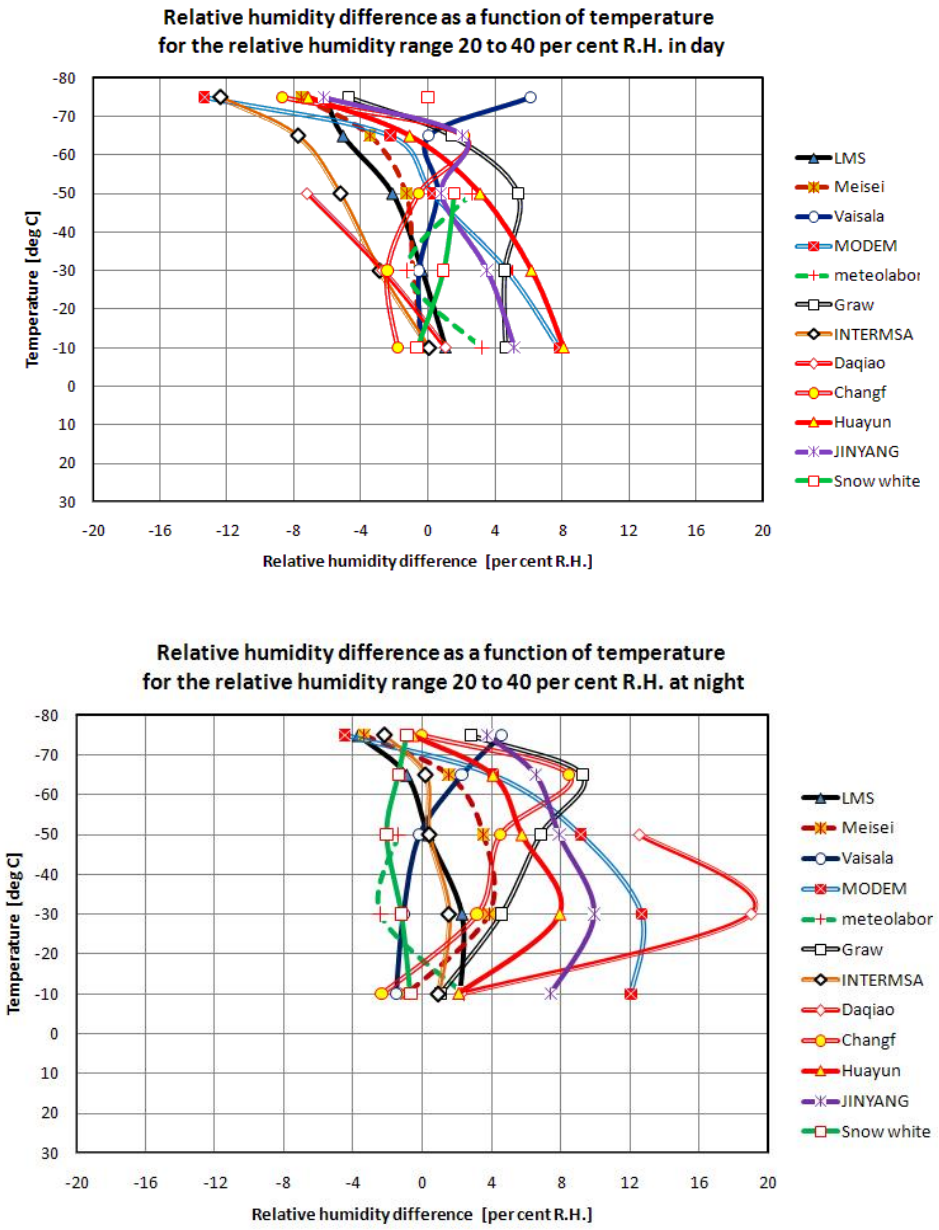

Fig. 8.1.9 Systematic bias (%) of relative humidity sensors from all QRS flights for the relative humidity band 20 to 40 per cent R.H. (Day-time top and Night-time bottom)

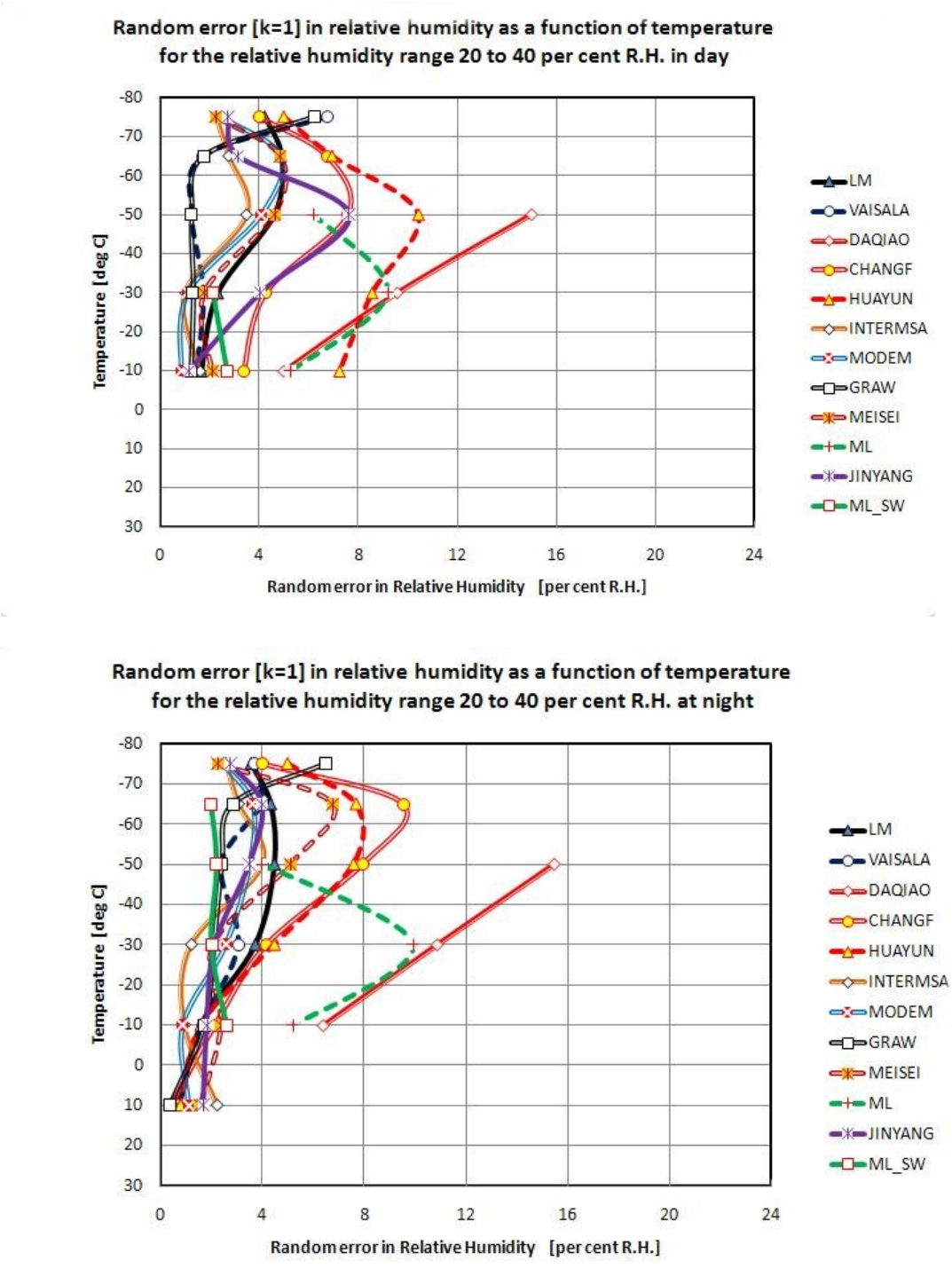

Fig. 8.1.10 Estimates of random error in relative humidity measurements for measurements from 20 to 40 per cent R.H. (Day-time top and Night-time bottom)

Finally, the group of plots for the lowest relative humidity band 0 to 20 per cent R.H., only observed above 5 km at Yangjiang are shown in Fig. 8.1.11 and 8.1.12. If the primary reason for day night bias is heat contamination of the humidity sensor in the day, then at these low R.H. values day-night difference should be small.

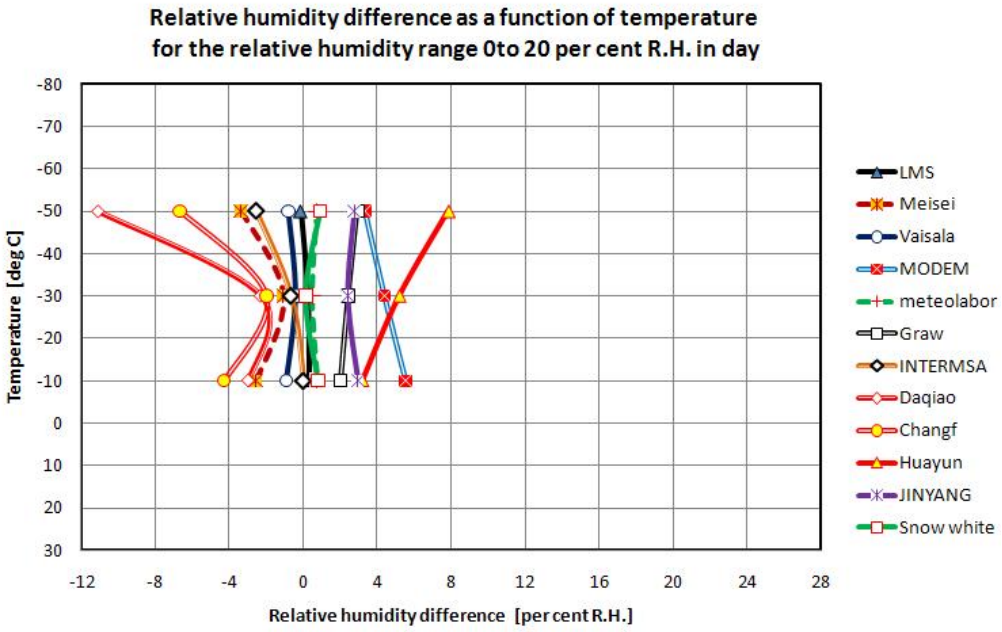

.

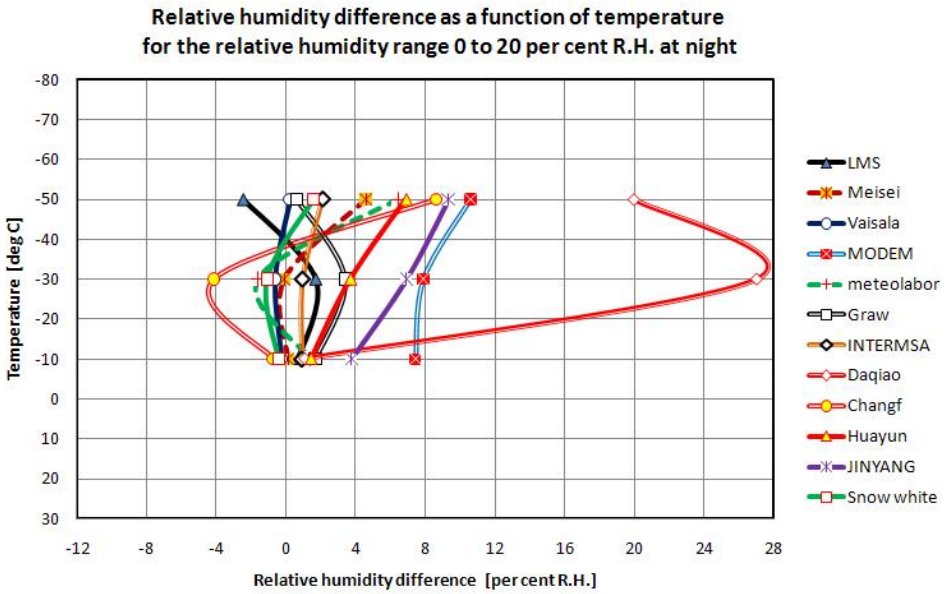

Fig. 8.1.11 Systematic bias (%) of relative humidity sensors from all QRS flights for the relative humidity band 0 to 20 per cent R.H. (Day-time top and Night-time bottom)

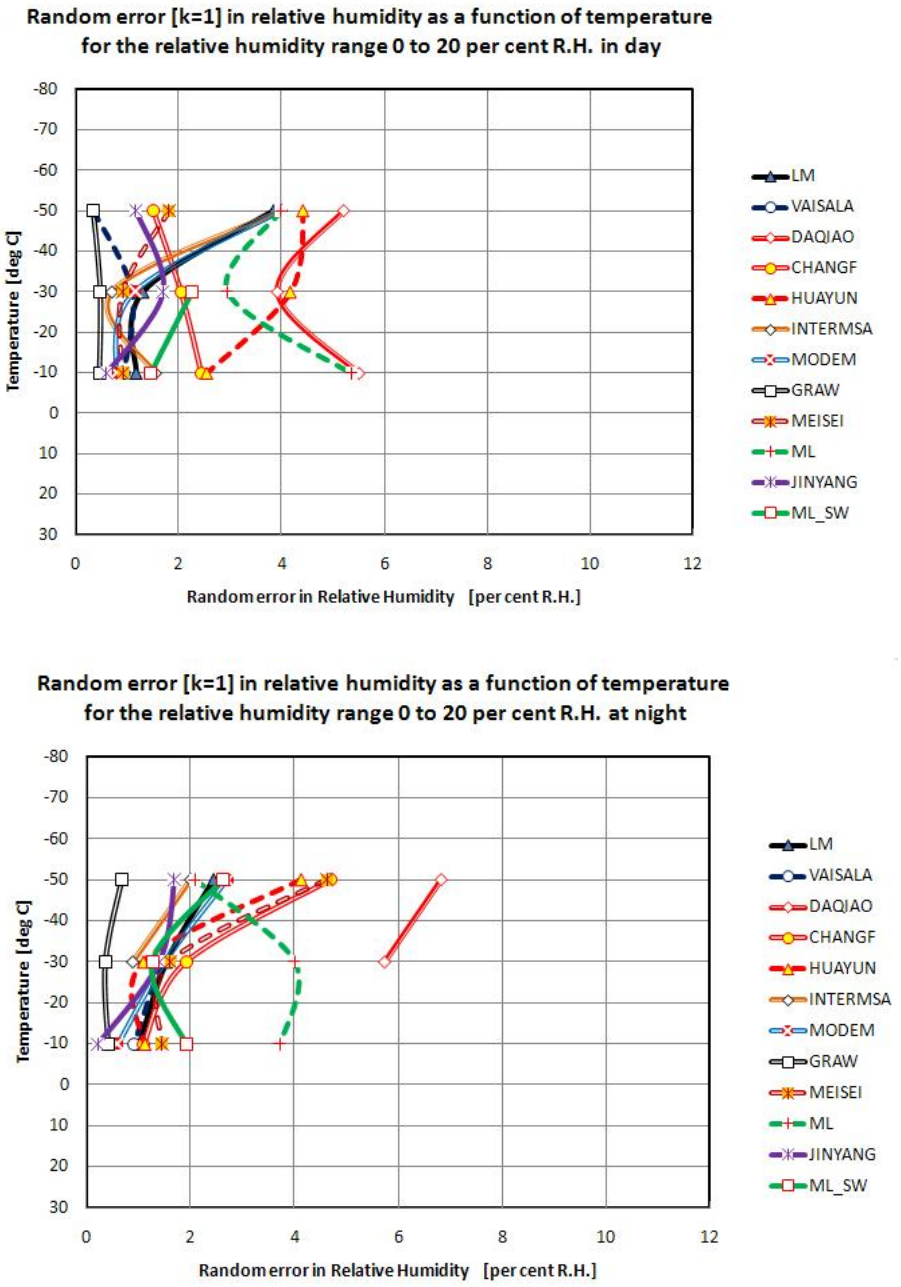

Fig. 8.1.12 Estimates of uncertainty in relative humidity measurements for measurements from 0 to 20 per cent R.H., Vaisala were close to LMS. (Day-time top and Night-time bottom)

The results in Fig. 8.1.12 represent very good sensor performance, since the measurements were made in shallow dry layers, not dry layers with extensive vertical extent, so any contamination around the sensor is likely to produce a significant bias, see Daqiao and Modem at night.

Comparing with the results from Mauritius, Snow White had much lower random errors in the 20 to 40 per cent R.H. band, but higher random errors were still observed in the 40 to 60 R.H. band especially at the lowest temperatures. This may be because of errors in the Snow White, or slower response of the other sensors. The LMS had much lower random errors at temperatures lower than -60 deg C than in Mauritius. So random errors were either similar or better than in Mauritius, and more systems were achieving this high standard.

The Daqiao radiosonde had large random errors for most of the time in almost all humidity bands. The Meteolabor radiosonde also had larger random errors than the other radiosondes. This sensor was not used in the Mauritius radiosonde test, since only Snow White measurements were reported by Meteolabor in Mauritius. Thus in Yangjiang, there were 10 humidity-sensing systems that had low uncertainties in the measurements in the low and middle troposphere, and these would all have satisfactory time constants of response at these heights.

Huayun measurements had higher random errors in daytime conditions at middle and lower relative humidity, and Changfeng had higher random errors at night in similar relative humidity bands at lowest temperatures. Overall, there were 8 humidity-sensing systems that were close together in terms of random error and well within operational user requirements for upper troposphere humidity. Here it is important to look at examples from individual ascents to identify whether good reproducibility is associated with an acceptable time constant of response in the sensing system.

The systematic bias estimates show that Modem night-time measurements had large positive bias greater than 10 per cent for much of the time in the lower and middle troposphere. Biases of this magnitude were also seen in the Mauritius test. Jinyang also had large positive biases at night, and InterMet strong negative bias at high humidity. Therefore, this leaves about 7 radiosonde types with better quality relative humidity measurements in the lower and middle troposphere.

In the upper troposphere, most of the conventional radiosonde humidity sensors are not responding fast enough to observe the correct relative humidity within 10 per cent, so many of the sensing systems, see Annexe D, like Vaisala and Graw, are using software corrections to obtain better estimates of the true value. The benefits and problems using these types of correction procedures are considered in detail when examining individual measurements in detail, later in this chapter and in Annex D.

The three radiosonde systems that have large positive or negative biases in the lower and middle troposphere, but low random errors in the measurements are Modem, Jinyang, and InterMet.

The day-night differences, corresponding to the systematic bias plots already shown are presented for all the QRS systems as a function of relative humidity in Fig. 8.1.13.

Day-night difference of relative humidity as a function of temperature and relative humidity for InterMet

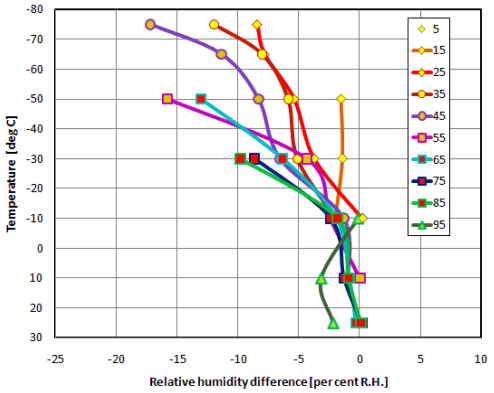

Day-night difference of relative humidity as a function of temperature and relative humidity for Modem

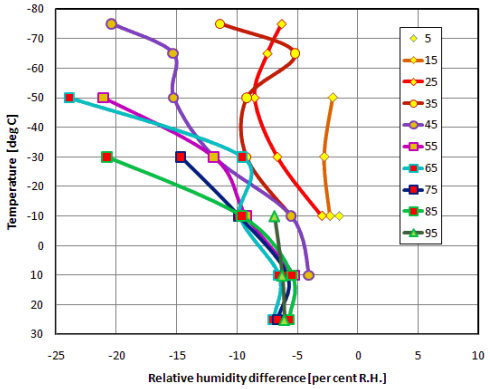

Day-night difference of relative humidity as a function of temperature and relative humidity for Graw

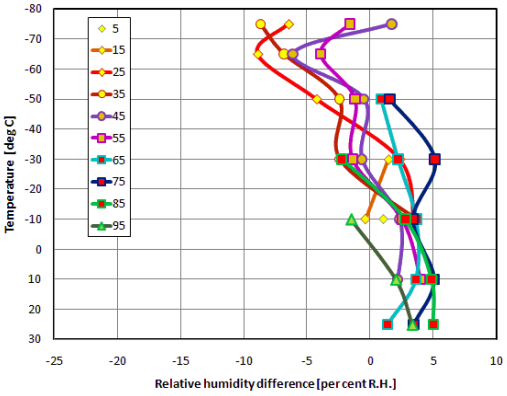

Day-night difference of relative humidity as a function of temperature and relative humidity for Meteolabor

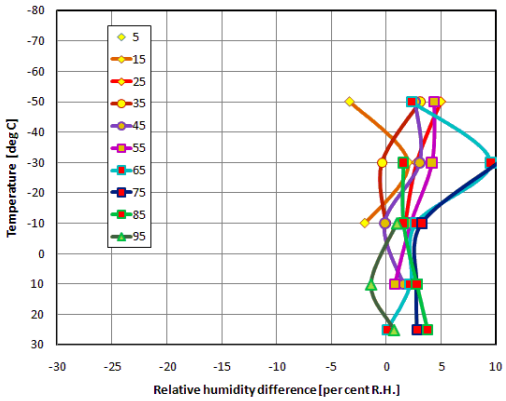

Day-night difference of relative humidity as a function of temperature and relative humidity for Daqiao

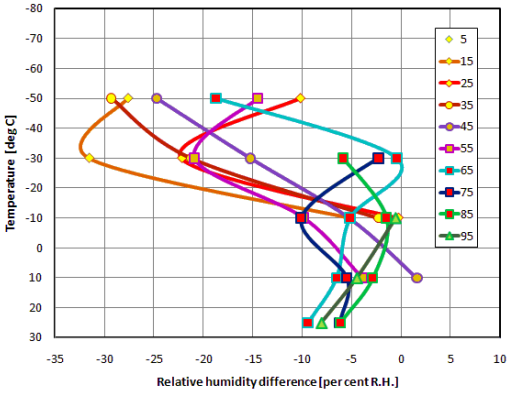

Day-night difference of relative humidity as a function of temperature and relative humidity for Jinyang

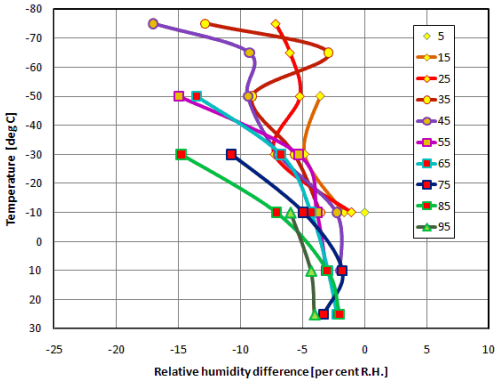

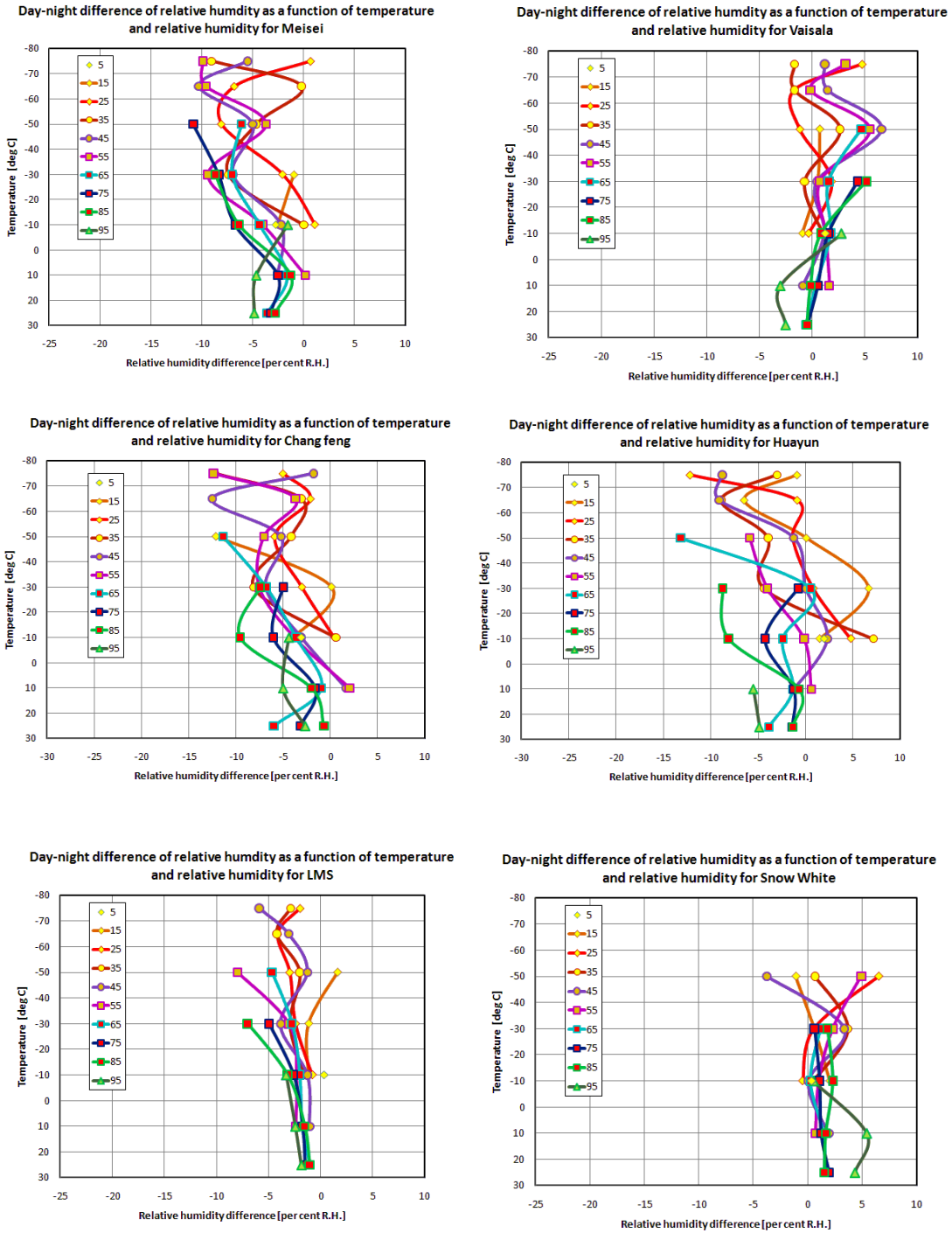

Figure 8.1.13 Day-night difference in systematic bias of relative humidity plotted against temperature for relative humidity bands centred 10 per cent R.H. apart, for all QRS.

Snow White has a small positive day-night difference, but remember that the two instruments are not identical and the daytime duct is likely to have positive bias around low cloud, and also generally some water vapour contamination at upper levels. The Meteolabor system also has small positive bias day to night, and is using a temperature sensor to measure the temperature of the relative humidity sensor. Vaisala had positive day-night humidity bias at higher humidity, indicating that possibly the correction scheme applied to day-time values may be a little too big there.

For the E+E sensors, LMS rely on a dedicated temperature sensor to measure the temperature of the humidity sensor, and have small negative day-night differences at all levels. InterMet have a similar sensor, but the system software was not working correctly, so the day-night differences were large at upper levels at temperatures lower than -20 deg C These were typical of a sensor with a temperature error, with small day-night difference at low relative humidity. Jinyang had quite similar day-night differences without a dedicated temperature sensor. Graw also did not use a dedicated temperature sensor, but added a software correction to daytime measurements, which varied from about 7 per cent near the ground to 15 per cent in the upper troposphere (see Annex D). The effect of this was to give a positive Graw day-night difference over much of the temperature range, but not at the coldest temperatures. Huayun day-night differences are not as coherent with temperature as the other systems, indicating that there were more problems with the way this sensor was implemented than in the other radiosondes using E+E sensor.

Modem also used a temperature sensor to measure the temperature of the relative humidity sensor. In this case, one of the main problems was the strong positive bias at night, and it is probable that software correcting for radiative effects on the daytime humidity temperature sensor was also applied to the night-time measurements contributing to the positive bias at night. In any case, the day-night differences at coldest temperatures have the characteristics of a humidity sensor with wrong temperature applied, whether it be night or day. Near the surface there appears to be a negative day-night difference of about -5 per cent R.H., which is there in all humidity bands.

Of all the sensors, Daqiao has the largest day-night difference. Near the ground this could be up to -10 per cent. The Daqiao systems does not use an aluminised protective cap, so even if the ventilation were good the humidity sensor will heat up much more than the other radiosonde systems in Yangjiang, so this low level negative bias may partly come from this. However, at the upper levels the negative day-night differences became very large, with the largest difference at low humidity rather than high humidity. This is the result of water vapour contamination at night and this may also contribute to the low level day-night differences.

Finally, Meisei and Changfeng day-night differences were quite similar, with evidence of the humidity sensor warming up in day for the layers from 0 to -60 deg C, and results difficult to interpret at the coldest temperatures.

8.1.3 Examples of relative humidity structure from individual flights

8.1.3.1 Lower and middle troposphere

The conditions in Yangjiang were extremely good for testing relative humidity sensors, because there was a lot of fine structure in the relative humidity profiles. Therefore, the uncertainties shown in the preceding section were not low because there was little vertical structure in the atmosphere. The examples shown below were chosen to illustrate this.

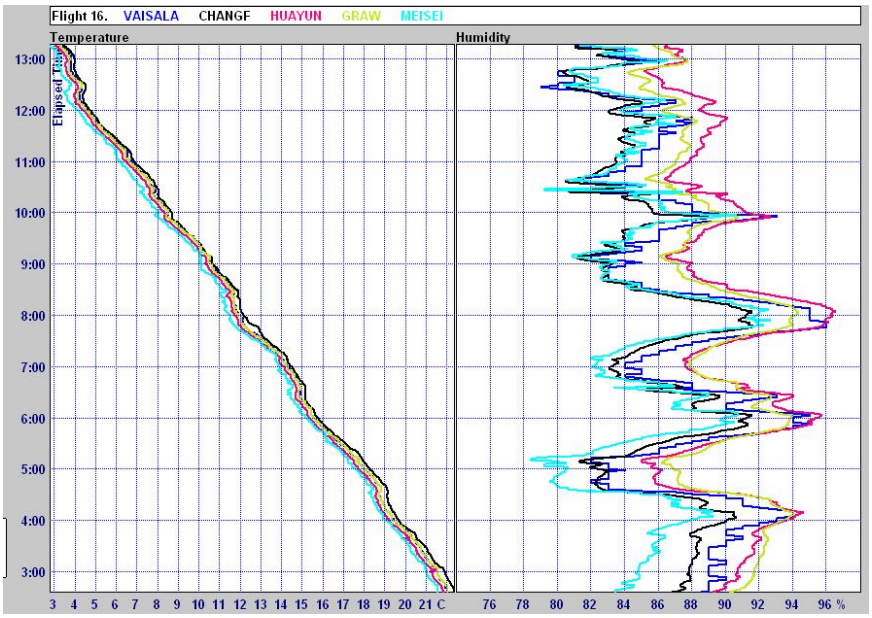

Fig. 8.1.14 (a) Sample of detailed vertical structure from an individual daytime flight, CHGM group plus Vaisala. Sample centred at about 3 km above the ground

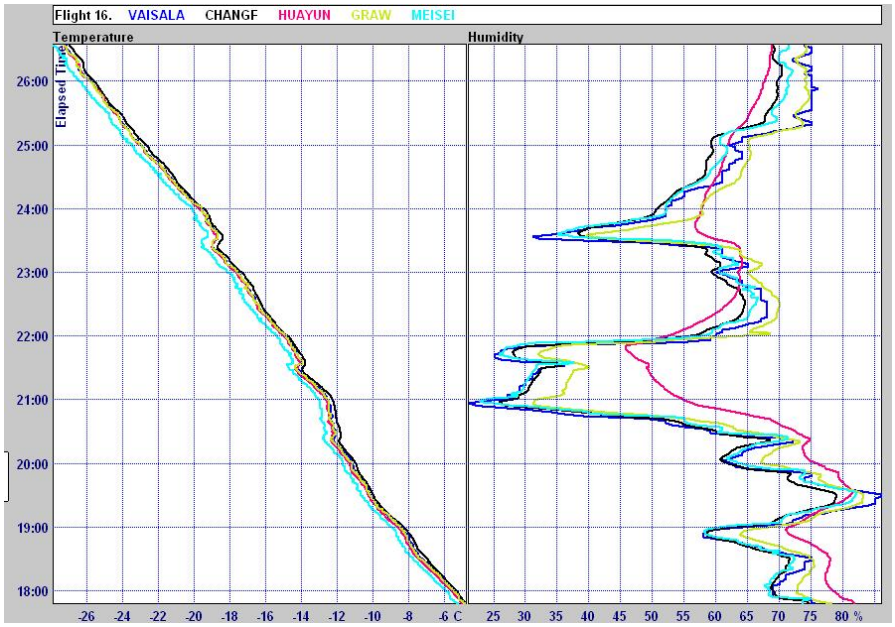

Fig. 8.1.14 (b) Sample of detailed vertical structure from an individual daytime flight, CHGM group plus Vaisala. Sample centred at about 8.5 km above the ground.

The first example (Fig. 8.1.14 (a)) is from a daytime flight, (flight 16), where the effects of small gravity waves in the humidity field were observed by the CHGM Group of QRS. In Fig. 8.1.14 (a), Vaisala shows slightly higher amplitude than the others, given the other sensors are covered by protective caps, with Graw showing least of the very detailed structures. Fig. 8.1.14 (b) shows later measurements in this flight at a height of 8.5 km, temperature of -20 deg C.

At this lower temperature, the Huayun sensor system is responding much more slowly than the other systems, even at -20 deg C. However, this is not true of all flights; see Fig. 8.1.15, where the Huayun is slightly slower than the other systems, but nowhere near as slow as in Fig. 8.1.14 (b). Thus, there was lack of consistency in the performance of the sensors incorporated into the Huayun radiosonde.

Fig. 8.1.15 Sample of detailed vertical structure from another individual daytime flight, CHGM group plus Vaisala. Sample centred at about 9 km above the ground.

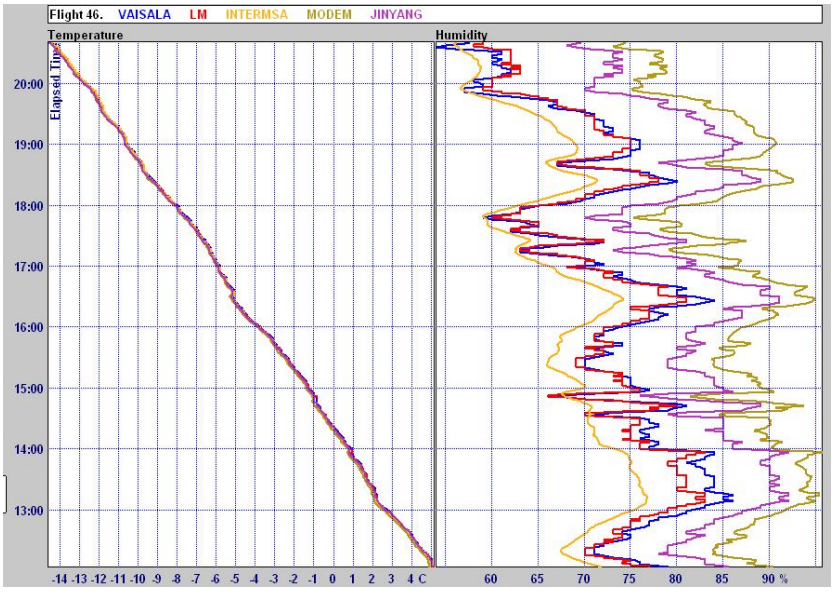

Fig. 8.1.16 (a) Sample of detailed vertical structure from an individual night time flight, LMIJ group plus Vaisala. Sample centred at about 6 km above the ground.

With the LMIJ group plus Vaisala in flight 46, LMS, Modem, Jinyang and Vaisala show similar detailed structure in the vertical (but not the same absolute values), but InterMet looks smoother, and has lower amplitude fluctuations, which could either be a difference in sensor exposure or processing software, see Fig. 8.1.16 (a).

Fig. 8.1.16 (b) Sample of detailed vertical structure from an individual night time flight, LMIJ group plus Vaisala. Sample centred at about 10.8 km above the ground

Higher in flight 46, Vaisala showed most detailed structure in a relatively dry layer, but Jinyang and Modem are showing more than InterMet and LMS which look similar but more smoothed than Jinyang, although both are nominally using similar sensors as Jinyang.

Fig. 8.1.17 (a) Sample of detailed vertical structure from an individual night time flight 17, LMIJ group plus Daqiao and Meteolabor (snow white). Sample centred at about 4.2 km above the ground

Detail from flight 17, day-time, are included in Fig. 8.17 (a) to test the ability of Daqiao, Meteolabor and Snow White to resolve fine structure in the lower and middle troposphere. Here, Snow White is fast enough to measure all the fine structure, InterMet is again too smooth, Daqiao is biased high, but shows the fine structure, and the basic Meteolabor sensor resolves a little better than InterMet.

Fig. 8.1.17 (b) Sample of detailed vertical structure from an individual night-time flight 17, LMIJ group plus Daqiao and Meteolabor (snow white). Sample centred at about 8 km above the ground

At a temperature of -15 deg C, see Fig. 8.1.17 (b), this Daqiao sensor is clearly much slower than the others are. However, in similar CHGM flight, see Fig. 8.1.18, the Daqiao sensor seems a little quicker, and the Huayun system is the slowest.

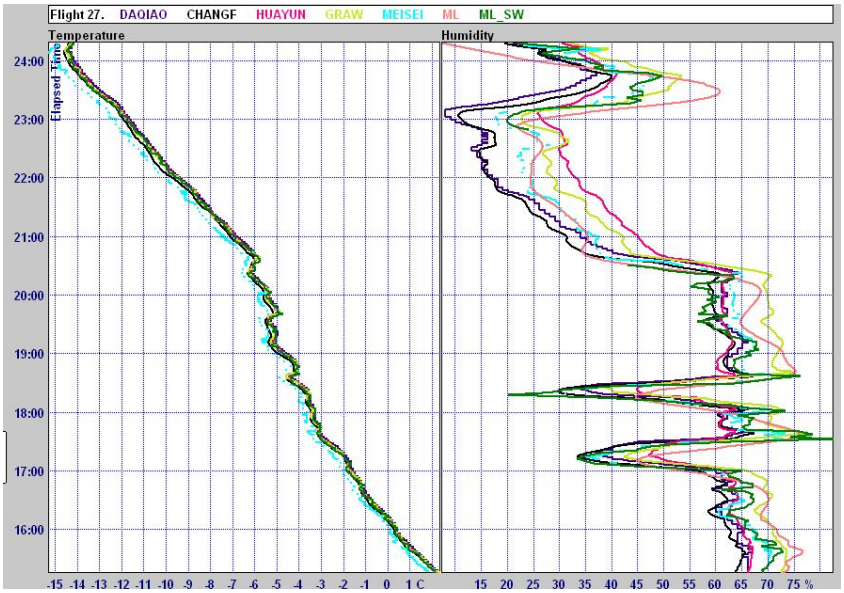

Fig. 8.1.18 Sample of detailed vertical structure from an individual day-time flight 27, CHGM group plus Daqiao and Meteolabor (Snow White). Sample centred at about 6.2 km above the ground.

Daqiao and Huayun radiosondes show evidence of a wide range of speed of response flight to flight. So every flight was examined in detail to assess the speed of response relative to the other radiosonde systems. The lowest temperature where the sensor was responding fast enough to resolve the humidity fine structure was identified. Very few Daqiao sensors were able to sense structure at temperatures lower than -50 deg C, and about a quarter did not work well at temperatures higher than -30 deg C. About a quarter of the Huayun systems, did not work well at temperatures higher than -40 deg C, and most of the other Huayun sensors were able to work well to temperatures between -40 and -60 deg C. The reasons for the problems with Daqiao and Huayun sensors are difficult to identify because there is no obvious pattern in the flight conditions where poor response occurred. The failures rates in these systems were too high for good quality operational measurements.

8.1.3.2 Upper troposphere

The upper troposphere and lower stratosphere present the greatest challenge to radiosonde relative humidity measurements, because of the low temperatures involved, down to -80 °C in Yangjiang, and because of the problems of contamination of water vapour picked up on passing through upper cloud, or in the lower layers of the atmosphere at warmer temperatures. Fig. 8.1.19 shows measurements in the upper troposphere from Flight 16. On Flight 16, the Graw data have been flagged out beyond minute 42.5, because in this early part of the test Graw were using software to make the reported relative humidity fall to a very low value once the tropopause had been identified from the temperature structure. From Flight 21 onwards, the set up was changed at the request of the WMO radiosonde expert. Then the user can see what actually happens and make his judgment about the performance of the sensor. After minute 47 in Flight 16, both Huayun and Changfeng may have applied software (not the same) to reduce the relative humidity down to a low value. Both sensors were initially responding very slowly to the drop in humidity that has occurred during the passage through the tropopause. This is considered in more detail later in this section.

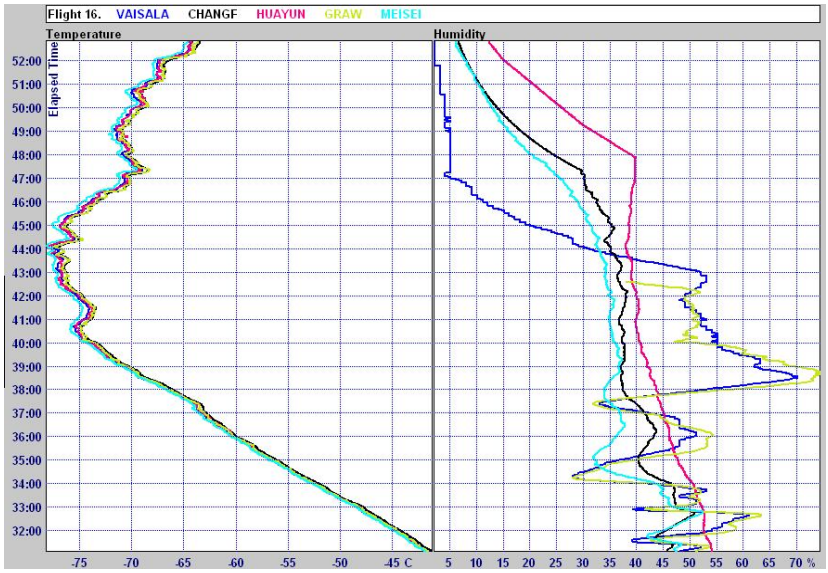

Fig. 8.1.19 Sample of detailed vertical structure from an individual daytime flight 16, CHGM group plus Vaisala. The two Chinese systems may have used software to reduce the relative humidity to a suitable value for the stratosphere.

<u>If a radiosonde operating system decides that reported values are not reliable, it should flag out the data and not report anything, rather than let the software invent values.</u>

The Vaisala time constant of response correction and daytime bias correction has led to a value of nearly 70 per cent at -65 deg C when the original raw value was about 40 per cent. Thus, the corrections have added about 30 per cent to the raw value. A similar high level of supersaturation with respect to ice was seen in a night flight (flight 43) with the SSI instrumentation. More work is required to establish the uncertainty in the corrected Graw and Vaisala observations. Another example of the effect of the time constant correction is shown in Fig. 8.1.20 (b), the raw and corrected data for the Vaisala flight shown in Fig. 8.1.1, where Vaisala report relatively low relative humidity at the upper level. Fig. 8.1.20 (a) shows the measurements from all the radiosonde types on Flight 13. The results from Graw, also time constant adjusted, support the general structure shown by Vaisala, with here the time constant of response of the other three sensors greater than 2 minutes. The raw Graw values can also be seen in Annexe D.

Fig. 8.1.20 (a) Temperature and relative humidity around the tropopause for Flight 13, with a dry layer present in the upper troposphere.

Usually the Vaisala time constant correction is not so big because the raw data is not changing rapidly with height. If these types of software correction are to be applied to routine operational measurements of relative humidity in the upper troposphere, it is essential that the procedures are well documented so that users of the data know what is happening and recognises the limitations of the technique. All sensors of a given radiosonde type must have similar time constants of response to justify using relatively large response time correction, and evidence needs to be supplied to show that this is the case. For instance in some Yangjiang flights it looks like errors/noise in some radiosonde measurements have been amplified instead of providing more reliable atmospheric structure.

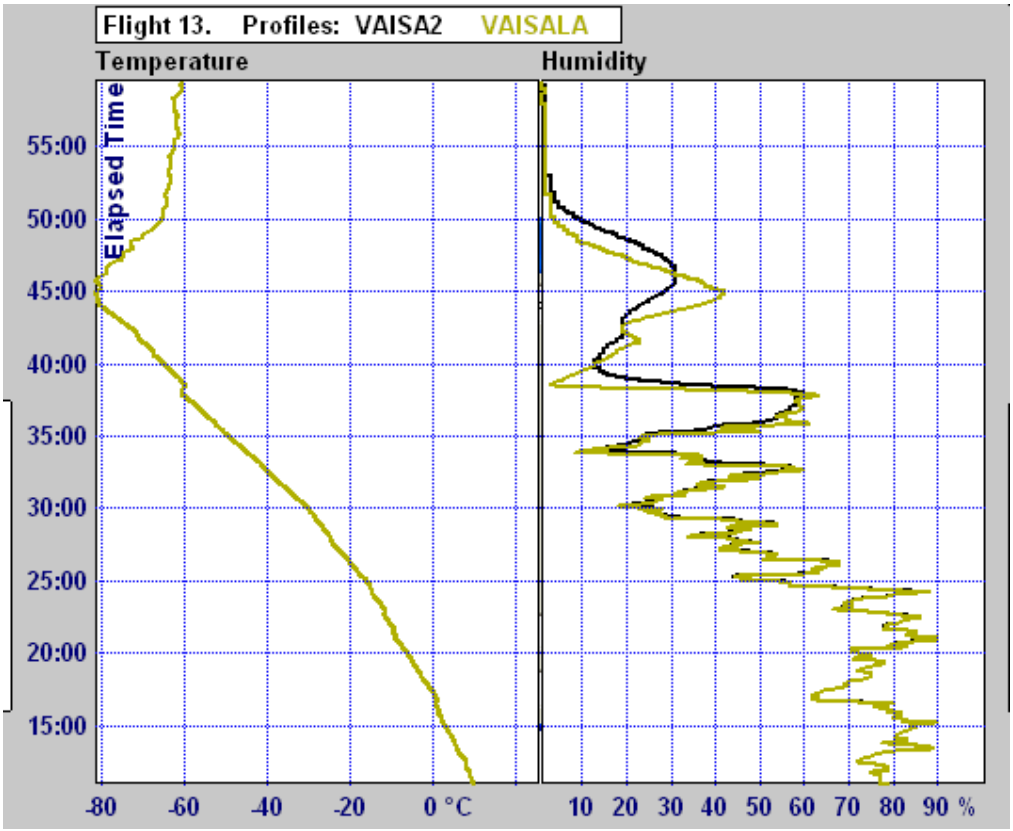

Fig. 8.1.20 (b) Comparison of Vaisala raw and corrected on flight 13 (a night-time flight).

In Flight 16, the Graw measurements show similar structure to Vaisala in the upper cloud, so the combination of basic measurements plus software adjustment for slow time constant in the Graw system has produced a similar result to Vaisala, but slightly higher supersaturation. Thus, it is quite important to ensure all sensors have identical time constants of response, and that this response time has been reliably identified.

Fig. 8.1.21 shows measurements by the LMIJ group in a cloud where Vaisala measure high levels of supersaturation with respect to ice at night. These systems have longer time constants than Vaisala raw, when responding to the large drop in relative humidity through the tropopause and do not always use software to reduce the values more quickly.

Fig. 8.1.22 shows Snow White measurements through a similar cloud on Flight 47. The Snow White shows dewpoints down to -90 deg C, frost point -86 deg C which are within a few degrees of the frost-points in the stratosphere observed by CFH, and thus do not merit flagging out. The speed of response of the sensor is high enough to respond to the transition in relative humidity through the tropopause, given the sensor is functioning correctly. On some flights the Snow White frost-point drops to -95 deg C, much lower than the CFH, and these have been flagged out, in agreement with Meteolabor and MeteoSwiss. In this flight the Snow White also shows the high degree of supersaturation with respect to ice, seen in the previous figures, although not over as deep a layer as implied by Graw measurements.

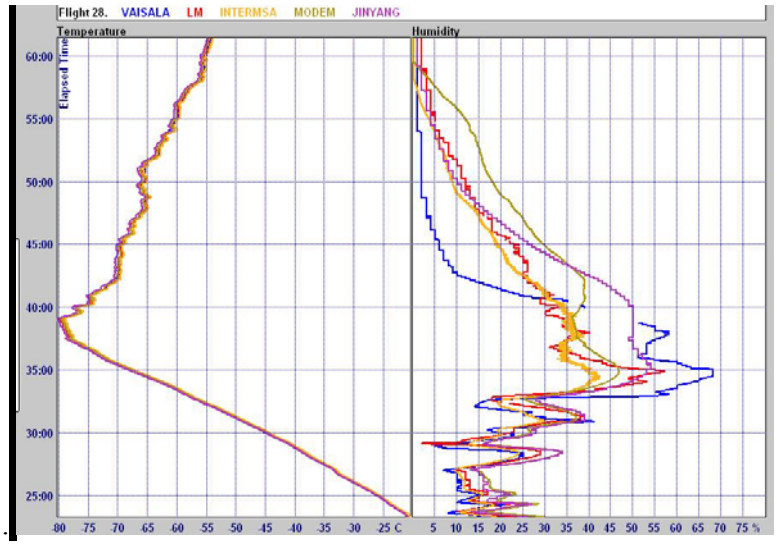

Fig. 8.1.21 Sample of detailed vertical structure from an individual night-time flight 28, LIMJ group plus Vaisala. Sample centred on the tropopause with high cloud.

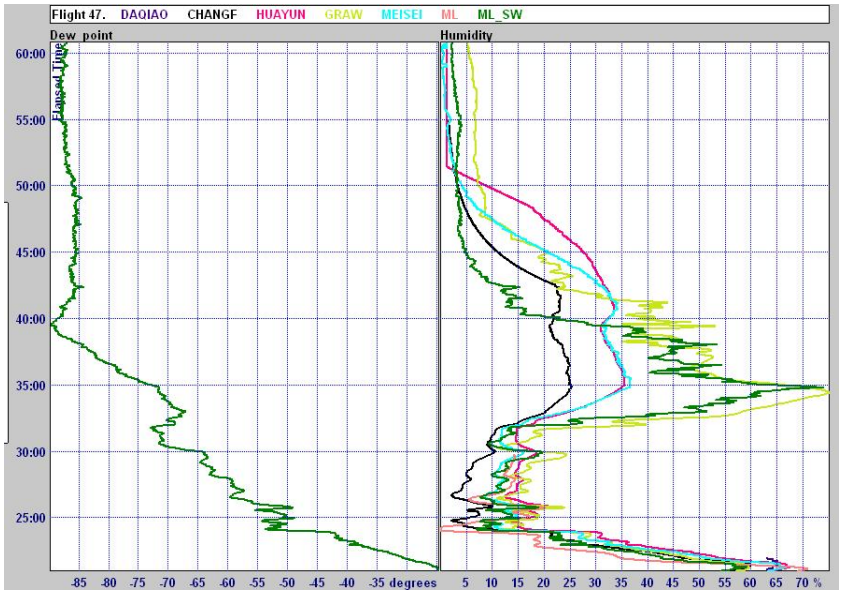

Fig. 8.1.22 Sample of detailed vertical structure in frost-point and relative humidity from an individual night-time flight 47, CHGM group plus Meteolabor (Snow White). Sample centred around the tropopause with high cloud.

Large disagreements between Graw and Snow white happened on some occasions. The low relative humidity measured in the upper troposphere before Typhoon Chantu arrived is shown in Fig. 8.1.23. The frost points measured by Snow white on this occasion are plausible in the cloud, but about 2 deg C too low in the layer where the temperature was rising immediately above the tropopause. Graw may have over-amplified a small increase in basic relative humidity near the tropopause, or Snow White is reading too low.

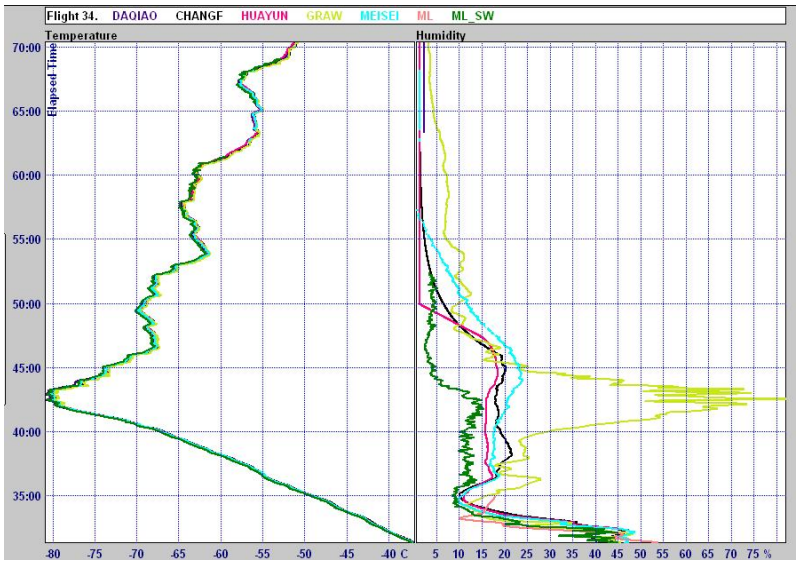

Fig. 8.1.23 Relative humidity measurements in the last test flight before typhoon Chanthu arrived near Yangjiang. The slow response sensors often showed a small increase in relative humidity when the temperature starts to warm again above the tropopause, so the rise here should not be taken as evidence that Snow-white was wrong.

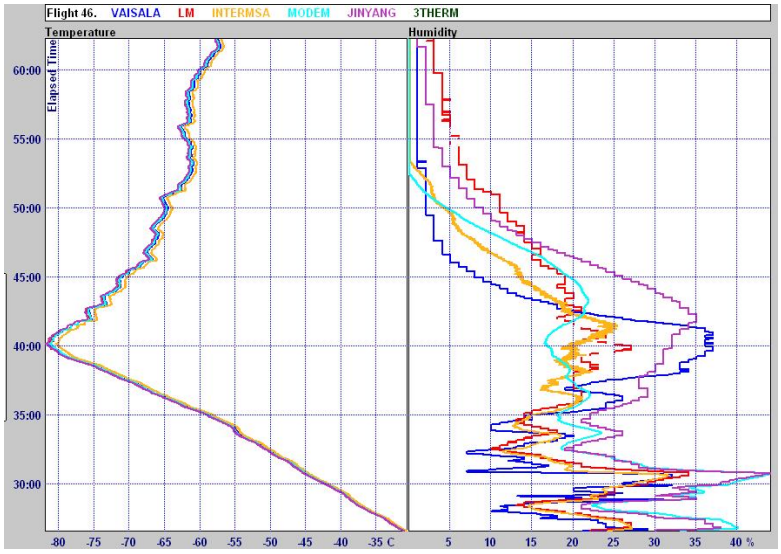

Fig.8.1.24 (a) Temperature and relative humidity as a function of time on a night time flight with dry conditions in the upper troposphere and no detectable cloud.

Another Vaisala flight, Flight 46 was showing relatively dry air in the upper troposphere in Fig. 8.1.1(b). Theses measurements that are definitely without ice contamination are shown in Fig. 8.1.24 (a). This flight shows the slower radiosondes often do not have a simple fall in humidity after the tropopause, but have some time delay and even increase before the drop in R.H. occurs. There is no reason to doubt the Vaisala measurements apart from the effect of the time constant correction in moving the maximum possibly a little too high above the tropopause. Fig. 8.1.24 (b) shows the effect of the Vaisala time constant correction near the tropopause. The maximum values were increased by about 3 per cent R.H. and the occurrence of the humidity maximum has shifted about one minute earlier in the flight.

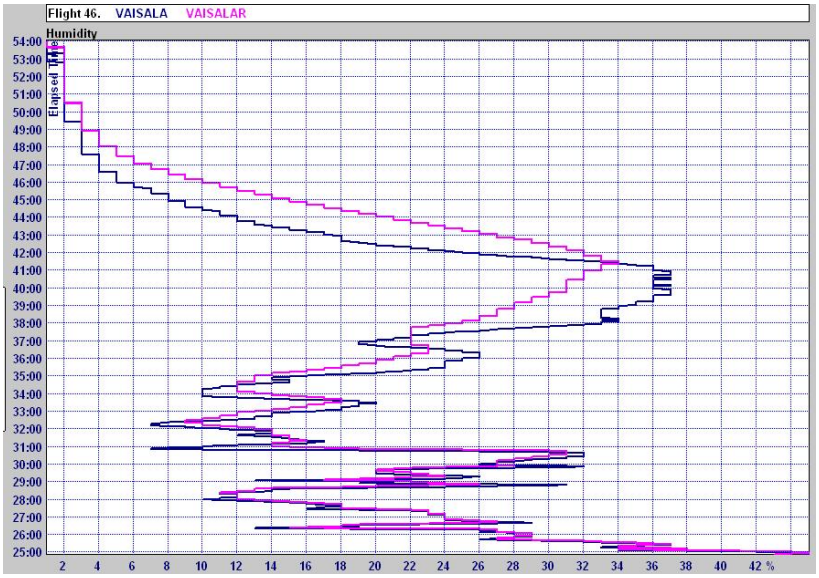

Fig. 8.1.24 (b) comparison of Vaisala raw and corrected values of relative humidity on this night-time flight.

8.1.3.3 Troposphere to lower stratosphere transition

Given the large amount of data in the upper troposphere, the transition from high to low humidity over a large number of flights is reviewed for each radiosonde type humidity sensor in Figs. 8.1.25 [CFH], 8.1.26 [Snow-White], and 8.1.27 [QRS] both in terms of relative humidity and in terms of water vapour mixing ratio. First, Figure 8.1.25(a) and (b) show the transitions from the tropopause to the stratosphere observed by the CHF instrument on the SSI flights. This uses the CHF data submitted to the WMO database, and so the values have not been averaged over 25 s intervals. However, this does not cause a problem here.

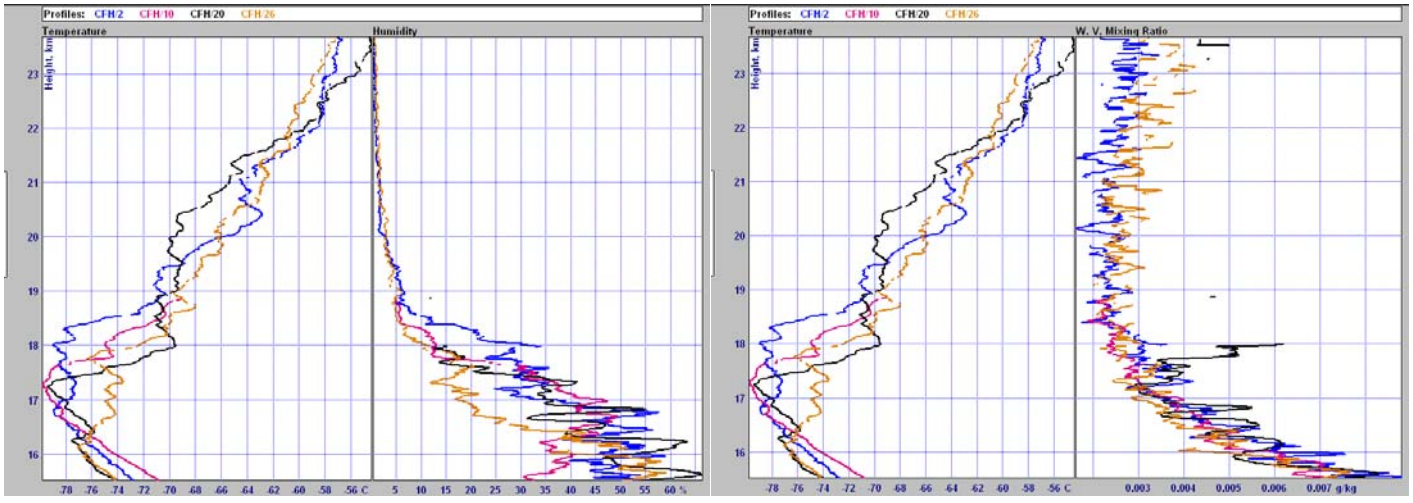

(a) CHF Flights 2 to 26

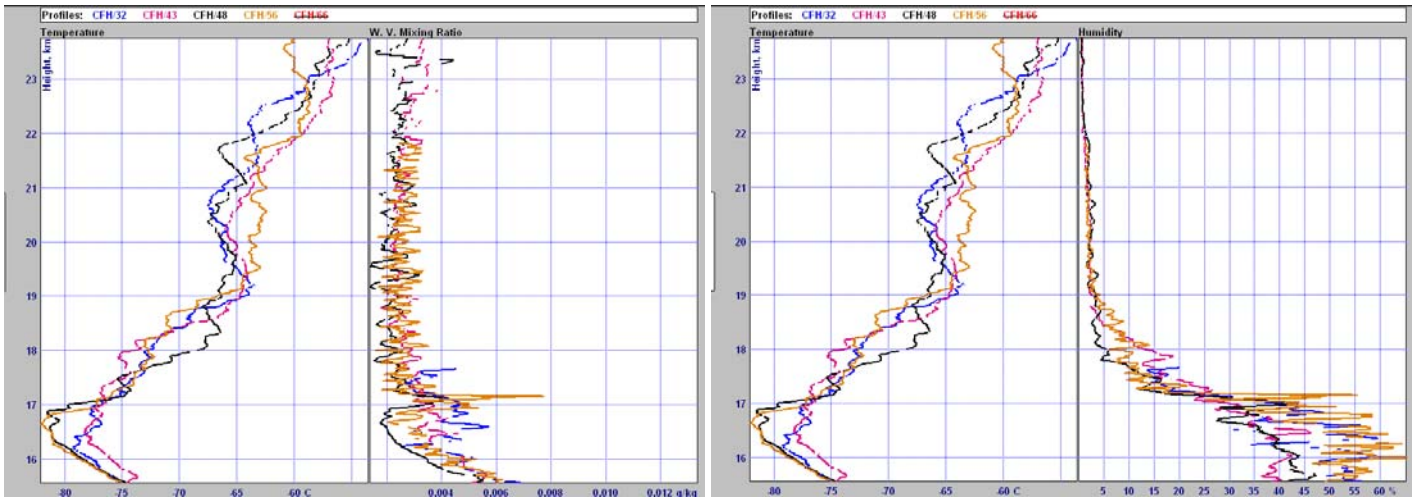

(b) Flights 32 to 56

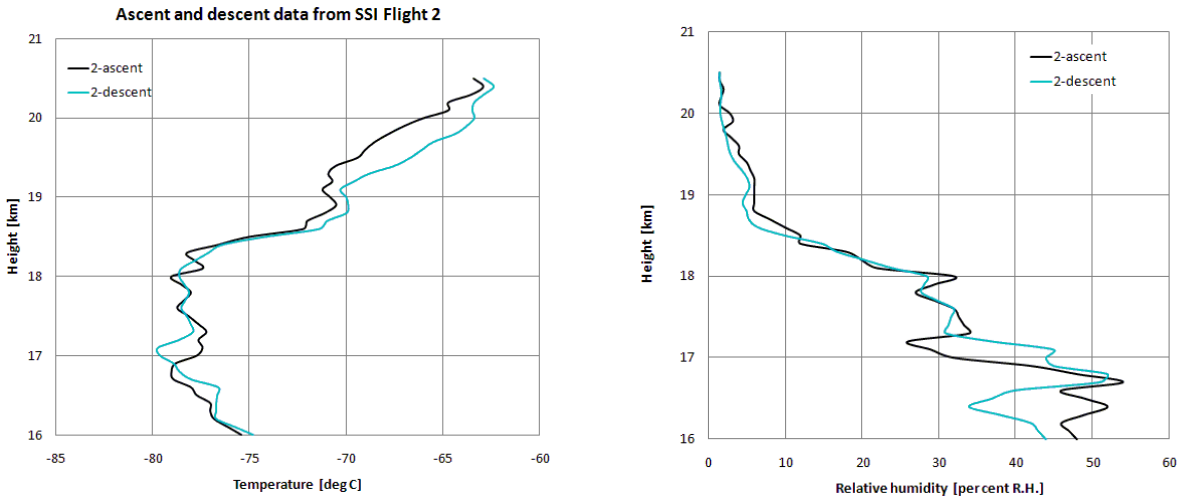

(c) CFH ascent and descent data from Flight 2

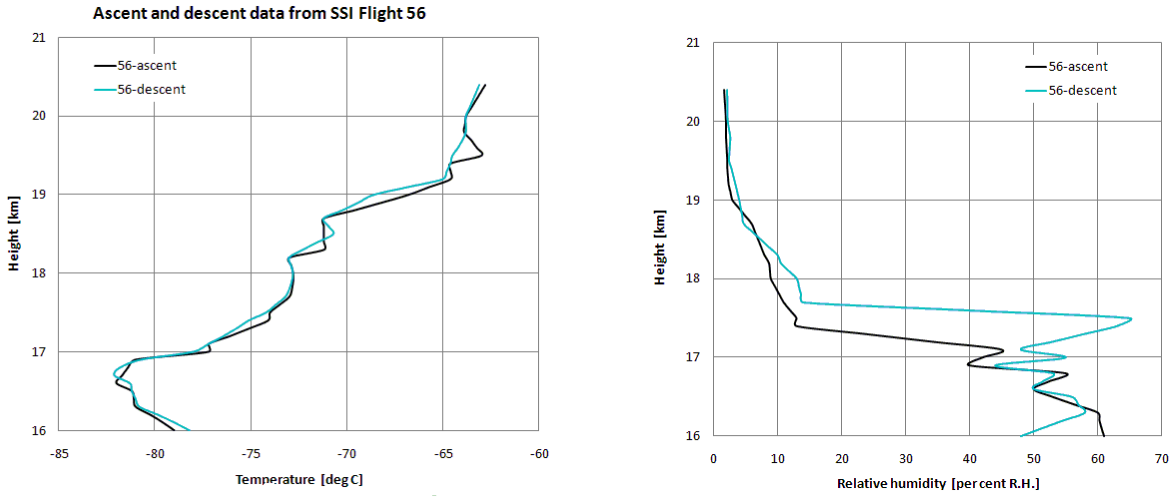

(d) CFH ascent and descent data from Flight 56

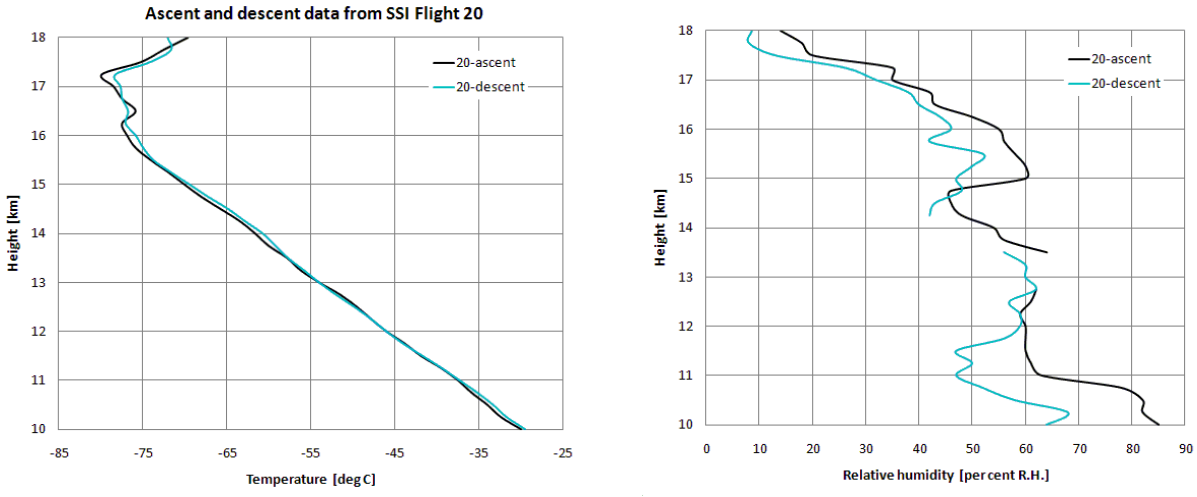

(e) CHF Ascent and descent mostly in the upper troposphere from Flight20

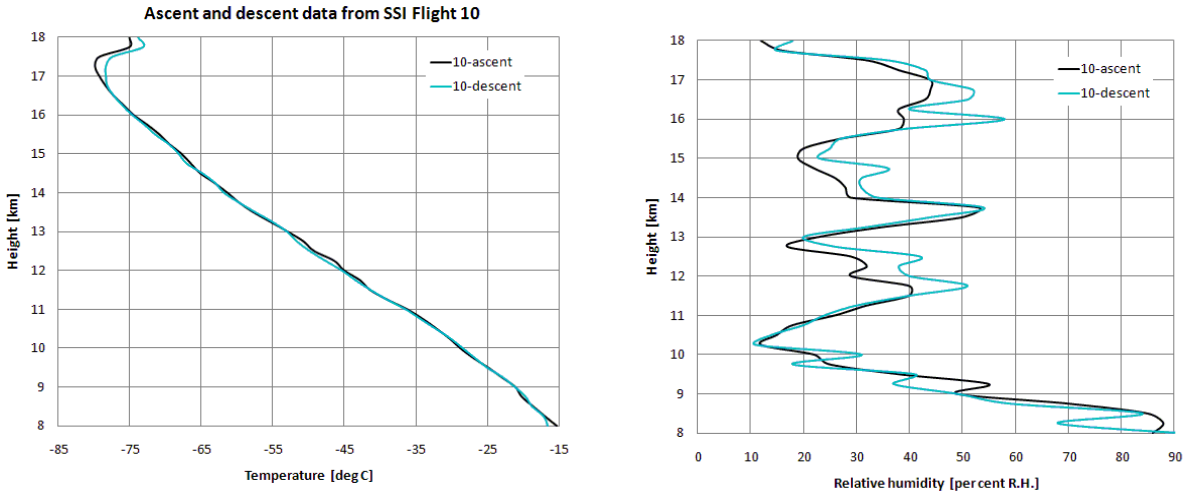

(f) CHF Ascent and descent mostly in the upper troposphere from Flight10

Figure 8.1.25 Measurements by CHF of the troposphere/stratosphere transition during SSI Flights, in terms of temperature, relative humidity and water vapour mixing ratio.

The CHF measurements in Figure 8.1.25 (a) and (b) show water vapour mixing ratio decreasing to values about 0.03 g/kg at 17 km to a minimum nearer 0.023 g/kg between 18 and 19 km. The comparison of ascent and descent observations in (c) to (f) show ascent and descent values so close that the ascent values are not in question, apart from in Flight 20 where above 17 km the ascent CHF relative humidity was high by about 10 per cent. This explains the anomalous mixing ratios at the end of flight 20 data in Fig. 8.1.25 (a).

These observations should be compared with those of Snow White in Figure 8.1.26 (a)/(b) and Fig. 8.1.28. Four of the 9 Snow Whites report much lower mixing ratios than CFH at heights between 15.5 and 18 km. The Snow White observations are not as reproducible as the 8 CFH measurements and it is not ready to be a working reference in the lower stratosphere. If the reasons for the low values on some of the flights can be identified, then Snow White might be used more routinely to measure the troposphere/stratosphere transition up to heights of 19 km. All the mixing ratios reported by Snow White increase with height to values larger than the CFH measurements. Without the inlet pipe protecting against contamination from the radiosonde body, the Snow White is more prone to contamination in the stratosphere than the CHF and even by 20 km is significantly contaminated relative to the CFH, which clearly is the most reliable measurement at this time.

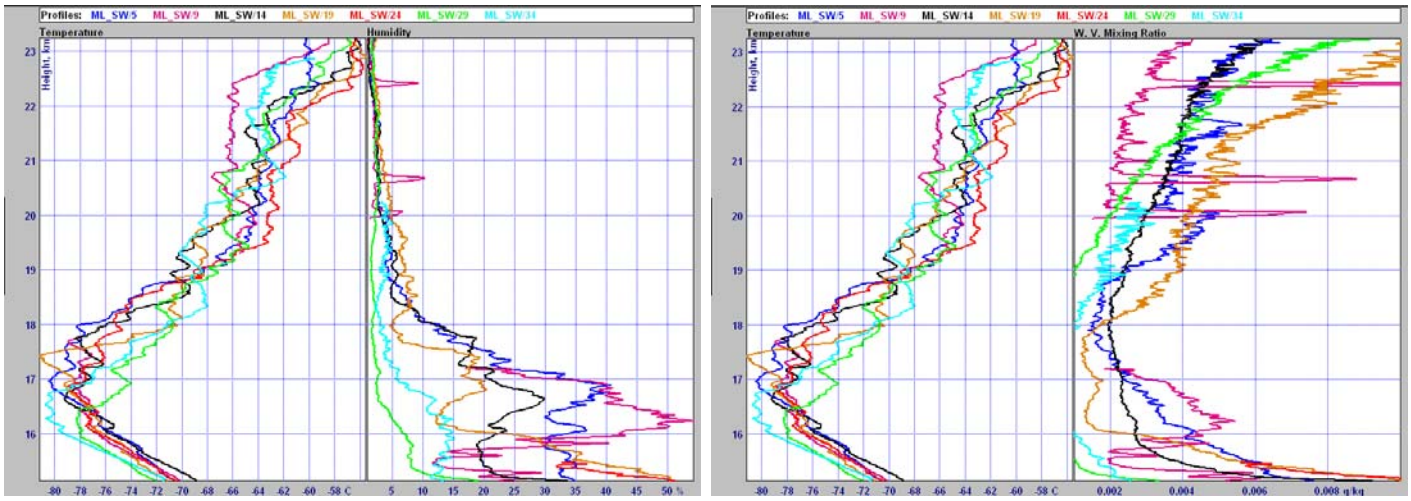

(a) Snow White night time ascents, Flights 5 to 34

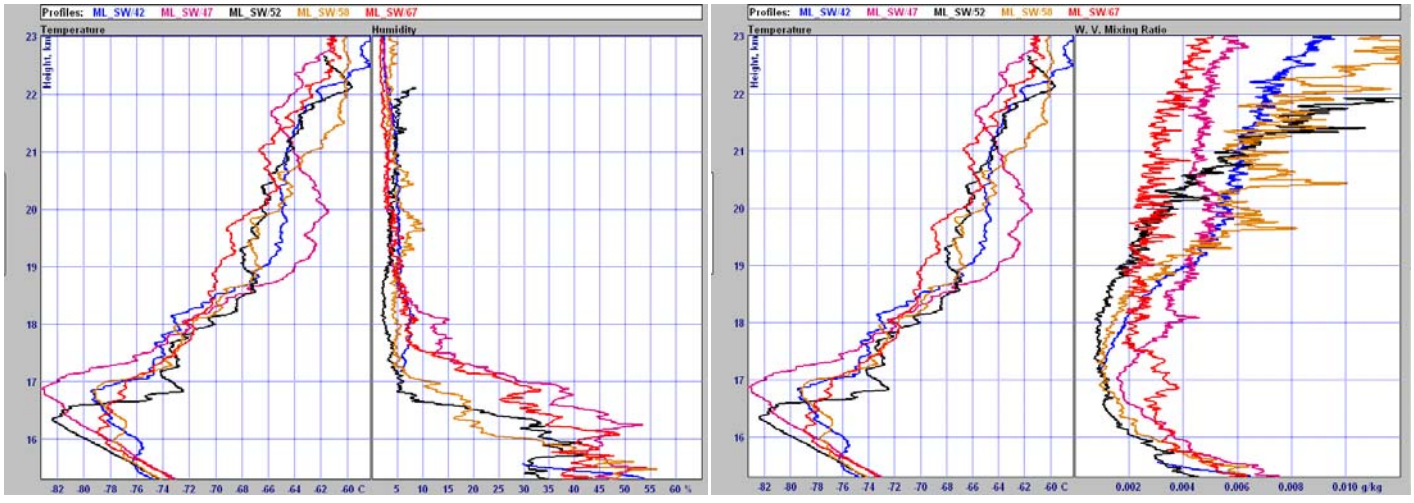

(b) Snow White night time ascents, Flights 42 to 67

Figure 8.1.26 Measurements by Snow White of the troposphere/stratosphere transition during QRS Flights, in terms of temperature, relative humidity and water vapour mixing ratio.

Vaisala measurements come closest to the CFH measurements for the troposphere/ stratosphere transition; see Fig. 8.1.27 (a) and (b). However, on some flights there is a local maximum in mixing ratio between 17 and 18 km, so that overall the lowest mixing ratio is reported at around 19 to 20 km. Vaisala needs to report relative humidity to a decimal place, rather than as an integer value, if the observations are to be used in this transition region. The effects in some flights of the R.H. changing in value by 1 per cent can be seen in the mixing ratios reported at heights between 21 and 23 km. There were about 10 flights with pronounced local maxima in mixing ratio above the tropopause, and of these about half were flights in cloud in the upper tropopause and half not. One question is does the pulse heating of the Vaisala humidity sensors need to continue to temperatures below -60 degC?

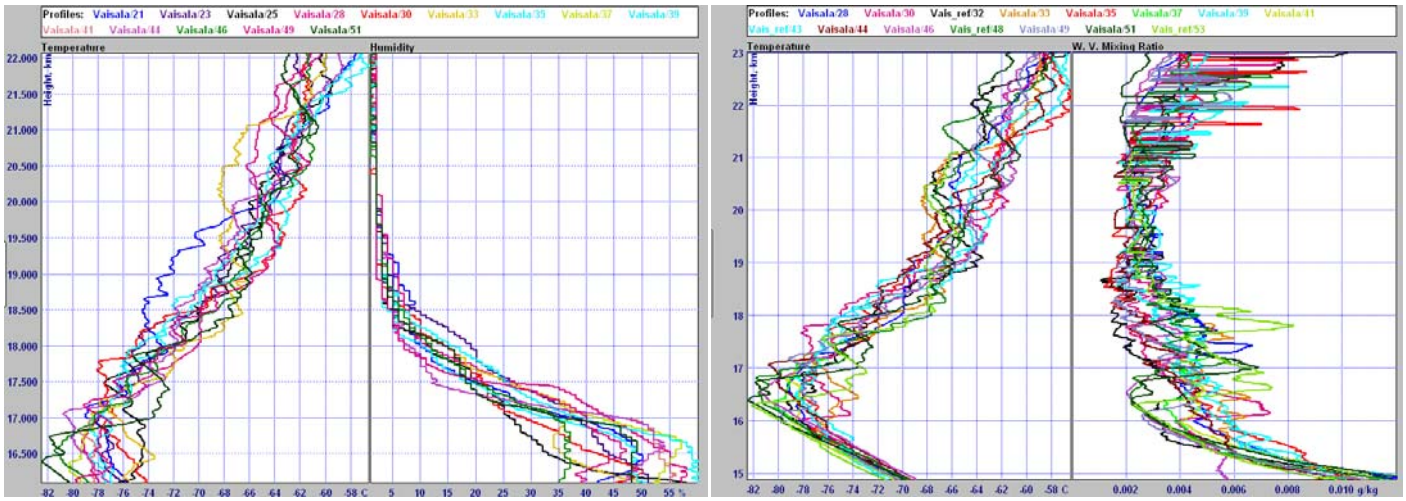

(a) Samples from the central part of the test for Vaisala

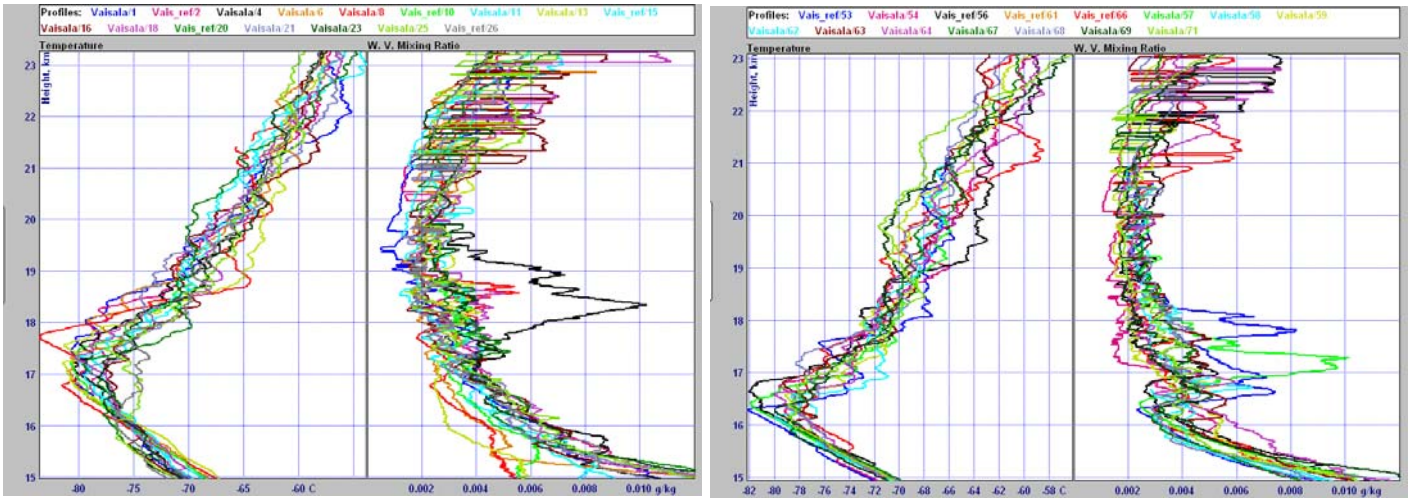

(b) Remainder of Vaisala mixing ratio measurements

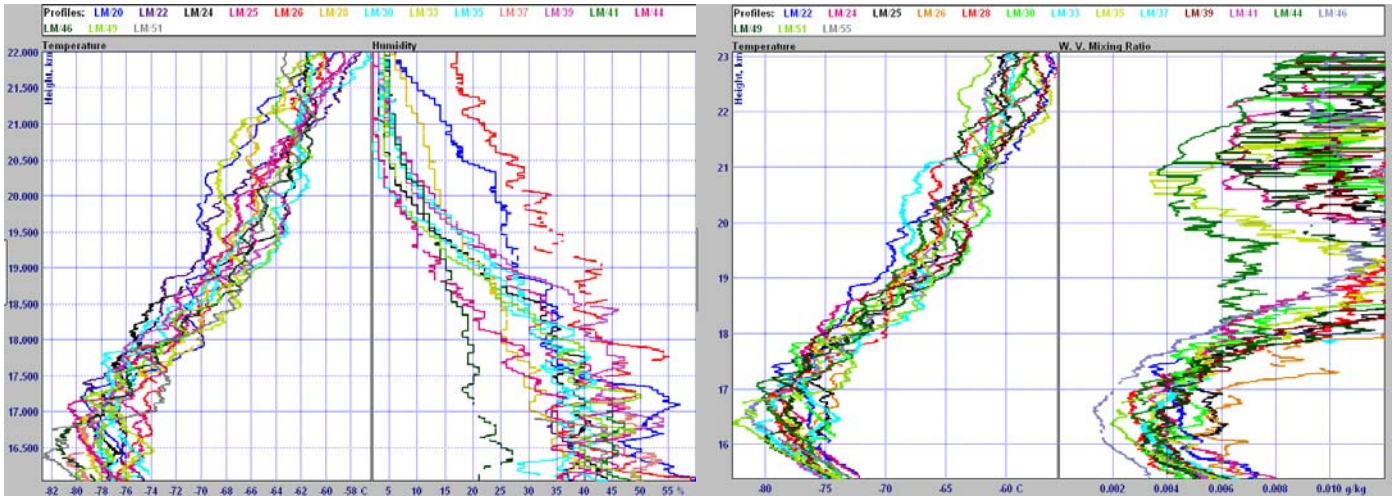

(c) LMS

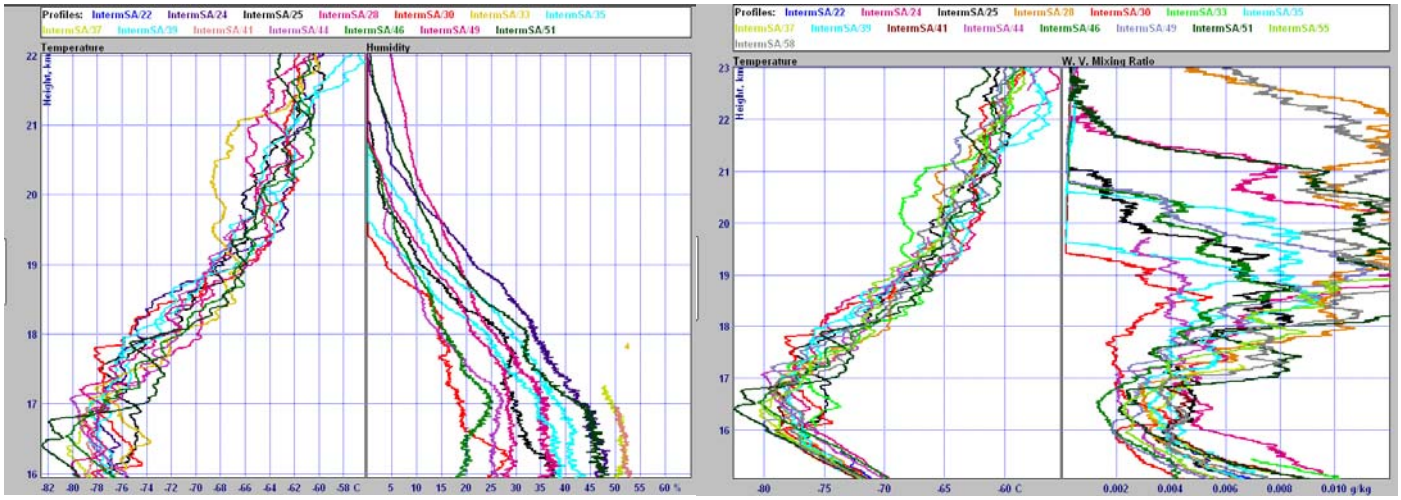

(d) InterMet

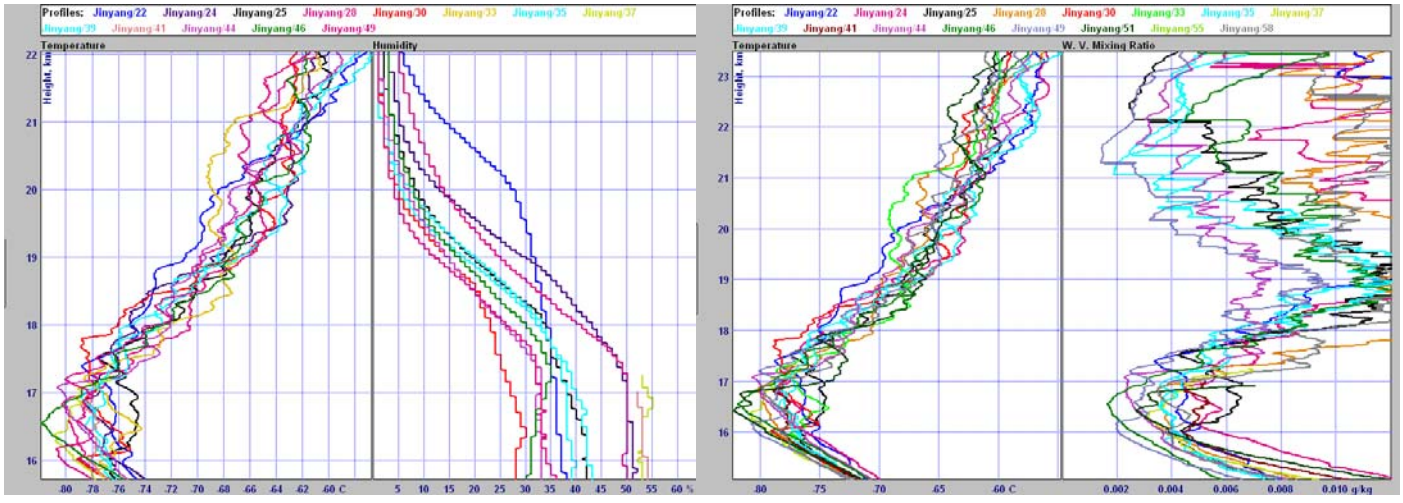

(e) Jinyang

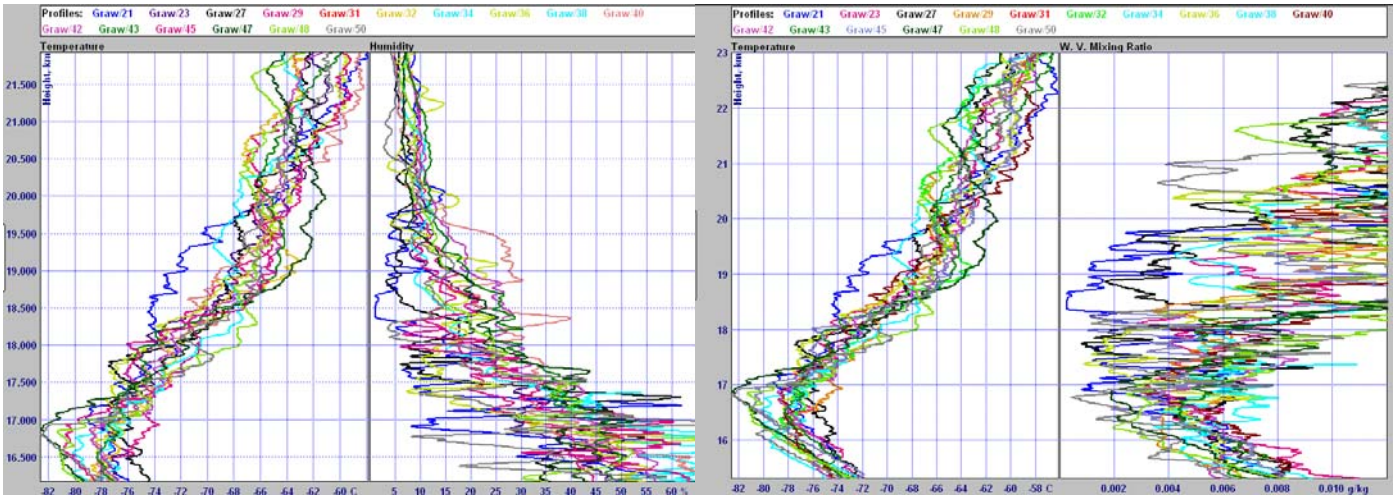

(g) Graw

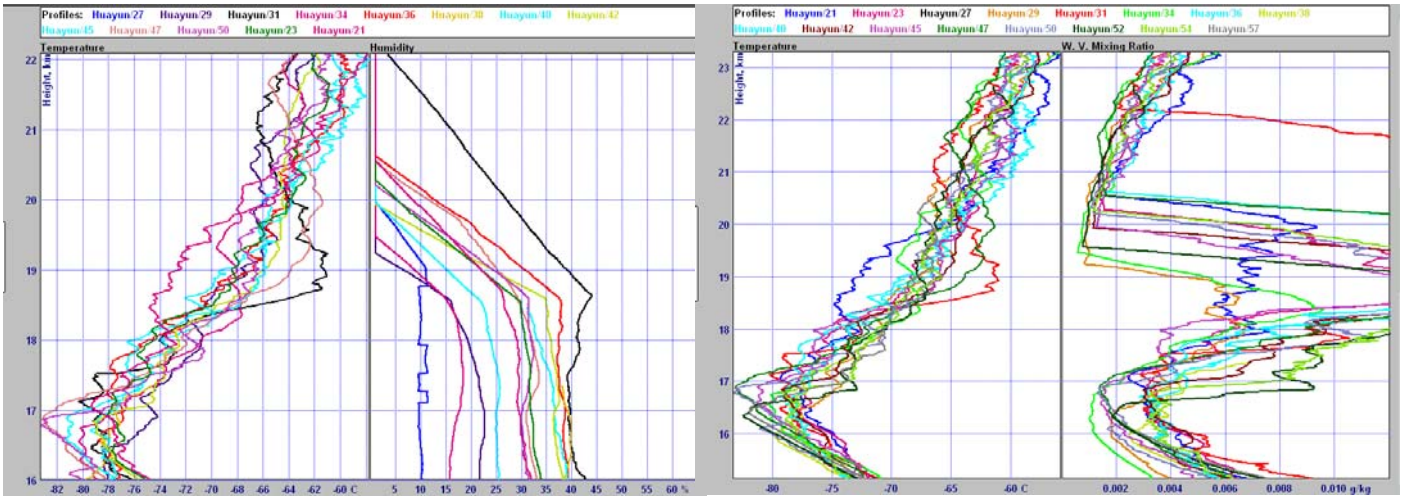

(h) Huayun

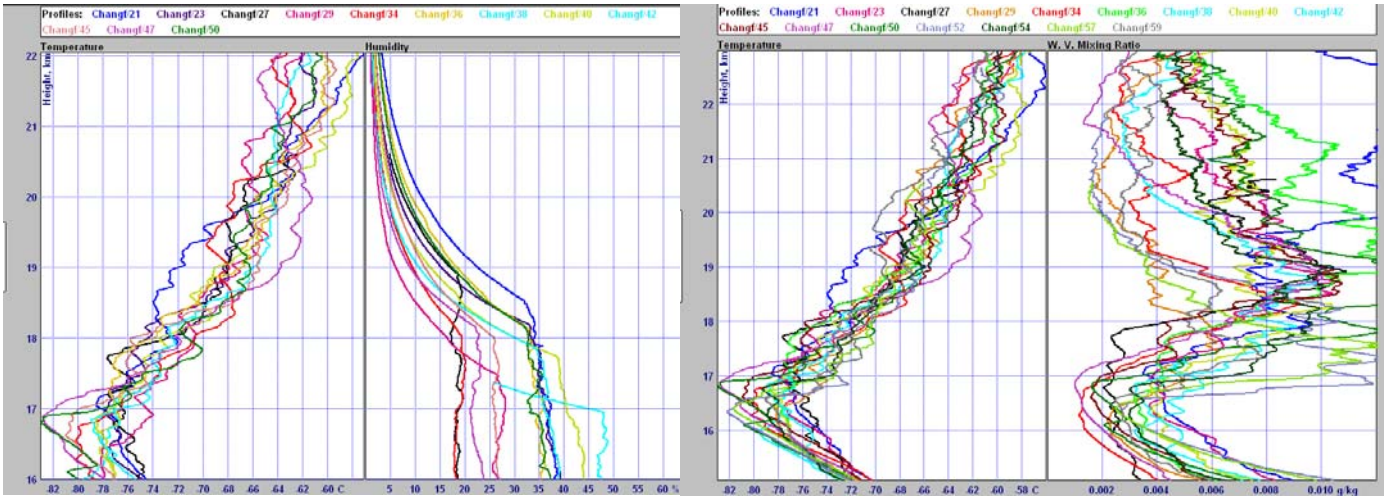

(i) ChangFeng

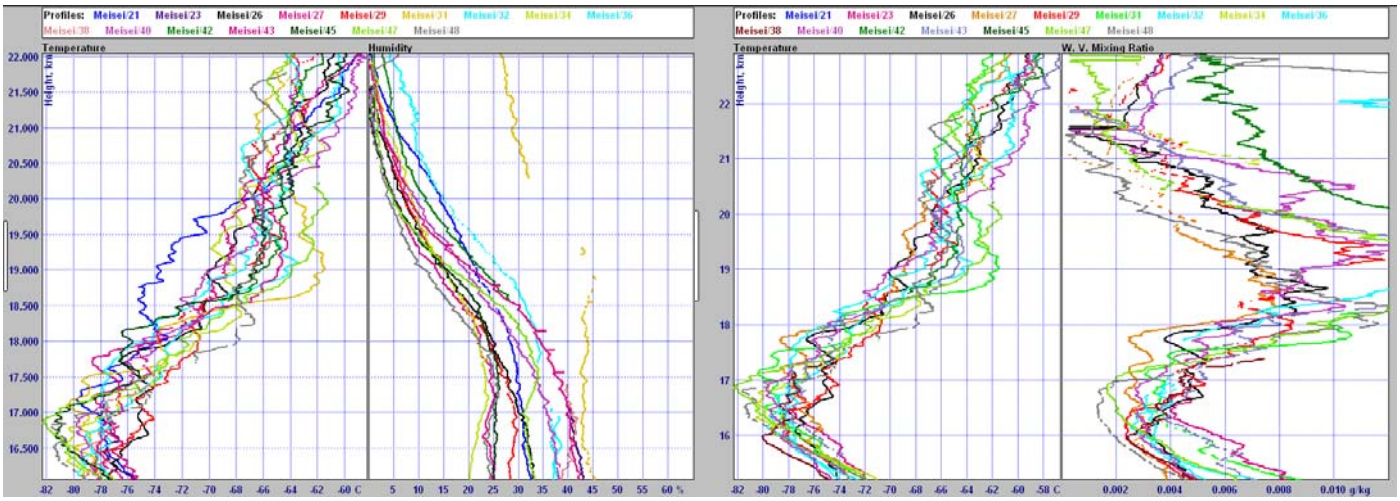

(j) Meisei

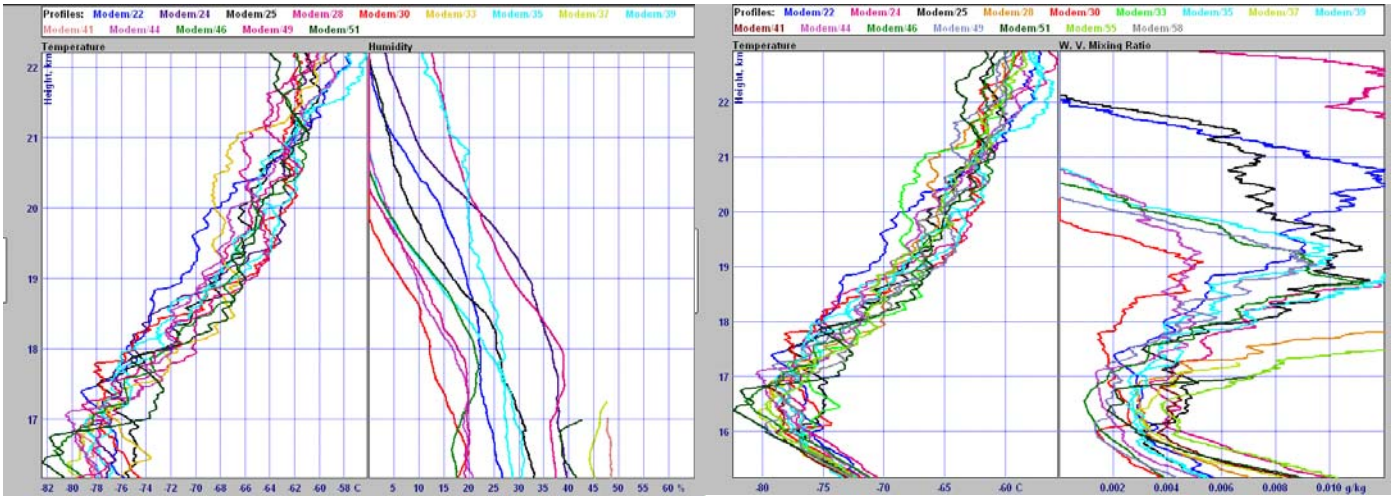

(k) Modem

Figure 8.1.27 Relative humidity and water vapour mixing ratio for the transition from upper troposphere to stratosphere, mainly sampled from flight 21 to 51, maximum height of tropopause, 18 km on Flight 27.

The E+E sensors response is very slow at temperature below -70 deg C and so the sensors are unable to measure the troposphere/stratosphere transition between 17 and 20 km in tropical conditions, as is also true for all the rest of the QRS radiosondes. At higher latitudes with a lower tropopause the sensors could be expected to cope better with this transition.

Snow White measurements in the tropopause/lower stratosphere transition were also checked against CFH measurements in Yangjiang, by averaging over several minutes in the vertical around three heights 18, 20 and 22 km (see Fig. 8.1.28). At 22 km, Snow White measurements show frostpoints that are consistently too high. At 18 km, the Snow White measurements are less consistent than CFH, but there is no reason to doubt that many are valid measurements. Without the inlet pipe protecting against contamination on the radiosonde body Snow White is much more prone to contamination and even by 20 km is significantly contaminated relative to the CFH, which clearly is the most reliable measurement at this time.

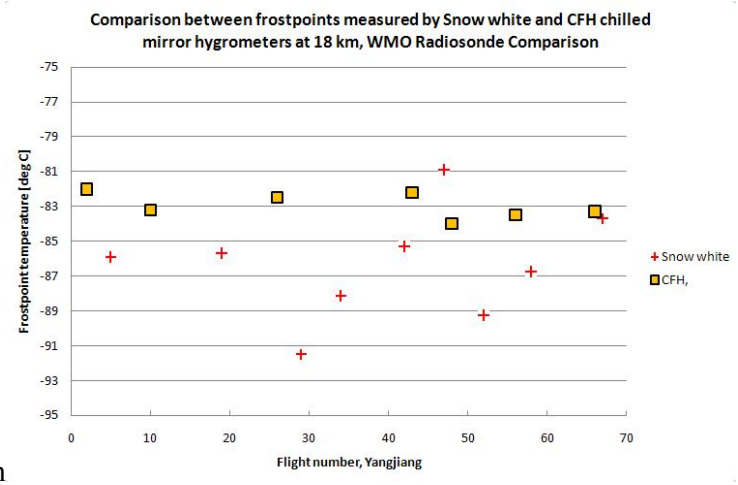

(a) 18km

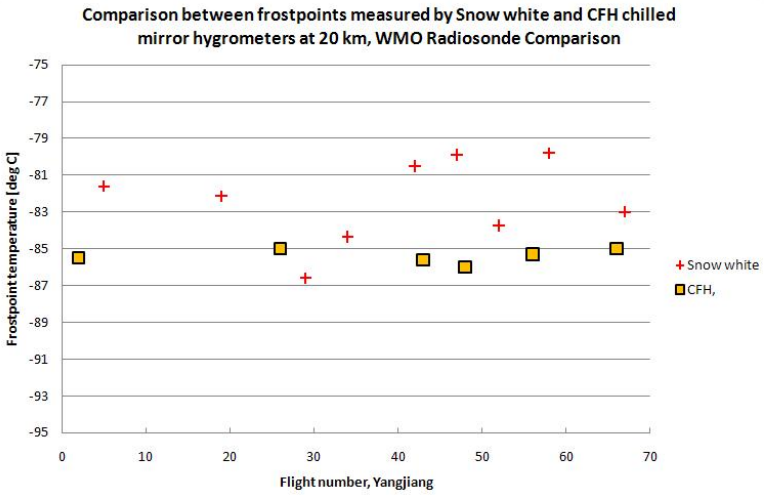

(b) 20km

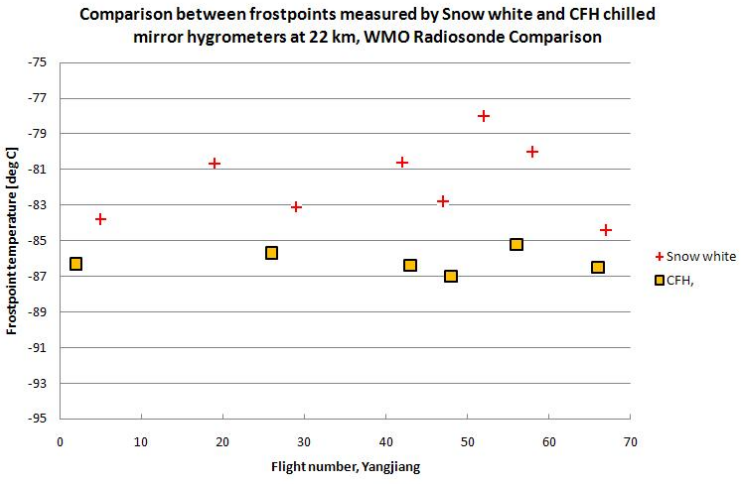

(c) 22 km

Fig. 8.1.28 Comparison of Snow White and CFH measurements of frostpoint in the lower stratosphere, from different flights in Yangjiang. Anomalous CFH and Snow White ascents from the troposphere have been flagged out.

8.2 SSI

8.2.1 Data analysis

The analysis compares the operational sensors on the SSI payload to the measurements provided from the CFH. As a first step, the altitude from each data file is used as the vertical axis. Although this approach is not ideal, since it does not consider potential systematic errors in the altitudes reported, this is considered negligible for comparisons in the troposphere and lowermost stratosphere, since altitude errors are more significant in the middle stratosphere than the regions below (see chapter 9). In addition, the visual examination of profiles for each flight confirms that there were no systematic shifts of RH with altitude for any flight. Thus, it is believed that small errors in altitude have insignificant effects on the results presented below.

Several CFH soundings suffered from excessive controller instability, which has subsequently been traced to a previously unidentified electronic issue. Fortunately, this electronic issue is believed to only decrease the CFH controller stability, not to introduce systematic errors. Thus it is possible to average the profile from the original 1 s resolution into 25 s bins, which are appropriate for the upper troposphere and lower stratosphere. Binning into 25 s intervals results in a vertical resolution of about 125 m. This approach has been validated in previous studies using the older NOAA frostpoint hygrometer (*Vömel et al., 2007b*). Averaging reduces the sensor oscillations and at the same time allows providing an estimate for the 25 s mean water vapor concentration.

For stratospheric water vapor observations contamination needs to be carefully evaluated and flagged. Any surface on the balloon train collects small amounts of water substance during the passage of the troposphere, which is subsequently released through desorption or evaporation in the stratosphere. Data where the measurements is believed to be contaminated or where the instrument performs mirror clearing cycles were flagged and removed from further analysis.

Usually, the best stratospheric observations can be obtained during slow descents, which can only be achieved using valved balloons (*Mastenbrook and Dinger, 1966, Mastenbrook and Dinger, 1960, Vömel et al., 1995*). During a valved balloon descent the measurement is no longer impacted by outgassing from the balloon, parachute, load line or any surface of the instrument rig. Outgassing within the sampling system can be minimized through proper design of the inlet and high air flow. However, the use of valved balloons in not always possible, in particular when hydrogen is used as lifting gas as was the case in Yangjiang. In these situations contamination from any surface above the instrument influences the measurement and causes systematic errors, which cannot be corrected and which have to be flagged as invalid measurements. It depends strongly on the amount of water substance that has been accumulated on the surfaces of the entire soundings system and ultimately limits the vertical range for water vapor measurements in the stratosphere (*Vömel et al., 2007a*). Stratospheric contamination is usually more severe in the tropics and for larger balloon payloads such as those launched in Yangjiang.

Fig. 8.2.1 shows the 1 second resolution water vapor profile measured by the CFH in sounding 43. The data, which are manually flagged as contaminated or as mirror clearing cycle are shown in blue and should not be used in analyses. Data that are considered good CFH measurements are shown in red. A water vapor profile measured by Aura/MLS during an overpass 120 km and 0.5 hr away is shown for guidance as example of a typical stratospheric water vapor profile. Aura MLS has been shown in previous studies to be in agreement with CFH for stratospheric water vapor measurements (*Read et al., 2007, Vömel et al., 2007c*).

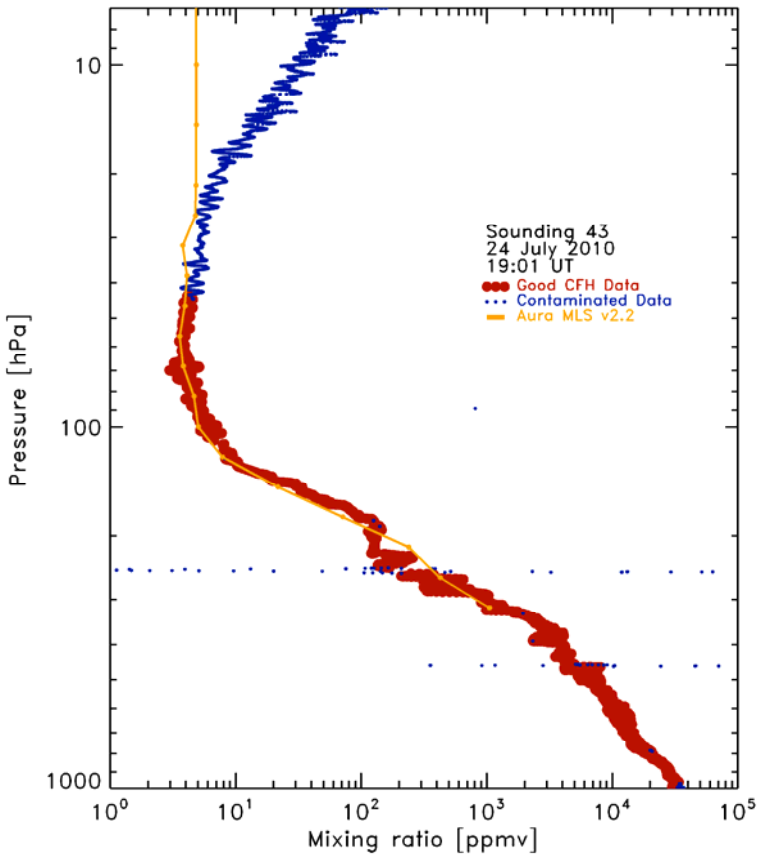

Figure 8.2.1: Stratospheric water vapor profile measured by the CFH. Good data are shown in red and flagged data (which should not be used) are shown in blue. The nearest Aura/MLS water vapor profile is shown for guidance

For soundings reaching the middle stratosphere water vapor measurements near the top of the profile are usually contaminated. For each sounding the altitude, where contamination was determined to become significant, was determined and all data above that altitude were flagged. Those flagged data should not be used in any analysis. Fig. 8.2.2 shows the number of soundings as function of altitude that provided good data. This figure also shows the variability of water vapor measurements within these soundings. Ten out of 12 soundings provided data up to the tropopause; six soundings provided data to about 22 km and three soundings to 25 km.

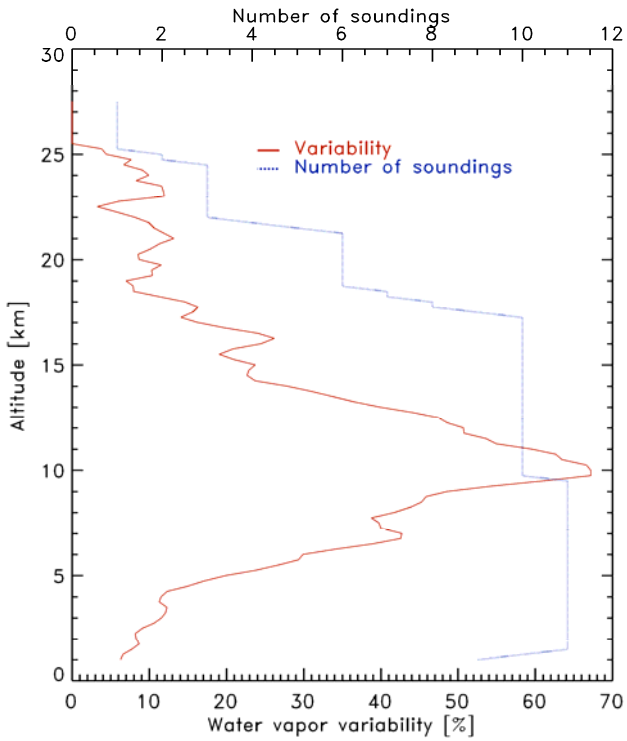

Figure 8.2.2 Number of soundings providing good data as function of altitude (in blue) and variability of water vapor mixing ratio within these soundings.

The variability within these observations is defined as the standard deviation of all water vapor mixing ratio measurements at a given altitude in percent of the mean value at that level. This variability does not distinguish between atmospheric and instrumental variability. The largest variability is found in the middle troposphere reaching a peak of more than 60% of the mean value and is controlled by the very large atmospheric variability found in the middle troposphere. In the stratosphere above the tropopause, this variability decreases rapidly and reaches values of around 10%. This variability still combines instrumental and atmospheric variability and is comparable to uncertainty of the mixing ratio measurements of the CFH in that altitude region (*Vömel et al., 2007a*). It has to be pointed out that Figure 8.2.2 shows the relative variability of mixing ratio, not the absolute variability of RH. Above the tropopause, water vapor and temperature are decoupled and water vapor becomes largely a passive tracer. Mixing ratio is therefore a much more appropriate quantity to describe the amount of stratospheric water vapor, whereas RH is typically unsuitable for stratospheric studies.

8.2.2 Results

Figure 8.2.3 shows two comparisons of RH profiles, on SSI flights. The mean and standard deviation profiles of RH differences between the operational sensors and CFH are shown later.

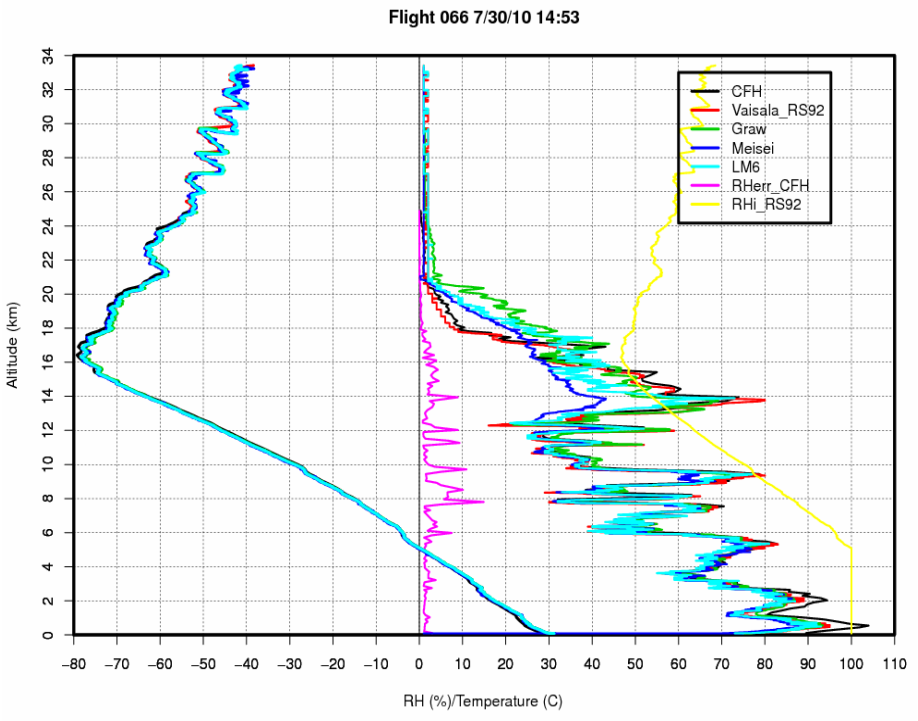

Figure 8.2.3 RH and temperature profiles from four radiosonde humidity sensors and the CFH on two SSI flights. The magenta lines show CFH RH uncertainty profiles (see 8.2.4 for details). Yellow lines are ice saturation RH calculated from the RS92 temperature profiles.

For Flight 53, the CFH was not attached to the center cross of the bamboo rig as shown in Figure 4.2.1, but rather it was suspended at the end of one of the bamboo rods (Figure 8.2.4, upper panel). In this sounding the CFH data are systematically wetter by about 20% than RS92 and LMS6 (Figure 8.2.4, lower panel); however, at this point it is not clear, whether this arrangement, a possible damage during the installation, or an unidentified issue contributed to this systematic error. This flight must be treated as an outlier and is excluded in the mean and standard deviation calculations shown below.

In the following parts, the vertical resolution of the data from the operational sensors has been reduced to match that of the reduced CFH resolution. This approach then allows a direct comparison with the output of the CFH. Ignoring the details of the very high resolution data allows use of the measurement uncertainty, which has been calculated for the CFH (see below) at this lower resolution.

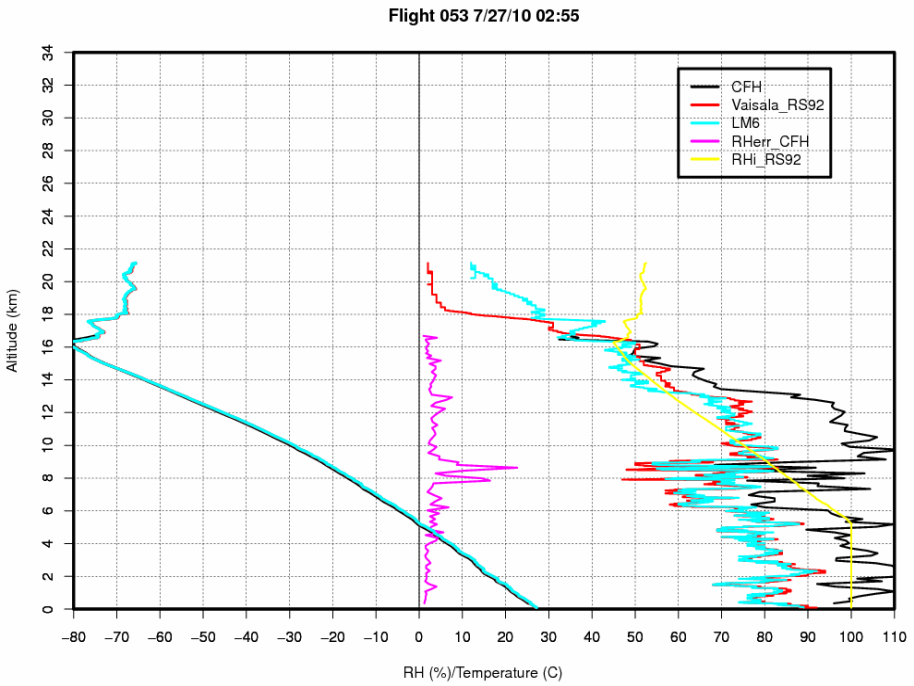

Figure 8.2.4 Upper panel shows the special configuration with CFH suspended on the side for Sounding #053. The lower panel is comparisons for Flight #053.

The comparisons shown in Figure 8.2.5 can be summarized separated into four regions: lower (0-3 km, LT), middle (3-10 km, MT) and upper (10-16 km, UT) troposphere, and lower stratosphere (>16 km, LS).

- LT: In the lower troposphere, the CFH seems consistently wetter than all other four sondes with maximum wet bias of 5-10% near the surface. The other four sondes agree well with each other. At this point this bias in the lower troposphere is unexplained and is possibly related to the CFH electronic issue that has been identified or improper control with liquid water on the mirror surface (*Miloshevich et al., 2009*).

- MT: The best agreement among all five RH sensors is achieved in the middle troposphere. Mean departures from CFH are generally within 2% RH on average although Meisei RS06-G shows a consistent wet bias in MT at night.

- UT: In the upper troposphere, during these SSI flights, the Vaisala RS92 has the best performance with little significant bias compared to CFH and captures both the magnitude and variability within the relative humidity profile. The Graw DFM-09 overestimates the relative humidity by on average 2-10%. Both the Meisei RS06-G and the LMS6 sensors exhibit dry biases in UT. The dry bias is larger in Meisei than that in LMS6 (see examples in Figure 8.2.3 and 8.2.4) and increases with altitude and reaches maximum near tropopause. The details of this bias can also be seen in the QRS evaluations in Figs. 8.1.4 and 8.1.6.

- LS: In the lower stratosphere, the Vaisala RS92 sensor again shows a closer agreement with CFH. However, this figure shows the absolute difference of RH from CFH, and large relative errors become hidden at small RH values. The other three show similar behaviors, with very large wet biases with peak values at ~18 km, as is also shown for a larger data set in Figs. 8.1.25.and 8.2.4), increases with altitude and reaches maximum near tropopause. The details of this bias can also be seen in the QRS evaluations in Figs. 8.1.4 and 8.1.6

The difference of the Meisei sensor to the CFH changes between day and night time measurements throughout the entire profile, indicating an insufficient treatment of the radiation errors. For the LMS6 sensor, this day-night difference is significant only in the upper troposphere.

Based on these results, we can conclude that the Vaisala RS92 version tested in China shows systematic errors of less than 2% RH and random errors of ~5% from the surface to the LS, whereas the Graw DFM-09, the Meisei RS06-G and the LMS6 exhibit significant biases in the upper troposphere and above.

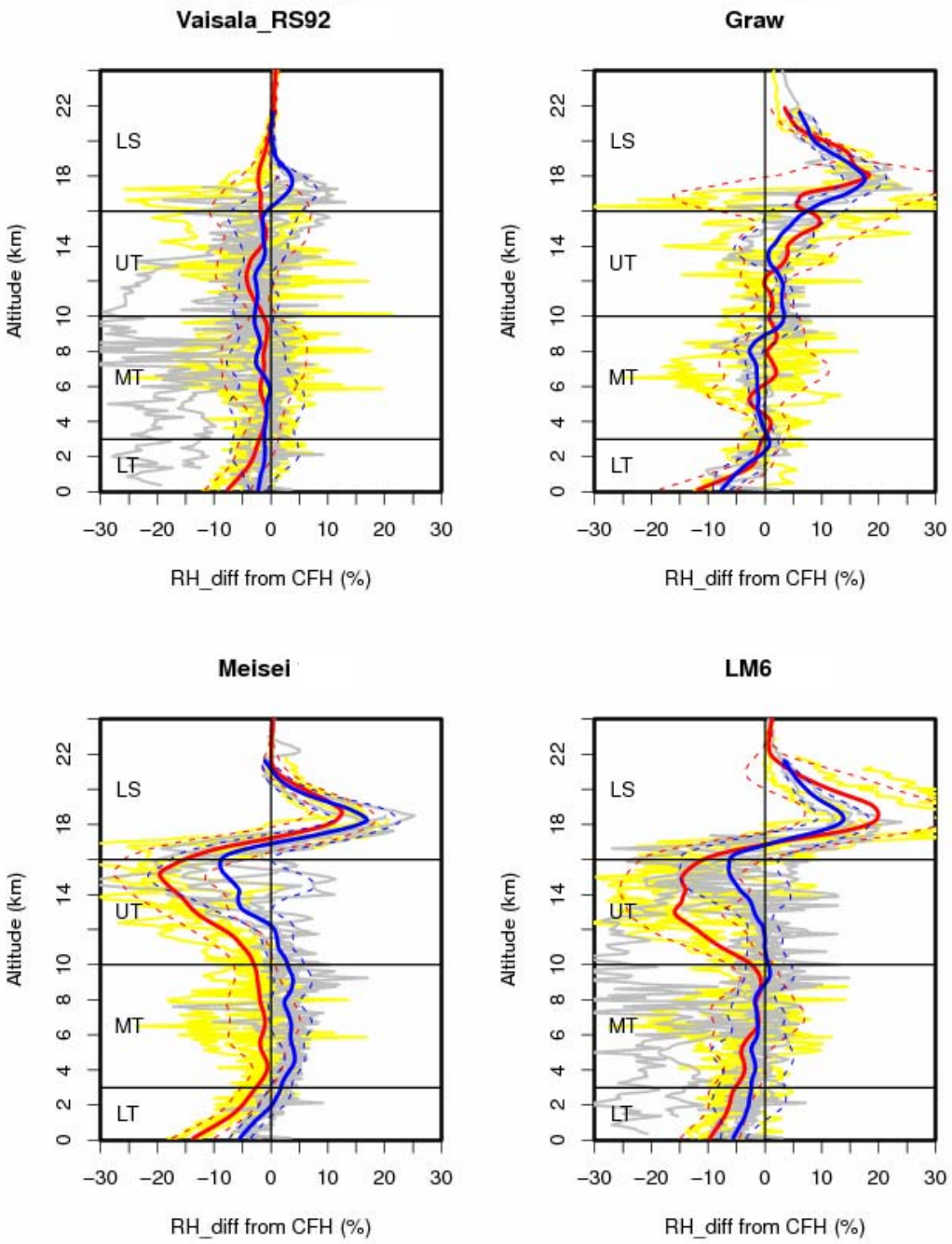

Figure 8.2.5 Profiles of RH differences between RS92, Graw, Meisei, LMS6 and CFH: Individual profiles are shown in yellow for daytime and grey for nighttime soudnings; daytime mean difference in solid red, and nighttime mean in solid blue; standard deviations are shown in dashed lines.

8.2.3 Humidity calibrations and corrections

The good performance of Vaisala RS92 humidity sensor shown in Figure 8.2.5 was not seen in previous intercomparisons and earlier studies have not seen such good agreement. For example, the daytime dry bias in RS92 humidity data has been studied extensively (e.g. *Vömel et al. 2007a*), whereas Figure 8.2.5 displays only very small mean differences between RS92 and CFH for both day and night. The improved humidity measurement accuracy in Vaisala RS92 is achieved through new correction algorithms added to the Vaisala DigiCORA software (*Vaisala, 2010*). The humidity corrections include time lag and daytime solar radiation corrections, which quite obviously improve the data quality significantly. The time lag and solar radiation corrections are adjustments of known systematic errors.

As described in Section 3.1, reference observations within GRUAN need to be well documented and must be traceable. This implies that the adjustments in the Vaisala relative humidity need to be documented (*Immler et al., 2010*). Therefore, in order to be qualified as a GRUAN reference sensor, in addition to meeting accuracy requirements, any corrections applied to raw measurements need to be disclosed. This has still to be done for any of the operational sensors, including the Vaisala RS92.

8.2.4 Uncertainty analysis

The chosen approach of GRUAN is to provide an uncertainty analysis with every data point (*Immler et al., 2010*). Here, the uncertainty analysis for CFH observations is described and subsequently used to quantify, whether the differences observed can be explained with the current understanding of the instruments, or whether unidentified systematic errors exist.

The uncertainty in frostpoint using the CFH is largely determined by the controller stability, with minor contributions from the calibration and installation of the temperature sensor used to measure the mirror temperature, as described by *Vömel et al.* (*1995*) and *Vömel et al.* (*2007a*). Although the controller behavior for the CFH instruments used in Yangjiang was not as good as expected, the approach to evaluate the uncertainty nevertheless remains valid and simply leads to a slightly larger uncertainty. The CFH has generally been slightly over-tuned, i.e. when optimally tuning has not been achieved, the deviation is generally on the side of oscillation rather than damping, This allows to avoid excessive time lag and so to get a better estimate of the atmospheric frostpoint temperature, which has been validated in previous studies using the older NOAA frostpoint hygrometer (*Vömel et al., 2007b*).

The best estimate for the frostpoint temperature in a 25 second time interval is the mean mirror temperature within that interval. More difficult is estimating the uncertainty within that time interval. Since both mirror temperature oscillations and atmospheric variation over that time are highly auto-correlated, using the standard deviation of all measurement points is not valid. However, a better estimate starts with the assumption, that the true mean value does not lie outside the range specified by a one standard deviation of the auto-correlated mirror temperatures. Following the *Guide to the Expression of Uncertainty in Measurement* (*JCGM/WG 1, 2008*) under this condition the width of the equally distributed range of possible values given by

the standard deviation is divided by $\sqrt{3}$ to give the best estimate for the 1-sigma uncertainty of the mean frostpoint temperature within that time interval. The total calibration and temperature uniformity uncertainty of 0.12 K is then added in quadrature.

Furthermore, a conservative estimate of 0.2 K for the 1-sigma uncertainty in air temperature is assumed to finally calculate the total uncertainty in RH. This procedure is done for each 25 s interval, which will lead to a vertical uncertainty profile for the frostpoint temperature measured by the CFH.

Figure 8.2.6 shows an example for the relative humidity profile measured by the CFH, the original 1-second resolution and the binned data with the 1-sigma uncertainty estimate described above. Note that the absolute uncertainty estimate for RH becomes small at low RH values found in dry tropospheric layers and above the tropopause.

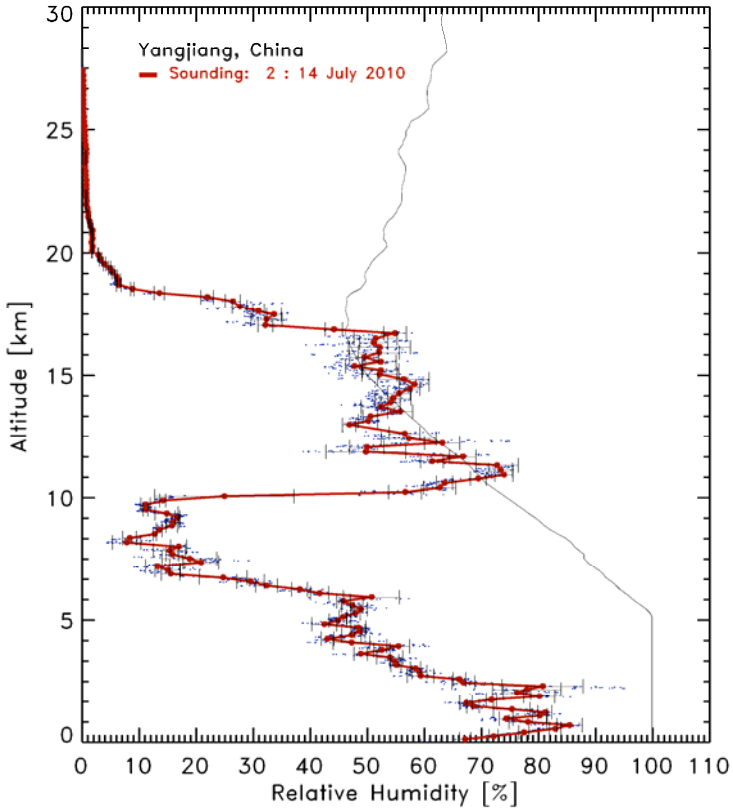

Figure 8.2.6 CFH profile of relative humidity with point by point uncertainty estimates. The thin solid line shows ice saturation.

The uncertainty profiles are then used in the consistency test described in section 3.2. This consistency test will provide insights on whether two RH measurements are consistent (i.e. differences can be explained with the current understanding of the factors contributing to the measurement uncertainty) in a quantitative measure. The consistency factor here is defined as:

$$k = \frac{|m_1 - m_2|}{\sqrt{u_1^2 + u_2^2}}$$

Since only one uncertainty estimate is available, the denominator uses only the uncertainty of the CFH, and the consistency factor is reduced to $k = |m_1 - m_2| / u_1$.

Figure 8.2.7 shows the vertical profiles for the consistency factor k for each individual sounding, as well as the mean and standard deviation of this factor over all soundings. For $k \leq 2$ the data are presumed to be in agreement, i.e. with the uncertainty given for the CFH and without specifying an uncertainty in the operational RH measurement, the difference can be explained with 95% probability, just considering the uncertainties of the CFH. In doing this the results presented in Fig. 8.2.7 are distorted by the underestimation of the standard deviation of the difference between the two observation. For values above $k \geq 1$, however, the differences still need to be called suspicious. With definitions, RS92 measurements are consistent with CFH measurements throughout the middle and upper tropospheric profile. The difference in the lower most troposphere is most likely a slight wet bias that has been noted earlier (*Miloshevich et al., 2009*). At the tropopause relative humidity generally has a maximum (*Vömel et al., 2002*) and drops rapidly in the stratosphere above. Small differences in RH rapidly increase to significant errors. For all sensors, this limits the sensitivity in the lower stratosphere.

Above the tropopause, the differences between the operational sensors and the CFH become very large, i.e. a multiple of the uncertainty of the CFH. This strongly points towards a loss of sensitivity to water vapor by the operational sensors above the tropopause

The consistency test provides some deeper insight into this comparison. The basis for this figure is a detailed understanding of the uncertainties of the CFH measurements and a simple assumption on the uncertainty of the operational sensors. To improve this evaluation, a better understanding of the sources of measurement uncertainty is needed, i.e. a better understanding of the sensors, their calibration, their implementation and their analysis. Sensors for which this information cannot be obtained either through disclosure by the manufacturer or carefully designed experiments, cannot be used as reference sensors. It is also necessary to be able to eliminate observations where anomalies occur that are not represented in the uncertainty model.

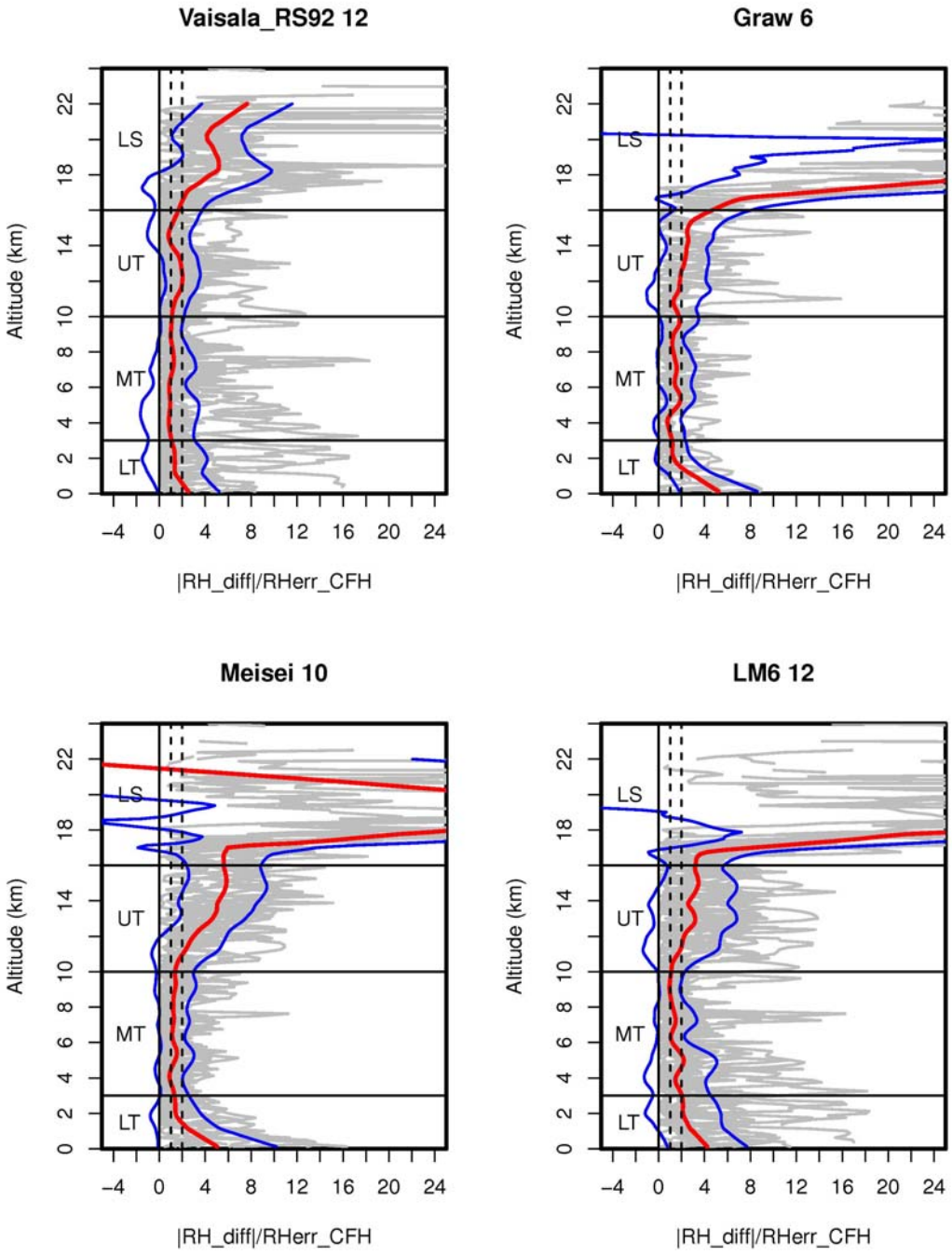

Figure 8.2.7 Profiles of consistency parameter (k) for individual profile (grey), mean (red) and mean +/- SD (blue). Vertical dashed lines represent k=1 and k=2.

8.2.5 Importance of the vapor pressure equation

Relative humidity over liquid water has been a common unit to express the amounts of water vapor in meteorology. Relative humidity is defined as the vapor pressure of water vapor in the air divided by the saturation vapor pressure of liquid water the air has at that given temperature. This unit easily relates to the amount of water vapor one might find within liquid clouds and is among others highly useful in modeling and studies leading to precipitation.

At cold temperatures, however, the use of relative humidity becomes ambiguous, since the saturation vapor pressure over liquid water is no longer well defined. This is due to the fact that bulk amounts of supercooled liquid water may exist only down to temperatures of around -30 deg C and any definition of the vapor pressure at colder temperatures depends on theoretical studies (Murphy and Koop, 2005), without the possibility of experimental verification. A number of different vapor pressure equations exist, which at cold temperatures may differ significantly.

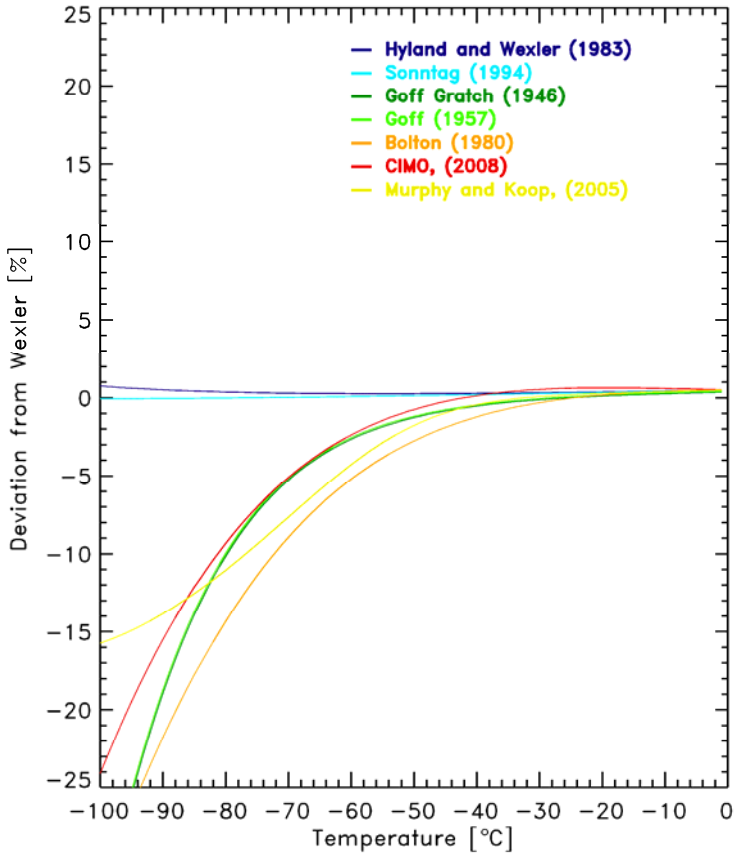

Figure 8.2.8 Relative difference of 7 vapor pressure equations over liquid relative to the equation by Wexler (1977).

Figure 8.2.8 shows the difference between 7 vapor pressure equations relative to the vapor pressure equation by Wexler (1977). No particular vapor pressure equation over liquid has any intrinsic advantage over any other. The curve by Wexler has only been chosen as reference here, since it is used by NIST. As can be seen from Figure 8.2.8,

the relative difference between all of these selected curves is negligible compared to typical measurement uncertainties in the temperature range of 0°C down to -40°C. Below this temperature, the relative difference is increasing and reaches values between 10% and 15% for these vapor pressure equations selected here. This difference is no longer negligible.

A relative humidity sensor is typically calibrated over a large temperature range including cold temperatures at which bulk amounts of liquid water no longer exist. The calibration equipment therefore is based on another physical property of water, among others the vapor pressure of ice, which can be readily measured under controlled laboratory conditions. To convert this measured property of water vapor into a corresponding value of relative humidity over liquid water a saturation vapor pressure has to be chosen; however, as mentioned, no unique definition of the vapor pressure equation exists.

This will not lead to problems, as long as the measurements obtained during a sounding are converted to partial pressure using the same vapor pressure equation. However, if a vapor pressure equation is used different from the equation used in calibration, then a systematic bias based on this inconsistency is artificially introduced in the data. For example, if during calibration at -80°C the equation by Wexler (1977) has been used to convert the partial pressure measurement of the calibration reference into relative humidity over liquid, but for an atmospheric observation the formulation by Bolton is used to convert the RH reading back into partial pressure, a systematic relative low bias of 15% would be introduced in the partial pressure calculated from the RH measurement.

Therefore manufacturers should take care of using the same vapor pressure equation over liquid that was used in the calibration equipment, to convert the RH reading back into partial pressure during measurement. Furthermore, the manufacturers should clearly indicate, which vapor pressure equation has been used, so that the user of the data would not accidentally make that mistake.

A brief survey among all manufacturers has shown that the equations by Wexler (1977), Hyland and Wexler (1983) and Sonntag (1994) are the most common equations. These three equations do not differ significantly over the temperature range of interest.

It is therefore recommended that only these three equations be used to convert relative humidity over liquid to partial pressure at cold temperatures, in particular by manufacturers, which are employing RH sensors capable of measuring water vapor at these cold temperatures. For RH sensors, which are no longer sensitive at temperatures below -40°C, this issue is not of importance.

8.3 Remote Sensing

8.3.1 Relative humidity reported in clouds detected by cloud radar and ceilometer

The cloud radar was able to identify relatively thick ice cloud up to a height of 16 km, see Fig. 8.3.1, which shows the cloud radar image for Flight 61. This image was from a measurement along the side of a big electrical storm and Flight 61 was ended by an electrical discharge at about 10 km, where the maximum signal is shown by the cloud radar. The cloud radar scan was made along the direction the balloon was expected to travel, so the radiosonde would not necessarily experience the conditions shown exactly above the site. The winds in the outflow from the thunderstorm above 10 km (as seen in flight 60), were similar to the average value from the surface to 10 km, with the winds immediately under the cloud weaker than this, so the balloon probably went through the upper cloud at 10 km which at launch was within 6 km of the cloud radar in the horizontal.

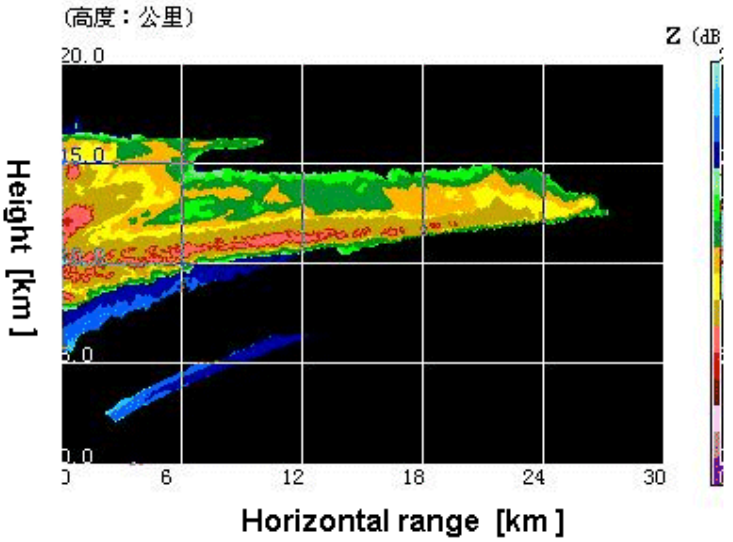

Fig. 8.3.1 Signal power, Z, as a function of range and height in km obtained from the cloud radar, Flight 61, terminated by electrical discharge from the side of a thunderstorm at 10 km

The Vaisala laser ceilometer, CL51, worked much better in Yangjiang than the CT75K system deployed in Mauritius for the preceding WMO radiosonde test. It was more sensitive at night, when on occasions it identified cloud as high as 12 km. This is shown in Fig. 8.3.2 together with the cloud radar image for this time. In this case the cloud was moving faster than the winds at lower levels, so the balloon ascended close to vertical, taking about 30 minutes to reach the bottom of the cloud, with the radiosonde experiencing conditions close to the ceilometer observation at about 01.15, i.e. cloud base below 10 km rather than 11 km at 00.46 when the balloon was launched. A cloud base of about 9.7 km was found in the radiosonde measurements on Flight 52. The radiosonde measurements on Flight 52, see Fig. 8.3.2(c) also indicated a very moist layer near 5 km, and the ceilometer shows some evidence of intermittent cloud starting at about 01.14, at a time when the balloon was near 9 km, so it is assumed that the ascent did not pass through this cloud. This method of

identfying cloud layers is used here to assess the relative humidity measured when the radiondes had a very high probability of passing through cloud.

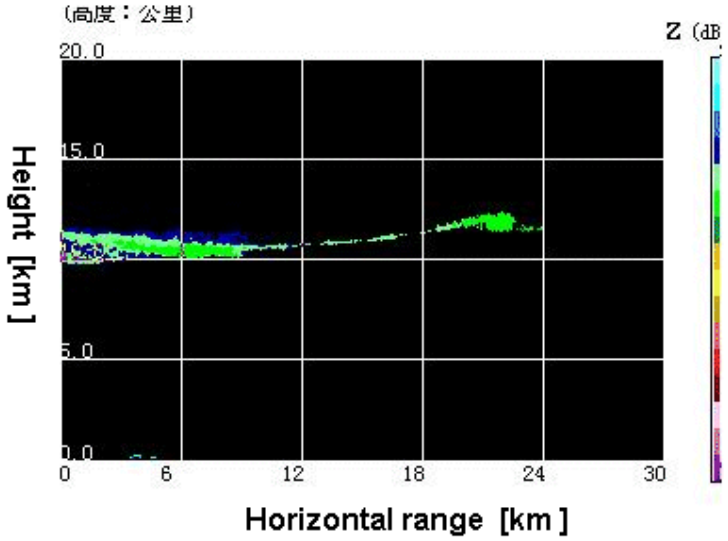

(a) Signal power, Z, as a function of range and height in km for Flight 52, measured at 00.48 local time,27.07.10

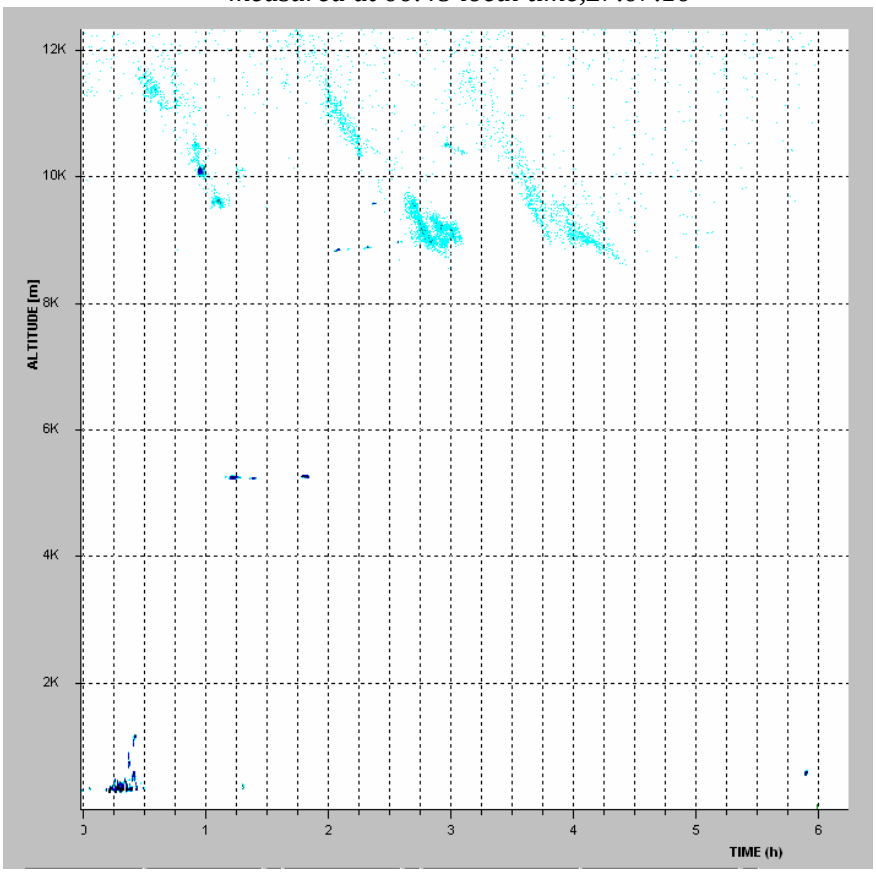

(b) Laser ceilometer back sactter for Flight 52, launched at 00.46,27.07.10

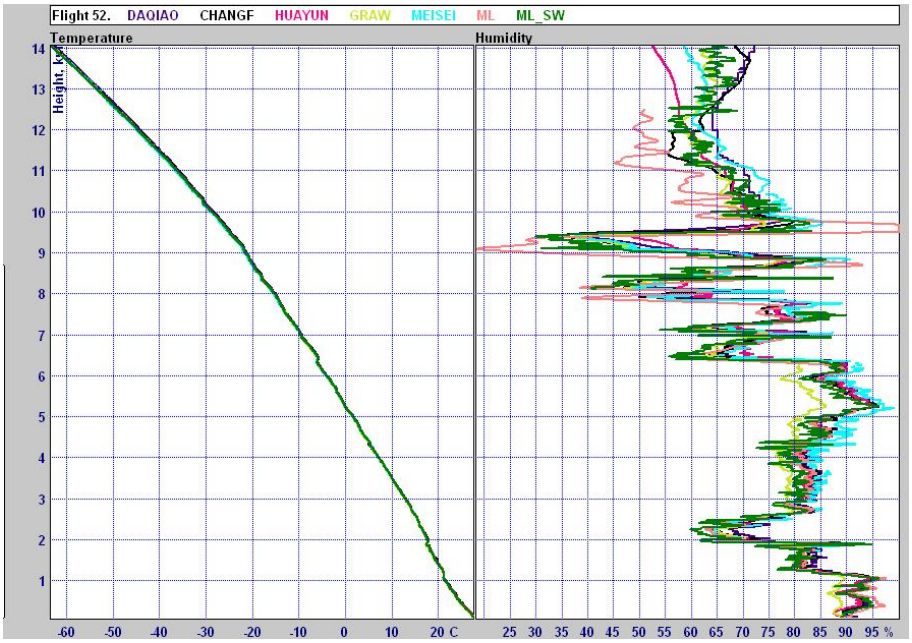

(c) Temperature and relative humidity for Flight 52 as a function of height

Fig. 8.3.2 Cloud radar and laser ceilometer measurements associated with the temperature and relative humdity measurements of Flight 52.

For most flights both laser ceilometer and cloud radar images were available and this gives a much fuller description of the environmental conditions than either system on its own. This is illustrated with two daytime radiosonde asecents on 21 July 2010 in Fig. 8.3.3. The laser ceilometer shows a layer of cloud base between 5 and 7 km from 14.00 onwards, but not all that much at 12.47 when Flight 31 was launched.

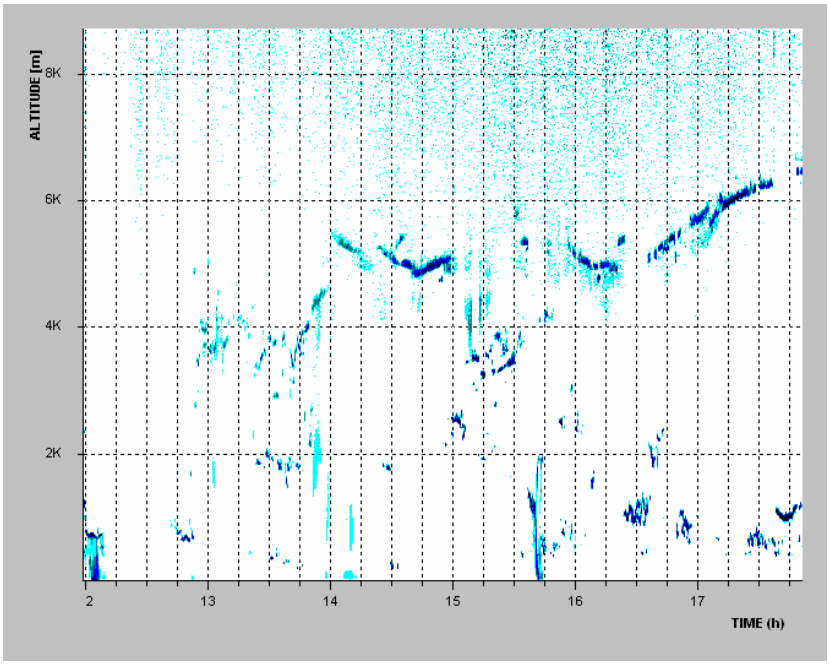

(a) Laser ceilometer backscatter plot for afternoon of 21.07.10

However, the cloud radar shows water and ice up to 15 km, see Fig. 8.3.3(b), and the radiosonde shows saturation at all levels above 5 km with drier layers near the ground and at 2.5 km and 4.5 km,see Fig. 8.3.3(c). The cloud radar images were not available to the launch supervisors in real time, and this is a pity since they would definitely have helped in decisions with respect to the viability of some of the launches. This flight was the severest test of the radiosonde relative humdity to cope with difficult conditions, with some but not all surviving.

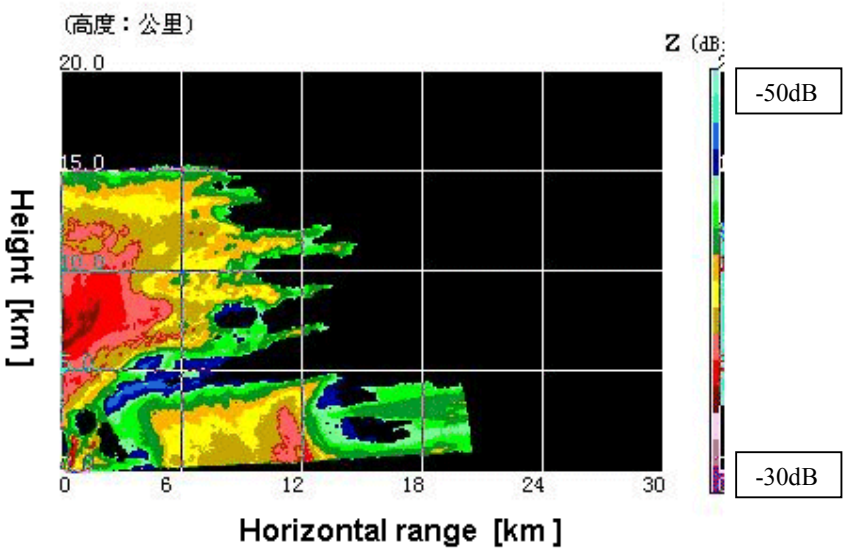

(b) Signal power, Z, as a function of range and height in km for Flight 31 at 12.47

(c) Temperature and relative humidity as a function of height, as measured on Flight 31

A second flight 32 was launched about 2 hours later. This was a SSI flight and the cloud radar image for that time is shown in Fig. 8.3.3(d) and the associated radiosonde measurements at Fig. 8.3.3(e).

.

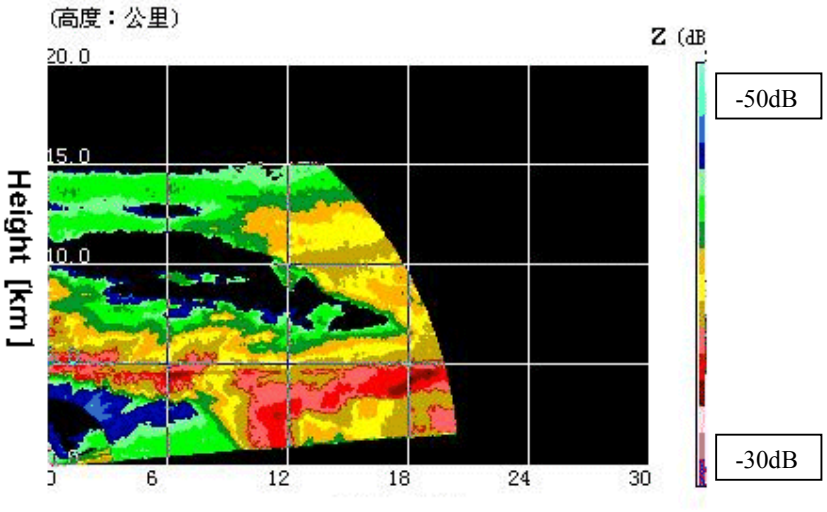

(d) Signal power, Z, as a function of range and height in km for Flight 32 at 14.45

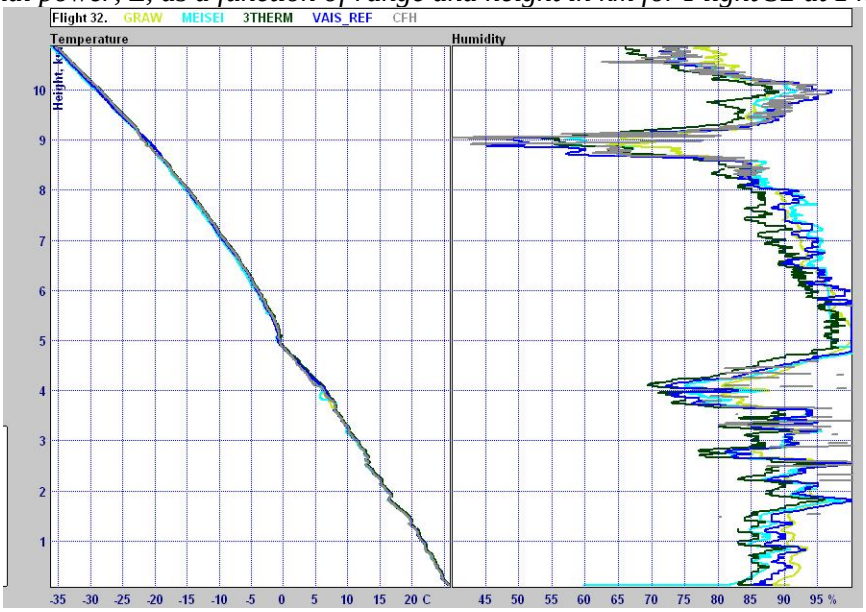

(e) Temperature and relative humdity as a function of height, as measured on Flight 32.

Fig. 8.3.3 Remote sensing and radiosonde ascents for the afternoon of 21.07.10

On Flight 32 the winds were strongest from 1 to 5 km so that the balloon moved forwards relative to the upper cloud, and ascended at heights from 5 to 10 km at a horizontal range of 4 km relative to the cloud radar. Hence the radiosondes saw a dry layer below 9 km rather than at 10 km as observed above the cloud radar. The cloud base is at 5 km as shown by the ceilometer, but the cloud radar sees the precipitation/drizzle falling into the dry layer and so shows strong signals in the relatively dry air below the cloud base for a further 1 km down to 4 km.

A final example is shown in Fig. 8.3.4 for Flight 19 at 00.51 on 18.07.10. This is a more uniform cloud layer which is located at a level where horizontal winds are week. So here the relatively strong winds at lower levels move the balloon forward relative to the upper cloud, and the radiosondes pass through the cloud layer at a horizontal range of about 18 km in relation to the cloud radar observation. The ceilometer shows a relatively uniform cloud base at about 8 km, but does in this case not actually sense the conditions experienced by the radiosondes, but just shows what happens at the zero horizontal range on the cloud radar plot.

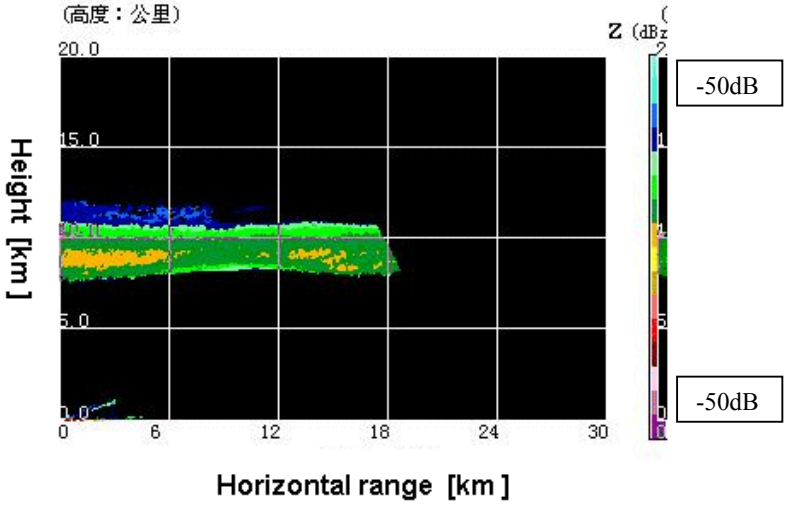

(a) Signal power, Z, as a function of range and height in km measured by cloud radar at Yangjiang on 00.51 18 July 2010, coincident with the launch of Flight 19.

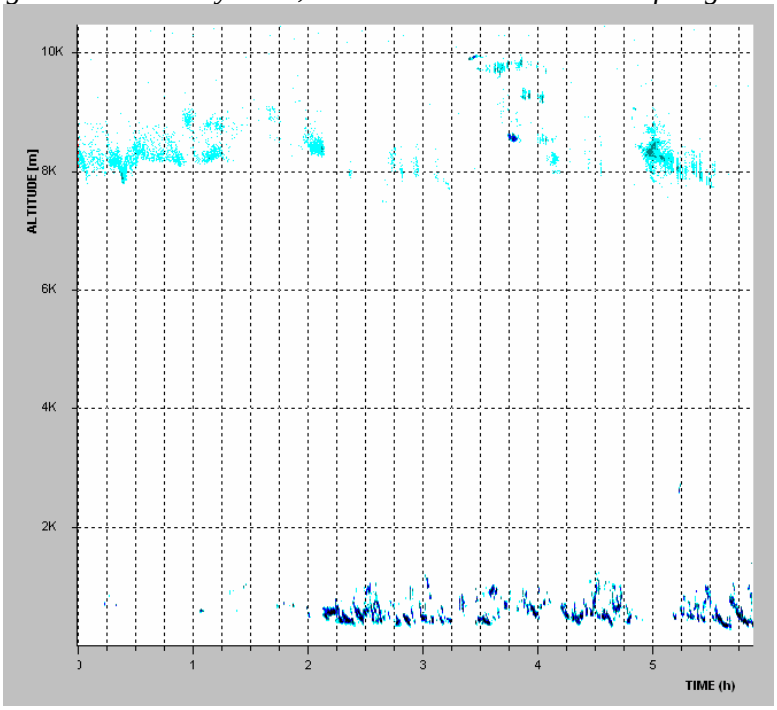

(b) Vaisala CL51 output for early morning 18.07.2010, where Flight 19 was launched at 00.51.

(c) Temperature and relative humidity structure as a function of height, for Flight 19, night time. In cloud from 8 to 10 km at least.

Fig. 8.3.4 Remote sensing and radiosonde ascents just after midnight on 18.07.10

The cloud radar and ceilometer show a cloud layer between 8 and at least 10 km. So it is possible to extract the relative humidity reported by each radiosomde system in this cloud, Flight 20, the SSI flight 2 hours later goes through similar cloud, and indicated values of relative humidity close to 85 per cent in the cloud, similar to LMS and Meteolabor. The film on the Snow White mirror was freezing at this time, and this is why there is a Snow White data gap in the cloud.

The cloud radar pictures were available for 54 of the 72 flights and these were used to identify when there was a high probability that the radiosondes were measuring in cloud. Also the infrared cooling of temperature sensors experienced by the white thermistors on Daqiao and the black and white LMS Multithermistors were used to identify when these radiosondes emerged from the top of a cloudy layer near the tropopause on night time flights.

Average values observed by each radiosonde type in cloud are plotted as a function temperature for day and night separately for Vaisala, LMS, Snow White and CFH in Fig. 8.3.5(a), for the remaining E+E sensors in Fig. 8.3.5(b) and for Changfeng, Daqiao, Meisei and Modem in Fig. 8.3.5(c). With most radiosond types there are plenty of samples for clouds between -50 and -70 deg C, and between -10 and -40 deg C. In Fig. 8.3.5(a), there are not so many CFH and Snow White measurements, so it has been assumed that daytime and nighttime measurements were of equivalent quality and the two merged together. Snow white does not show very much supersaturation with respect to ice, but CFH shows about +10 per cent, given some flights with unrealistically high positive bias were omitted. The truth probably lies somewhere between CFH, but both systems have limitations and need relatively large samples to provide best estimates of truth.

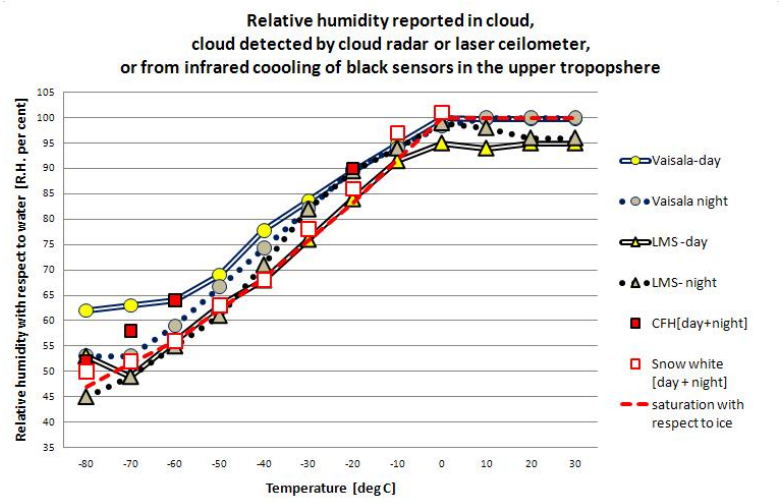

(a) CFH, LMS, Snow –White and Vaisala

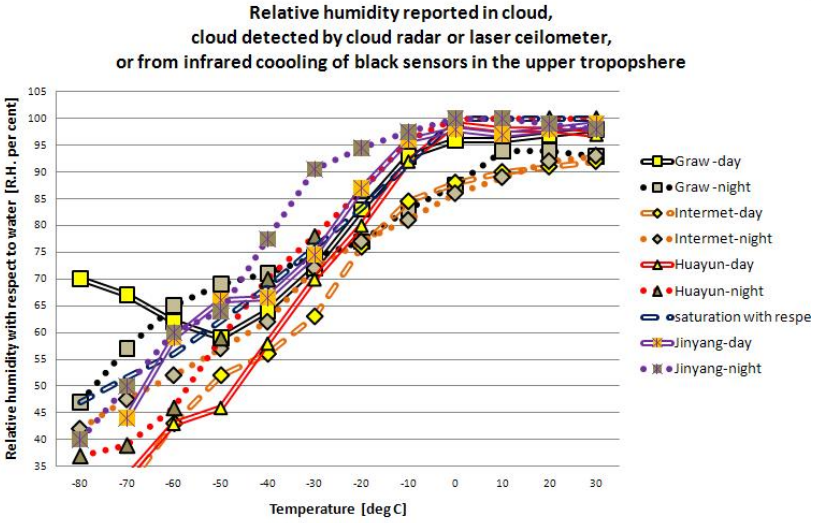

(b) Graw, Huayun, InterMet SA and Jinyang

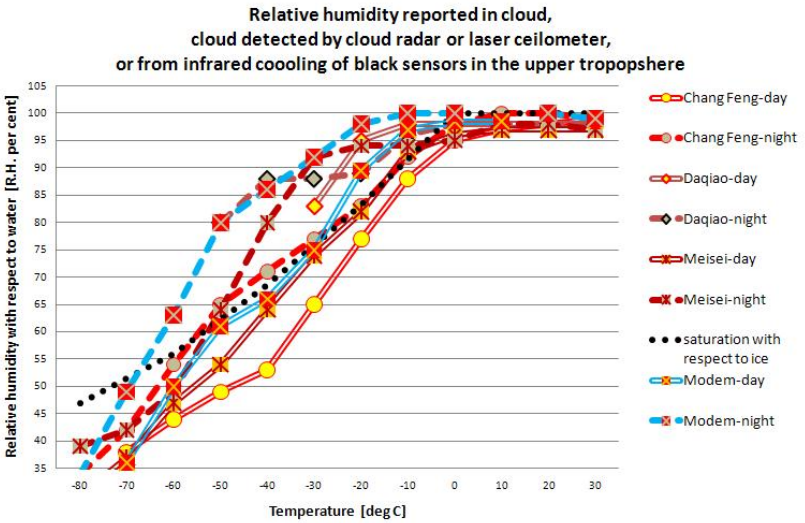

(c) Changfeng, Daqiao, Meisei and Modem

Fig. 8.3.5 Relative humidity reported in clouds identified by remote sensing

Vaisala measurements show differences between day and night at temperature lower than -60 deg C, with the daytime measurements showing higher supersaturation than those at night. Vaisala time constant corrections at night at temperatures lower than -60 deg C lead to reported values higher than raw by about 3 per cent on average. In the day the Vaisala reported values are about 16 per cent higher than raw on average. The results shown here suggest that this daytime correction may be too high and taken together with the bias plots in Fig. 8.1.6 suggest that the correction should be about 3 to 5 per cent lower than used. This may require further testing in the tropics. In clouds above 0 deg C, the average raw relative humidity reported by Vaisala was just larger than 101 per cent. This could be true, so does not confirm an inaccuracy in Vaisala measurements.

In order to cross check the results at temperatures at temperatures higher than -10 deg C, against the larger data set considered in section 8.1, the systematic bias plots are presented as a function of height for the relative humidity band 90 to 100 per cent in Fig. 8.3.6.

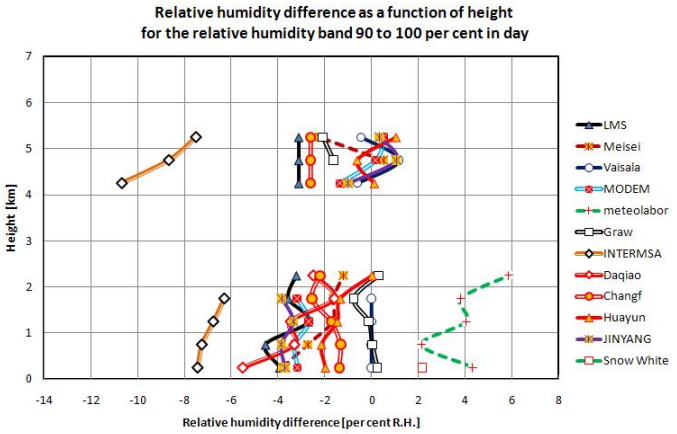

(a) Day

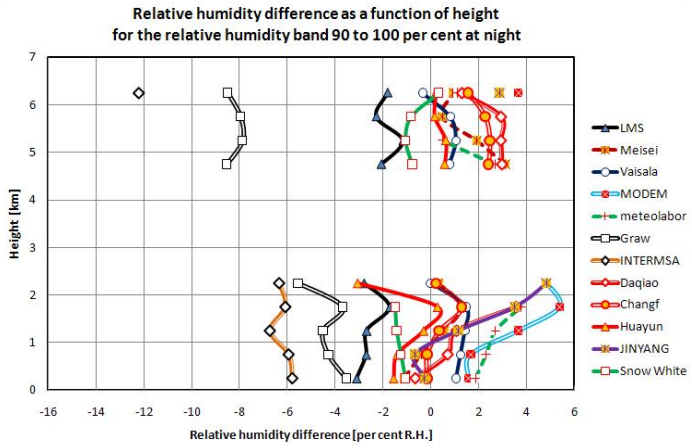

(b) Night

Fig. 8.3.6 Systematic bias in relative humidity as a function of height for the relative humidity band 90 to 100 per cent for heights from 0 to 6 .5 km.

LMS does not report relative humdity near 100 per cent in water clouds above 0 deg C, and there seemed to be a difference between day time and nighttime measurements at temperatures between 15 and -30 deg C. In Fig. 8.3.6 this difference seems to have daytime measurements about 2 per cent lower than night time. This difference can also be seen at slightly lower relative humdity in the IWV day-night comparisons in the following section.

In Fig. 8.3.5(b), Graw (night, in particular) and InterMet (similar day and night) did not report near 100 per cent in water clouds above 0 degC, and this is confirmed in Fig. 8.3.6. InterMet was always too low in cloud at all temperatures, and has a calibration difference relative to the other E+E sensors at these higher humidities. All the E+E sensors in this group apart from Graw showed relative humidity in cloud too low at temperatures lower than -60 deg C. Graw were applying software corrections and in the day time this seemd to give values which were too high at temperature lower than -60 deg C.

Jinyang at night showed higher superstauration between -20 and -50 degC than appears plausible, and in Fig. 8.3.5 (c) it can be seen that Modem, Meisei, and Daqiao had similar problems. Work needs to be performed to check that this is not a contamination problem caused by the protective caps.

All the radiosonde systems in Fig. 8.3.5 (c) have low systematic bias in water clouds above 0 deg C, but also all of them report values too low in cloud at temperatures lower than -50 deg C.

8.4 Comparison of radiosonde measurements of integrated water vapour with GPS remote sensing of water vapour near Yangjiang

Yangjiang is relatively close to five operational sites in the operational GPS network, and an additional sensor was added at Yangjiang itself. Enping and Yangchun are further inland than Yangjiang. The time when radiosonde measurements were made are shown in Fig. 8.4.1.

As in Mauritius, integrated water vapour (IWV) computed from each type of radiosonde were compared with simultaneous values of integrated water vapour from the GPS network. As there were some data gaps in the GPS from the Yangjiang site, it was found that a larger data set giving lower uncertainty in the comparisons was found by using an average of GPS measurements from Yangjiang, Enping and Yangchun. Most of the radiosonde ascents drifted inland from Yangjiang, towards either Enping or Yangchun. The range of values observed on this day were typical of most of the test and there was only limited periods with the value observed lower than 50 $kg.m^{-2}$.

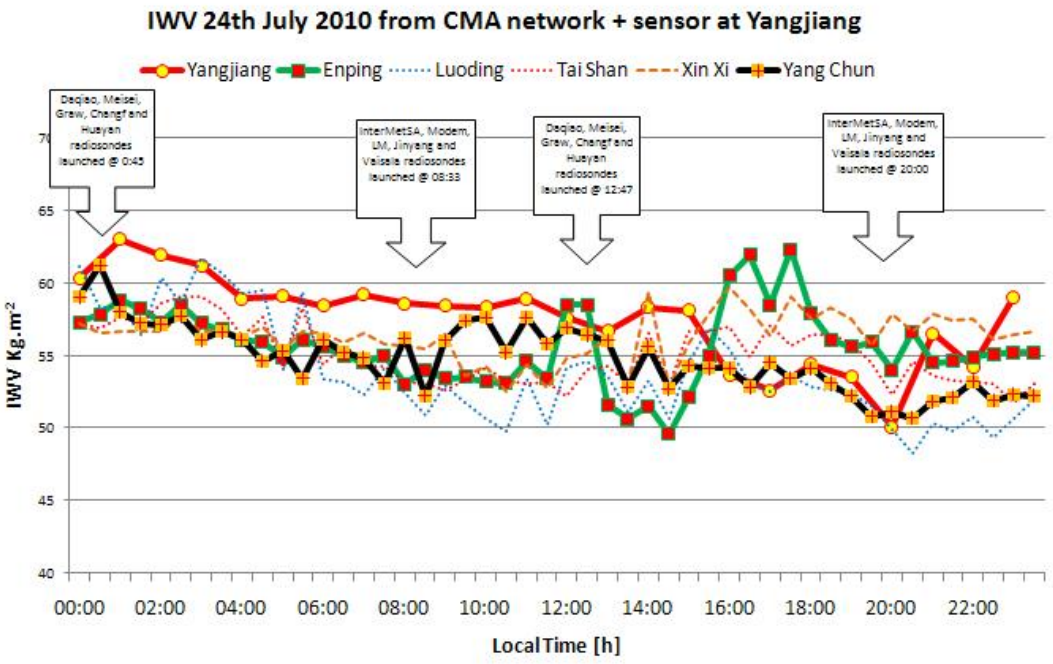

Fig. 8.4.1 Example of GPS IWV measurements for 24 July 2010, as supplied by CMA. The Yangjiang sensor was at the observatory, and Enping and Yangchun were the closest stations to Yangjiang to the north.

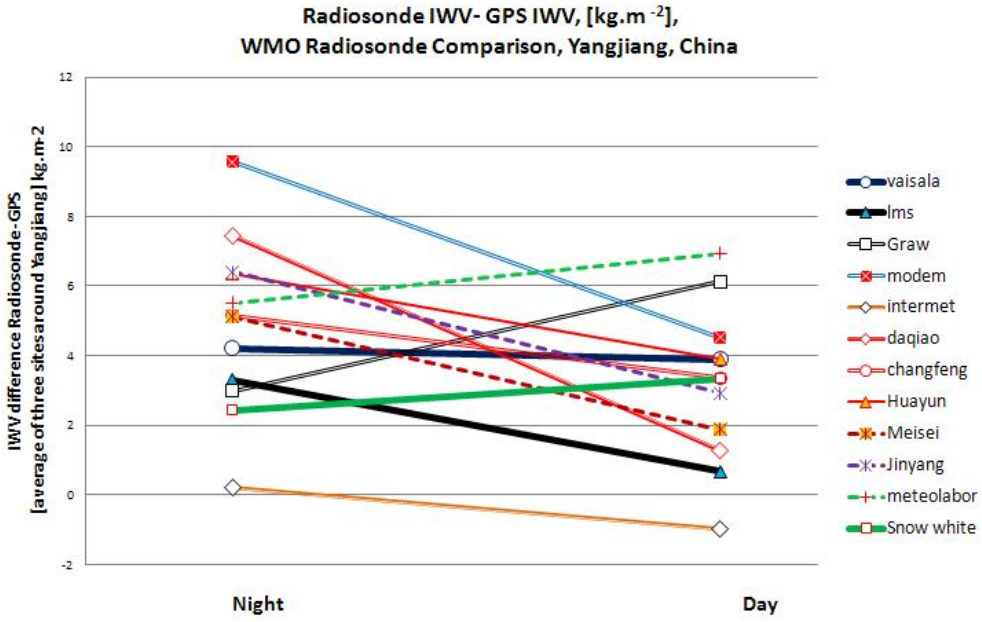

Fig. 8.4.2 Results of systematic bias in comparisons of integrated water vapour from each radiosonde type with simultaneous Yangjiang, Enping and Yangchun GPS integrated water vapour measurements.

The systematic bias between radiosonde and GPS water vapour for day and night are shown in Fig. 8.4.2. The random error [k=1] associated with each systematic bias apart from Daqiao was 0.65 $kg.m^{-2}$ at night and 0.5 $kg.m^{-2}$ during the day. With Daqiao measurements, the random error in the systematic bias was 1 $kg.m^{-2}$. Thus, this comparison with GPS confirms the poorer reproducibility of Daqiao measurements. If most random errors in the radiosonde IWV were derived from measurements with a random error in relative humidity of 3 to 4 per cent, then the random error in the average of the GPS measurements is found to be about 1.5 $kg.m^{-2}$ at night and 1.2 $kg.m^{-2}$ in the day.

Those radiosondes expected to have low day-night difference in the lower troposphere from previous WMO radiosonde Comparisons (Snow White and Vaisala) show little day-night difference in Fig. 8.4.2 in comparison with GPS. Therefore, it would appear the systematic errors of the GPS measurements were similar between day and night observations, and the references day to night in the statistical analysis in the lower and middle troposphere are not unreasonable.

The average values from the radiosondes do not agree with the GPS measurements in Fig. 8.4.2. InterMet is shown in Figs. 8.3.3 and 8.3.4 to give values too low in cloud, and this low bias extends down to about 60 per cent R.H., see Figs. 8.1.2 and 8.1.4, so is not correct. It is probable that an average of LMS and Vaisala + Snow White + Changfeng should be within 1.5 $kg.m^{-2}$ of the “truth”, given the random errors and systematic biases noted earlier.

GPS water vapour measurements do have biases that depend on the processing and the adequacy of the network used in processing. These have been examined in Europe for instance; de Haan, http://egvap.dmi.dk/3-monitoring-validation-products-de-Haan.pdf. The biases in Yangjiang may be a bit larger than found by some authors, but the measurements are consistent with the flight-testing results, showing that there was good skill in the GPS measurements.

9 Comparison of simultaneous geopotential height measurements

9.1 Introduction

All the radiosonde systems apart from Daqiao used the GPS system to measure geometric height and then convert this to geopotential height. This procedure does not need any knowledge of the virtual temperature or pressure distribution with height.

Daqiao were using a pressure sensor, which then used virtual temperature plus surface pressure and the pressure in flight to produce a value for geopotential height, see the relevant chapter of the CIMO Guide. This pressure sensor also allowed Daqiao operators to judge when the tracking of the secondary radar was in error for a short time. (Height was available from the secondary radar data)

The references used in the statistical processing of the geopotential height comparisons are shown in Table 9.1

Height range, [km]	Group working references	Linking radiosondes	Typical uncertainty in LMS-Changfeng link, [gpm]	Reference for systematic difference plot	Category
0 to 16	LMS, Changfeng	Vaisala, Meteolabor, Daqiao	<3	LMS, Vaisala, Modem, Graw, Meteolabor, InterMet, Huayun Changfeng	Day+night
16 to 24	LMS, Changfeng	Vaisala, Meteolabor, Daqiao	<4	LMS, Vaisala, Modem, Graw, Meteolabor, InterMet, Huayun, Changfeng	Day+night
24 to 32	LMS, Changfeng	Vaisala, Meteolabor,	<6	LMS, Vaisala, Modem, Graw, Meteolabor, InterMet, Huayun, Changfeng	Day+night

Table 9.1: References used in the processing of the geopotential height statistics and the resultant error in linking the results from the LMIJ and CHGM groups

9.2 Examples of height comparisons from individual flights

Examples of comparisons from a LMIJ group flight and CHGM group flight are shown in Figs. 9.2.1 and 9.2.2. Flight 49 was selected randomly for the LMIJ group, not because agreement was exceptionally good. The systematic differences between GPS heights of different radiosondes were much larger than the random error of the systems against the average. Vaisala have now realised that there was an incorrect setting for the height of their GPS antenna at Yangjiang and this made all their heights 5m too low. In addition, the systematic differences depend to some extent on the algorithms used to interpolate between the surface and the time shortly after launch when the GPS measurements were reliable. The assumption of uniform rate of ascent after launch seemed to come closest to the way the balloons lifted on most flights in Yangjiang. In addition, if the time of launch is incorrectly identified then this will also introduce error in routine operational flights.

Flight 47 was chosen more carefully to show an ascent where the pressure sensor did not produce its largest errors in the stratosphere. The performance of the GPS systems was similar to those in Fig. 9.2.1, apart from Graw. However, the reason for this has been identified and rectified, so the subsequent statistical results use data with the error rectified.

On many Meisei flights the random errors in height were larger at times when the balloon rate of ascent was changing rapidly with time, which in Fig. 9.2.2 was between minutes 30 and 40. Meisei now propose to change the filtering used in the computation to provide heights that are more reliable. In addition at least 5 flights were found where Meisei tracking was faulty for most of the flight, and it was agreed by the final review meeting that these could be flagged out, given that Meisei would test to try and understand what caused the problem.

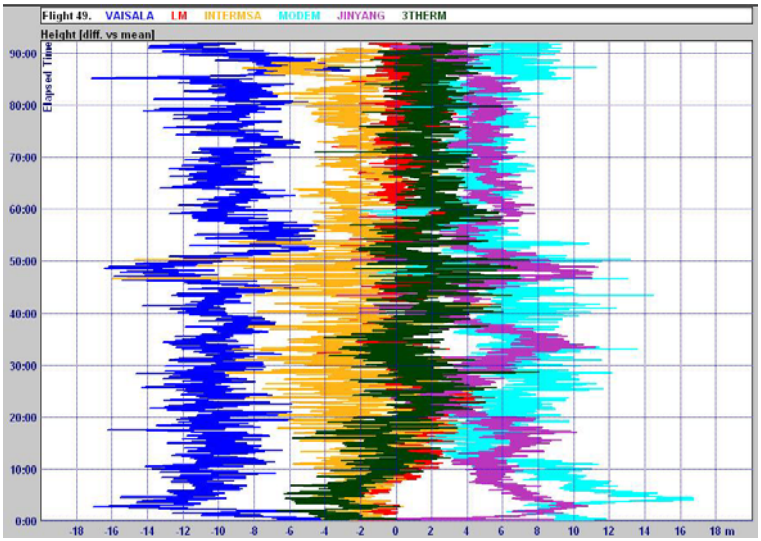

Fig. 9.2.1 Example of differences between simultaneous height measurements from the LMIJ group + Vaisala, as a function of time into flight. The zero difference at each height is the average of all the measurements. All measurements derived using GPS measurements

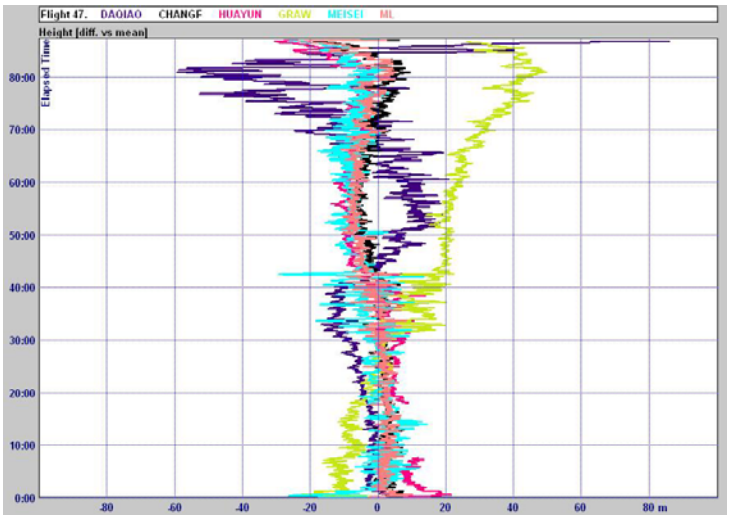

Fig. 9.2.2 Example of differences between simultaneous height measurements from the CHGM group + Daqiao, as a function of time into flight. The zero difference at each height is the average of all the measurements. All measurements derived using GPS measurements apart from Daqiao. Graw measurements did not follow the other GPS systems, and the reason has been identified and rectified.

9.3 Statistical results of geopotential height comparisons

The results of combining the information from the two groups of quality radiosonde systems to show the systematic bias between the different systems is shown in Fig. 9.3.1. The results are based on the difference between at least 28 flights up to 100 hPa and slightly lower numbers of flights at the uppermost levels. The pressure sensor used by Daqiao works well up to 24 km, but cannot match the reproducibility of the GPS height measurements above 24 km. This can be seen from the random error estimates shown in Fig. 9.3.

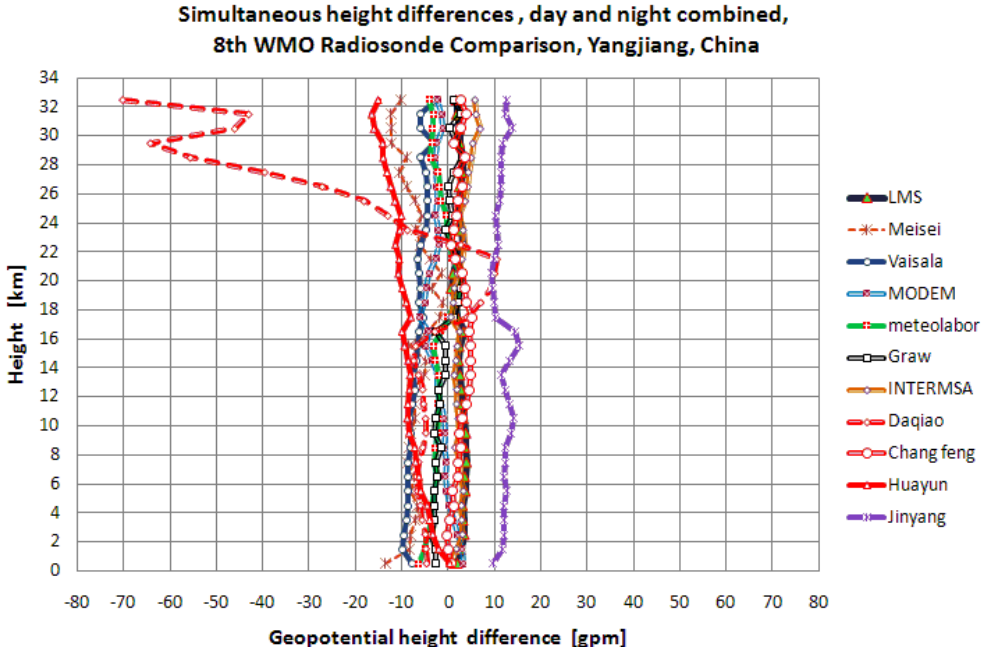

Fig. 9.3.1 Systematic bias between simultaneous geopotential heights [gpm], daytime and night-time measurements combined.

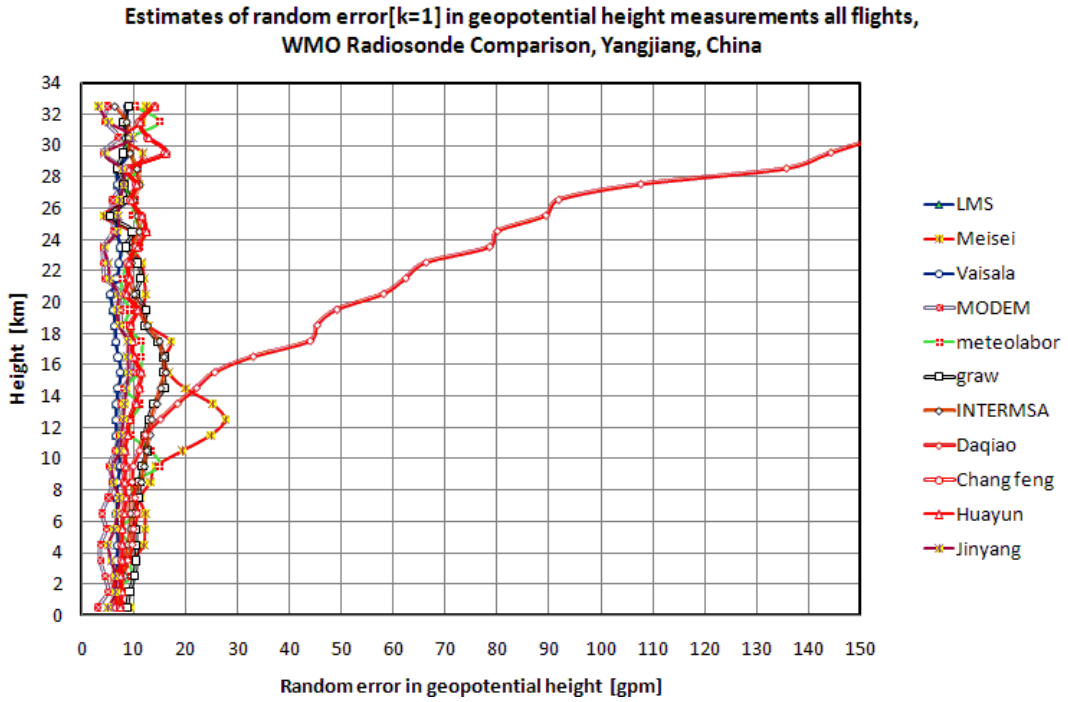

Fig. 9.3.2 Random error (k=1) of geopotential heights [gpm] measurements, daytime and night time measurements combined.

The random errors in Meisei heights are larger in the upper troposphere because of the problem with the filtering.

The current statement of accuracy required for geopotential height measurements of a significant level, e.g. tropopause, capping inversion, jet stream maximum is stated as 1 per cent near the surface decreasing to 0.5 per cent near 100 hPa in the current CIMO Guide. This is impossible for any system to meet in the boundary layer. Given the existing requirements for pressure in the CIMO Guide, it is suggested that the accuracy requirement and equivalent for pressure, given in Table 9.2.1, should be considered for future use. This relaxes the height requirement to 15 m, a requirement which can be validated with correctly functioning GPS radiosondes, and seems accurate enough for determining the height of inversions and fog top/cloud base and top near the ground, given the representativeness errors which are associated with measuring the heights whether with remote sensing (ceilometer/cloud radar) or with radiosondes.

If the proposal in Table 9.2.1 were accepted as suitable for the CIMO Guide, then Daqiao would fulfil all the height requirements for operational radiosondes up to about 28 km.

Height [km]	Accuracy requirement for geopotential height [gpm]	Accuracy requirement for pressure [hPa]
1	15	1.5
3	15	1.5
6	20	1.5
10	30	1.5
16	60	1.0
20	100	1.0
24	100	0.5
32	120	0.2

Table 9.2.1: Proposed revised accuracy statement (k=1) for measuring heights/ pressures of significant levels, such as capping inversions or the tropopause in the troposphere and heights/pressures of temperature and wind structures in the stratosphere.

With the GPS height measurements, the most difficult part of the accuracy requirement to meet is from the surface to about 3 km, but all the most reproducible GPS systems should be able to meet it. The weakness in some systems is the systematic bias shortly after launch. In future, the project leader should check the launch and antenna co-ordinates used by the participants, including survey height, to eliminate unnecessary inconsistencies before the test starts.

The low errors in the heights from GPS radiosondes eliminate one of the main problems for climate scientists with historical radiosonde measurements in the stratosphere, where the errors from the pressure sensors in height assignments were often producing bigger temperature errors than the errors in the temperature sensor itself. Unfortunately, it is almost impossible to trace the systematic errors in these old radiosondes. In this context, the performance of the Daqiao pressure sensor in Yangjiang was of good quality, although not quite as good as the Vaisala pressure sensor in Mauritius.

Note: for the SSI systems, the MTR reported height as geometric, not geopotential height to facilitate comparison with lidars and other remote sensing systems and the CFH would benefit from better height measurements than were provided by its host radiosonde in Yangjiang.

10 Comparison of simultaneous pressure measurements

10.1 Introduction

In this section, only the Daqiao measurement is the results of a direct sensor measurements and all the rest are the results of computation from the geopotential height derived from the GPS geometric height. The computation from the geometric height uses the temperature and relative humidity measurements from the radiosonde and is similar in principle to that used for Russian radiosonde measurements (see the CIMO Guide) where in that case height measurements come from secondary radar. All the radiosonde systems apart from Daqiao used the GPS system to measure geometric height and then convert this to geopotential height. This procedure does not need any knowledge of the virtual temperature or pressure distribution with height.

The references used in the statistical processing of the pressure comparisons are shown in Table 10.1

Height range, [km]	Group working references	Linking radiosondes	Typical uncertainty in LMS-Changfeng link, [hPa]	Reference for systematic difference plot	Category
0 to 8	LMS, Changfeng	Vaisala, Meteolabor, Daqiao	<0.05	LMS, Modem, Huayun, Changfeng, Daqiao, Vaisala	Day+night
8 to 22	LMS, Changfeng	Vaisala, Meteolabor, Daqiao	<0.08	LMS, Modem, Huayun, Changfeng, Daqiao, Vaisala	Day+night
24 to 32	LMS, Changfeng	Vaisala, Meteolabor,	<0.01	LMS, Modem, Huayun, Changfeng, Daqiao, Vaisala	Day+night

Table 10.1: References used in the processing of the pressure statistics and the resultant error in linking the results from the LMIJ and CHGM groups

10.2 Examples of pressure comparisons from individual flights

Examples of comparisons from a LMIJ group flight and CHGM group flight are shown in Figs. 10.2.1 and 10.2.2. These correspond to the height differences for the same groups shown in Figs. 9.2.1 and 9.2.2

When the Meteolabor pressures were examined, it was found that there were 2 flights with large anomalies in the histogram of pressures versus Changfeng measurements (Flight 36 and 38) and one flight where the values were very inconsistent as a function of height (Flight 67). The data from these flights were hidden; otherwise, there was negligible editing of the pressure data.

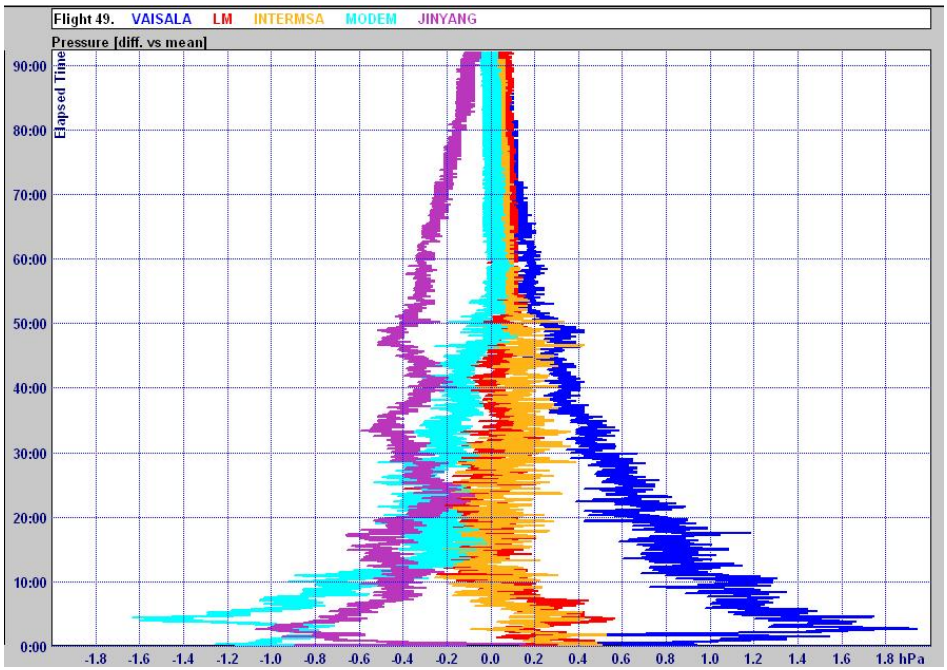

Fig. 10.2.1 Example of differences between simultaneous pressure measurements from the LMIJ group + Vaisala, as a function of time into flight. The zero difference at each height is the average of all the measurements. All measurements derived using GPS measurements

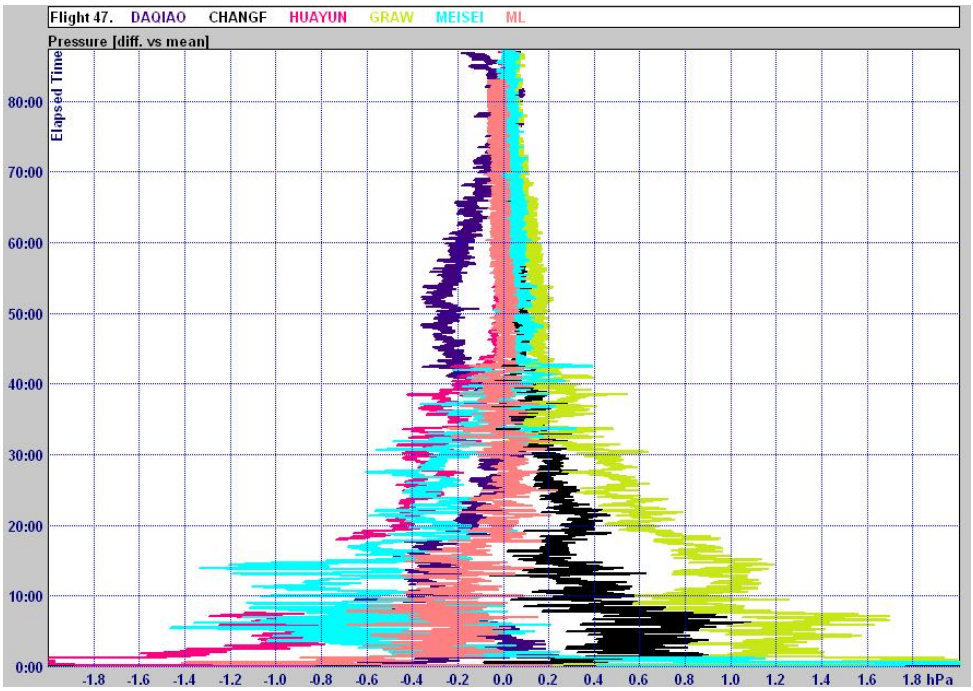

Fig. 10.2.2 Example of differences between simultaneous pressure measurements from the CHGM group + Daqiao, as a function of time into flight. The zero difference at each height is the average of all the measurements. All measurements derived using GPS measurements apart from Daqiao. Graw measurements did not follow the other GPS systems and the reason has now been identified and rectified.

10.3 Statistical results of pressure comparisons

The results of combining the information from the two groups of quality radiosonde systems to show the systematic bias between the different systems are shown in Fig. 10.3.1. The results are based on the difference between at least 28 flights up to 100 hPa and slightly lower numbers of flights at the uppermost levels. The corresponding random error estimates are shown in Fig. 10.3.2.

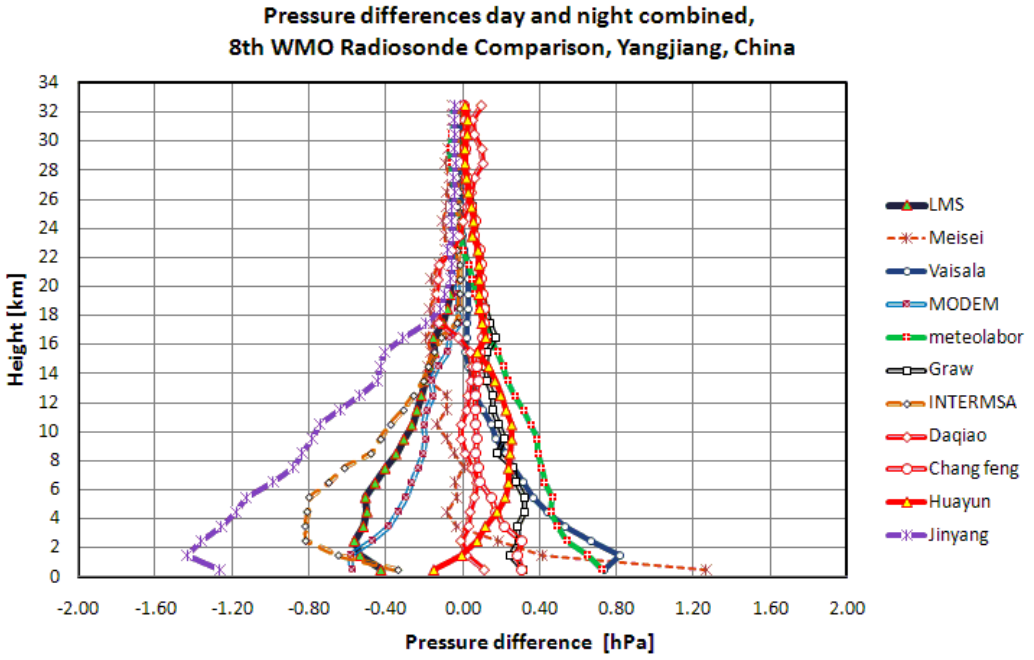

Fig. 10.3.1 Systematic bias between simultaneous pressures [hPa], day-time and night-time measurements combined.

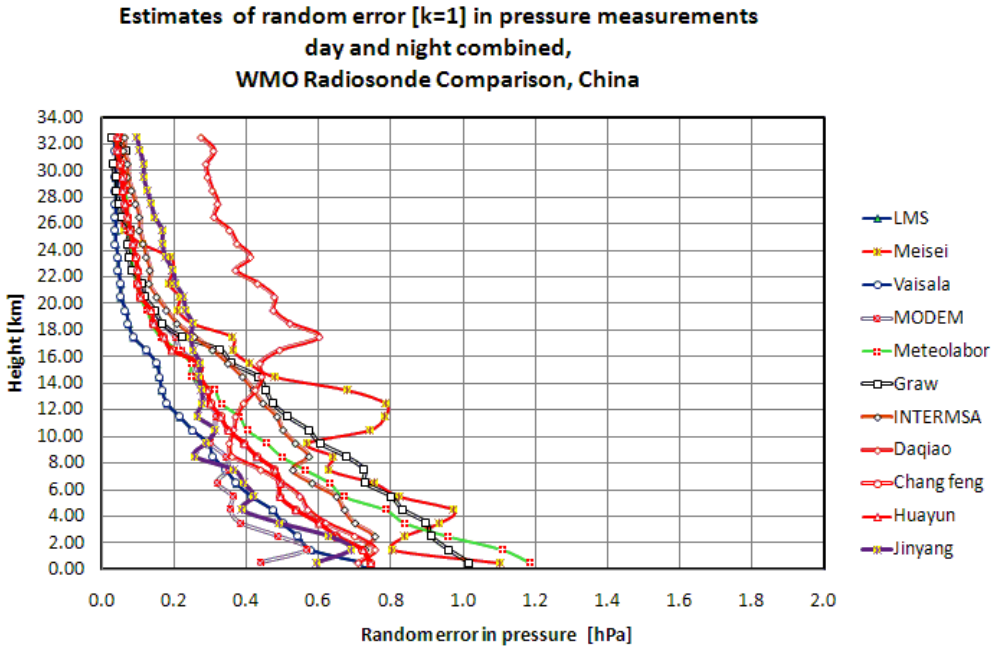

Fig. 10.3.2 Random error (k=1) of pressure [hPa] measurements, day-time and night-time measurements combined

The main issue in these results concerns the performance near the ground. Vaisala kindly provided the raw data from most of their flights and this contained observations from the pressure sensor on the radiosonde, which was otherwise not used in the reported data submitted for the test. The pressure sensor observations in Vaisala Raw near the ground are compared to the actual pressures reported near the ground for all Vaisala comparison flight. This shows that pressures were about 1 hPa too low up to 200 m above the ground, with the bias then reducing to about -0.8 hPa at 1 km above the ground, random error in both measurements probably from 0.5 hPa, reducing to 0.3 hPa see Fig. 10.3.3

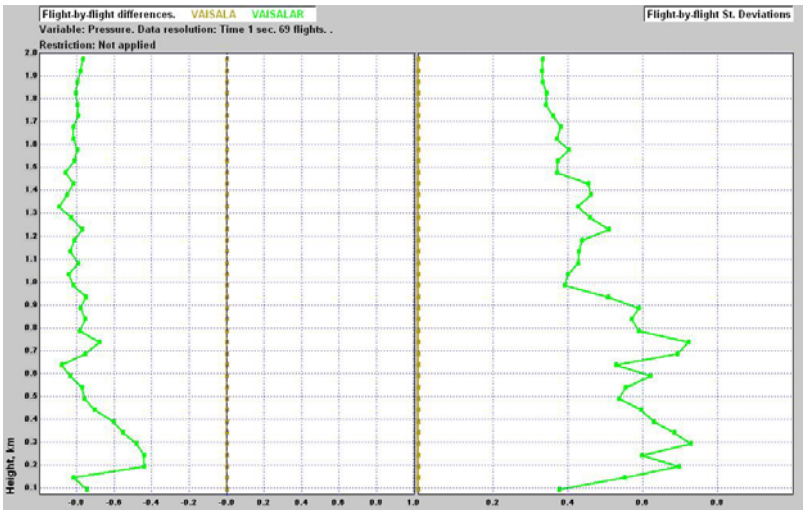

Figure 10.3.3 Comparison of Vaisala RS92 pressure sensor observations (VaisalaR) with the values from the GPS measurements (Vaisala) in the first 2 km of the flight, for 32 QRS flights. Vaisala found that the height of their GPS antenna was in error by 5 m, and this would have the effect on pressure shown for Flight 49 in Fig. 10.3.4.

Fig. 10.3.4 Effect of GPS heights 5 m too low on the Vaisala pressure computation as a function of time into flight, for Flight 49, with pressure too low near the ground.

Because of this result, the reference for the plots in Fig. 10.3.1 was changed to that shown in Table 10.1, with InterMet omitted, and Daqiao added to the group. This then brought the zero line closer to the two pressure sensors (Daqiao and what the Vaisala pressure sensor indicated at low levels). Thus, it seems probable that the zero line in Fig. 10.3.1 is close to the truth.

Pressure is probably the most difficult meteorological variable to compare reliably, because an error of 1s in synchronisation can produce a systematic bias of 0.6 hPa near the surface. However, the results in Fig. 10.3.1 suggest that manufacturers should check how they are processing their data close to the ground, to try to minimise errors in the height and pressure computations, when locking to the surface values.

Meteolabor have found that the data were not being tied correctly to the surface height at Yangjiang, and this error has now been corrected in the operational system, in Switzerland. Meteolabor will have to check whether this problem was also leading to the high random errors at low levels and the flights that had to have pressure data hidden.

The Graw observations shown in Figs. 10.3.1 and 10.3.2 are the results of two sets of reprocessing, first to remove an error in the geopotential height computation, and then to remove another error in the pressure computation.

The random errors in Meisei measurements were originally too large to meet the standards proposed in Table 9.1, or in the CIMO Guide, but with 5 flights flagged out the results are much better in Fig. 10.3.2.

11 Comparison of simultaneous wind measurements

11.1 Introduction

All radiosondes In Yangjiang apart from the Daqiao systems measured winds from GPS tracking of the radiosonde. The GPS engines differ from radiosonde to radiosonde and the resultant winds differ from system to system in the filtering applied to smooth the winds and to remove the motion of the radiosondes relative to the balloon, as the radiosondes swing together in a circular pendulum motion under the balloon. The Daqiao system uses a secondary radar to track the radiosonde, measuring the angle from which the signals come and the range from the radar. This system is in widespread operational use in China.

Winds in the troposphere were of varying magnitude and direction. In the stratosphere, there were relatively strong easterly winds throughout the experiment, as can be seen in Fig. 11.1.1. This shows a summary of winds once per day throughout the test. The choice of the radiosonde type for this plot is arbitrary, since as can be seen in Figs. 11.1.2 and 11.1.4 it is not possible to discriminate differences in measurement quality between the various radiosonde systems on a plot with this scale.

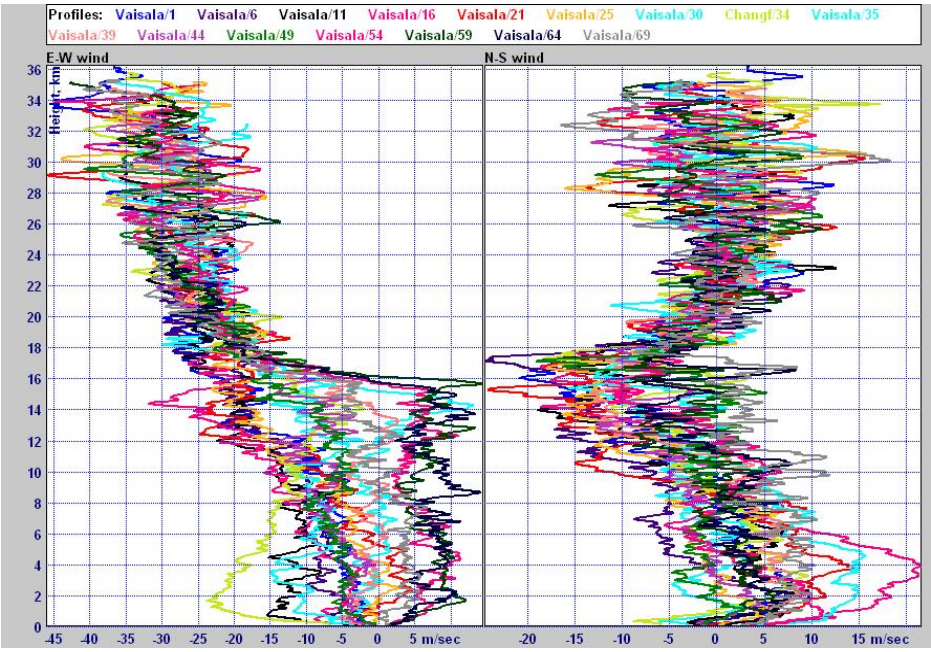

Fig. 11.1.1 Summary of winds observed during the WMO Radiosonde Comparison Yangjiang presented in terms of E-W component [positive value westerly wind], and N-S component [positive value southerly wind].

The strongest easterly wind components were observed as a small typhoon, Chanthu, was to the south of Yangjiang; see Fig. 11.1.2 where the observations from all the radiosondes on this ascent are shown. The strongest southerly components were five days earlier when typhoon Conson was approaching Yangjiang but then passed west of Hainan Island into Vietnam. Fig. 11.1.4 shows the winds just over a day later when the Chanthu had passed north of Yangjiang, positioned about 100 km to the west of the site. In most flights, it is impossible to tell the difference between the different systems on this type of summary plot.

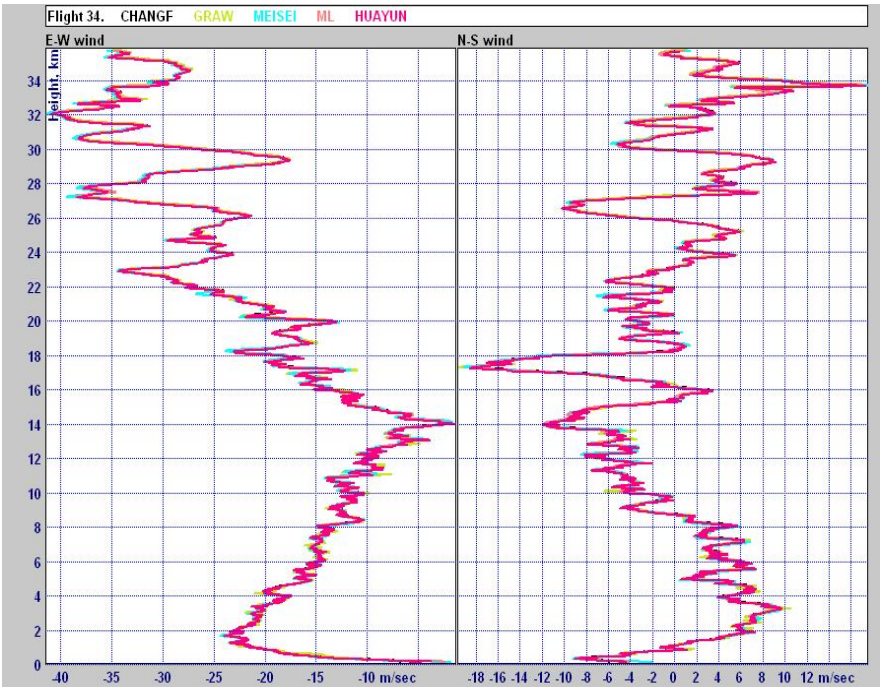

Fig. 11.1.2 Winds as a function of height, measured on Flight 34, as typhoon Chanthu approached Yangjiang

In Fig. 11.1.2, there were strong southeasterly winds at 3 km above a layer of northeasterly winds below 1 km. The wind profiler installed for the comparison operated throughout the typhoon period and Fig. 11.1.3 shows the measurements from the wind profiler compared with the radiosondes at times close to the launch of Flight 34. The statistics of such comparisons will be presented in section 11.4. On this flight, the wind profiler measurements were in general agreement with the structure of the radiosonde winds in the vertical.

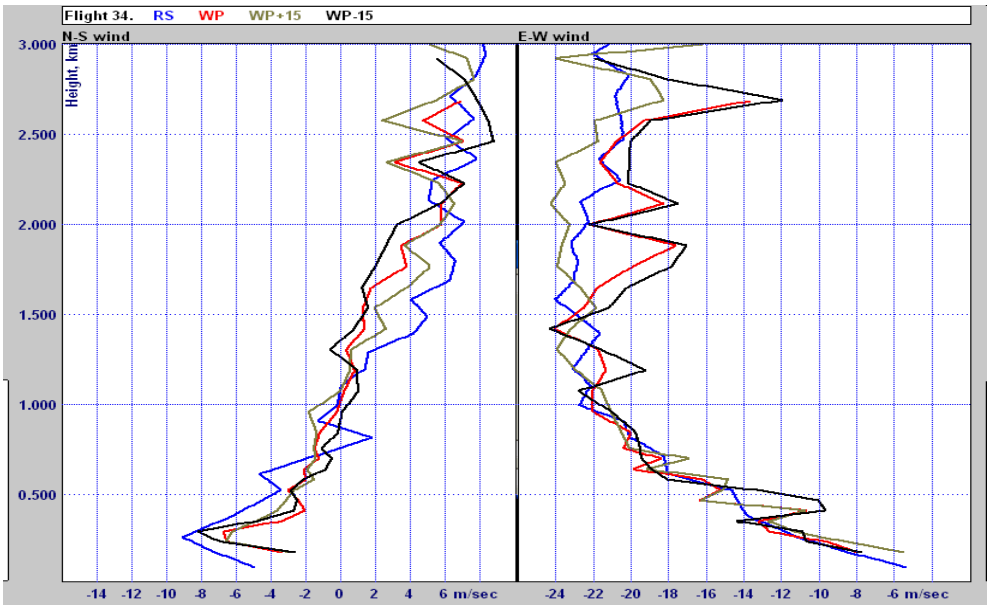

Fig. 11.1.3 Comparison of wind profiler measurements with the radiosonde on flight 34. WP profiler winds are centred at the launch time, WP-15 15 minutes before, and WP+15 15 minutes later.

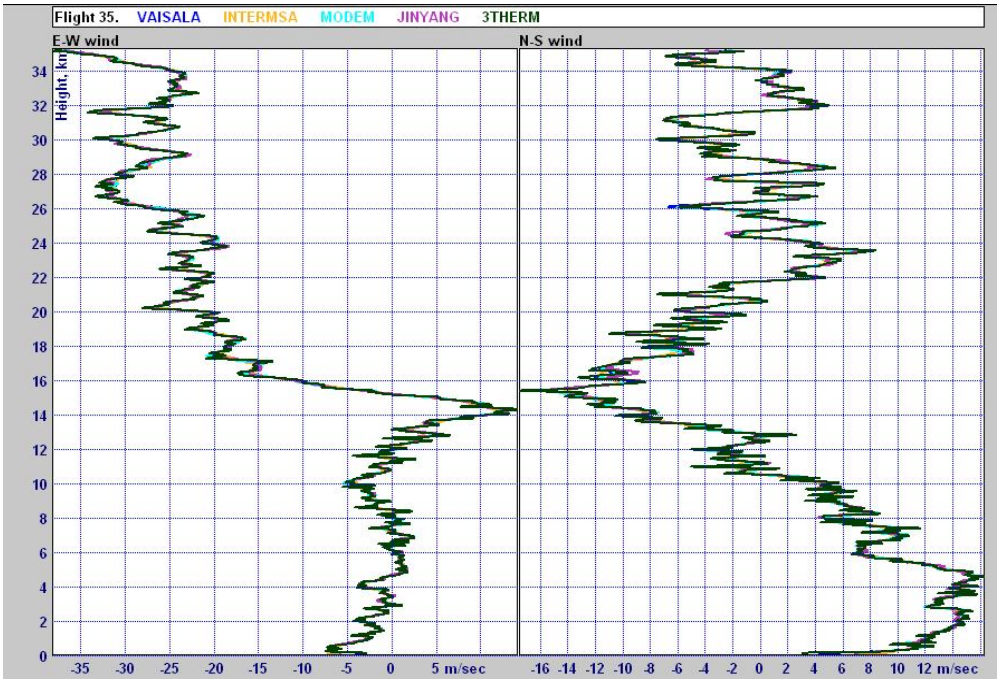

Fig. 11.1.4 Winds as a function of height, measured on Flight 35, as typhoon Chanthu has passed to the north west of Yangjiang

After the passage of the typhoon there was now a northeasterly flow between 11 and 15 km, which brought very moist air/ upper cloud across Yangjiang after the typhoon.

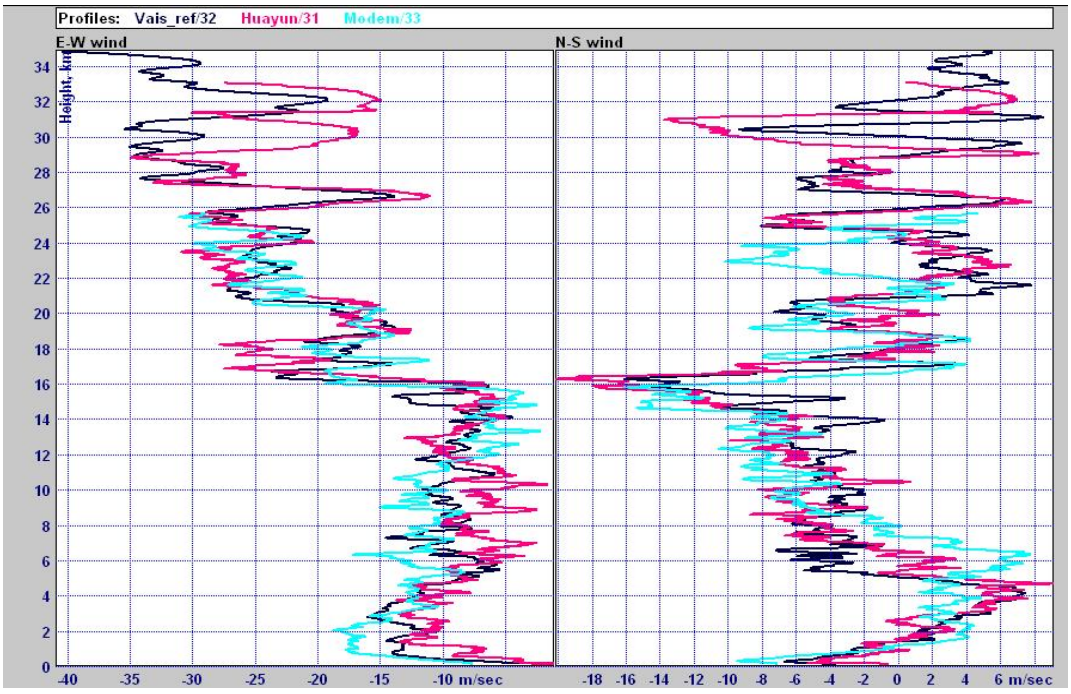

Fig. 11.1.5 Wind measurements as a function of height from 12.47, (31), 14.45 (32, SSI) and 19.59 (33), local times, on 21.07.2010, Yangjiang.

In each radiosonde wind profile there is quite a lot of small scale structure. Whilst some of this short lived, other variations in the vertical associated for instance with quasi-inertial gravity wave are of quite large horizontal extent and so can be seen in subsequent ascents. Winds from two QRS flights and an interleaved SSI flight are compared in Fig. 11.1.5. Much, but not all, of the vertical structure in the stratosphere persisted between these three flights. The radiosonde measurements in each ascent were equivalent in measurement capability.

One of the scientific uses for radiosonde wind measurements in the stratosphere and upper troposphere is for the study of gravity waves, so it is important that these variations in wind be archived for the future at sufficient radiosonde stations worldwide. At Yangjiang, the gravity waves at upper levels were not only seen as variations in u and v in the vertical with wavelengths 2 to 4 km, but also produce variations in the vertical velocity of the balloon, see measurements from the upper part of Flight 31 compared with the balloon rate of ascent in Fig. 11.1.6.

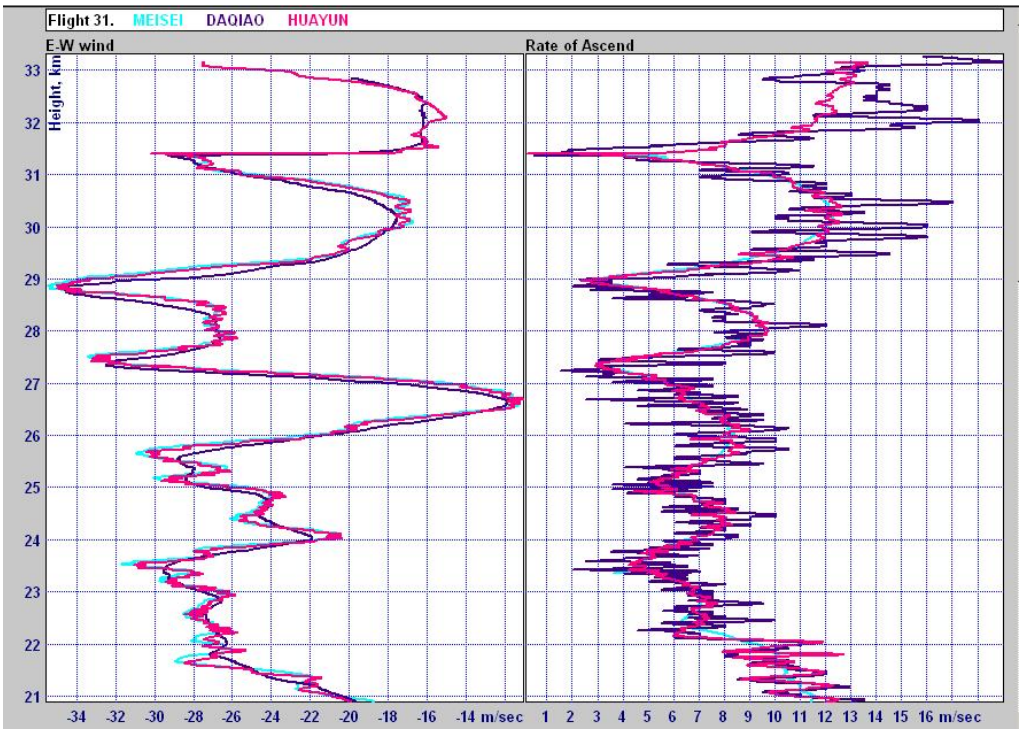

Fig. 11.1.6. Comparison of E-W wind components with variation in the rate of ascent of the balloon estimated from the radiosonde height measurements

The consequence of the gravity wave activity in the stratosphere is that to define the mean wind accurately at a given level for climate purposes, it is necessary to take many more measurements than you would expect from the high measurements quality achieved with GPS radiosonde systems.

11.2 Evaluation of radiosonde wind measurements

In this section, the relative performance of the GPS wind measurements is mostly compared in terms of orthogonal wind components, since the error estimates obtained by this method are not directly dependent on the strength of the winds, whereas the errors when comparing wind directions are strongly dependent on wind speed at low wind speed.

11.2.1 Examples of comparisons from individual flights

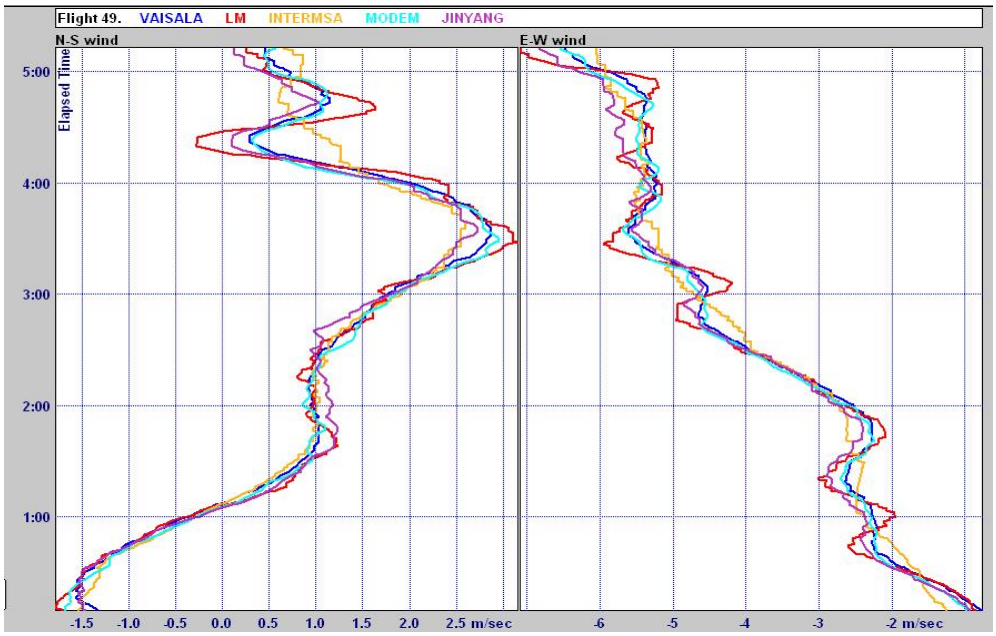

(a) Immediately after launch

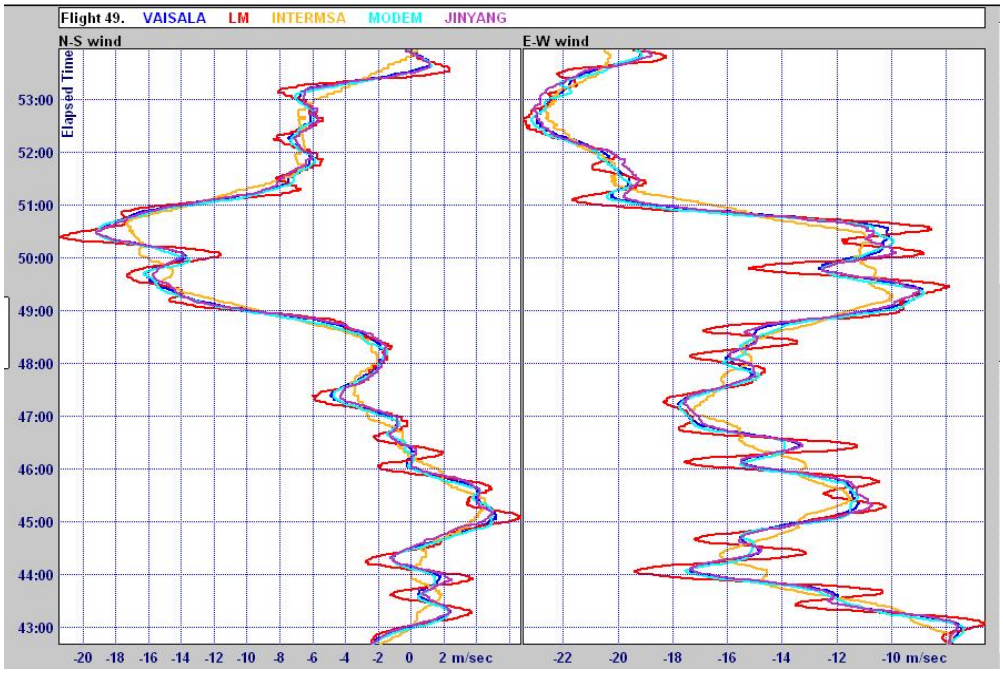

(b) Upper troposphere

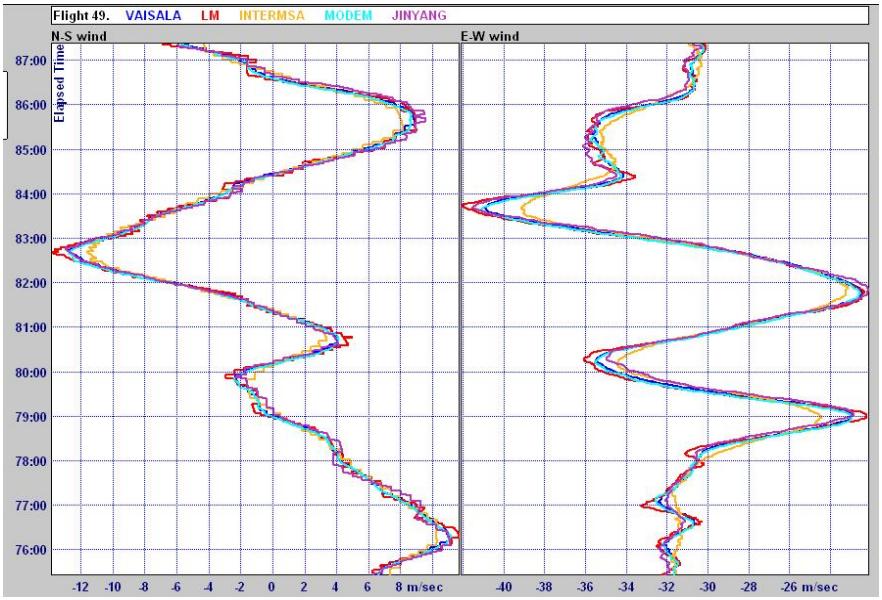

(c) Near end of flight

Fig. 11.2.1 Excerpts of simultaneous wind component measurements by the LMIJ group + Vasiala on Flight 49

Fig. 11.2.1. shows three excerpts of the second by second comparison data obtained during one flight. Here, all the wind measurement systems in the LMIJ group + Vaisala worked reliably after launch and throughout the ascent. The measurements of the different systems differ in the software filtering applied, with LMS showing most detail in fine structure and InterMet the least detail.

Similar excerpts for the CHGM group + Daqiao and Meteolabor are shown in Fig. 11.2.2.

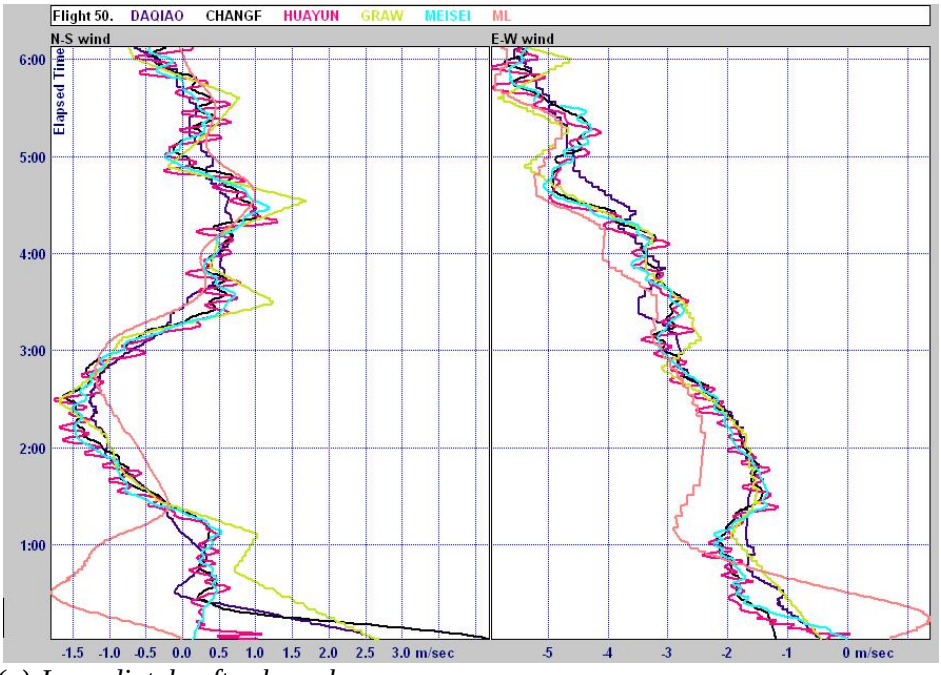

(a) Immediately after launch

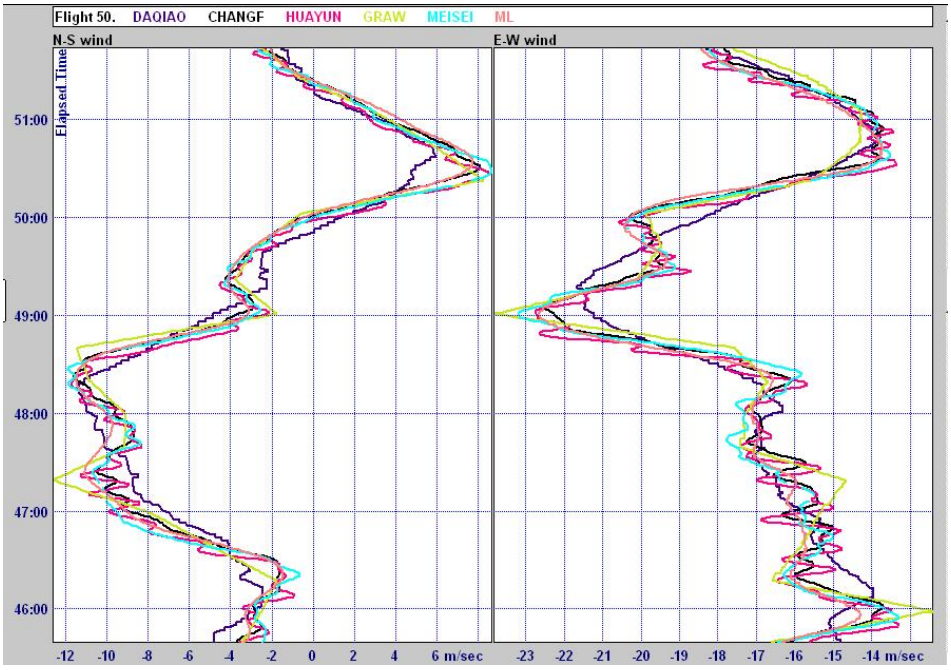

(b) Upper troposphere

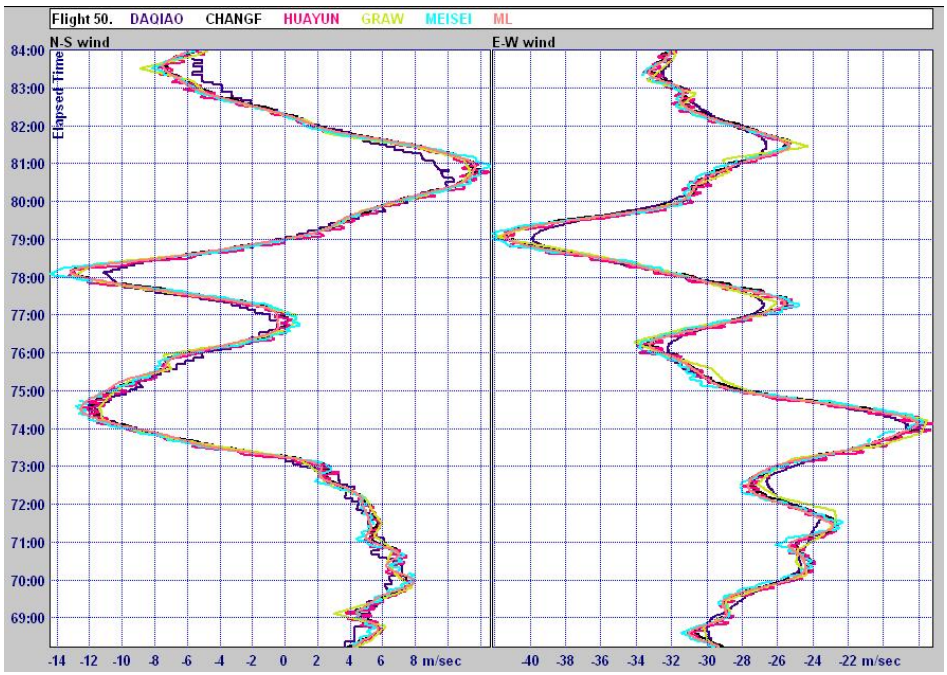

(c) Near end of flight

Fig. 11.2.2 Excerpts of simultaneous wind component measurements by the CHGM group plus Daqiao and Meteolabor on Flight 50.

The CHGM group had some problems in generating reliable winds in the first 30 s after launch and in two cases in the first minute after launch. Meisei and Huayun appear the most reliable near the surface. In order to launch the Daqiao on the multiple radiosonde rig, it was not possible to use the standard operational procedures for launch used with secondary radar, so the Daqiao measurements near the ground should not be taken as what happens on operational flights in China.
The Daqiao winds were of good quality compared to the GPS measurements, but do not have quite as high vertical resolution. After the first couple of minutes the agreement between all systems was good.

A close look at Graw measurements shows that the software differs from the other systems, and appears to be interpolating linearly between values chosen at 10 to 15 s apart. Thus from time to time this process produces small outliers (1 ms^{-1}) relative to the other radiosonde systems.

Note: The filtering used by a given radiosonde system may be particularly designed for individual flights on a given length of suspension, so may not always be best tuned for the in flight movement of the multiple radiosonde rig relative to the balloon. Nearly all the measurements shown here would be considered satisfactory for routine operational use, see processed statistics in next section.

11.3 Results of statistical processing

The WSTAT statistical package was used to compute the systematic bias and standard deviations of the wind component differences for the two groups of QRS, using Modem as the group reference for the LMIJ group and Changfeng as the group reference for the CHGM group. The group references were chosen as the two systems which were on most of the group ascents and whose filtering was in the middle of the group in terms of resolving vertical structure.

The comparison data were first processed in 2 km averages, checking the low uncertainty which should be obtained when averaging over a depth of the atmosphere that averages out the effects of the smaller scale vertical structure, and then also in 250 m averages in the vertical, a vertical resolution suitable for routine operational use in the troposphere. Daytime and night-time measurements were treated together as no significant difference could be found between the two categories.

The number of flights compared from the main group members was at least 25 at all heights up to 20 km, reducing because of early balloon burst to around 20 at 30 km. The results of each group also contained results for the linking radiosondes, Vaisala, Daqiao and Meteolabor from at least half the number of flights of the main group members. The link data set for Vaisala was the largest. Problems in individual flights can increase the standard deviations associated with the link radiosondes in a smaller data sample, which was happening to some extent with Daqiao in the stratosphere, and Meteolabor in the troposphere.

The results of averaging the winds over 2 km in the vertical are shown in Fig. 11.3.1 for the LMIJ group and in Fig. 11.3.2 for the CHGM group.

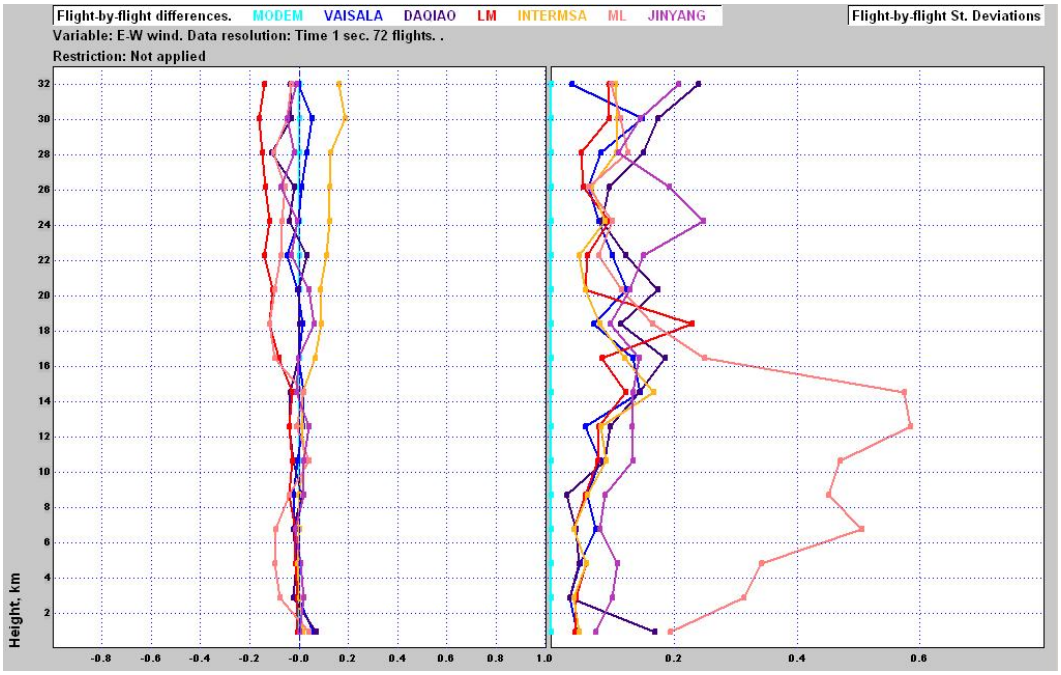

(a) E-W component LMIJ Group, Modem group reference

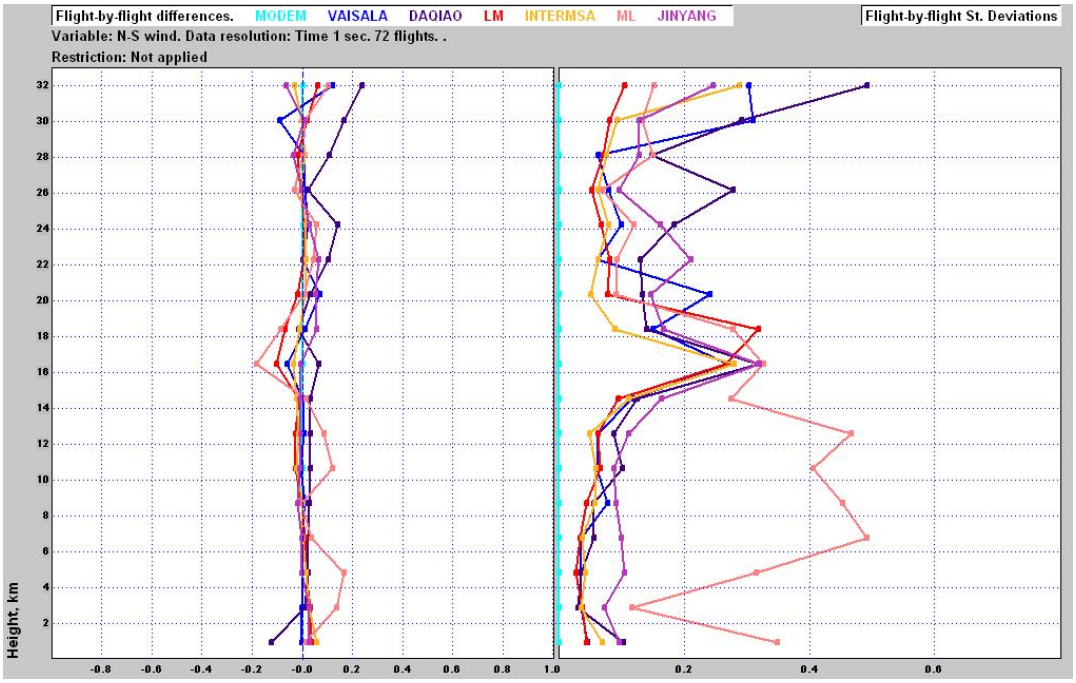

(b) N-S component, LMIJ Group, Modem group reference

Fig. 11.3.1 Systematic bias and standard deviations of differences relative to Modem averaged flight by flight over 2 km in the vertical for the LMIJ group plus linking radiosondes.

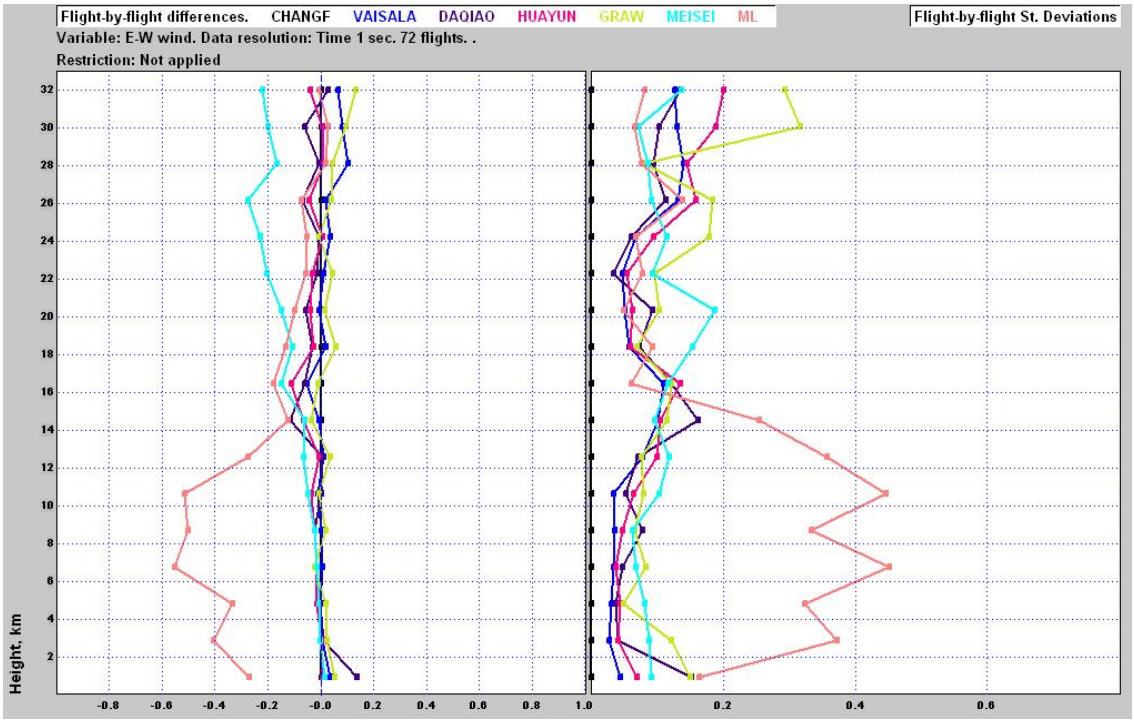

(a) E-W component CHGM Group, Changfeng group reference

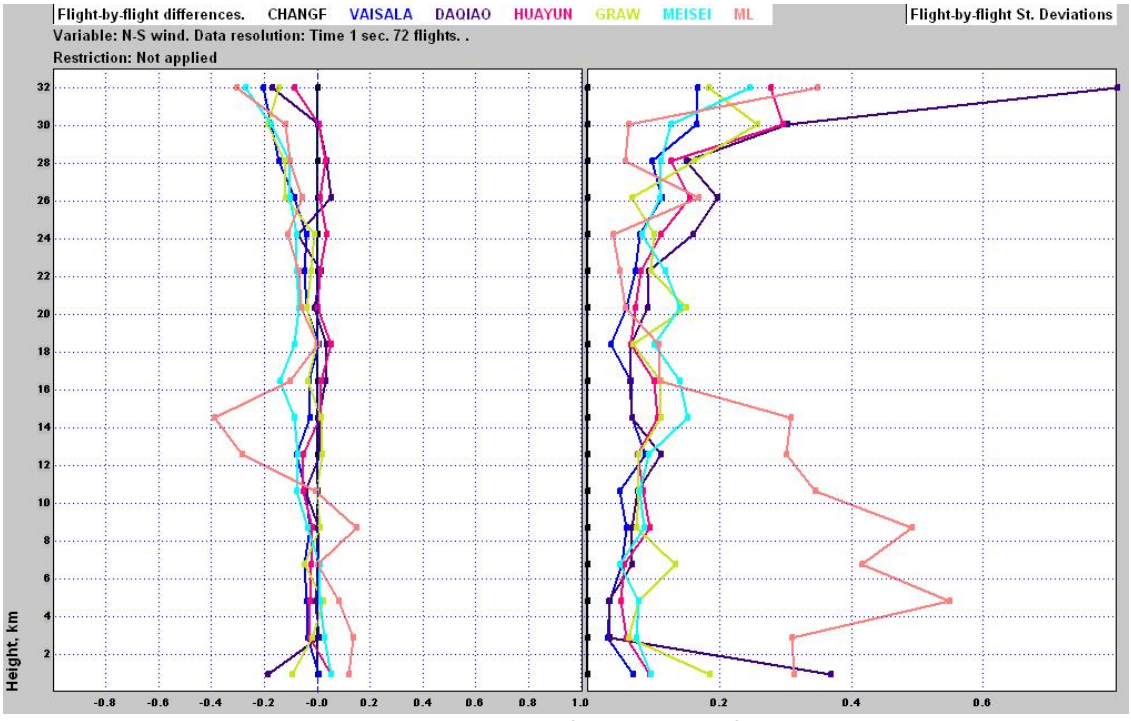

(b) N-S component, CHGM Group, Changfeng group reference

Fig. 11.3.2 Systematic bias and standard deviations of differences relative to Changfeng averaged flight by flight over 2 km in the vertical for the CHGM group plus linking radiosondes.

All the radiosonde system winds, apart from Meteolabor, have low bias in their differences relative to the group references, with standard deviations compatible with random errors less than or equal to about 0.1 ms^{-1}. For some reason, Meteolabor measured more accurately in the stratosphere at long ranges, than at shorter ranges in the troposphere. Subsequent investigation by Meteolabor found a software error in the wind computations that only produced significant errors when winds were less than 5 ms^{-1}. The results of similar processing but using averages over 250 m in the vertical are shown in Fig. 11.3.3 and Fig. 11.3.4.

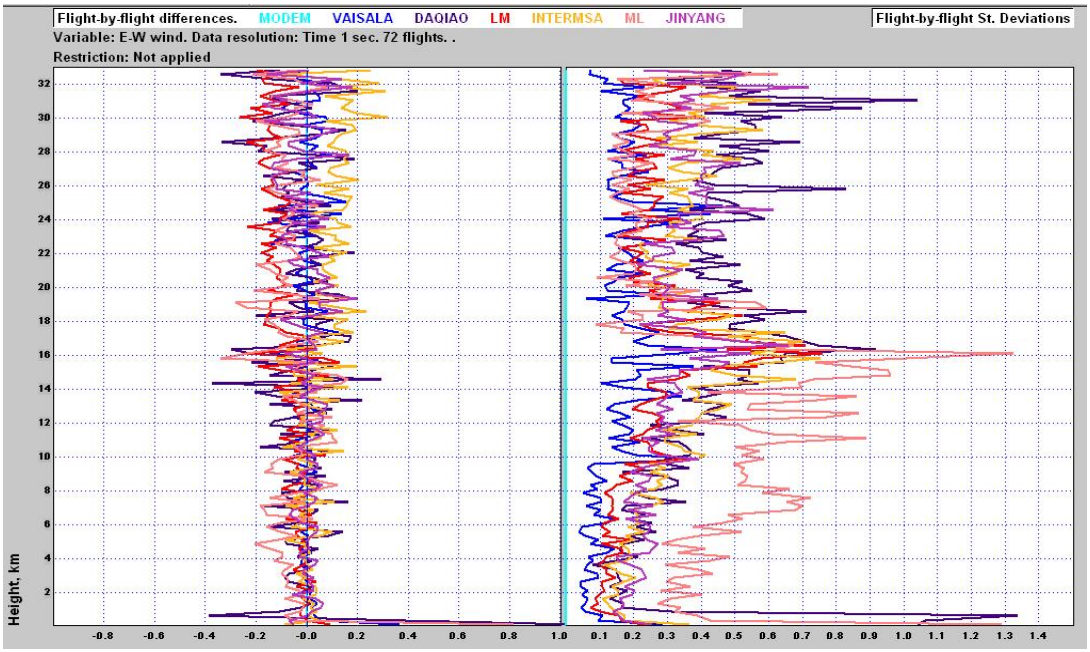

(a) E-W component LMIJ Group, Modem group reference

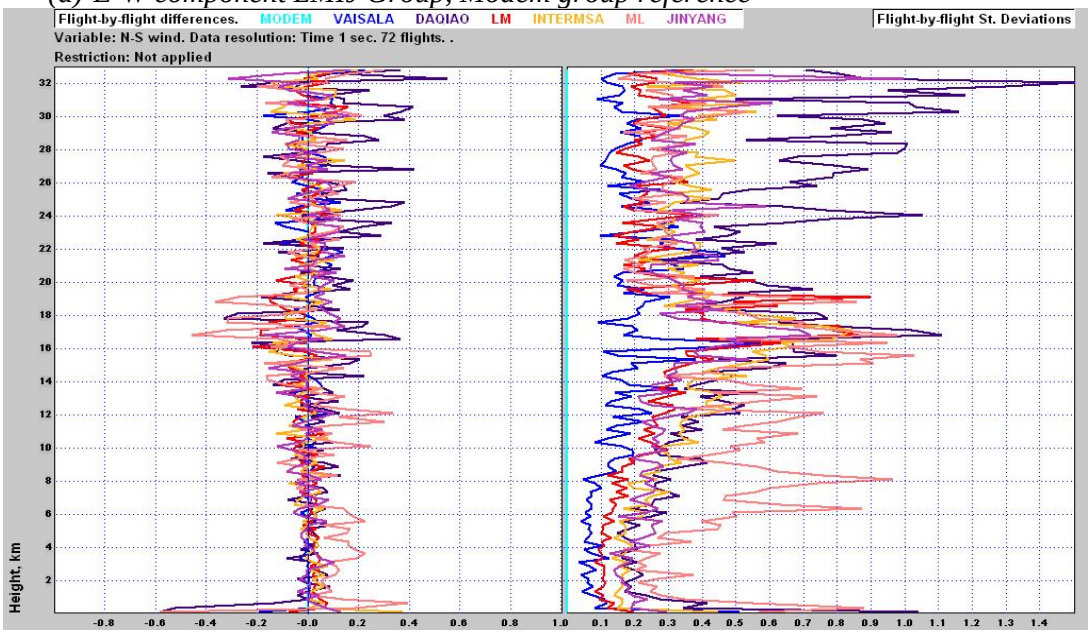

(b) N-S component, LMIJ Group, Modem group reference

Fig. 11.3.3 Systematic bias and standard deviations of differences relative to Modem, averaged flight by flight over 250 m in the vertical for the LMIJ group plus linking radiosondes.

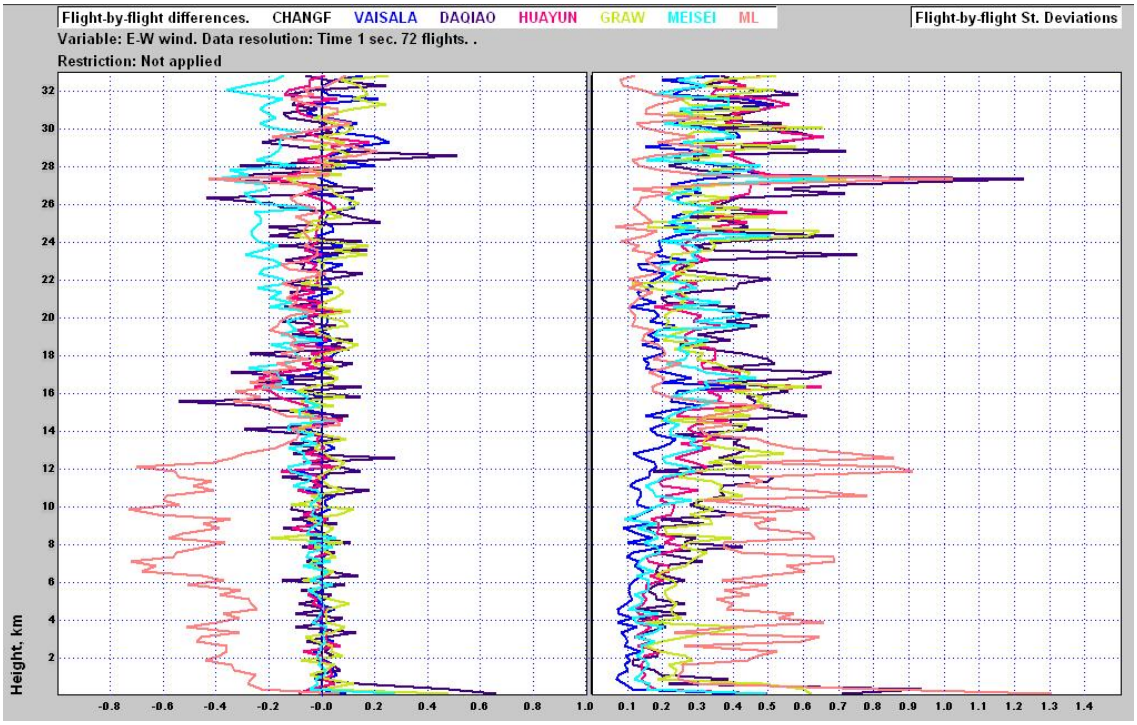

(a) E-W component CHGM Group, Changfeng group reference

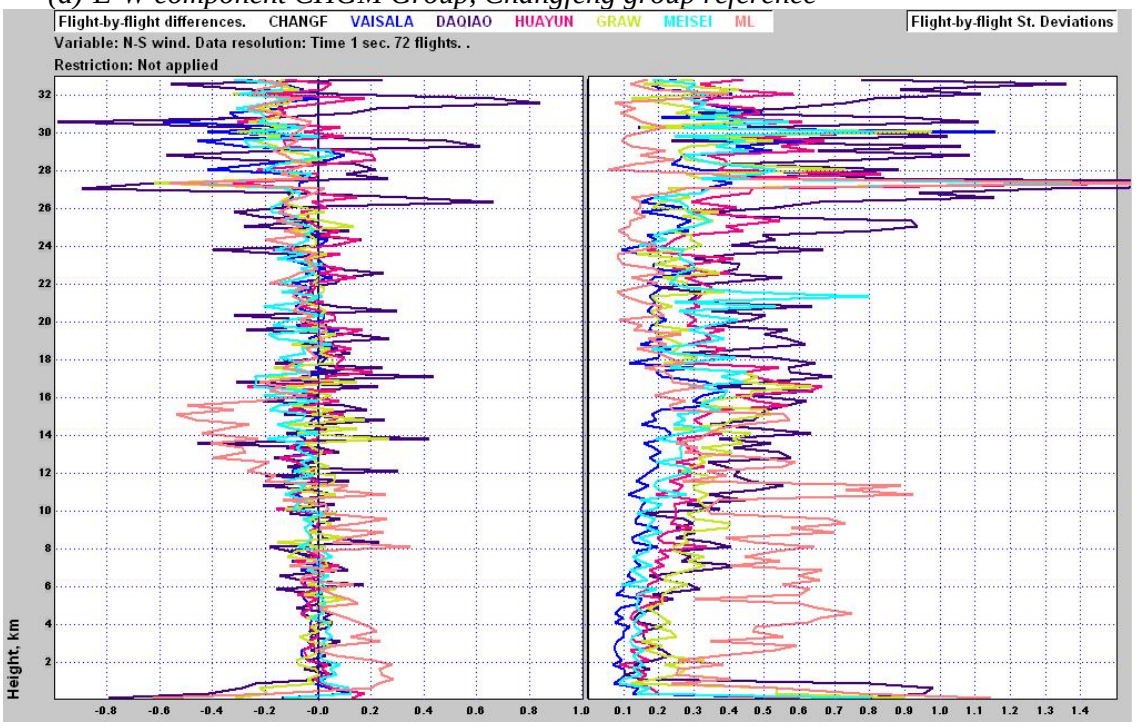

(b) N-S component, CHGM Group, Changfeng group reference

Fig. 11.3.4 Systematic bias and standard deviations of differences relative to Changfeng, averaged flight by flight over 250 m in the vertical for the CHGM group plus linking radiosondes.

At the higher resolution, the differences in resolving fine structure lead to larger standard deviations relative to the group references. The errors in Meteolabor were caused by a mixture of good flights with little systematic bias over relatively deep layers and others when the winds were in error by more then 0.5 ms^{-1} over several km in the vertical. The systems did not reliably deliver the measurement quality expected of correctly functioning GPS wind finding systems.

Both Meteolabor and Daqiao had problems immediately after launch, and in the case of Daqiao this was probably caused by problems in locking the secondary radiosonde onto the radiosonde because of the method used in launching the flight rigs in the test.

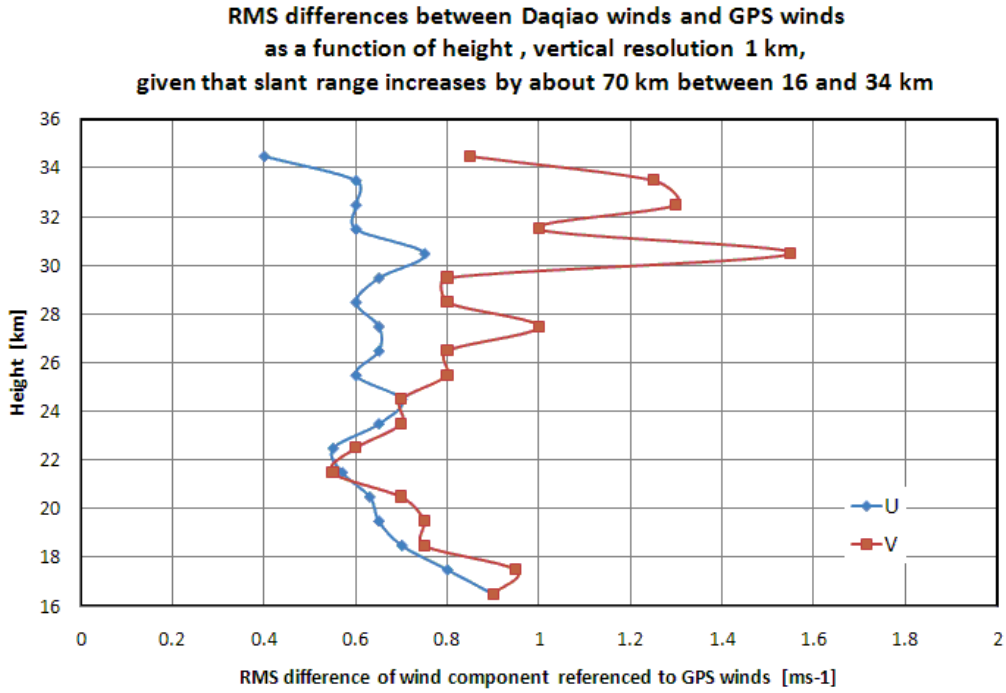

Figure 11.3.5 Results of amalgamating the RMS differences of Daqiao winds against the two group references, as a function of height and therefore approximately as a function of slant range.

At long ranges in the stratosphere, Daqiao showed large rms deviations against the group references in the N-S component than the E-W component, see Fig. 11.3.5. This would be because at increasing slant range the secondary radar was not producing increasing errors in the measurements along the axis of the radar antenna to the east, but there was some increase in the tracking errors in the direction perpendicular to the radar antenna axis. At the greatest heights, the slant range was typically about 80 to 110 km. Thus, the Daqiao measurements are well within operational accuracy requirements for winds in the stratosphere, even at these longer ranges.

The accuracy requirement (k=1) for winds in the CIMO Guide can be converted into a requirement of random error (k=1) in each orthogonal wind component of 1 ms^{-1} in the troposphere, and 1.5 ms^{-1} in the stratosphere, when systematic biases are very small.

Meteolabor wind measurements were very close to the limit and need to be improved to be sure always to fall within the requirement in the troposphere, otherwise all the systems were good for operational use, given vertical resolution required in the troposphere is about 300 m and in the stratosphere between 1 and 2 km.

11.4 Comparison of radiosonde and wind profiler winds

Simultaneous wind profiler winds were available for 62 of the Comparison ascents. The wind profiler had to be switched off when there were power supply problems to the site near the start of the intercomparison. The wind profiler was producing independent wind measurements for sampling periods of about 15 minutes. Fig. 11.4.1 shows one of the windier days at low levels where the wind profiler agrees closely with the radiosonde wind structure in the N-S wind component.

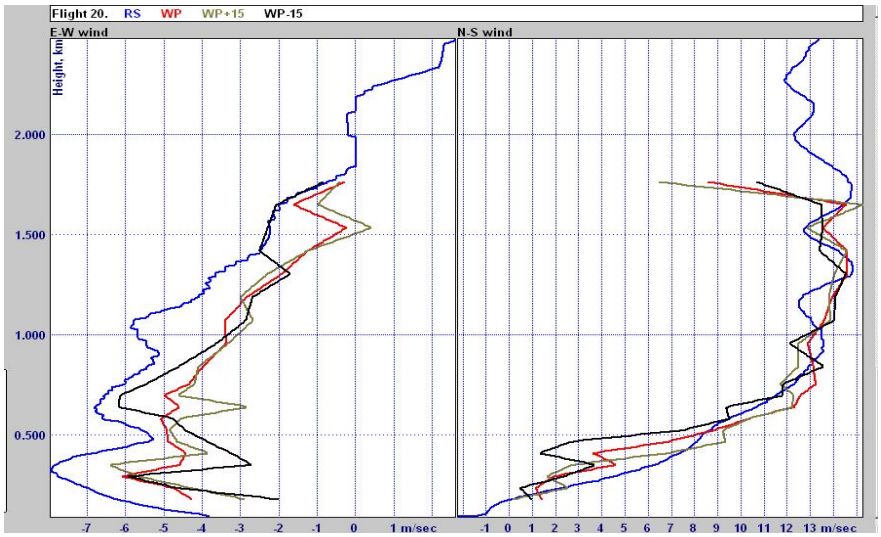

Fig. 11.4.1 Comparison of wind profiler measurements with the radiosonde on flight 20. WP profiler winds are centred at the launch time, WP-15 15 minutes before, and WP+15 15 minutes later

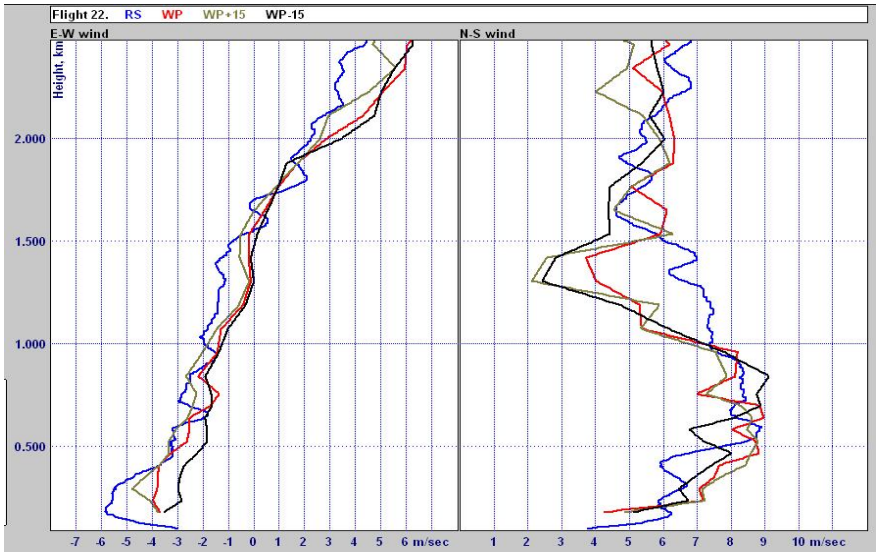

Fig. 11.4.2 Comparison of wind profiler measurements with the radiosonde on flight 22. WP profiler winds are centred at the launch time, WP-15 15 minutes before, and WP+15 15 minutes later.

Two flights later, the wind profiler signals were better at upper levels and the wind profiler could report a complete vertical profile up to 2.5 km. The E-W component is measured very accurately, but there is a significant difference relative to the radiosonde from 1 to 1.5 km for all three wind profiler samples in the N-S component. As the wind profiler signals were good at the time, it is possible that the radiosonde sample taken in 1.5 minutes between 1 and 1.5 km does not represent a good average value over 15 minutes, or more likely the winds at this level directly above the site were not the same as 2 km north where the radiosondes were. Thus, where structure in the boundary is required over a site, the wind profiler may offer a more representative measurement as long as it is functioning correctly. Many wind profilers have difficulties in measuring accurate horizontal winds when winds are very weak. The system at Yangjiang seemed to cope quite well, see Fig. 11.4.3.

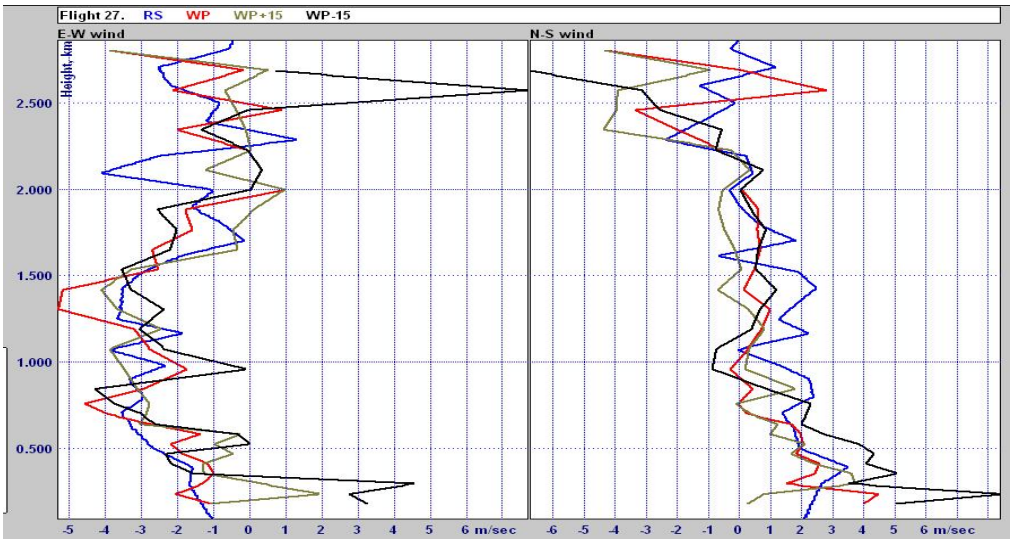

Fig. 11.4.3 Comparison of wind profiler measurements with the radiosonde on flight 27, WP, profiler winds are centred at the launch time, WP-15 15 minutes before, and WP+15 15 minutes later.

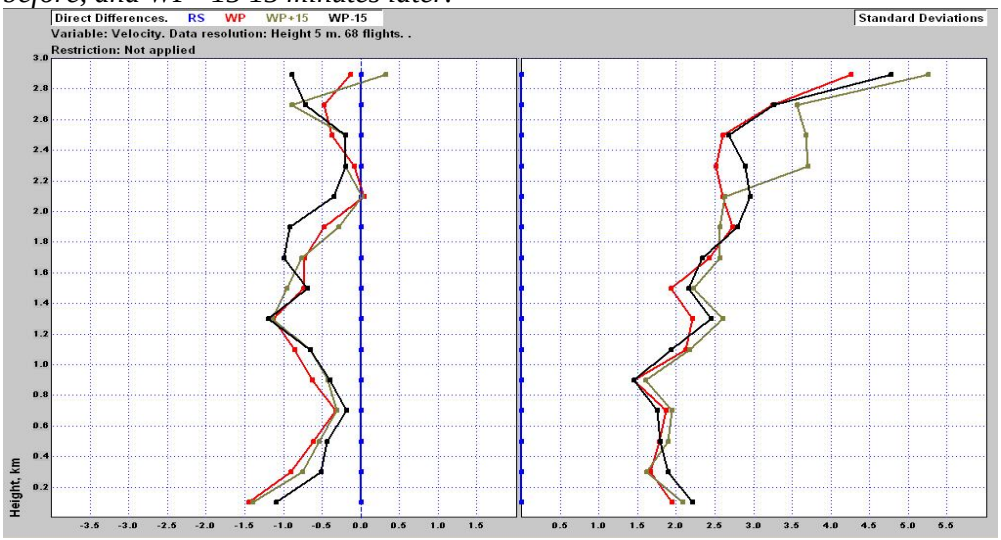

Fig. 11.4.4 Comparison of wind profiler velocity measurements with radiosonde winds at Yangjiang, showing systematic bias and the standard deviations of the comparisons between the two systems.

Wind profiler wind speeds were compared against radiosondes as a function of height using the WSTAT software (see Fig. 11.4.4). There were about 60 wind profiler measurements at each level below 2 km, reducing to 40 measurements at 3 km.

The slightly larger negative bias between 1 and 1.8 km, was probably linked to several occasions similar to that shown in Fig. 11.4.2. In any case the standard deviations shown are not purely the result of the random errors in each system, but also have a significant contribution from representativeness errors from the different sampling volumes and duration of the two measurements. The increase in standard deviations at the upper level is caused by the poorer quality of the wind profiler winds, as it is difficult to tune the wind profiler quality control to eliminate all spurious winds when the wind profiler signals get weak. In analysing the data, we have tried to give a correct representation of how the wind profiler was working, so we have eliminated some clearly spurious observations at upper level, which undoubtedly would have been removed if there had been more time to spend with the system at Yangjiang. It usually takes several months to get a new system optimised for a given site.

The magnitude of systematic bias and random errors as a function of the orthogonal wind components is shown in Fig. 11.4.5. These show that when the E-W component became strong, the systematic bias at stronger wind speed did not increase significantly, and the standard deviations of the differences with respect to the radiosonde were effectively independent of the E-W wind. However, when the N-S component became stronger in southerly winds the systematic bias became much larger than in the rest of the measurements, and the standard deviation of the differences much higher. This is caused by the type of difference shown in Fig. 11.4.2, and as such is probably not an instrument error, but caused by the variation of horizontal winds behind and over the Yangjiang hill when there were significant southerly winds.

The wind profiler was able to provide continuous records of the surface winds throughout the periods when the typhoons were approaching, and could provide winds during these events when it was not raining, which was a considerable part of the time. Wind profilers should be considered as a useful supplement to Doppler weather radar observations of wind in severe weather to fill gaps in the observing networks.

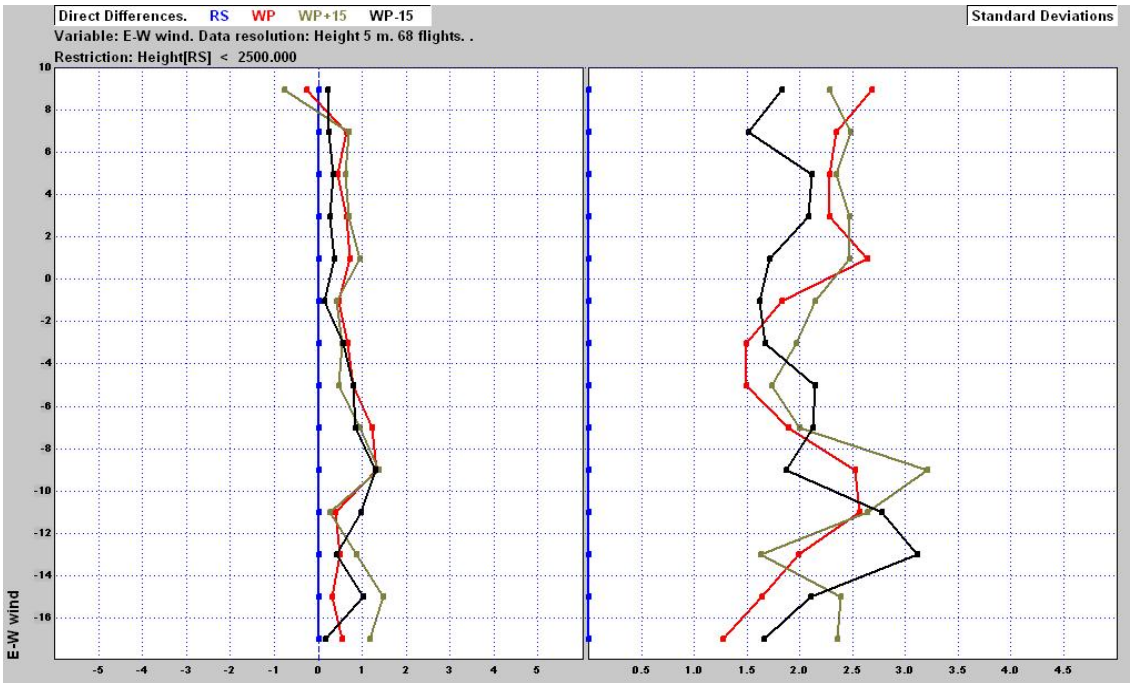

(a) E-W component

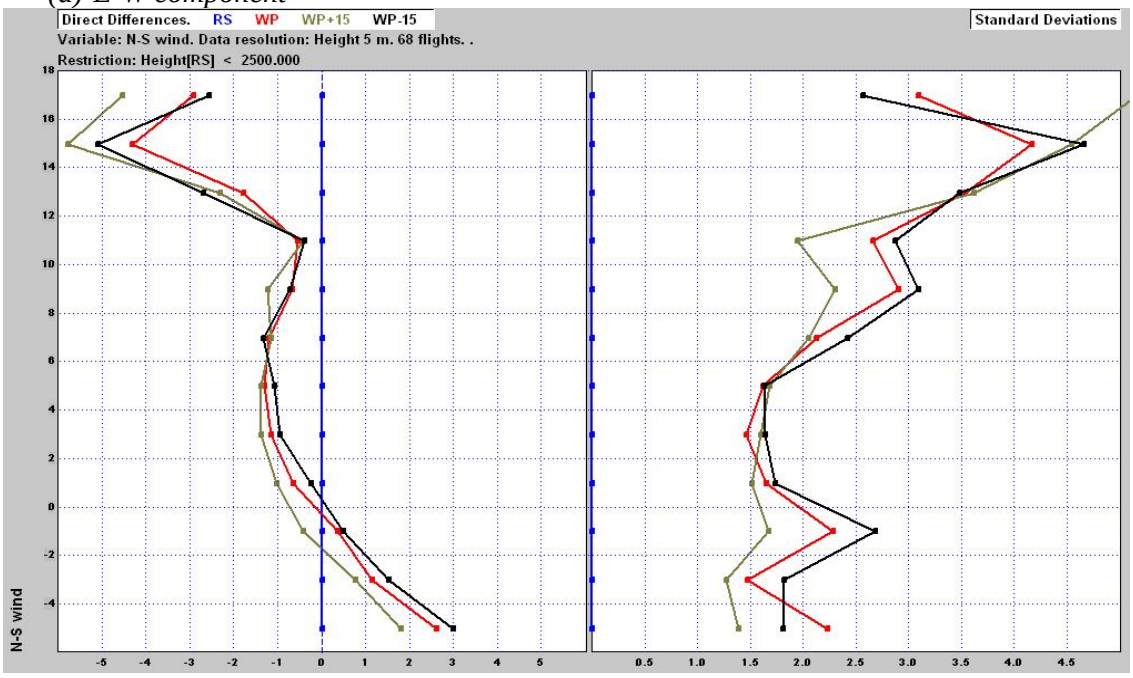

(b) N-S component

Fig. 11.4.5 Comparison of wind profiler wind component measurements with radiosondes as a function of the orthogonal wind component measured by the radiosonde for heights from 100 m to 2.5 km.

12 Conclusions

12.1 QRS performance

The quality of measurements produced by the various radiosonde types has been assessed in Table 12.1 using the systematic bias and random error from the evaluations of the different meteorological variables in the preceding chapters. The marking scheme is described in Table 12.2 and the standards used described in Tables 12.3 to 12.6. The standards for best GRUAN operations will need to be reviewed by the GRUAN community but represent CIMO's view of the best performance that could be reasonably expected at this time, given more than one radiosonde type is required for GRUAN use. More than one radiosonde type is necessary to identify and avoid difficulties if one radiosonde type has production engineering problems, which lead to unexpected anomalous performance. Operational experience shows that production-engineering problems occur with all main operational radiosonde types.

It is recommended that the requirement for operational relative humidity measurements in the lower and middle troposphere is made less stringent than in the CIMO guide. The limits in the CIMO guide were set tight to ensure that poorly performing equipment was improved to be able to meet most known user requirements. However, in practice this meant the operational standard was too close to the highest standard that could be expected for GRUAN and made scoring of the relative performance of the relative humidity sensors problematic.

For relative humidity at temperatures lower than -40 deg C in the troposphere, [in Yangjiang up to about 100 hPa], a new set of performance standards have been generated in Table 12.4, based on current knowledge of the performance of the better relative humidity sensor. These standards may need adjustment before use in the next edition of the CIMO Guide.

At these lower temperatures, Meteolabor and Daqiao were not assessed in Table 12.1 because few useful measurements were obtained at the lower temperatures. Also daytime measurements by Snow White were few in number at these levels, partly because it was chosen to fly Snow Whites mostly at night where they were most useful.

It was also found impossible to use the existing accuracy requirements for height and pressure in the CIMO Guide to score for Table 12.1. Thus, the standards have been changed to something that can be used for this purpose. In the past, the requirement for pressure accuracy near the surface of 1 hPa was suitable to ensure good pressure sensor performance, but using GPS height measurements for pressure is difficult to evaluate. Thus, it is suggested that a height standard of 15 m is used near the surface, corresponding to a pressure standard of 1.5 hPa. This needs to be checked with the users, but is consistent with the type of representativeness error found in measuring low inversions or cloud base and cloud top.

	InterMet	Modem	Graw	Meteo-labor	Daqiao	Jinyang	Meisei	Changfeng	Huayun	LMS	Vaisala	Snow-white	Multi-thermistor
2 years operations	Yes	Yes	No	No	Yes	No	No	No	No	Yes	Yes	Yes	Yes
Used in:-	global	global		Switz.	China	Korea				global	global	global	USA
Temperature, Night, height.<16 km	4.5	5	4.5	5	4.25	4.75	5	4.75	5	5	5	See Meteolabor	5
Temperature, Night, height > 16 km	3.25	5	4.5	5	3.25	3.75	5	4.75	5	5	5	See Meteolabor	5
Temperature, day, height <16 km	4.75	5	4.5	5	4.5	4.5	4	5	5	5	5	See Meteolabor	5
Temperature, day, Height >16 km	3.25	5	4.25	4.75	3.75	3.5	4.25	4.5	2.75	5	5	See Meteolabor	4.25
Protection for Evap. cooling errors	No	No	No	No	No	No	No	No	No	No	Yes	See Meteolabor	No
Humidity T>-40 deg C, night	4.5	3[1]	5	4.25	2.75	3.75	4.75	5	4	5	5	5	See LMS
Humidity T>-40 deg C, day	4.25	4.25[1]	4.75	3.25	4	4.75	5	4.25	3.75	5	5	5	See LMS
Humidity, Upper trop. T<-40 deg C, night	4.5	4.25	4.5	xx	xx	4	4	3.5	3.25	4.75	5	5	See LMS
Humidity, Upper trop. T<-40 deg C, day	2.5	3	4.25	xx	xx	4.25	3	3	2.75	4.5	4.5	xx	See LMS
Height P higher than 100 hPa	5	5	5[2]	5	4.75	4.25[5]	4[6]	5	5	5	5[7]	See Meteolabor	See LMS
Height P lower than 100 hPa	5	5	5[2]	5	3.25	5	5[6]	5	5	5	5	See Meteolabor	See LMS
Pressure Higher than100hPa	4	5	4.5[2]	4[3]	4.75	3.5[5]	4.5[6]	5	5	5	5[7]	See Meteolabor	See LMS
Pressure Lower than 100hPa	4.75	4.75	4.5[2]	4.75[3]	3.25	4.25	4.25[6]	5	4.75	5	5	See Meteolabor	See LMS
Wind, troposphere	5	5	5	3[4]	5	5	5	5	5	5	5	See Meteolabor	See LMS
Wind ,stratosphere	5	5	5	5	4.5	5	5	5	5	5	5	See Meteolabor	See LMS

Table 12.1: Summary of operational performance of QRS as measured in Yangjiang; see Tables 12.2 to 12.7 for the origin of the marking standards. Note: Scoring system was made more sensitive to differences between the systems, so uncertainty scored to nearest decimal place, and then averaged with average value reported with a resolution of 0.25. The evaluation of relative humidity is much more complex than the other meteorological variables, because the results to be considered are in many more categories than affect any of the other variables.

Footnotes:

[1]Factory error in the calibration of the radiosondes used in Yangjiang has been found, with the values about 5 per cent too high, verified from UK Met Office operational experience with Modem. If corrected it would be expected that this scoring would increase in the range 0.5 to 1.0. Also with the agreement of the project team, no humidity ground correction was applied during the test.

[2]After reprocessing data twice to correct the algorithms.

[3] Problem caused by software. Problem with locking GPS measurements to the ground solved after comparison and implemented for MeteoSwiss at Payerne.

[4] Problem caused by software. Error in computing winds at low wind speeds identified after comparison and correction implemented for MeteoSwiss at Payerne.

[5]This rank will be improved by a new Altitude offset and Launch Point Algorithm. The improved algorithm is now used in KMA (Korea Meteorological Agency).

[6]After removal of about 10 per cent poor tracking. Further improvement will be made when reason for poor tracking corrected, and also improved filtering to reduce errors associated with the effects of variable balloon rate of ascent at Yangjiang.

[7]Incorrect GPS antenna height setting corrected

Mark	Status
1	Minimum acceptable performance, given current available technology
2	Close to the accuracy requirement for operations in the CIMO Guide
3	Just meets the operational requirements of the CIMO Guide
4	Better than operational requirements of CIMO Guide, but still needs some improvement to become ideal for GRUAN
5	As good as can be expected fro GRUAN at the moment
6	Documentation of error corrections and processing supplied to GRUAN Lead Centre

Table12.2: Marking Categories used in Table 12.1 for evaluating QRS performance from Yangjiang. The minimum acceptable quality standard is probably not met by some of the current operational radiosondes, but these radiosonde systems need to be replaced as soon as possible, particularly for relative humidity measurements

Temperature accuracy (k=1)

	Temperature, surface to 100 HPa	Temperature 100 hPa to 10 hPa	Score	
Minimum	1	2	1	
			2	Not far short of operations standard
Operations	0.5	1	3	
			4	Better than operations standard, but need some improvement for GRUAN
Potential for GRUAN	0.3	0.6	5	Performance good enough for GRUAN
Ready for GRUAN			6	Necessary documentation complete for GRUAN

Table 12.3: Standards used to quantify performance of temperature measurements

Relative humidity (k=1)

	Relative humidity, T > -40 deg C	Relative humidity T<-40 deg C, in the troposphere	Score	
Minimum	20	30	1	
Moderate	14	23	2	Not far short of operations, meets moderate standard
Operations	7.5*	15*	3	
	5	10	4	Better than operations standard, but need some improvement for GRUAN
Potential for GRUAN	3	5	5	Performance ideal for GRUAN
Ready for GRUAN			6	Necessary documentation complete for GRUAN

*Revised limit, given current knowledge of relative humidity sensor performance.

Table 12.4 Standards used to quantify performance of relative humidity measurements

Geopotential height of significant levels (k=1)

	Surface to 100 hPa [gpm]	100hPa to10 hPa [gpm]	Score	
Minimum	40 at 1km 200 at 16 km	300	1	
Moderate			2	Not far short of operations
Operations	15* at 1km 20 at 5 km 30 at 10 km 60 at 16 km	100 20km 120 32 km	3	Proposed, Table 9.1
				Better than operations standard, but need some improvement for GRUAN
Potential for GRUAN	10	20	5	Performance ideal for GRUAN
Ready for GRUAN			6	Necessary documentation complete for GRUAN

*Revised limit , given current knowledge of GPS geopotential height capability

Table 12.5: Standards used to quantify performance of geopotential height measurements

Pressure (k=1)

	Surface to 100 hPa [hPa]	100hPa to10 hPa [hPa]	Score	
Minimum	4 at 1km 4 at 10 km 3 at 16 km	1.5 at 24 km 0.6 at 32 km	1	
Moderate			2	Not far short of operations
Operations	1.5 at 1km 1.5 at 10km 1 at 16 km	0.5 at 24km 0.2 at 32 km	3	Proposed, Table9.1
			4	Better than operations standard, but need some improvement for GRUAN
Potential for GRUAN	1 at 1 km 0.3 at 16 km	0.1 at 24km 0.04 at 32 km	5	Performance ideal for GRUAN
Ready for GRUAN			6	Necessary documentation complete for GRUAN

Table 12.6: Standards used to quantify performance of pressure measurements

Orthogonal Wind components (k=1)

	Surface to 100 hPa [$m.s^{-1}$]	100hPa to10 hPa [ms^{-1}]	Score	
Minimum	3	5	1	
Moderate			2	Not far short of operations
Operations	1	1.5	3	Proposed, Table9.1
				Better than operations standard, but need some improvement for GRUAN
Potential for GRUAN	0.5	0.5	5	Performance ideal for GRUAN
Ready for GRUAN			6	Necessary documentation complete for GRUAN

Table 12.7: Standards used to quantify performance of E-W and N-S wind components, vertical resolution = 300 m

The standards for wind measurements have been translated into equivalent wind component measurements standards in Table 12.7. These are easier to use for evaluation of winds, since they can be applied whatever the wind speed, and have been quoted with an associated vertical resolution. If purchasing a GPS wind finding system, it is recommended that tighter performance limits are used to ensure that the system purchased functions correctly. GPS should always produce measurements of better quality than the operational standard.

All the other current standards above need suitable vertical resolution requirements added to present a complete picture. For instance, what vertical resolution is required for relative humidity in the upper troposphere in the tropics, 250 m, 500 m, 1 km? If this is established it would then be possible to establish standards about time constant of response errors, and so judge when a sensor gets too slow that its values should not be reported rather than a correction applied if vertical resolution could be introduced as one of the categories evaluated, the scoring system in Table 12.1 would be improved for upper troposphere relative humidity in the future.

12.1.1 Temperature

The evaluation in Table 12.1 shows all the radiosonde types making night time measurements to a high standard. There is some degradation in quality in daytime, mostly caused by poor exposures of the sensors to the free atmosphere, or because the sensor was not far enough away from the radiosonde body to avoid sensing air that has already been heated by flowing over the top of the radiosonde. Chapter 7 provides details of what needs to be done to obtain the best performance, and improving performance should not require extremely costly modifications. All these radiosondes could measure the 100hPa geopotential height with a random error of less than 20 m; whereas there are many operational radiosondes still in use that can only manage to measure this height with an error between 30 and 60 m. In the tropics errors as large as 60 m for this parameter damage forecasts.

At this time it should not be assumed that any of the radiosondes types are reproducible to a systematic bias of 0.1 K in any conditions worldwide. The results from Yangjiang show that there must be other limitations to the temperature quality than just solar heating and traceability to national metrological standards e.g. stability of the sounding system during flight. At night, these are definitely the limiting factors. In daytime some improvement in the accuracy of the solar correction schemes, and references such as the Multithermistor radiosonde should be possible and are required if daytime measurements in the stratosphere are to be of most use to climatology, since it appears at the moment that systematic bias in the stratosphere is still a limiting error, and this will not be stable from location to location.

12.1.2 Relative humidity

The humidity sensors performance was evaluated in each of the five relative humidity bands and an average mark made from the individual markings. At temperatures higher than -40 deg C, all the relative humidity sensors had good reproducibility, apart from Jinyang and Meteolabor. Many radiosonde types made measurements of poorer quality at night than in the day. Modem, Daqiao, Jinyang, Huayun and Meisei had systematic positive biases over much of the relative humidity range, too large for good quality. In the day, the positive bias of Modem, Jinyang, Huayun, Daqiao and Meisei was much less. However, Meteolabor, and Graw to a lesser extent had daytime positive bias that reduced quality. InterMet also had a large negative daytime bias at high R.H. If the origins of these large biases (poor calibration, poor referencing, poor sensor ventilation, hygroscopic material in the cap or around the sensor, faulty software utilising humidity temperature sensor measurements) could be fixed then most of the quality problems would be solved for relatively dry conditions. It was impossible to prove whether Vaisala or Snow White had the correct values at night. Snow White had faster response in the upper levels than Vaisala, so it cannot be assumed that Vaisala was always correct. However, the differences between them were not so great, and the measurements both probably merit 5. The LMS measurements in cloud were lower than saturation with respect to ice, so had slightly larger errors. In the daytime, the problem is much more complex with Vaisala indicated higher supersaturation in upper cloud in the day than at night, which could suggest that its daytime correction was too high. The CFH measurements did show that the level of supersaturation found by Vaisala in these upper layers was not in large error, so 4.5 seems the fairest mark for Vaisala and LMS in the daytime at this stage.

Huayun has slightly lower marks at the higher levels in the day, because the random errors in the measurements were significantly higher than the rest of the radiosonde types still working

in this layer, and this may have been the result of poor positioning of the relative humidity sensor relative to the radiosonde body.

12.1.3 Geopotential heights of significant levels

These heights are used to assign the heights of temperature measurements. The operational acceptance standards in Table 12.5 are those proposed in table 9.1. The accuracy requirement for GRUAN is suggested since it assures that errors in the temperature from a height error are less than or equal to 0.1 deg C.

Meisei measurements had poor reproducibility in the troposphere, which ought to be a problem that could be quickly fixed. Other wise, GPS height measurements give the potential for very low height assignment errors in temperature from the surface to 35 km. Here there were very many more satisfactory systems than there had been in Mauritius.

Minimising the systematic height bias when locking to surface measurements could be improved in some systems.

The Daqiao system had good pressure sensor performance, suitable for operations, but not able to give the very small height assignment errors at pressures lower than 20 hPa for climatology.

12.1.4 Pressure

The standards in Table 12.6 were based on the proposals in Table 9.1 and try to be compatible within reason with the height standards in Table 12.5.

Methods of computing pressure from geopotential heights for some radiosonde types need to be checked, because in some cases, radiosonde systems with good heights and temperatures were not computing pressure without introducing larger errors than in other radiosonde types. Meteolabor have already found and fixed the problem in their software after returning from Yangjiang.

Here, the Daqiao pressure sensor can be seen to perform quite well relative to the computations from some of the GPS radiosonde types. GPS radiosondes tend to be much more expensive than those used with the secondary radar system, so for operational purposes there is no reason not to use this type of radiosonde. However, if the measurements at some sites are also required for climate purposes then it would be better to use GPS [or other satellite radio navigation system] radiosondes.

12.1.5 Orthogonal wind components

The values in Table 12.7 for operational acceptance are just a typical transform from wind speed and direction to equivalent values for the orthogonal wind components.

All the systems have high markings against the standards. For some reason, Meteolabor winds were poor in the troposphere, but not in the stratosphere.

Daqiao winds at longer slant ranges were slightly noisier in the stratosphere than in the troposphere.

12.1.6 Summary

Although much progress has been made with relative humidity measurements since the Mauritius test, some of the faults found in Mauritius still persist, showing that these need to be addressed quickly now. Relative humidity measurements are still the most difficult to perform and often are the main difference in the performance of the different radiosonde types. Unlike temperature measurements, the best performance is often found in the day, suggesting that contamination after passing through moist levels is worse at night than in the day, or at least balanced by other errors in the day.

In attempting to measure uncertainty through a comparison test, it is necessary to use large data sets, 15 flights to compare is not a luxury, it is necessary if the evaluation is to be representative and fair to all the participants. This number is only satisfactory if the quality of the measurements is good, and that is why poorly performing systems should not be allowed to participate in this type of test. Individual test flights should not be used to represent the typical performance of the radiosonde type.

12.2 SSI issues, including measurement uncertainty

- The QRS flights have been used to demonstrate the methods of generating uncertainty required for GRUAN operations. Thus, manufacturers are being asked to work with the GRUAN Lead centre to develop models of their measurement uncertainty, so that these can be reported with the measurements submitted to GRUAN.
- In any case, even for operations, software corrections that are applied to basic measurements need to be documented, especially for time constant of response and solar heating, whether temperature or relative humidity. The operational community needs to understand what is happening and to evaluate whether they think the corrections are likely to be reliable.
- What is clear is that some manufacturers are able to produce records of the basic measurements before any of these corrections have been applied, but others cannot. In order to diagnose problems in this type of in future it is essential that the expert analysing the measurements has access to a **reliable basic database for every radiosonde type, which can be reported openly.** In this test, the raw data has been extremely useful in understanding the filtering applied to many daytime temperature measurements, but this is not available generally for all to see.
- SSI Instruments (CFH, etc…) need specialized staff to provide reliable measurements, so are only suitable for use at sites where suitable staff are available. Thus, they can be expected to be used in specialised investigations, but not in most of the operational GRUAN measurements.
- Only CFH provided measurements that could be used in the stratosphere, but the other instrument show encouraging signs of development. The method in which SSI instruments were flown in Yangjiang produced contamination of the CFH. Further consideration would need to be given to minimize contamination in stratospheric water vapour measurement (including the environments) and possibly paying more attention to obtaining descent data.
- While Vaisala reference system had provided promising data in dry conditions in previous tests, it experienced problems in the lower stratosphere in the wet conditions

of Yangjiang. It was encouraging to see that manufacturers were investing in developing sensors for stratospheric measurements. It is highly recommended that manufacturers continue these developments in view of meeting the requirements of the climate community.

- The Meisei MTR instrument was mainly used to identify short lived temperature pulses, either negative or positive, probably originating from the methods used to suspend the radiosondes. The temperatures need some improvement in stability to be useful for assessing the performance of other radiosonde types. In any case for GRUAN, all this needs to be documented, and a full uncertainty analysis performed.
- In a similar fashion, full documentation about the uncertainties of the Multithermistor instrument is necessary before it could usefully be used for temperature measurements in GRUAN.

12.3 Usefulness of remote sensing

- The GPS water vapour measurements proved of large value in evaluating the differences in performance of the relative humidity sensors between radiosonde types and between day and night.
- The cloud radar and laser ceilometer records have been used to define the cloud conditions on all the flights, and these measurements were essential for understanding issues like infrared temperature errors and the ascents, which passed through clouds. The radiosonde expert analysing the test records would have found it very hard to understand what was happening without the information.
- The data set merited more analysis than has yet taken place. Unfortunately, the CIMO experts who were designated to deal with this issue were not available by the time of the Comparison test, and it proved impossible to find a suitable replacement expert at short notice. This needs to be planned better in future, where there may even be problems in finding a suitable radiosonde expert to deal with the test. Work required is non-trivial to achieve substantial results.
- In some cases, access to the data became more complicated than expected, so any collaboration on analysis needs to be planned further in advance than happened on this occasion.

12.4 Organisational issues

The whole intercomparison has been well organized from both WMO (especially project team) and CMA, good collaboration and efficient communication among project team, participants and LOC has made the intercomparison go smoothly. Some experience could be extracted as follows:

- The necessary preparatory meetings are fundamental in not only agreeing the participants, but clarifying detail requirements for the host country (CMA) including responsibility for host country, intercomparison site infrastructure (in particular releasing field) and local logistics.
- The releasing training held in advance for operating staffs is very important, as well as the releasing practice and test flights just before the formal intercomparison. This

ensured that all the launches of the 72 flights made during the intercomparison were successful.

- Well planned import and export procedure carried by Chinese company-China national Huayun Technology Development Corporation, has benefited manufacturers and facilitated the intercomparison.
- Centralized accommodation is convenient for LOC to arrange transportation and other logistic.
- Necessary backup power supply is essential for flight data acquisition as well as UPS for every manufacturer.
- Daily weather forecasting from local meteorological bureau provided useful background information for both project team decision-making and logistic, especially focused on heavy rain, strong wind and typhoon.

12.5 Advantages to CMA

- Through hosting Yangjiang intercomparison, CMA has obtained much benefit and learned lots of experience from it. Firstly the gap between Chinese radiosonde and other advanced radiosonde has been found, in particular relative humidity measurement, it will guide Chinese manufacturers to improve radiosonde quality.
- Secondly, CMA has gotten better understanding of new developed China-made remote sensing instrument such as cloud radar, all-sky imager and wind profiler through intercomparison with amount of radiosonde launching.
- Thirdly, CMA has established an experienced group team for not only intercomparison, but organizing the international activities. Furthermore, it will promote the capability of upper-air intercomparison for CMA, e.g. establishment of standard flow, improvement of intercomparison method, enrichment of data analysis technology, and obviously be beneficial to radiosonde system evaluation.

13. Recommendations

13.1 Operations

13.1.1 Benefits/impact of this intercomparison for WMO Members

- Members can use the results of this test to facilitate acquisition of systems for national purposes, minimising additional performance testing on a national level.
- The test results confirm that pressure sensors are no longer needed for operational GPS radiosondes (with an expected long term impact on lowering the cost of some radiosondes).
- Advice has been provided to GRUAN on the potential operational radiosondes for use in GRUAN, and those radiosonde types wishing to participate in GRUAN have been informed on the GRUAN requirement for building an uncertainty model to be applied in flight to their radiosonde measurements.
- It is recommended that the suitable radiosondes for the GUAN network would score at least an overall category 4 for the important climate variables in Table 12.1. This can then be used to guide procurement of suitable systems.
- Within China, the use of the secondary radar system is suitable for good quality operational measurements, but needs to be matched to a radiosonde with a humidity sensor that meets China national user requirements.

13.1.2 Advice to Members

- Adequate signal reception is essential to achieve the performance shown in this test and this must be taken into account in deciding what ground equipment is necessary with a given Radiosonde. In the past many systems, especially in some of the remoter areas, have not performed correctly because of under-investment in the ground system.
- In making decisions about procurement of new radiosonde equipment, some choice has to be made between the price of the radiosonde and the level of performance that is acceptable for the requirements of the country and the surrounding region. The results in this report should mean that there is a wider choice than before. However, what it is not possible to test is the reliability of the supplier, the long term reliability of production, and the level of operational back up support provided by the manufacturer, and this needs to be negotiated in any contract placed.
- For those members who wish to contribute observations for climate monitoring, care should be taken to procure systems which have small systematic biases.
- Those Members using operational radiosonde which would not get an average score of 3 (for each meteorological variable of table 12.1), if the standards proposed in this report were applied in their network should make every effort to replace the equipment with equipment which can meet the standards, as soon as possible.

13.2 Climate

- In many parts of the worlds gravity wave activity is significant in the stratosphere, in particular, so that any measurement of temperature and wind structure contains departures from the mean wind or temperature field required by the climatologist. This was illustrated to some extent in Fig. 11.1.1. Figure 13.2.1 shows a similar type of plot for the temperature measurements as a function of height from 16 consecutive flights at Yangjiang, with the radiosonde types used of very similar performance. Nearly all the variation with time above 18 km is the result of gravity wave activity. This level of natural variability arising from the gravity wave activity needs to be taken into account when planning how many radiosonde observations are needed to measure the mean temperature profile and hence detect certain magnitudes of temperature trend.

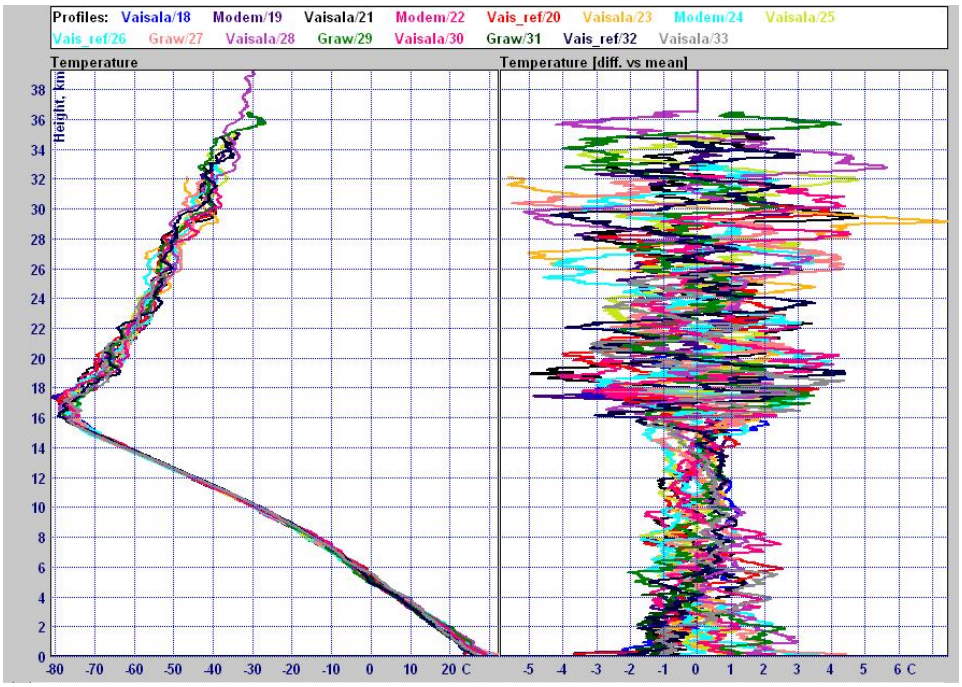

Fig. 13.2.1 Temperature profiles measured from 16 consecutive test flights at Yangjiang as a function of height, and then the differences from the average value for the 16 flights.

- The GRUAN network needs to use radiosonde systems where the main error sources have been minimised by good design, factory calibration and operational procedures, and ground processing software. This report is intended to indicate how far the new operational systems have progressed along this path, and so allow suitable choices of equipment to be made for GRUAN, and then to go through the full uncertainty documentation process that is required for the operations.
- GRUAN also needs to work with the manufacturers to develop the documentation for uncertainty estimates that can be reported as part of the GRUAN network operations.
- The Scientific Sounding Instruments have special characteristics, e.g. measuring water vapour accurately in the stratosphere and the uppermost troposphere, or very high temperature speed of response. It should not be assumed that they have better engineering, greater reliability, better radiofrequency links, better basic calibration or better reproducibility than several of the best operational radiosondes: - for relative

humidity down to -70 deg C, and for the rest of the climate variables measured by radiosonde from the surface to 35 km.

13.3 Manufacturers

- If manufacturers make corrections to the basic data they need to document them (time constant correction for humidity and temperature, radiation corrections, method of data filtering to remove day-time temperature noise) and make the documentation open to users.
- Basic Raw data are essential to diagnose problems of radiosondes during a test. Therefore, in future intercomparisons, raw data must be provided to the project team and then be allowed to be used in the final report as required. Currently, this information is not always available from the ground system, or comes in a range of variants from a given manufacturer that undermines confidence in the information. Please can the software be developed so that there is only one version of the basic raw data, with this being ready for the next phase of when testing (either international test or for national procurement exercises).
- If a radiosonde operating system decides that reported values are not reliable, it should flag out the data and not report anything, rather than let the software invent values. Interpolation of missing data should be minimised as far as possible and manufacturers are encouraged not to interpolate data over gaps larger than 1 minute.
- In future, only three formulae should be used for the water vapour pressure equation at temperatures lower than -50 deg C, when working on calibration of relative humidity sensors at these low temperatures. These are Wexler (1977), Hyland and Wexler (1983) and Sonntag (1994).
- Manufacturers are recommended to improve calibration of relative humidity sensors, dealing with the systematic biases that persist, and taking care of calibration at low temperatures.
- With temperature sensors, manufacturers are requested to take note of the CIMO Guide (7th edition, 2008) and not to paint temperature sensors white which can lead to significant infra-red errors.
- Providing temperature sensors with as good exposure as possible, is the key to low random errors in measurements in the stratosphere. (For example the MTR instrument was able to detect modified air passed over a thin bamboo cane 2 m above the sensor.) Similarly the temperature sensor **must** be well above and away from the radiosonde body.
- Manufacturers now need to provide better protection against evaporative cooling when emerging from cloud into dry layers. This is important for the issues of forecasting low cloud in numerical weather prediction models.

13.4 Future activities

- The results, conclusions and technical recommendations from this test need to be used to update the CIMO Guide as soon as possible. This should include the clarification of the algorithms for computing geopotential height from geometric height.
- The part of the CIMO Guide related to instrument intercomparisons need to be reviewed and updated. For instance, the design model of support rig frame should be

formalized and included in CIMO guide, e.g. proper rig material selection, design method considering various simultaneous radiosondes launching model, suitable rig length and radiosonde suspending height from frame to balloon for preventing from extra heat contamination, along with rope length advice between balloon and support frame, as well as different balloon launching method with respect to various ground wind condition, and standard intercomparison procedure, e.g. launching flow, regulation and standard data processing method.

- For an intercomparison of this size, consideration should be given to the analysis of the results and writing of the report as it can almost not be done by an expert beside their normal work.
- In view of the size of the intercomparison, it is recommended that in the future only those systems that are widely used should be taking part in the intercomparison. Thus, the aim of any future comparison must be well defined and agreed by all parties to justify the level of investment and manpower resources required to do the comparison successfully.
- If part of the aim of future comparisons will be to measure water vapour in the stratosphere as accurately as possible during the experiment, then deployment of instrumentation such as CFH may be best done on its own individual flights where observing methods can be optimised.
- The planning process for this test recognised that it would be necessary to incorporate testing of Russian and Indian Radiosondes, as requested in the next CIMO intersessional period.
- When system manufacturer's correct significant errors identified in this Comparison, there must be a process by which these systems can be retested. To accommodate such retesting small scale tests should be performed to demonstrate that the problem(s) have been rectified. This would best be done at one of the CIMO Lead centres for upper air testing, or other recognised test site, and then it should be possible to post test results of these small-scale tests to a suitable WMO information site.
- When a new radiosonde type is developed during the period between WMO Intercomparisons, it is suggested that initial small scale pilot intercomparisons are performed with one of the best quality radiosondes. Without such testing a radiosonde should not be allowed to take part in a Regional or Global WMO Radiosonde Comparison.

14 Acknoledgements

We are very grateful for all the resources made available by the Administrator of China Meteorological Administration, Dr. Zheng Guoguang.

The success of the test was mainly dependent on the facilities and staff plus volunteers provided by the China Meteorological Administration. Dr. Zhou Heng, as part of the CIMO Management Group, facilitated coordination and implementation of the Project both in Yangjiang, and in the preparatory meetings.

Financial and logistical support was provided by DWD, NOAA and Chinese Academy of Sciences (Institute for Atmospheric Physics) for the SSI operations.

The WMO Project team appreciated the high level of expertise and collaboration from Chinese colleagues working in Yangjiang.

Isabelle Ruedi and Miroslav Ondras, WMO Observing and Information Systems Department organized vital preparations for the test and provided help during the field phase of the test.

Mr. Sergey Kurnosenko did an invaluable job in generating the Intercomparison database and processing software. We were very grateful that he took time to support this work, after a break of five years.

The test could not have been successfully completed without the funding and manpower resources provided by all the radiosonde manufacturers. We are grateful to Vaisala for providing the laser ceilometer used for the test, and to CMA for organizing a wide range of valuable remote sensing systems.

This report has benefited greatly from comments by the manufacturers and the IOC members and associated experts, especially Prof. Bertrand Calpini, President of CIMO.

15 References

Bolton, D., The computation of equivalent potential temperature, Monthly Weather Report, 108, 1046-1053, 1980.

Fujiwara, M., M. Shiotani, F. Hasebe, H. Vömel, S. J. Oltmans, P. W. Ruppert, T. Horinouchi, and T. Tsuda (2003a), Performance of the Meteolabor ''Snow White'' chilled-mirror hygrometer in the tropical troposphere: Comparisons with the Vaisala RS80 A/H-Humicap sensors, J. Atmos. Oceanic Technol., 20, 1534– 1542.

GCOS-112, GCOS Reference Upper-Air Network (GRUAN): Justification, requirements, siting and instrumentation options. WMO/TD-No. 1379, 2007.

GCOS-121, GCOS Reference Upper Air Network (GRUAN): Report of the GRUAN Implementation Meeting, Lindenberg, Germany, 26-28 February 2008.

GCOS-134, GRUAN Implementation Plan 2009-2013. WMO/TD-No. 1506, 2009.

Guide to Meteorological Instruments and Methods of Observation, WMO-No 8, 7th edition, Geneva, 2008. (CIMO Guide)

Hyland, R. W. and A. Wexler, Formulations for the Thermodynamic Properties of the saturated Phases of H_2O from 173.15 K to 473.15 K, ASHRAE Trans, 89(2A), 500-519, 1983.

Immler, F.J., J. Dykema, T. Gardiner, D.N. Whiteman, P.W. Thorne, and H. Vömel, Reference Quality Upper-Air Measurements: guidance for developing GRUAN data products, *Atmos. Meas. Tech*., 3, 1217–1231, 2010.

JCGM/WG 1: Evaluation of measurement data Guide to the expression of uncertainty in measurement, International Bureau of Weights and Measures/Bureau International des Poids et Mesures, www.bipm.org/utils/common/documents/jcgm/JCGM_200_2008_E.pdf, Working Group 1 of the Joint Committee for Guides in Metrology, 2008.

Mastenbrook, H. J., 1966: A control system for ascent-descent balloon soundings of the atmosphere. J. Appl. Meteor., 5, 737–740.

Mastenbrook, H. J., and J. E. Dinger, 1960: The measurement of water vapor distribution in the stratosphere, Naval Research Laboratory Tech. Rep. NRL 5551, Washington, DC, 35 pp.

Miloshevich, L. M., H. Vömel, D. N. Whiteman, T. Leblanc, Accuracy assessment and correction of Vaisala RS92 radiosonde water vapor measurements, *J. Geophys. Res., 114*, doi:10.1029/2008JD011565, 2009.

Murphy, D. M. and T. Koop, Review of the vapour pressures of ice and supercooled water for atmospheric applications, Quart. J. Royal Met. Soc, 131, 1539-1565, 2005.

Nash, J., R. Smout, T. Oakley, B. Pathack, S. Kurnosenko, WMO Intercomparison of High Quality Radiosonde Systems, Vacoas, Mauritius, 2-25 February 2005. (http://www.wmo.int/pages/prog/www/IMOP/reports/2003-2007/RSO-IC-2005_Final_Report.pdf)

Read, W. G., et al., Aura Microwave Limb Sounder Upper Tropospheric and Lower Stratospheric H_2O and RHi Validation, *J. Geophys. Res., 112*, D24S35, doi:10.1029/2007JD008752, 2007..

Schmidlin, F. J., J. K. Luers, and P. D. Huffman, Preliminary estimates of radiosonde thermistor errors, *NASA Technical Paper 2637*, 15 pp, 1986

Sippican Inc., Fast Response Thermistor, *Sippican Technical Bulletin*, March 2003

Shimizu, K. and Hasebe, F., Fast-response high-resolution temperature sonde aimed at contamination-free profile observations, *Atmos. Meas. Tech*., 3, 1673-1681, doi:10.5194/amt-3-1673-2010, 2010.

Sonntag, D., Advancements in the field of hygrometry, Meteorol. Z., N. F., 3, 51-66, 1994

Vaisala, available on http://www.vaisala.com/Vaisala%20Documents/Vaisala%20News%20Articles/VN184/VN184_16_WMOIntercomparisonofRadiosondeSystemsinChina.pdf, 2010.

Vömel, H., S. J. Oltmans, D. J. Hofmann, T. Deshler, and J. M. Rosen, The evolution of the dehydration in the Antarctic stratospheric vortex, *J. Geophys. Res., 100,* 13919-13926, 1995.

Vömel, H., S. J. Oltmans, F. Hasebe, M. Shiotani, M. Fujiwara, N. Nishi, M. Agama, J. Cornejo, F. Paredes, and H. Enriquez, Balloon-borne observations of water vapor and ozone in the tropical upper troposphere and lower stratosphere, *J. Geophys. Res., 10.1029/2001JD000707,* 2002.

Vömel, H., D. E. David, and K. Smith, Accuracy of tropospheric and stratospheric water vapor measurements by the cryogenic frost point hygrometer: Instrumental details and observations, *J. Geophys. Res., 112,* D08305, doi:10.1029/2006JD007224, 2007a.

Vömel H., V. Yushkov, S. Khaykin, L. Korshunov, E. Kyrö, and R.Kivi, Intercomparisons of stratospheric water vapor sensors: FLASH-B and NOAA/CMDL frost point hygrometer, *J. Atmos. Oceanic Technol., 24*, 941–952, 2007b.

Vömel, H., J. E. Barnes, R. N. Forno, M. Fujiwara, F. Hasebe, S. Iwasaki, R.Kivi, N. Komala, E. Kyrö, T. Leblanc, B. Morel, S.-Y. Ogino, W. G. Read, S. C. Ryan, S. Saraspriya, H. Selkirk, M. Shiotani, J. Valverde Canossa, D. N. Whiteman, Validation of Aura/MLS Water Vapor by Balloon Borne Cryogenic Frostpoint Hygrometer Measurements, *J. Geophys. Res., 112,* D24S37, doi:10.1029/2007JD008698, 2007c.

Wexler, A., Vapor pressure formulation for ice, Journal of Research of the National Bureau of Standards-A. 81A, 5-20, 1977.

Annex – A Project Team, International and CMA Participants.

1	Tim Oakley	WMO/UK Met Office	Project Leader
2	John Nash	WMO/UK Met Office	Radiosonde Test Expert
3	Sergey KURNOSENKO	WMO	Data Manager
4	Romanens Gonzague	WMO/Meteoswiss	Data Processing Expert
5	Holger VÖMEL	GRUAN/DWD	GRUAN/SSI Expert
6	Mark Smees	WMO/UK Met Office	Remote Sensing Expert
7	Li Wei	CMA	Local Project Leader
8	Miroslav Ondras	WMO	Secretariat
9	Isabelle Rüedi	WMO	Secretariat
10	Franz Immler	GRUAN/DWD	GRUAN Scientist
11	Masatomo Fujiwara	GRUAN/Hokkaido University	GRUAN Scientist
12	Junhong Wang	GRUAN/NCAR	GRUAN Scientist
13	Bian Jianchun	GRUAN/CAS/IAP	GRUAN Scientist
14	Bai Zhixuan	GRUAN/CAS/IAP	GRUAN Support
15	Zhang Jinqiang	GRUAN/CAS/IAP	GRUAN Support
13	Christo le Roux	InterMet Africa	Manufacturer
14	Shaun Wentzel	InterMet Africa	Manufacturer
16	Georges Ricaud	Modem/France	Manufacturer
17	Christophe Raux	Modem/France	Manufacturer
18	Patrick Charpentier	Modem/France	Manufacturer
19	Benjamin Charpentier	Modem/France	Manufacturer
20	Samuel Mesmin	Modem/France	Manufacturer
21	Sarah Alkemade	Graw/Germany	Manufacturer
22	Alexander Kotik	Graw/Germany	Manufacturer
23	Rolf Maag	Meteolabor/Switzerland	Manufacturer
24	Levrat Gilbert	MeteoSwiss	System Expert
25	Thomas Brossi	Meteolabor/Switzerland	Manufacturer
26	He Dinghong	Daqiao/China	Manufacturer
27	Chen Jian	Daqiao/China	Manufacturer
28	Yang Yuerong	Daqiao/China	Manufacturer
29	Piao Yifang	Daqiao/China	Manufacturer
30	Zhu Hua	Daqiao/China	Manufacturer
31	Jiang Luanjuan	Daqiao/China	Manufacturer
32	Gap Bong Bak	Jinyang/Korea	Manufacturer
33	Seung Gu Yang	Jinyang/Korea	Manufacturer
34	Soo Dong Han	Jinyang/Korea	Manufacturer
35	Sunghoon Jung	Jinyang/Korea	Manufacturer
36	Taekyu Ahn	Jinyang/Korea	Manufacturer
37	Kensaku Shimizu	Meisei/Japan	Manufacturer
38	Kohei Kai	Meisei/Japan	Manufacturer
39	Sakari Kajosaari	Vaisala Oyj/Finland	Manufacturer
40	Jarmo Franssila	Vaisala Oyj/Finland	Manufacturer
41	Mikko Krapu	Vaisala Oyj/Finland	Manufacturer
42	Markku Heikkinen	Vaisala Oyj/Finland	Manufacturer
43	Hannu Jauhiainen	Vaisala Oyj/Finland	Manufacturer
44	Tapio Tikkanen	Vaisala Oyj/Finland	Manufacturer
45	Petri Tupamaki	Vaisala Oyj/Finland	Manufacturer
46	Peng Wenwu	Changfeng/China	Manufacturer
47	Huang Xiaojie	Changfeng/China	Manufacturer
48	Zhou Yibing	Changfeng/China	Manufacturer
49	Yuan Tianfu	Changfeng/China	Manufacturer
50	Yang Jiachun	Huayun/China	Manufacturer
51	Zhang Qihai	Huayun/China	Manufacturer
52	Xin Tao	Huayun/China	Manufacturer
53	Hu Zhe	Huayun/China	Manufacturer
54	John Gordon Grant	Lockheed Martin/USA	Manufacturer
55	Matthew John Cardoza	Lockheed Martin/USA	Manufacturer
56	LIM Byeong Cheol	KMA/Korea	Observer
57	Kim Ki Hoon	KMA/Korea	Observer
58	Alexander Kats	Roshydromet/Russia	Observer
59	Andrey Dubovetskiy	Roshydromet/Russia	Observer

60	Zhou Heng	CMA	Director of foreign affairs department
61	Li Bai	CMA	Deputy director of meteorological observation centre
62	Liang Jianyin	CMA	Deputy director of Guangdong provincial meteorological bureau
63	Chen Yongqing	CMA	Member of LOC
64	Liu Zuoting	CMA	Member of LOC
65	Ao Zhenlang	CMA	Member of LOC
66	Ruan Shilin	CMA	Director of Yangjiang municipal meteorological bureau
67	Tan Jianrong	CMA	Member of LOC
68	Liang Guofeng	CMA	Member of LOC
69	Li Feng	CMA	Leader of remote sensing
70	Yu Jun	CMA	Member of LOC
71	Xing Yi	CMA	Leader of data centre
72	Wu lei	CMA	Member of data centre
73	Liu Fengqin	CMA	Member of data centre
74	Yan Dongxue	CMA	Member of LOC
75	Wei Jinwu	CMA	Member of LOC
76	Lin Zhengchun	CMA	Member of LOC (Doctor)
77	Yang Rongkang	CMA	Leader of releasing team 1
78	Zhang Weimin	CMA	Member of releasing team 1
79	Zhao Lunjia	CMA	Member of releasing team 1
80	Luo Xiongguang	CMA	Member of releasing team 1
81	Zhao Peitao	CMA	Leader of releasing team 2
82	Wang Zhiwen	CMA	Member of releasing team 2
83	Li Jiebo	CMA	Member of releasing team 2
84	Zhang Yinting	CMA	Member of releasing team 2
85	Guo Qiyun	CMA	Leader of releasing team 3
86	Sun Minfeng	CMA	Member of releasing team 3
87	Chen Cungen	CMA	Member of releasing team 3
88	Zhang Jian	CMA	Member of releasing team 3
89	Ma Guidong	CMA	Local staff
90	Feng Huasheng	CMA	Local staff
91	Zhao Jie	CMA	Local staff
92	Zhang Li	CMA	Local staff
93	Guo Zhenmian	CMA	Local staff
94	Yang Chaohui	CMA	Local staff
95	Ruan Yongzheng	CMA	Local staff
96	Zhang Yangsheng	CMA	Local staff
97	Zhou Lin	CMA	Local staff
98	Wu Ning	CMA	Local staff
99	Yin Hongnan	CMA	Local staff
100	Yan Zhihong	CMA	Local staff
101	Zeng Guangyu	CMA	Local staff
102	Wu Songwei	CMA	Local staff

Annex – B Yangjiang Station Information

Investigation Report on Yangjiang International Intercomparison Station Site

(I) The Station's Climatic Data

1. Basic climatic data of the station

Yangjiang station started its upper-air sounding in May 1966. Yangjiang station is situated in the south of the Tropic of Cancer, with an altitude of 88m. At 21°50′north latitude and 111°58′east longitude, it is of tropical climate with plentiful rainfall all the year around. Its humidity at 500-hPa is 33% in March and the amount of precipitation from May to Sept. is about 54%~67%. The annual mean ground temperature stands at about 22.6°C, while the annual mean surface humidity is around 81%. The troposphere height at Yangjiang station is about 16780m, while the height of zero-degree layer is about 4808m. The number of days with the sounding temperature below -80°C reaches more than 140 days all the year round, while the annual ground wind speed is about 3.9m/s on average, with the maximum ground wind speed reaching 7.6m/s (See Table 1.1 for details).

Table 1.1 Monthly Statistics of Climatic Data of Yangjiang Station in Recent 3 Years

Month	Mean temp.	Mean humidity	Mean precipitation	Mean surface wind speed	Mean maximum wind speed	500hPa monthly mean humidity	Upper-air sounding troposphere height	Upper-air sounding 0° layer height
1	14.9	71	33.1	4.4	7.8	15	16968	4448
2	16.1	81	36.3	3.8	7.1	18	16747	4027
3	19.0	85	70.7	3.9	7.1	33	16927	4361
4	22.3	88	101.5	3.9	7.6	41	16997	4715
5	25.3	86	489.5	3.8	7.4	58	17061	5021
6	27.2	90	501.9	3.7	7.9	67	16855	5215
7	28.2	85	191.4	3.8	7.5	59	16596	5271
8	27.4	87	375.8	3.7	7.8	58	16475	5270
9	26.8	80	189.8	3.9	7.7	54	16582	5183
10	25.2	77	52.3	3.8	7.3	38	16715	5096
11	20.8	65	44.5	4.5	8.2	30	16576	4711
12	17.5	66	12.2	4.4	8.0	13	16861	4375
Annual mean	22.6	81	209.0	3.9	7.6	40	16780	4808

2. Typhoon landing status

In 2006, Typhoon Prapiroon made landfall at the south China coastal area between Yangxi County and Dianbai County in western Guangdong at 7:20 p.m. on 3 Aug.. With a central pressure of 975 hPa and a speed of 33 meters per second, the maximum wind power reached 12 degrees at the Beaufort Scale near its eye.

Tropical Storm Kammuri formed in the northern part of the South China Sea on 5 August 2008 and intensified into strong tropical storm on the morning of 6 August. After an evening landfall from Xitou Town, Yangxi County in Guangdong province with the strength of severe

tropical storm, the maximum wind power reached 10 degrees (25m/sec) on the Beaufort Scale near its eye.

In 2009, the tropical storm Soudelor made landfall on the morning of 12 July between Yangjiang and Xuwen in Guangdong.

(II) Clearance Conditions of the Station

1. Upper-air wind observation environment

Yangjiang station is built atop an independent mountain, free from occlusion from high mountains or other buildings. The antenna of its L-band radar sounding system for its operation is erected on the top of duty room (2-storey building). There is a new generation weather radar building 50m true east of the antenna with an occlusion elevation angle exceeding 5 degrees and an electric wire iron tower northwest of the antenna with an occlusion elevation angle also exceeding 5 degrees, while there is no occlusion in other directions (See Fig. 1.1 for Eight azimuth diagrams of the site for flying sounding balloon and Fig. 1.2 for Ground obstacles occlusion diagram). Yangjiang station's ground prevailing winds are northeaster and southeaster. The weather radar building is at the windward side of the site of flying sounding balloon for the international sonde intercomparison, therefore, generally there will be no influence on sounding balloon flying (See Fig. 1.3 for wind rose diagram).

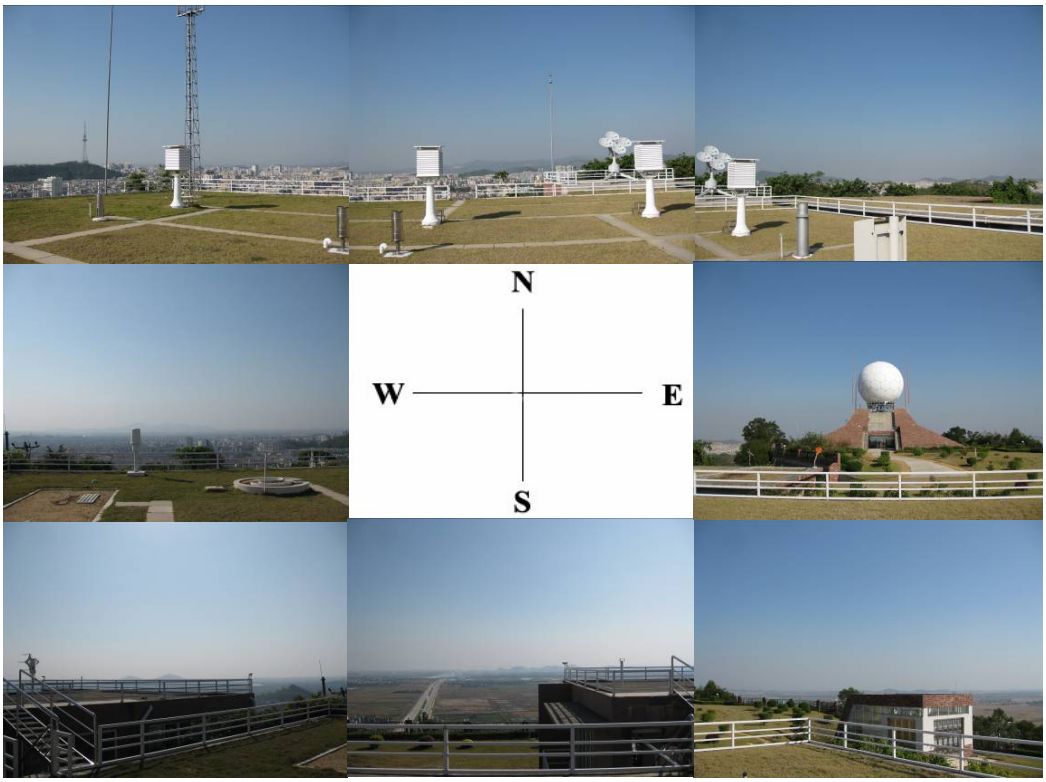

Fig. 1.1 Eight azimuth diagrams of the site for antenna erecting

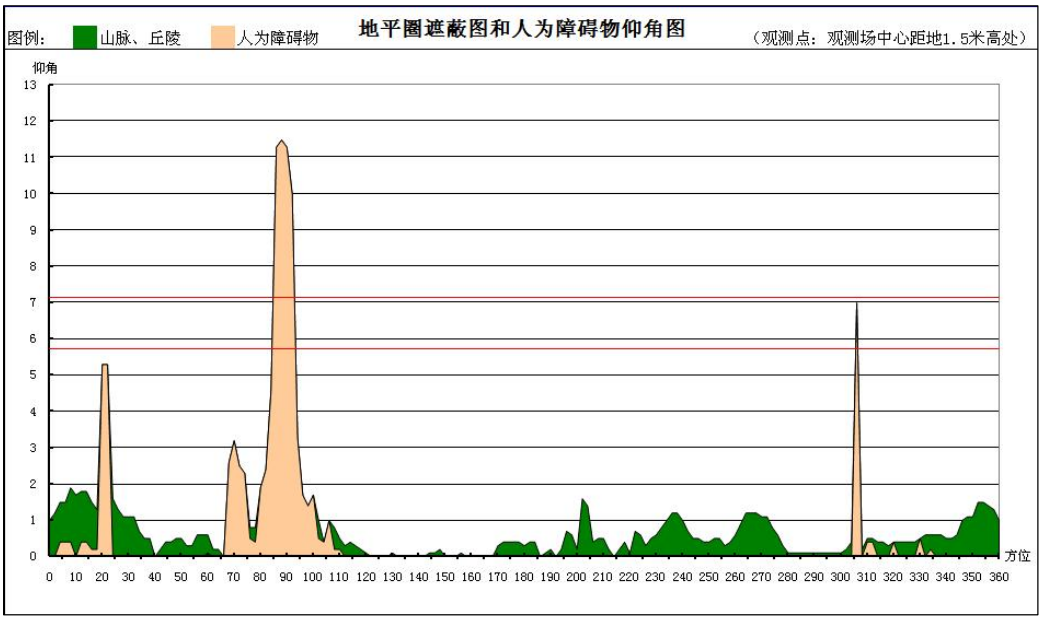

Fig. 1.2 Ground obstacles blocking angle diagram

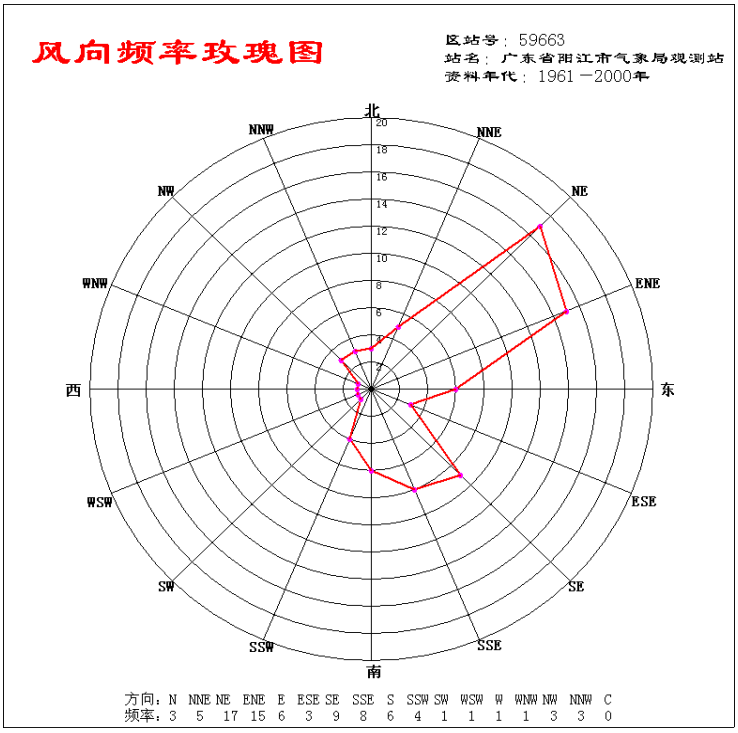

Fig. 1.3 Wind rose diagram

2. Airspace conditions

There is no airport at Yangjiang. There is no large airport within 100 km of the air sounding station but only a small civil airport within about 15 km-Heshan airport. Within 60 km, 4 air routes will pass above the station, and the upper horizontal distance to Guangzhou air route is about 10 km and that to Shenzhen air route is about 20 km (See Fig. 1.4).

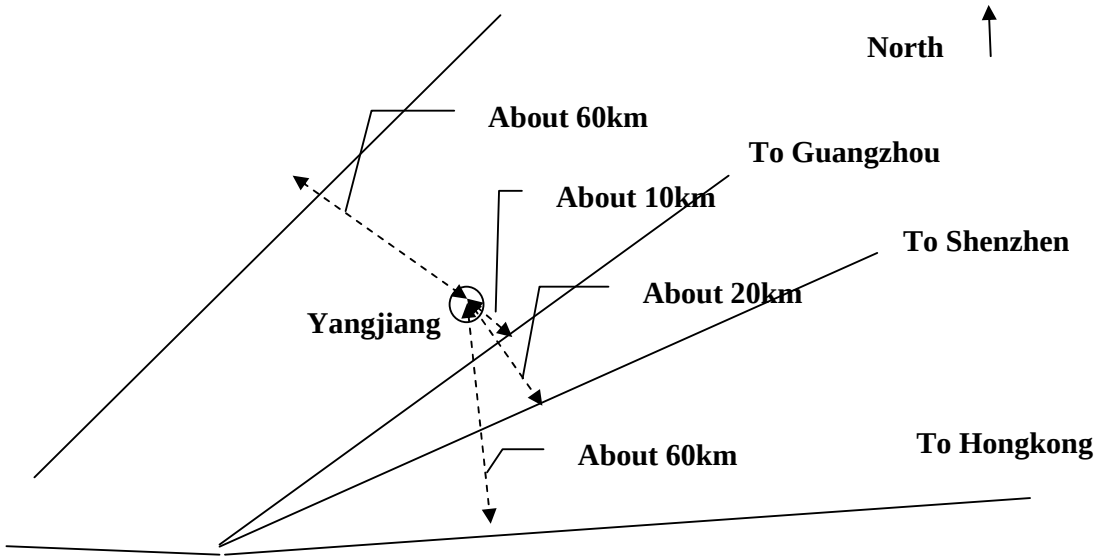

Fig. 1.4 Airspace diagram

3. Electromagnetic environment

The permissible electromagnetic frequency for China's GPS sounding is 400.3 MHz ~406 MHz, and the operating frequency of operatioanl L-band radar sounding system is 1675±10 MHz, while there is no electromagnetic interference within these 2 frequency ranges at Yangjiang station.

(III) Hydrogen Production and Supply Conditions

At present, Yangjiang station has already ceased hydrogen production and started to buy hydrogen. There are many hydrogen providers at Yangjiang that can provide compressed hydrogen in tanks. According to the updating and upgrading arrangement for hydrogen production equipments from China Meteorological Administration, the hydrogen production equipments of the souding station in 2009 will all be replaced by Handan-made water-electrolytic hydrogen production equipments.

(IV) Living and Transportation Conditions

Situated within the urban district of Yangjiang, the traffic of Yangjiang air sounding station is really convenient. Several hotels above 3-star level within 2 km can fully meet the accommodation, catering the needs of the international intercomparison participants. Yangjiang's main inter-provincial means of communication are train and long-distance bus. To pass the customs, the foreign personnel can enter Shenzhen customs via Hongkong, and then they can reach Yangjiang by inter-provincial means of communication or it is for Guangdong Provincial Meteorological Bureau to dispatch cars to pick them up at Shenzhen and send them to Yangjiang. Yangjiang station is equipped with vehicles for operation, and it can make corresponding arrangements to pick up and send off intercomparison personnel during the international intercomparison period.

(V) Professional Staff

There are 6 professional staff at Yangjiang station who can undertake such operations as flying sounding balloon, hydrogen production and sonde binding. In addition, professional staff with favorable technical skills can be transferred from Guangdong Provincial Meteorological Bureau and other stations throughout the country to undertake such operations as flying sounding balloon during this intercomparison.

(VI) Site Alteration

There is not much redundant area within the Yangjiang station. During the international intercomparison, operational sondes of 8 models as well as research-model sonde and other ground remote sensing sounding equipments will be involved in the intercomparison, therefore, the site layout shall be designed overall to make full use of the existing area. At present, Yangjiang station has carried out alteration planning over the existing site within the station and divided the site into the following functional areas (See Fig. 1.5):

1. Area for flying sounding balloon:

Intercomparison balloon-flying area takes advantage of the **original balloon flying area**[1]. The hydrogen production room situated to the south of the balloon flying area is moved southwards and new water-electrolytic hydrogen production equipments are installed.

2. Area for hydrogen production and storage:

The original hydrogen production room is still in operation, **the new hydrogen production room[2]** is now in the process of land-levelling operation. As the hydrogen consumption volume for sonde intercomparison increases, the real-time hydrogen yield of the water-electrolytic hydrogen equipments cannot meet the demand of the intercomparison, thereupon, it is scheduled to buy hydrogen during the intercomparison period.

3. Area for sounding data summary:

According to the requirements of WMO sonde international intercomparison, the host country shall be responsible for the organization and summary of the intercomparison sounding data as well as the compilation of preliminary report of the intercomparison. This area is comparatively independent, and it is expected to be in the outer room of the station's **current duty room[3]** or within the **original duty room[4]**.

4. Area for working group meeting:

During the intercomparison period, various problems encountered shall be negotiated and coordinated. The area for working group meeting is scheduled to be on the first floor of the **weather radar building[5]**.

5. Area for ground receiving equipments:

This area is the working area of all producers participating in the intercomparison. Yangjiang station works out 2 solutions-open and close solutions. The open one lies in the outer room of the **current duty room[3]**, and all the ground receiving equipments and personnel are within the same indoor space. It is convenient for management, but the current conditions make it too crowded; while the close one lies in **the original duty room[4]** which boasts 8 independent rooms of $10m^2$, 7 of which are equipped with independent bathrooms.

6. Area for erecting receiving equipments' antennas:

It adopts open solution, with the area for erecting receiving equipments' antennas being on the top of the building of the **current duty room[3]**. It is comparatively crowded to erect over 8 antennas. If close solution is adopted, the area for erecting receiving equipments' antennas shall be atop of the building of the **original duty room[4]** (only 1 storey) where there is abundant area.

7. Area for ground remote sensing equipments:

Area to the north of the original duty room is **the area for erecting ground remote sensing equipment[6].**

(VII) Investigation Conclusion

Situated at the top of the mountain, Yangjiang station has a favorable clearance condition. The station's climate environment accords with the high moisture conditions required by the international sonde intercomparison. The station possesses a strong technical capacity. There is not much redundant area within the Yangjiang station which is now carrying out alteration

according to the international intercomparison site. Yangjiang station has accumulated relevant experience through evaluation and test of China's home-made GPS sonde and possesses obvious advantage. Besides Yangjiang station, China Meteorological Administration also considers Haikou meteorological air sounding station in Hainan as the alternative intercomparison site.

Annex – C Yangjiang Site Plan

Distribution Map

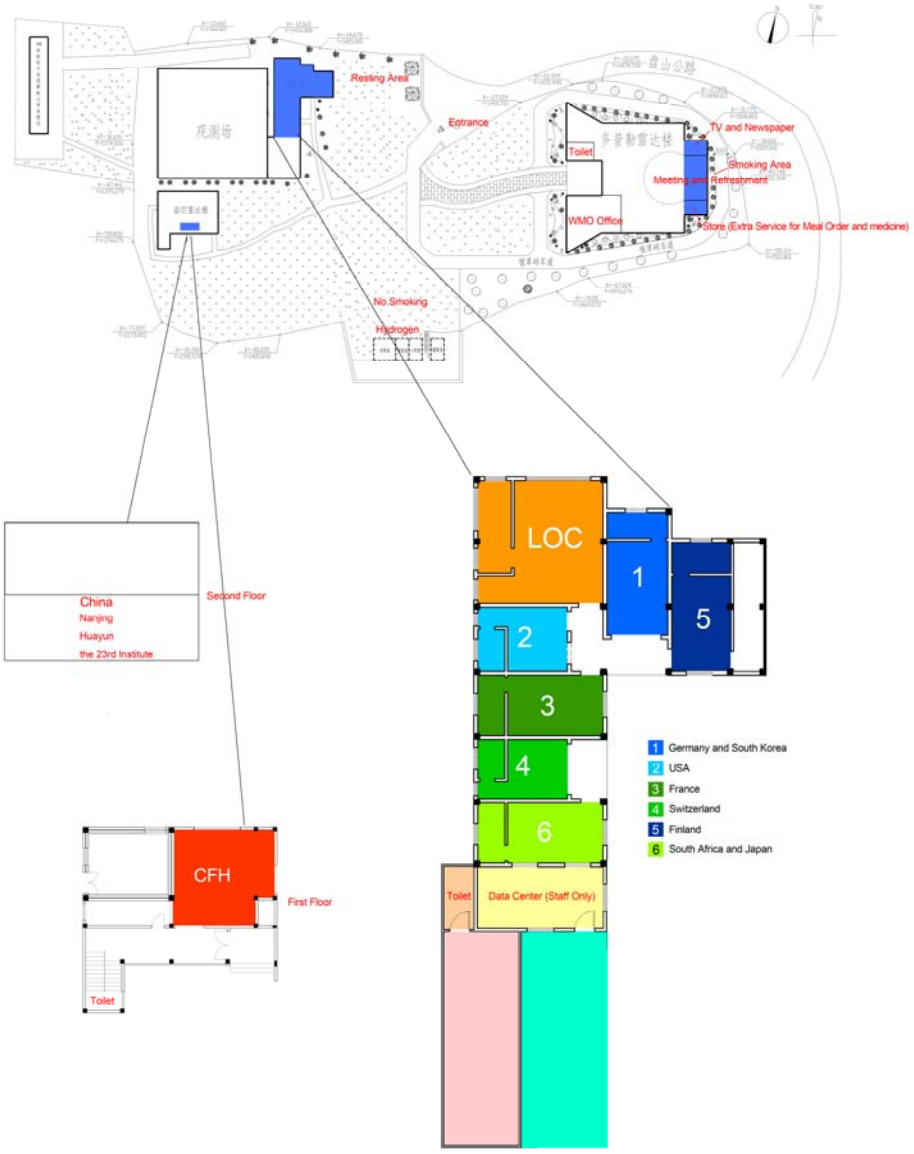

Annex – D Routine processing and corrections being applied to QRS systems

D1 Introduction

The purpose of this section is to provide examples of some of the processing that is applied to temperature and relative humidity observations by various manufacturers. Fundamental issues raised by this are:

- What evidence needs to be supplied to justify the correction that is made? How does a manufacturer check that they are using a procedure useful for meteorologists or climate scientists?
- Does the correction procedure lead to a better result for users, or does it introduce other problems, and are these other problems acceptable to the user?
- When correcting for slow time constant of response, how reliable are the time constants, is the structure being generated meaningful or largely noise?

It is suggested that the CIMO Expert Team on Standardisation consider drafting recommendations for what evidence is required to support correction schemes, e.g. laboratory tests, in flight-testing against high quality measurements, theoretical uncertainty models plus identification of the reason for the error.

One concern is that if test results such as those at Yangjiang were used to adjust the measurements, without understanding the reason for the systematic differences, the corrections become arbitrary and not based on an understanding of the sensing system limitations. It is essential that every effort is made to eliminate design deficiencies in the basic radiosonde sensing systems, rather than covering up flaws by using arbitrary software adjustments.

Users of observations in numerical weather prediction models tend to want to correct observations with their own software, since they can support sophisticated corrections utilising other information in the numerical model, as for instance for many satellite observations and GPS water vapour sensing. This is essential if the correction requires knowledge of other meteorological variables in the numerical model. However, if the correction requires knowledge of some variables which are not represented in the numerical model, e.g. use of a humidity temperature sensor to evaluate humidity observations, with this data not made available to users, then the correction is best applied in the radiosonde system software.

For climate purposes, it is essential that manufacturers keep a public record of changes to their software, especially the temperature and humidity correction software.

D2 Temperature (Night)

Graw apply a correction for time constant of response to the temperature sensor both at night and in the day. Figure D2.1 (a) shows how this software works near the tropopause. At this height, the software has eliminated some spurious measurements between minute 43 and 44. The correction for time constant of response does not have much effect although there are some examples where short term fluctuations in temperature have slightly larger amplitude in the reported values than in the raw, e.g. between minute 46 and 47.

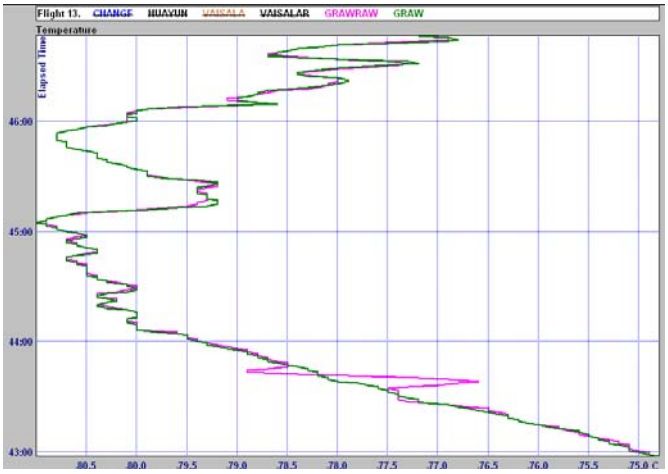

(a)

(b)

Figure D2.1 Examples of Graw raw and reported data from a night time temperature flight, flight 13.

In the later stages of flight 13, where the time constant of response was slower, and the temperature corrections more significant, the reported values are much noisier than the raw data. It appears that the time constant correction in this circumstance amplifies the noise (e.g. see minute 84 to 85) and does not lead to an improved representation of the temperature structure. This is not always true, and Figure D3.1 (b) shows an example where the corrections are more stable with time.

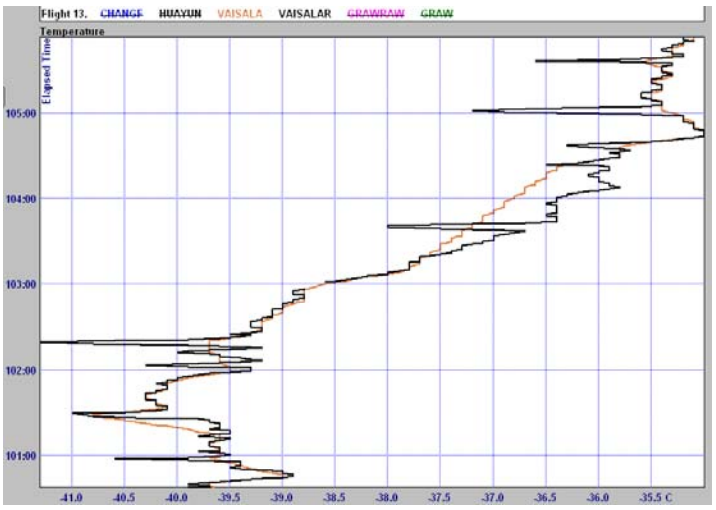

(a)Vaisala

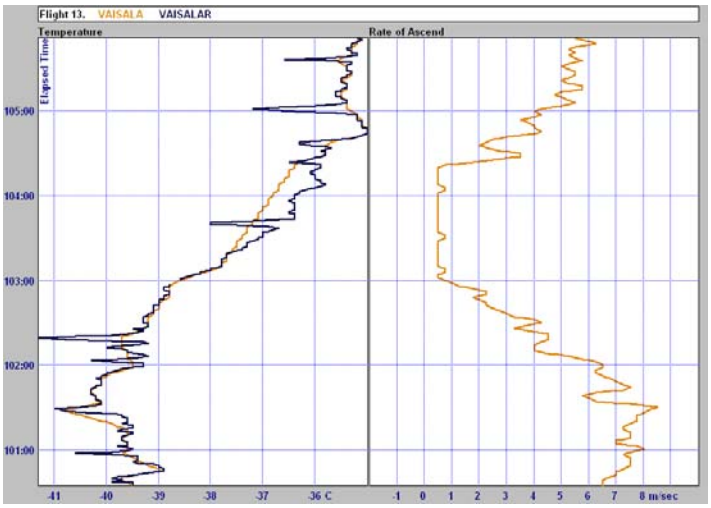

(b) Vaisala +rate of ascent, showing interpolation is caused by Vaisala software reaction to a period of very low rate of ascent.

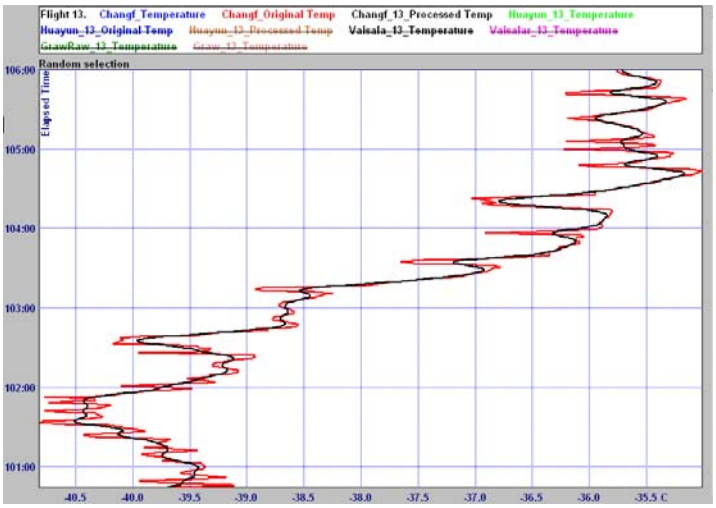

(c) Changfeng

Figure D2.2 Examples of nigth-time temperature measurements from the end of Flight 13 by Vaisala and Changfeng radiosondes, near 35 km.

Figure D2.2 shows examples of night-time software adjusting the impact of the negative spikes seen by both Vaisala and Changfeng on this flight. In the case of Vaisala the quality control is rejecting some of the signals in the raw data and interpolating across more than a minute, see minutes 103 to 104.5 This was a result of the Vaisala software reaction to a portion of the flight where the rate of ascent was very low. The software is intended to avoid problems where for very short periods of the ascent the radiosonde may fall with time before continuing to ascend, since this can cause problems in the TEMP message, if all the detail is reported.The negative spikes may be of similar origin to those observed by the MTR, see section 7.2.3. There are very few instances of these negative spikes in the raw data of any of the other night-time flights at Yangjiang. These negative spikes only occurred near the end of the flight. Figure D2.3 shows measurements by Huayun on the same flight.

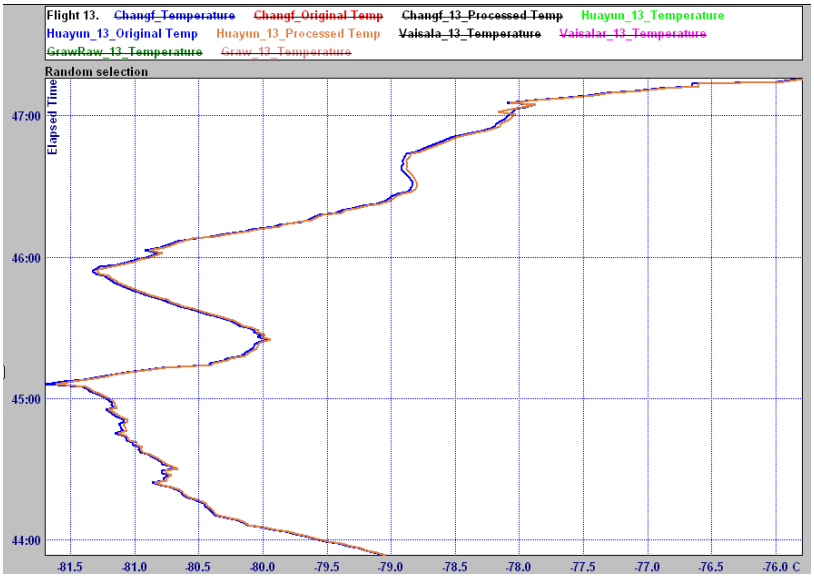

(a) Near the tropopause

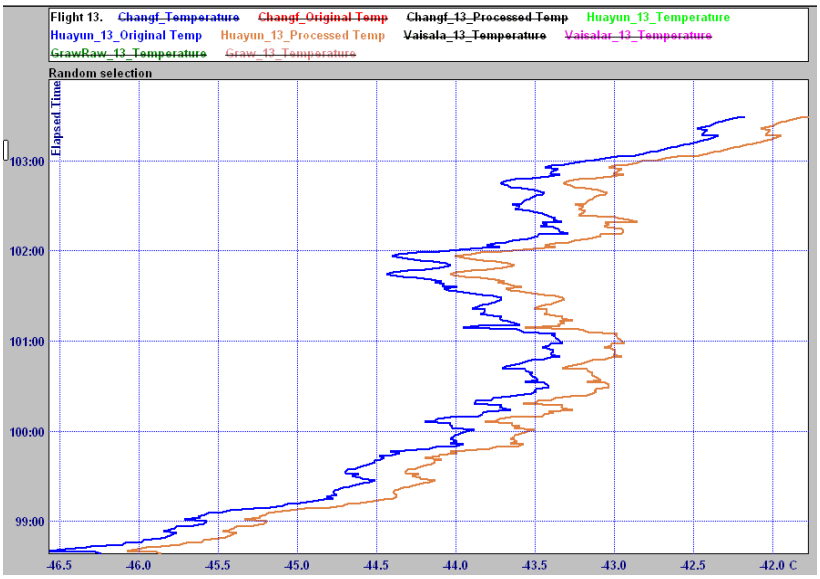

(b) At upper levels, near 35 km

Figure D2.3 Examples of night-time temperature measurements by Huayun on Flight 13

Figure D2.3 shows that whilst raw and processed Huayun temperatures are very similar near the tropopause, at 35 km Huayun has added a temperature correction of at least 0.4 deg C to the temperature. The reason for this is unclear. Corrections should not be made unless there is evidence that an error has been identified.

Figure D2.4 shows InterMet data from the end of a very high night flight, and compares this to the Vaisala data. The Vaisala raw shows some negative spikes, but InterMet does not indicate these at all.

The examples shown in Figure D2.4 give an impression of the level of pre-processing applied to night-time temperature measurements. Without the information shown here, it becomes very difficult to interpret the comparisons of reported temperature from this intercomparison, e.g. the Huayun night-time correction.

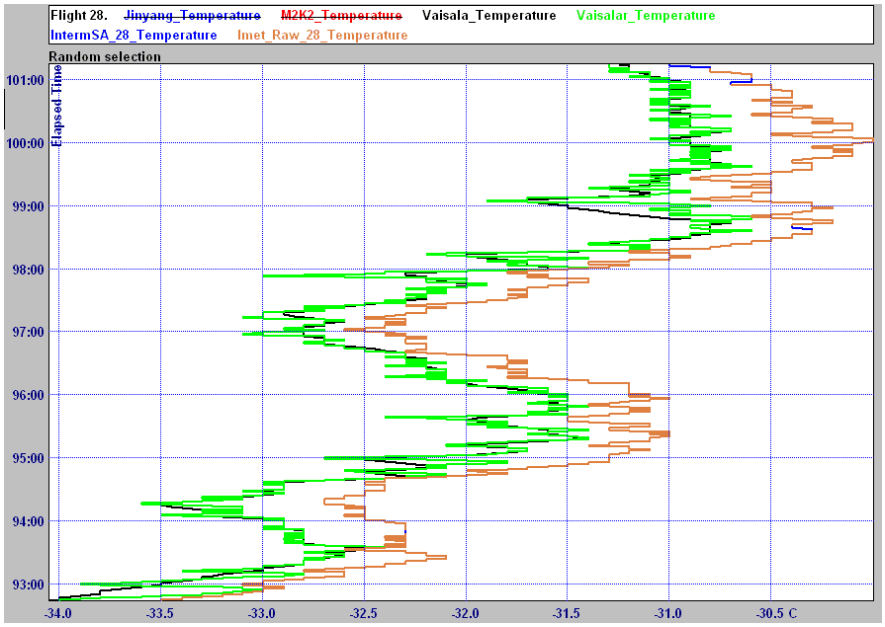

Figure D2.4 Raw InterMet temperatures compared to raw and edited Vaisala data at the end of Flight 28, near 38 km. The reported InterMet values were the same as the raw.

D2 summary

- Manufacturers need to ensure that their system reports reliable data, without excessive interpolation in the vertical, and be willing not to report data if the quality is poor.

- Users of the data would probably prefer to correct for time constant of response in temperature observations themselves, and see less noisy data in the operational reports, given that the sensors now are very much faster than 20 years ago.

- It is clearly helpful to users that manufacturers provide assessments of the time constant of response of their temperature sensing systems.

D3 Temperature (day)

Daytime radiosonde temperature measurements often have a lot more short-term fluctuations than night-time, so the filtering applied to daytime measurements is not necessarily the same as that used at night.

Examples of Graw measurements are shown in Figure D3.1 (a) and (b). Near the tropopause, a solar radiation correction of about 0.5 deg C is applied, and the effects of the time constant of response correction can be seen more clearly in this example. At the upper level, the data from this flight is of better quality, so the noise induced by the time constant of response correction is much less than in the night-time example. The solar radiation correction at about 34 km was just over 1 deg C. Is the time constant of response correction for Graw correct at these upper levels? Has the correction lowered the maximum near minute 76.7 too much? How was the time constant measured? For GRUAN purposes the raw data would need to be stored until the evidence for the corrections was checked and agreed. Compared to many of the following plots, the Graw sensing system gives very clean daytime measurements with the raw data showing very little evidence of spurious short-term fluctuations.

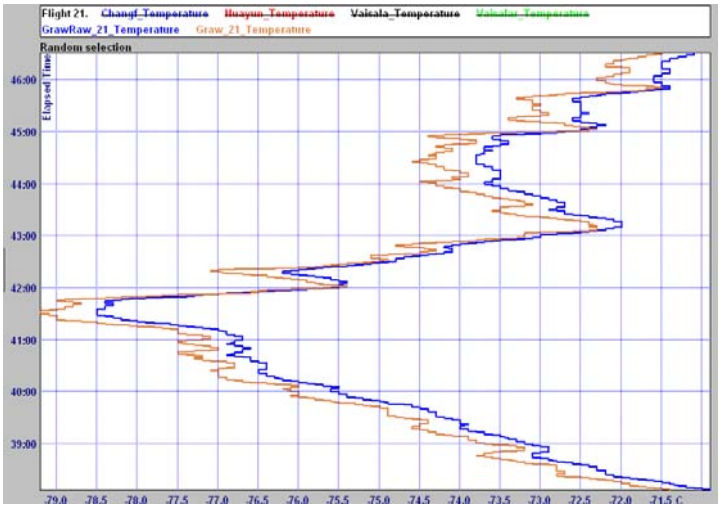

(a) Near the tropopause

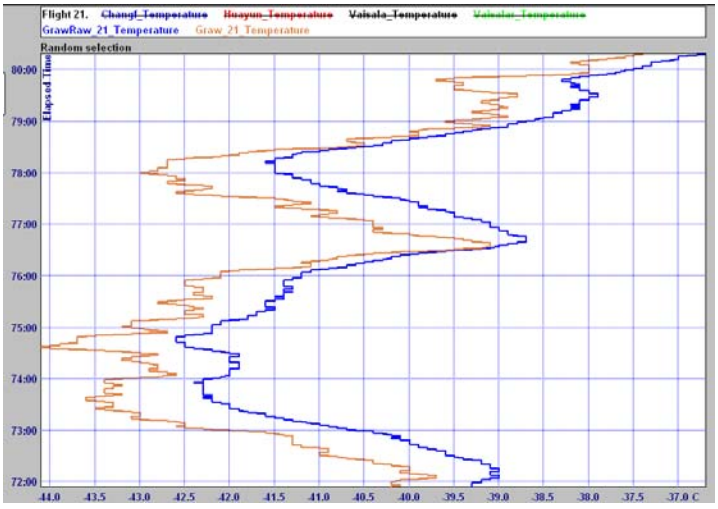

(b) At upper levels near 34 km

Figure D3.1 Examples of Graw raw and processed daytime temperature measurements.

Both Modem and InterMet have taken actions to improve the exposure of their temperature sensors in the daytime in recent years. Consequently, their measurements do not now require a lot of additional filtering in the daytime to remove short-term fluctuations, although Figure D3.2 shows that a few fluctuations still occur occasionally at very high levels. InterMet's solar radiation correction was about 1.2 deg C near 34 km.

(a) InterMet raw and processed day time measurements near 34 km

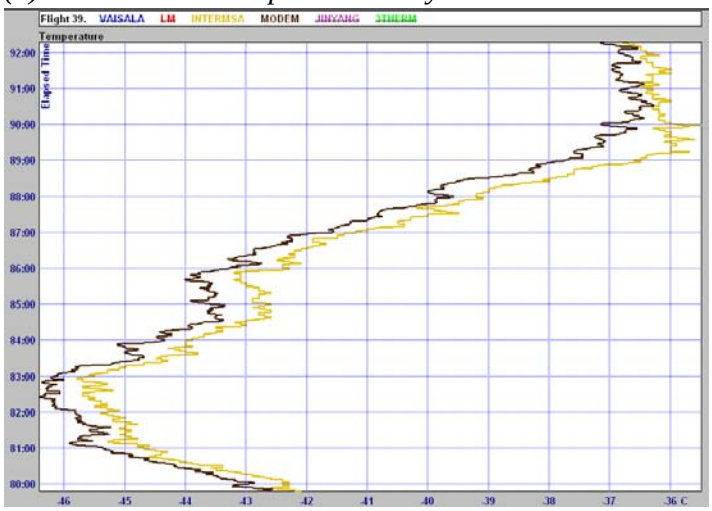

(b) Modem compared to InterMet, both with minimal filtering near 34 km

Figure D3.2 Comparison of InterMet and Modem measurements from Flight 39 in the daytime at about 34 km.

LMS and the Multithermistor are also compared to InterMet on this flight (Fig. D3.3), at 24 and 34 km. Again, there are occasional short-term fluctuations, but the temperature measurements of these systems with little filtering, track each other well, apart from right at the end of the flight.

(a) Near 24 km

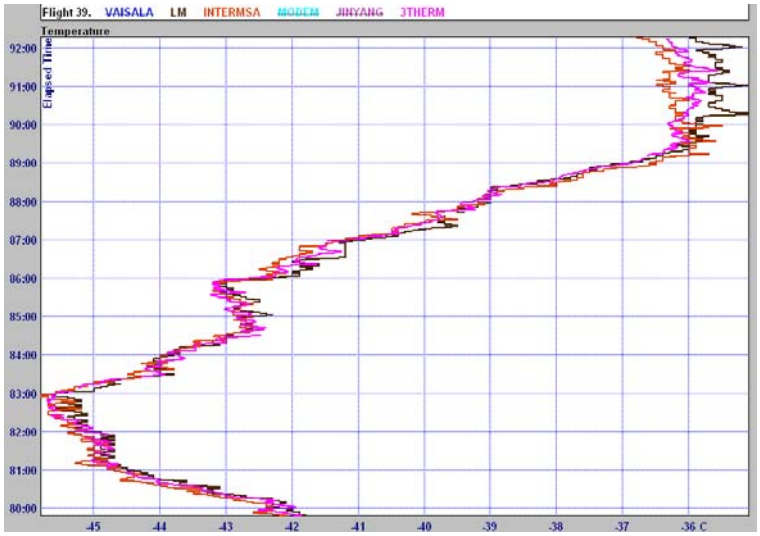

(b) Near 34 km

Figure D3.3 Comparison of InterMet, LMS and Multithermistor measurements from Flight 39 in the daytime.

Figure D3.4 shows Vaisala processed and raw for the same heights as the comparison in Fig. D3.3. Vaisala and InterMet processed values are very close at 24 km, and it can be seen that the Vaisala raw has short fluctuations of peak-to-peak amplitude about 0.5 deg C, which the Vaisala filtering removes very effectively at this height. However, at 34 km the positive pulses which cause the short term fluctuations have increased in amplitude to around 1.5 deg C, and because these pulses are irregular due to the complex motion of the radiosonde in flight, the filtering is not so effective. In individual radiosonde ascents, the radiosonde is more irregular than on the test flights so it is more difficult to recognise the positive pulses in the raw data.

(a) Near 24 km, Vaisala and Vaisala raw (VAISALAR) compared to processed InterMet

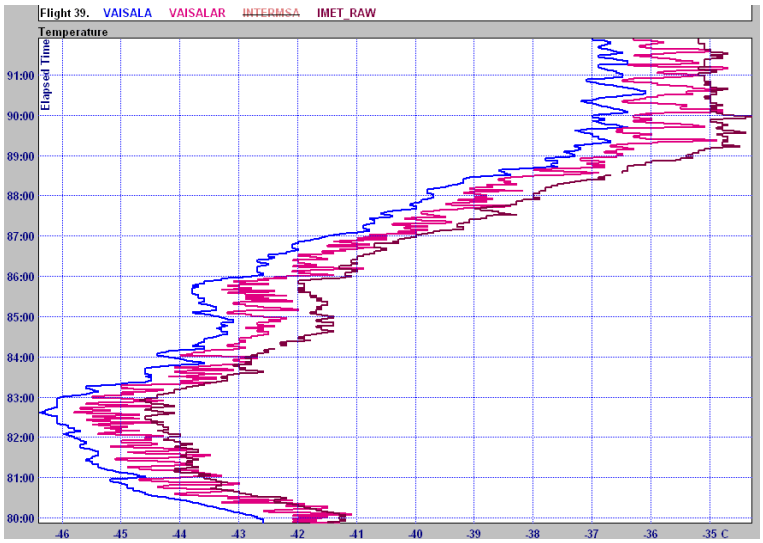

(a) Near 34 km, Vaisala compared to raw InterMet, for clarity, InterMet raw and processed have the same short-term fluctuations.

Figure D3.4 Comparison of InterMet and Vaisala measurements from Flight 39 in the daytime.

The positive pulses come from the air which has been heated by passing over the Vaisala sensor support frame and then passes over the temperature sensor itself. This only occurs for certain geometry as the radiosonde rotates, hence the frequency of occurrence of the positive pulses can be as high as the period of rotation of the radiosonde rig under the balloon. This is usually near 12 s, but can be less than this from time to time as the radiosonde is also rotating relative to the balloon rig. The other radiosondes on this flight did not see this problem, so it is not caused primarily by heat shed from the balloon or the rig.

The Changfeng radiosonde has a very similar sensor support to Vaisala, see chapter 4.

(a) Near 23 km

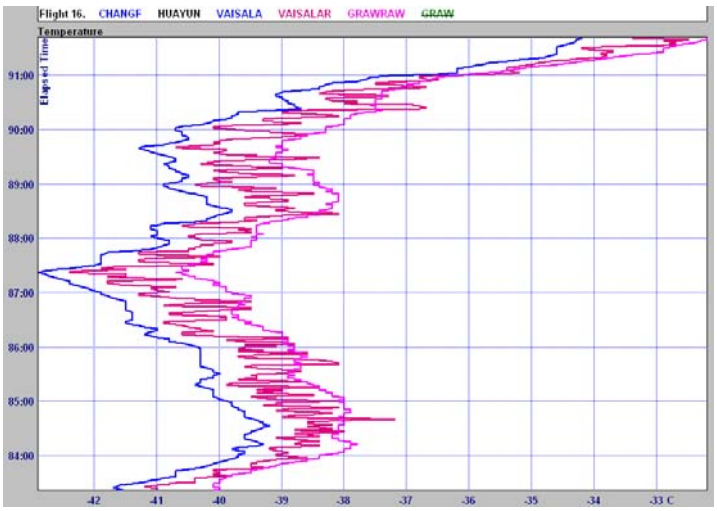

(b) Near 34 km

Figure D3.5 Comparison of raw Graw and Vaisala measurements from Flight 16 in the daytime.

In Figure D3.5, the Vaisala measurements are compared with raw Graw from a daytime flight 16. These Vaisala measurements show the same characteristics as those in Fig. D3.4. Then in Figure D3.6, the Vaisala raw measurements are compared with raw and processed Changfeng measurements from the same flight. The Changfeng measurements have similar positive pulses to Vaisala at similar frequencies, but not correlated with Vaisala.

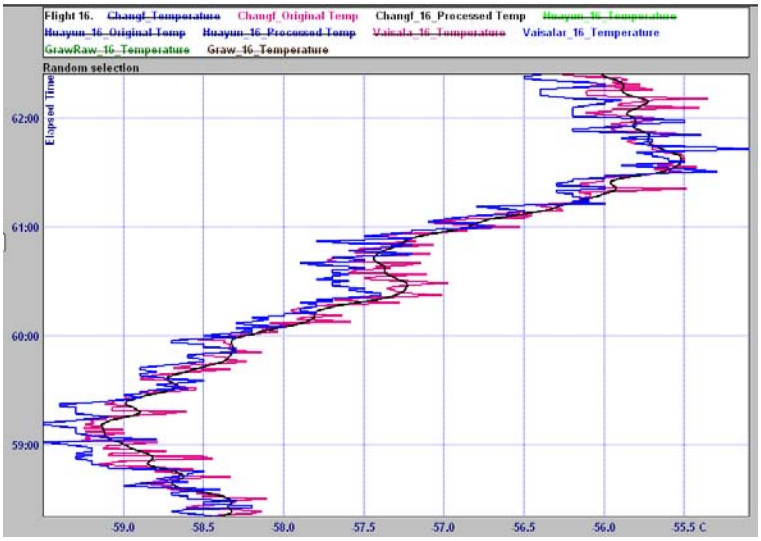

(a) Near 23 km

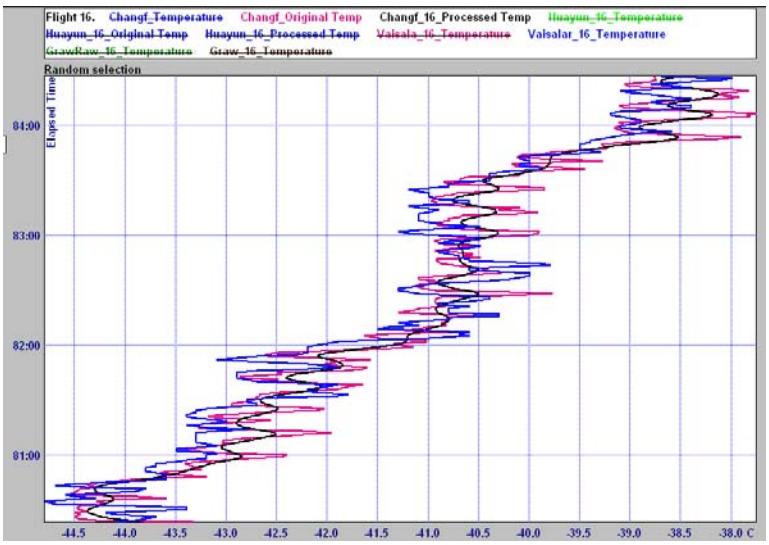

(b) Near 33 km

Figure D3.6 Comparison of Changfeng, raw and processed, and Vaisala raw measurements from Flight 16 in the daytime.

Figure D3.6 shows that Changfeng software deals with the positive peaks in a different manner to Vaisala, but the result is similar, with the filtering effective at 24 km but not at the highest levels.

Huayun raw and processed temperature is compared to raw Graw in Figure D3.7.

(a) Near 24 km

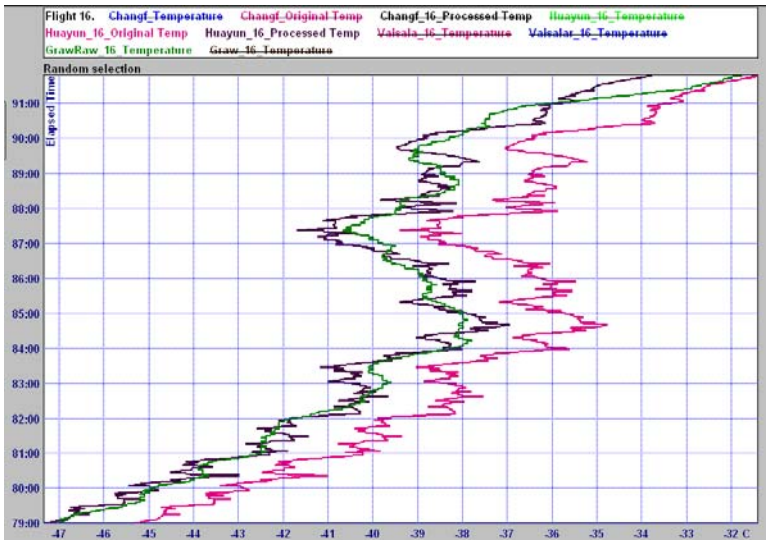

(b) Near 34 km

Figure D3.7 Comparison of Huayun, raw and processed, and Graw raw

Huayun apply a solar correction of about 1.2 deg C at 24 km and about 2 deg C at 34 km, however there is no other filtering unlike Changfeng, Daqiao and Vaisala. There are no frequent narrow positive pulses, because the temperature sensor mount is quite different to Vaisala and Changfeng. The changes in systematic bias are less rapid, e.g. between minute 83 and 87, because the sensor is sensing air heated above ambient for longer periods than in the case of Vaisala and Changfeng. They are not related to problems with Huayun time constant of response.

D3 Summary

- In general solar radiation corrections have grown smaller with quicker temperature sensors. Those still using larger corrections should check their design, since larger corrections should not be necessary with a fast sensor with low reflectivity coating.
- If a sensor is exposed correctly and is far enough from the radiosonde body, it should not have large numbers of positive temperature spikes at upper levels in daytime.
- Avoid supporting the sensor with a guard ring support unless there is absolutely no alternative. Good exposure of the sensor allows day-time temperatures to be made without the need to filter out frequent temperature spikes.

D4 Introduction to relative humidity

There is a long history of corrections applied to temperature measurements. However, software corrections to relative humidity measurements seem to have started since the previous WMO Radiosonde Comparison in Mauritius.

Once it was recognised that this was happening, the IOC attempted to summarise the situation with the manufacturers who participated in the Yangjiang Intercomparison. The results of this small questionnaire are shown in Table D4.1.

Radiosonde Type	Dedicated temperature sensor to measure humidity sensor T?	Software Adjustment for slow time constant of response?	Time constant used All values shown are for 63% response time:	Software to correct for day-time low bias in humidity?	Other specialised Correction Please specify?
InterMet	Yes	Yes	-40 °C: 5s -70°C: 225s	No	No
Modem	Yes	No	-40°C: 9s -70°C: 21.5s (Not applied)	Yes	NA
Graw	No	Yes	-40°C: 15s -70°C: 250s	Yes	
Snow White	Yes	N/A	N/A	No	Frostp/DP
Meteolabor	Yes	Yes	-40°C: 120s -70°C: 240s	No	No
Daqiao	No	No	No	No	Adds humidity difference between ground check value and ambient value to upper-air data
Jinyang	No	No	No	No	No
Meisei	No	No	No	No	No
Changfeng	No	No	No	No	No
Huayun	No	No	No	No	No
LMS	Yes	Yes	-40 °C: < 20s -70°C: Not given	No	No
Vaisala	No	Yes	-40°C: 8s -70°C: 73s	Yes	No

Table D4.1: Software corrections applied to relative humidity measurements

D5 Relative humidity (night)

Three of the participants in Yangjiang were able to provide information showing the effect of time constant of response corrections. Some examples of Vaisala measurements are shown in section 8.1, but another Vaisala example from Flight 8 is shown in Figure D5.1. This was a flight with no upper cloud. The time constant correction affects measurements lower than -40 deg C.

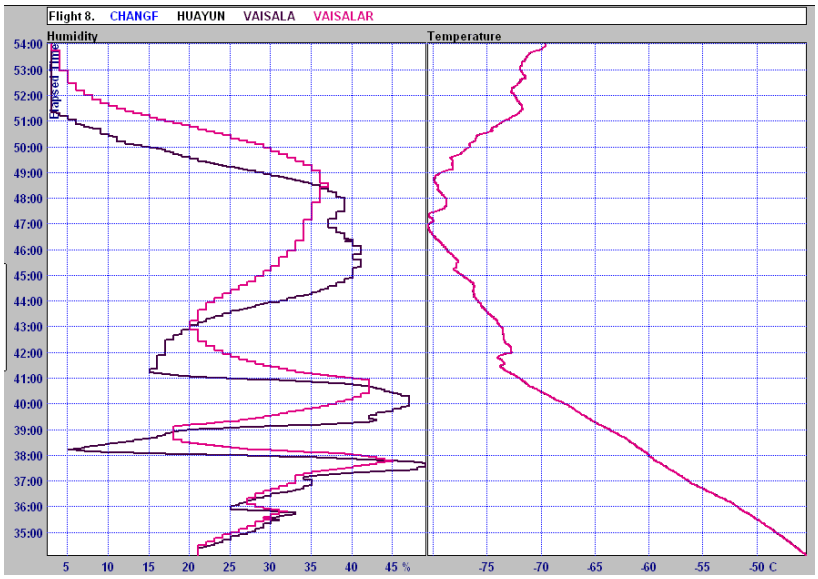

Figure D5.1 Raw and corrected night time Vaisala measurements of relative humidity on Flight 8

Vaisala provided the raw data from all the QRS flights, so it is possible to see what overall changes at night were introduced by this correction, see Figure D5.2.

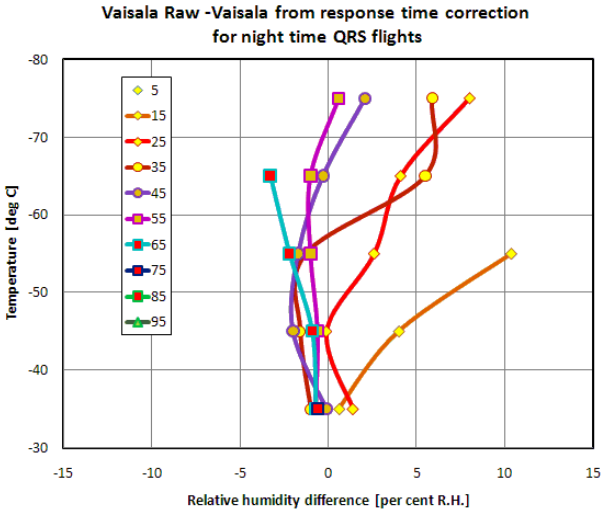

Figure D5.2 Difference between Vaisala Raw and processed Vaisala for all Vaisala night QRS flights, a positive value means the processed values are lower than the raw.

Thus, the Vaisala correction scheme made the largest differences at night in situations where the raw data were also at low humidity, producing a positive bias of the raw values relative to the processed values. All data in Figure D5.2 have contributions from at least 4 flights.

The effect of the InterMet time constant of response correction can be seen in Figure D5.3 where the results are compared to the processed Vaisala output on the same flight.

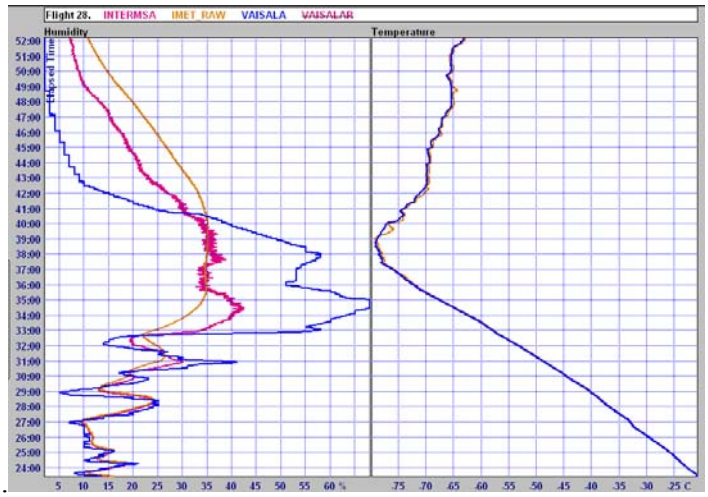

Figure D5.3 Raw and corrected night time measurements of InterMet relative humidity on Flight 28, compared to Vaisala processed output

The InterMet correction improves the representation of the vertical structure, and does not increase the noise in the processed data by too much, but cannot represent the troposphere /stratosphere transition correctly. The overall effect of the time constant correction on both day and night InterMet flights can be seen in Figure D5.4.

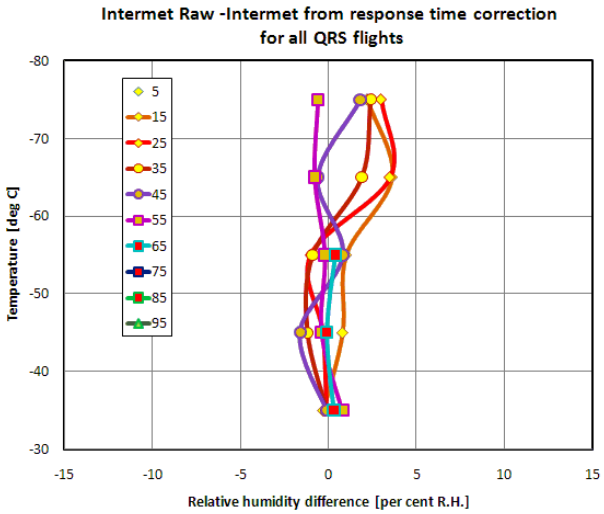

Figure D5.4 Difference between InterMet Raw and processed InterMet for all InterMet QRS flights, a positive value means the processed values are lower than the raw.

Thus, the InterMet correction slow response correction scheme has less effect than that of Vaisala, even though the response of the E+E sensor is slower than that of Vaisala at upper levels. Figure D5.5 shows the raw and corrected InterMet values compared to the raw Vaisala measurements from Flight 68 at night, and this confirms that a larger slow response correction is probably needed to bring InterMet measurements closer to the correct value at temperatures lower than -50 deg C in the conditions found at Yangjiang.

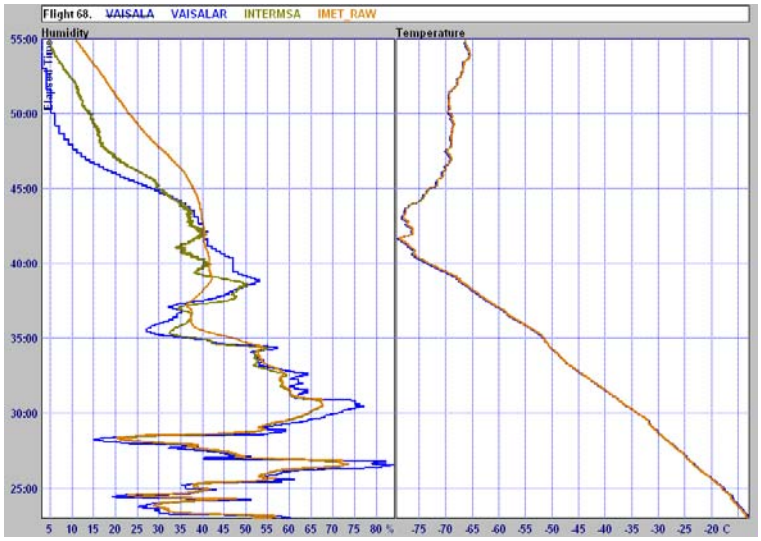

Figure D5.5 Raw and processed InterMet relative humidity compared with Vaisala uncorrected values at night, Flight 68

The effect of Graw's correction for slow response is shown in Figure D5.6. This is the flight for which Vaisala corrections are presented in Figure 8.1.20. The increase in relative humidity after minute 42.5 corresponds to an extremely small increase in relative humidity in the basic measurements.

Figure D5.6 Raw and corrected night-time measurements of Graw relative humidity on Flight13.

Up to minute 42.5, the Graw correction scheme has improved the profile to be similar to Vaisala basic measurements. However, to get closer to the Vaisala processed values would require a bigger correction between minutes 30 and 42. The correction later than minute 42.5 raises the issue of the sensor being too slow to correct, but more work needs to be done to define the limit for this type of correction.

D5 summary

- Corrections for slow response can be beneficial in improving relative humidity profiles in the upper troposphere, probably for time constants up to as long as 2 or 3 minutes.

- Some sensors have time constants of response closer to 4 minutes at the lowest temperatures in Yangjiang, and trying to use the same technique with these measurements is dangerous, because the sensing system performance is not always sufficiently reliable. There are plenty of examples in Yangjiang of the slower sensors showing structure above the tropopause that is not real, see Fig. D5.7. The slow response correction can then amplify very small variations in relative humidity into significant atmospheric structure, sometimes this is correct, but when there is contamination it is quite spurious. In Yangjiang, where corrections for such slow response were applied, the result looked reasonable in about 65 per cent of the cases and quite wrong the rest of the time.

Figure D5.7 Example of relative humidity structure near the tropopause, where the main drop in relative humidity was at about minute 41.5 into flight, but all the other sensors show variations in relative humidity after this which were nothing to do with atmospheric variation in relative humidity.

D6 Relative humidity (day)

In the daytime, both Vaisala and Graw make significant changes to the raw humidity measurements to compensate for the effect of solar heating causing the humidity sensor to be a different temperature to the main temperature sensor. As can be seen from Table D4.1 many other systems are using a separate sensor attached to or deployed near the humidity sensor, so that the effect can be measured and then corrected without making a general assumption about the heating that has occurred on a specific flight, which is going to depend on both solar elevation and cloud cover.

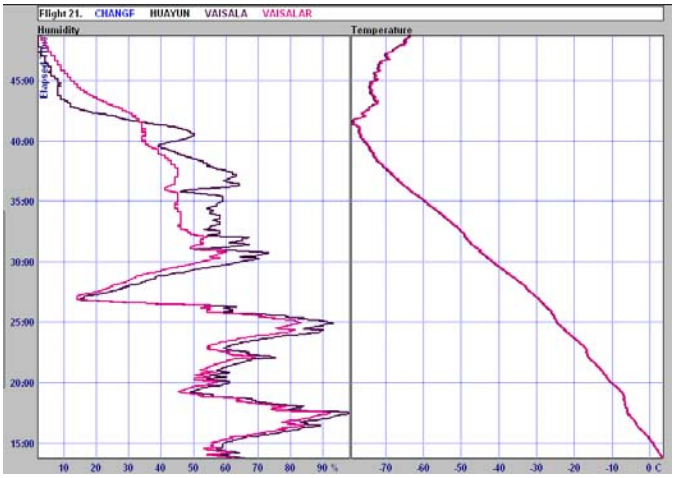

Figure D6.1 Raw and processed Vaisala relative humidity for a daytime flight, Flight 21.

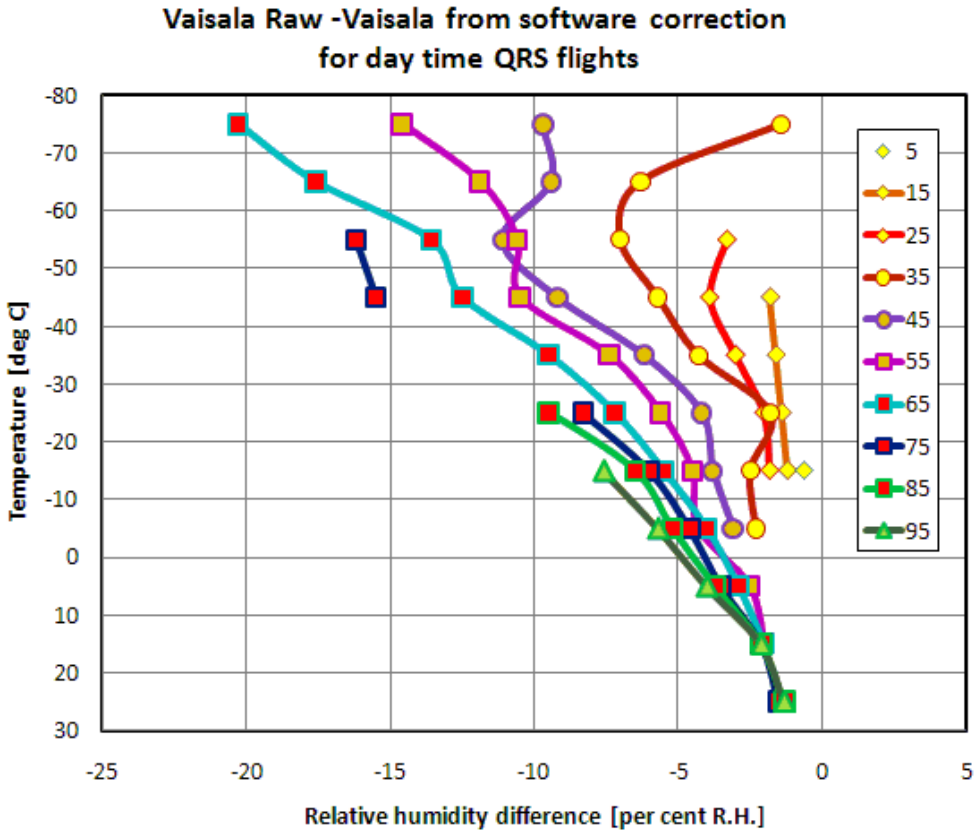

Figure D6.2 Vaisala raw – Vaisala processed for all daytime QRS flights, where a negative value means Vaisala processed is higher than Vaisala raw.

The effect of the daytime correction scheme (a combination of the slow response correction and a solar heating error correction) can be seen in Figure D6.1. In this case, the solar heating correction affects measurements throughout the flight, increasing in amplitude with height. The effects of the daytime correction of Vaisala Raw on all the Vaisala flights is summarised in Figure D6.2.

The day-night difference plots for relative humidity in Fig.8.1.13 in the main report imply that the correction scheme is too large at high humidity for Yangjiang conditions by about 5 per cent R.H. at -25 deg C, 5 per cent R.H. at -55 deg C, and about 3 per cent R.H. at -75 deg C. The discrepancies were probably associated with occasions with high cloud cover. For measurements in the upper levels the accuracy of this correction scheme is probably the limiting factor on daytime Vaisala measurements.

Vaisala humidity sensors are directly exposed to solar heating, but in the case of Graw the sensor is covered by an aluminised cap, so it may not be so straightforward to try and build a model of the temperature difference between the humidity sensor and the main temperature sensor.

Figures D6.3 and D6.4 show examples of the difference between Graw basic and Graw processed daytime relative humidity. This includes the effects of time constant of response correction and of the correction for solar heating.

The example in Figure D6.3 is from an SSI flight, so it is safe to conclude that the Graw basic data have been overcorrected between minute 44 and 47. The most probable reason for this was that the sensor on this flight was responding faster than normal, and the root of the problem is in the time constant of response correction.

In the second example in Figure D6.4, the time constant correction has been effective between minute 33 and 44, and the vertical structure from Vaisala and Graw was similar. After minute 44, the Graw correction scheme seems to be unstable for some reason and although the relative humidity drops relatively quickly above the tropopause, the values are noisy.

It is not easy to identify the solar heating correction from these examples, but it seems the solar correction increased relative humidity by about 7 per cent R.H. at high humidity near the ground and about 12 per cent R.H. at -60 deg C. When referenced to Figure 8.1.13 in the main report this would imply that the correct daytime adjustment for Yangjiang conditions is about 3 per cent near the ground and about 15 per cent at -60 deg C. This means the correction ought to have a similar dependence in the vertical to the Vaisala correction scheme.

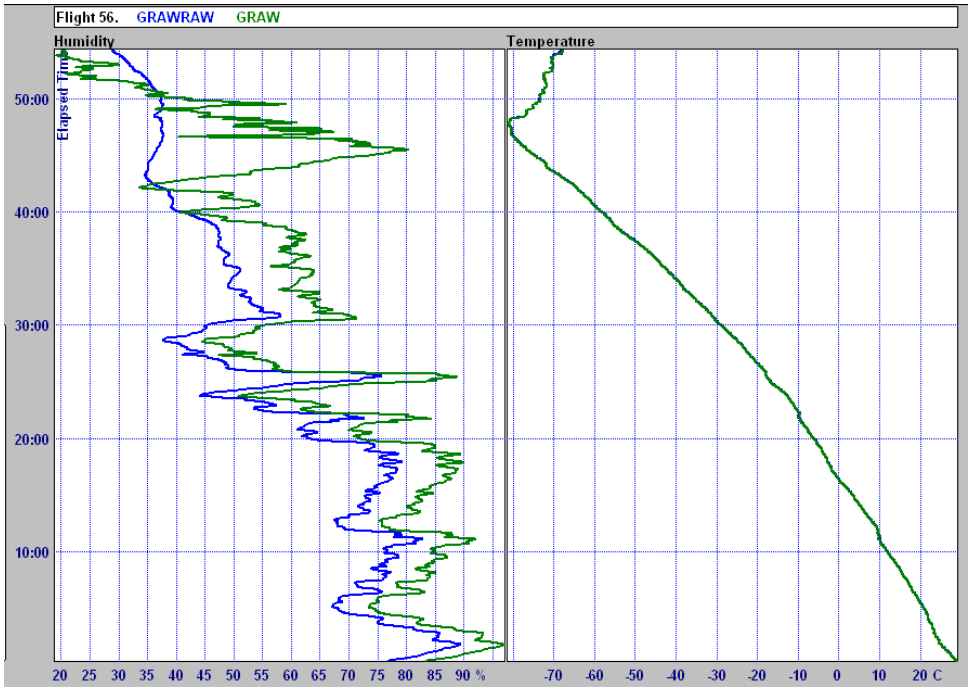

(a) Comparison of Graw Raw and processed, Flight 56

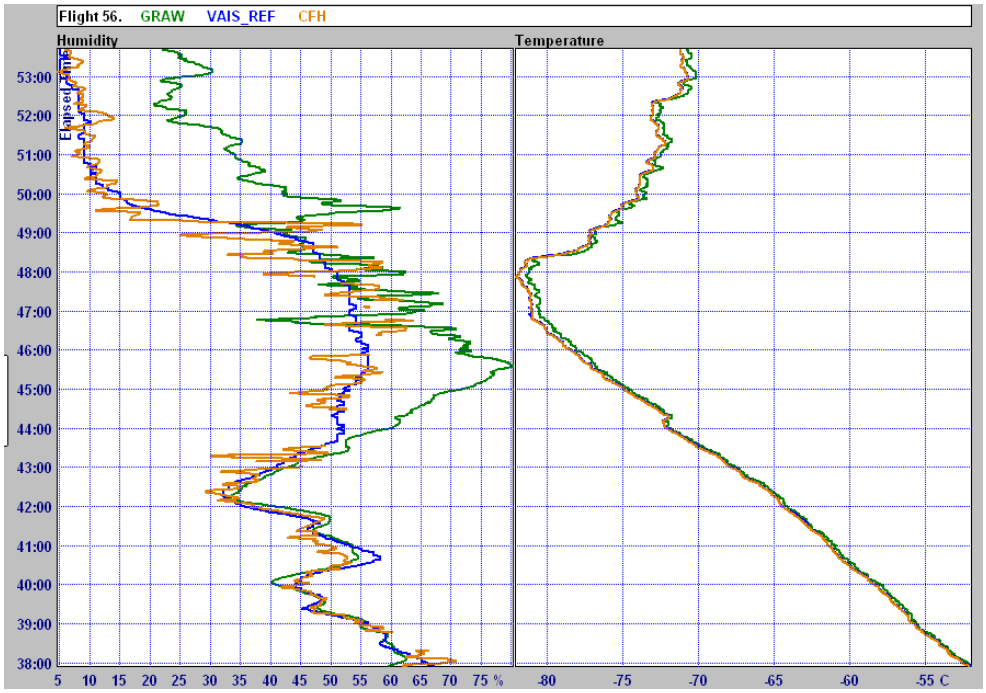

(b) Comparison with Vaisala and CFH on Flight 56

Figure D6.3 Example of daytime correction of Graw raw, taken from SSI Flight 56.

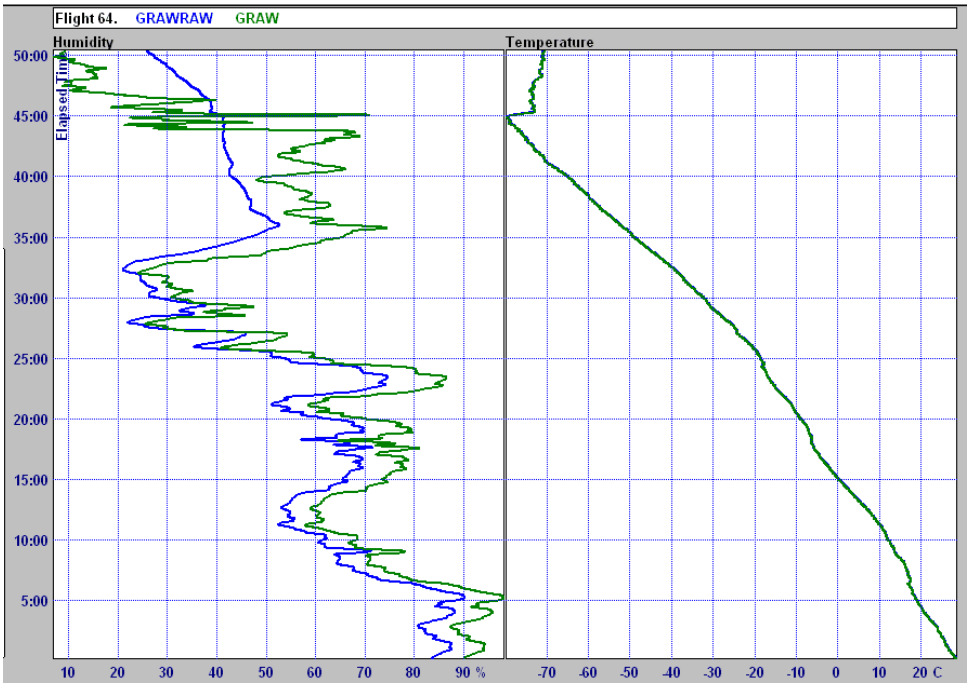

(a) Comparison of Graw Raw and processed, Flight 64

(b) Comparison of Graw with Vaisala on Flight 64

Figure D6.4 Example of daytime correction of Graw raw, taken from QRS Flight 64.

D6 Summary

- The daytime corrections for the temperature difference between the relative humidity sensor and the main temperature sensor are not small at upper levels. The correction accuracy will depend on the validity of the model, which needs to take into account the likelihood of increased cloud cover when observing high humidity. This correction is likely to be the limiting factor on daytime systematic bias in relative humidity measurements at upper levels.
- In the long term for GRUAN, it would be better if the temperature of the humidity sensor was measured directly, so that the solar heating correction was unnecessary.
- Testing at Yangjiang showed that sensing the temperature of the humidity sensor has not yet been implemented successfully by all manufacturers using the technique.

D7 Troposphere/stratosphere transition for relative humidity.

Some manufacturers have been requested to reduce relative humidity values to the low values found in the stratosphere, using software, when the sensor fails to repond. This was either to drop the relative humidity linearly or exponentially to the low value thought likely to be reasonable. The temperature measurements were used to determine when the drop in relative humidity occurs.

If the customer does not want misleading observations reported and the manufacturer knows that the humidity sensor is too slow at the low temperatures near the tropopause to measure the change, then the relative humidity data should not be reported after the tropopause, rather than adjusted arbitrarily by software which does not give the correct results, see Figure 8.1.27.

Note: Most of the sensors in Yangjiang may be fast enough to measure troposphere/ stratosphere transitions at higher latitude but good quality measurements in the tropics are more difficult because of the very low temperatures.

Annex – E Accuracy Requirements for Upper-Air Measurements (CIMO Guide)

Extracted from WMO Guide to Meteorological Instruments and Methods of Observation (WMO-No. 8, 2008)

Annex 12A

Accuracy Requirements (standard error) for Upper-air Measurements for Synoptic Meteorology, Interpreted for Conventional Upper-air and Wind Measurements

Variable	*Range*	*Accuracy requirement*
Pressure	From surface to 100 hPa 100 to 10 hPa	1 hPa to 2 hPa near 100 hPa 2 per cent
Temperature	From surface to 100 hPa 100 to 10 hPa	0.5 K 1.0 K
Relative humidity	Troposphere	5 per cent (RH)
Wind direction	From surface to 100 hPa	5°, for less than 15 m s^{-1} 2.5° at higher speeds
	From 100 to 10 hPa	5°
Wind speed	From surface to 100 hPa	1 m s^{-1}
	From 100 to 10 hPa	2 m s^{-1}
Geopotential height of signifcant level	From surface to 100 hPa	1 per cent near the surface decreasing to 0.5 per cent at 100 hPa

Annex – F Launch metadata

Information

- All times are local (UTC +8)
- Temperature in degrees Celsius
- Relative Humidity %
- Wind Direction in degrees true
- Wind Speed in metres per second
- Cloud amount n/n = amount high cloud/amount low cloud
- Cloud amount in tenths
- Pressure corrected for 88m (AMSL) launch site
- Rate of Ascent is from surface to 100 hPa

Flight No.	Launch		Manufacture	15 minutes before launch										Time to cloud (s)	Rate of ascent m/s	Additional information
	Date (L)	Time (L)		Pressure hPa	Temperature °C	Humidity %	Wind		Visibility km	Significant Weather	General cloud		Local cloud			
							Direction	Speed			Amount	Type	Amount	Type		
1	14/07/2010	08:00	Vaisala, Meisei, Graw, Changfeng, Huayun	998.3	28.7	83	047	3.6	30	Nil	10-/4	Ci, Cu	4/0	Ci	///	6.5	
2	14/07/2010	12:58	CFH, Multi-Therm, Vaisala Sci, Meisei sci	998.6	32.3	53	185	2.4	50	Nil	9/2	Ci, Cu	8/0	Ci	///	6.6	
3	14/07/2010	14:49	InterMet, Modem, Sippican, Jinyang, Meteolabor, Daqiao	997.9	32.0	60	152	4.9	50	Nil	10-/3	Ci, Cb	-	-	///	6.3	
4	14/07/2010	20:01	Vaisala, Meisei, Graw, Changfeng, Huayun	997.3	29.2	83	129	2.4	20	Nil	10-/1	Ci, Cu	10-/0	Ci	///	6.09	
5	15/07/2010	00:52	InterMet, Modem, Sippican, Jinyang, Meteolabor+SW, Daqiao	997.5	27.5	88	044	2.2	30	Nil	0/0	-	0/0	-	///	6.72	
6	15/07/2010	08:31	Vaisala, Meisei, Graw, Changfeng, Huayun	997.7	29.3	76	050	4.6	18	Nil	6/2	Ci, Cu	5/0	Ci	///	6.08	
7	15/07/2010	14:17	InterMet, Modem, Sippican, Jinyang, Meteolabor+SW, Daqiao	996.9	28.0	68	157	4.3	10	Slight rain with thunder in preceding hour	10-/10-	Cb, Cu	10-/10-	Cu	///	6.84	
8	15/07/2010	20:01	Vaisala, Meisei, Graw, Changfeng, Huayun	995.9	28.8	77	093	3.6	15	Nil	5/5	Sc	5/5	Sc	///	6.05	

Flight No.	Launch		Manufacture	15 minutes before launch											Time to cloud (s)	Rate of ascent m/s	Additional information
	Date (L)	Time (L)		Pressure hPa	Temperature °C	Humidity %	Wind		Visibility km	Significant Weather	General cloud		Local cloud				
							Direction	Speed			Amount	Type	Amount	Type			
9	16/07/2010	00:58	InterMet, Modem, Sippican, Jinyang, Meteolabor+SW, Daqiao	997.0	26.4	86	065	6.7	50	Shower of rain in preceding hour	5/5	Cu	5/5	Cu	///	7.51	
10	16/07/2010	03:00	CFH, Multi-Therm, Vaisala Sci, Meisei Sci	996.0	25.5	95	047	5.4	25	Shower of rain in preceding hour	10-/10-	Sc, Fn	10-/10-	Sc, Fc	///	7.38	
11	16/07/2010	08:35	Vaisala, Meisei, Graw, Changfeng, Huayun	996.3	27.1	84	097	5.8	40	Nil	8/0	Ac, Ci	10-/0	Ac	///	6.71	
12	16/07/2010	14:45	InterMet, Modem, Sippican, Jinyang, Meteolabor+SW, Daqiao	995.8	25.9	96	083	5.4	20	Rain	10-/8	Cu,Sc,Ci,Fn	10/10	Sc	///	5.98	
13	16/07/2010	20:04	Vaisala, Meisei, Graw, Changfeng, Huayun	996.7	25.2	94	075	4.4	5	Rain	10/10	Sc, Cu	10/10	Sc	///	6.32	
14	17/07/2010	00:46	InterMet, Modem, Sippican, Jinyang, Meteolabor+SW, Daqiao	997.7	24.9	96	065	3.7	30	Nil	1/1	Sc	0/0	Sc	///	6.26	
15	17/07/2010	02:56	CFH, Multi-Therm, Vaisala Sci, Meisei Sci	996.7	25.3	93	081	6.4	4	Shower	10-/10-	Sc, Cu	10-/10-	Sc, Cu	///	5.91	
16	17/07/2010	08:31	Vaisala, Meisei, Graw, Changfeng, Huayun	998.3	26.9	88	140	6.8	25	Nil	10-/10-	Sc, Cu	10-/10-	Sc, Cu	///	6.16	
17	17/07/2010	14:53	InterMet, Sippican, Jinyang, Meteolabor+SW, Daqiao	998.6	28.7	79	132	8.4	40	Nil	10-/3	Ci,Cu,Ac	10-/0	Ci, Ac	///	6.82	
18	17/07/2010	19:54	Vaisala, Meisei, Graw, Changfeng, Huayun	999.9	24.8	96	160	3.7	25	Rain	10/10	Sc,Fc	10/10	Sc, Fc	///	6.74	
19	18/07/2010	00:51	InterMet, Modem, Sippican, Jinyang, Meteolabor+SW, Daqiao	1001.4	23.9	96	043	4.8	28	Nil	10-/0	Ac	10-/0	Ac	///	6.85	
20	18/07/2010	03:07	CFH, Multi-Therm, Vaisala Sci, Meisei Sci	1000.6	23.8	96	054	4.3	15	Nil	10-/10-	Sc	10-/10-	Sc	203	6.93	

8th WMO Intercomparison of Radiosonde Systems July 2010, Yangjiang, China

Flight No.	Launch		Manufacture	15 minutes before launch											Time to cloud (s)	Rate of ascent m/s	Additional information
	Date (L)	Time (L)		Pressure hPa	Temperature °C	Humidity %	Wind		Visibility km	Significant Weather	General cloud		Local cloud				
							Direction	Speed			Amount	Type	Amount	Type			
21	18/07/2010	08:32	Vaisala, Meisei, Graw, Changfeng, Huayun	1000.9	26.1	89	058	4.7	14	Nil	9/6	Cu, Ac	10-/10-	Cu	///	6.80	
22	18/07/2010	14:47	InterMet, Modem, Sippican, Jinyang, Meteolabor, Daqiao	1000.0	29.9	79	141	6.6	40	Nil	9/8	Cu,Ac,Ci	3/3	Cu	///	6.78	
23	18/07/2010	20:00	Vaisala, Meisei, Graw, Changfeng, Huayun	1000.2	28.2	88	177	3.8	40	Nil	7/6	Cu,Fc,Ci	9/9	Cu, Ci	68	6.86	
24	19/07/2010	00:46	InterMet, Modem, Sippican, Jinyang, Meteolabor+SW, Daqiao	1000.2	27.0	94	094	2.0	25	Nil	3/3	Cu, Fc	2/2	Cu, Fc	///	7.09	
25	20/07/2010	08:32	InterMet, Modem, Sippican, Jinyang, Vaisala	999.4	29.1	82	102	1.2	24	Nil	10-/0	Ci, Cu	10-/0	Ci	///	6.88	
26	20/07/2010	12:51	CFH, Multi-Therm, Vaisala Sci, Meisei Sci	999.5	31.4	60	147	3.4	40	Nil	10-/3	Ci, Cu	10-/0	Ci	///	6.44	
27	20/07/2010	14:55	Daqiao, Meisei, Graw, Changfeng, Huayun, Meteolabor+SW	998.2	31.4	60	172	3.8	40	Nil	10-/2	Ci Cu	10-/0	Ci	///	5.64	
28	20/07/2010	20:00	InterMet, Modem, Sippican, Jinyang, Vaisala	997.1	29.1	82	175	2.1	20	Nil	10-/0	Ci, Ac	10-/0	Ac	///	7.17	
29	21/07/2010	00:47	Daqiao, Meisei, Graw, Changfeng, Huayun, Meteolabor+SW	998.1	28.1	81	081	1.9	30	Nil	8/0	Ac	10-/0	Ac	///	6.80	
30	21/07/2010	08:38	InterMet, Modem, Sippican, Jinyang, Vaisala, Multi-Therm	997.1	28.1	84	051	4.3	20	Nil	10-/5	Sc, Ac	10-/10-	Sc	///	6.04	
31	21/07/2010	12:47	Daqiao, Meisei, Graw, Changfeng, Huayun, Meteolabor	996.6	26.6	86	083	3.8	25	Thunder shower	10-/10-	Cb, Cu	10-/10-	Cb, Cu	///	6.20	
32	21/07/2010	14:45	CFH, Multi-Therm, Vaisala Sci, Meisei Sci, Graw	995.7	25.4	92	052	6.4	40	Shower	10/10	Sc, Cb	10/10	SC, Cb	///	6.14	

8th WMO Intercomparison of Radiosonde Systems July 2010, Yangjiang, China

Flight No.	Launch		Manufacture	15 minutes before launch											Time to cloud (s)	Rate of ascent m/s	Additional information
	Date (L)	Time (L)		Pressure hPa	Temperature °C	Humidity %	Wind		Visibility km	Significant Weather	General cloud		Local cloud				
							Direction	Speed			Amount	Type	Amount	Type			
33	21/07/2010	19:59	InterMet, Modem, Sippican, Jinyang, Vaisala	994.4	26.4	85	053	9.4	30	Nil	10-/10-	Sc	10-/10-	Sc	///	6.00	
34	22/07/2010	00:45	Daqiao, Meisei, Graw, Changfeng, Huayun, Meteolabor+SW	994.6	26.1	89	049	9.1	20	Nil	8/2	Ac, Fc	10-/10-	Ac	63	6.47	
35	23/07/2010	08:34	InterMet, Modem, Sippican, Jinyang, Vaisala, Multi-Therm	995.6	26.9	94	138	8.5	20	Nil	10-/10-	Cu,Fc, Sc	10-/10-	Cu	60	6.54	
36	23/07/2010	12:53	Daqiao, Meisei, Graw, Changfeng, Huayun, Meteolabor+SW	996.2	27.8	92	149	7.2	20	Nil	10-/10-	Cu, Fc	10-/10-	Cu	50	6.42	
37	23/07/2010	20:07	InterMet, Modem, Sippican, Jinyang, Vaisala	995.6	27.2	93	141	7.3	25	Nil	10-/9	Cu,Fc,Sc,Ci	10-/10-	Sc, Cu, Fc	///	5.80	
38	24/07/2010	00:45	Daqiao, Meisei, Graw, Changfeng, Huayun, Meteolabor+SW	998.0	27.1	94	123	5.2	20	Nil	10-/9	Cu,Fc,Ci	8/8	Cu, Fc	///	6.06	
39	24/07/2010	08:33	InterMet, Modem, Sippican, Jinyang, Vaisala, Multi-Therm	998.0	27.5	92	137	3.9	35	Nil	10-/8	Cu, Ci, Fc	10-/4	Ci, Cu	82	6.53	
40	24/07/2010	12:47	Daqiao, Meisei, Graw, Changfeng, Huayun, Meteolabor+SW	998.0	29.5	78	156	5.3	40	Nil	10-/7	Ci, Cu	10-/5	Cu, Ci	///	5.31	
41	24/07/2010	20:00	InterMet, Modem, Sippican, Jinyang, Vaisala, Multi-Therm	997.2	27.5	85	134	3.4	50	Lightning	10-/1	Ci, Cb	10-/0	Ci	///	5.86	
42	25/07/2010	00:48	Daqiao, Meisei, Graw, Changfeng, Huayun, Meteolabor+SW	998.1	27.0	88	066	1.9	40	Nil	10-/2	Ci, Cu	10-/0	Ci	///	6.50	
43	25/07/2010	03:01	CFH, Multi-Therm, Vaisala Sci, Meisei Sci, Graw	997.0	26.5	92	058	1.5	40	Nil	6/6	Cu, Fc, Ci	10-/10-	Cu	///	5.70	

8th WMO Intercomparison of Radiosonde Systems July 2010, Yangjiang, China

Flight No.	Launch		Manufacture	15 minutes before launch											Time to cloud (s)	Rate of ascent m/s	Additional information
	Date (L)	Time (L)		Pressure hPa	Temperature °C	Humidity %	Wind		Visibility km	Significant Weather	General cloud		Local cloud				
							Direction	Speed			Amount	Type	Amount	Type			
44	25/07/2010	08:30	InterMet, Modem, Sippican, Jinyang, Vaisala, Multi-Therm	997.5	28.8	83	037	2.6	15	Nil	10-/9	Ci, Cu	10-/2	Ci, Cu	///	5.78	
45	25/07/2010	12:43	Daqiao, Meisei, Graw, Changfeng, Huayun, Meteolabor	998.1	28.4	85	097	1.2	45	Nil	10-/10-	Cu	10-/10-	Cu	///	6.30	
46	25/07/2010	19:59	InterMet, Modem, Sippican, Jinyang, Vaisala	997.0	28.0	81	128	2.3	40	Nil	3/0	Ac	0/0	-	///	6.84	
47	26/07/2010	00:45	Daqiao, Meisei, Graw, Changfeng, Huayun, Meteolabor+SW	998.3	26.9	90	033	1.9	30	Nil	10-/0	Ci, Cu	10-/0	Ci	///	7.19	
48	26/07/2010	02:50	CFH, Multi-Therm, Vaisala Sci, Meisei Sci, Graw	997.7	26.3	94	052	1.5	18	Nil	10-/0	Ci, Sc	10-/0	Ci	///	6.38	
49	26/07/2010	08:31	InterMet, Modem, Sippican, Jinyang, Vaisala, Multi-Therm	997.5	27.9	83	004	1.1	30	Nil	10-/0	Ci, cu	10-/0	Ci	///	5.62	
50	26/07/2010	12:48	Daqiao, Meisei, Graw, Changfeng, Huayun, Meteolabor	997.6	28.5	76	164	4.4	10	Nil	10-/10-	Cu	10-/10-	Cu	///	5.86	
51	26/07/2010	20:00	InterMet, Modem, Sippican, Jinyang, Vaisala	997.3	28.1	86	139	2.9	37	Nil	10-/2	Ci, Ac, Cu	10-/2	Ci, Ac, Cu	///	6.97	
52	27/07/2010	00:46	Daqiao, Meisei, Graw, Changfeng, Huayun, Meteolabor	998.4	27.1	90	201	2.4	50	Nil	10-/3	Ci, Cu, Fc	10-/0	Ci	///	6.33	
53	27/07/2010	02:55	CFH, Multi-Therm, Vaisala Sci	997.3	26.9	92	228	1.6	40	Nil	10-/0	Ci	10-/0	Ci	///	6.63	
54	28/07/2010	08:34	Vaisala, Meisei, Graw, Changfeng, Huayun, Multi-Therm	997.9	28.8	85	201	8.4	30	Nil	10-/7	Cu, Sc, Ci	10-/10-	Sc	133	5.86	

8th WMO Intercomparison of Radiosonde Systems July 2010, Yangjiang, China

Flight No.	Launch		Manufacture	15 minutes before launch											Time to cloud (s)	Rate of ascent m/s	Additional information
	Date (L)	Time (L)		Pressure hPa	Temperature °C	Humidity %	Wind		Visibility km	Significant Weather	General cloud		Local cloud				
							Direction	Speed			Amount	Type	Amount	Type			
55	28/07/2010	12:50	InterMet, Modem, Sippican, Jinyang, Meteolabor, Daqiao	997.7	29.4	83	220	4.3	35	Thunder	10-/10-	Cu, Cb	10-/10-	Cb	///	5.13	After launch rig possibly hit by lightning.
56	28/07/2010	15:05	CFH, Multi-Therm, Vaisala Sci, Meisei, Graw	996.7	30.2	79	203	6.0	35	Nil	10-/6	Cu,Ci,Ac,Fc	10-/0	Ci, Ac	97	5.82	
57	28/07/2010	20:03	Vaisala, Meisei, Graw, Changfeng, Huayun, Sippican	998.0	5.3	96	042	2.7	25	Lightning	10-/10-	Sc,Cb,Cu,Ac	10-/10-	Sc, Cu, Ac	///	6.67	
58	29/07/2010	01:06	InterMet, Modem, Sippican, Jinyang, Meteolabor, Daqiao, Vaisala	997.1	25.8	95	339	1.8	15	Nil	10-/3	Ci, Sc	10-/0	Ci	///	7.29	RS92 added to flight, hung in centre of rig on Vaisala 30m unwinder
59	29/07/2010	08:35	Vaisala, Meisei, Grwa, Changfeng, Huayun	997.1	28.5	85	241	0.2	25	Nil	8/2	Ci,Ac,Cu,Fc	8/0	Ci, Ac	///	6.05	
60	29/07/2010	12:46	InterMet, Modem, Sippican, Jinyang, Meteolabor, Daqiao	996.7	31.2	72	178	5.1	45	Nil	7/4	Cu, Ci	1/0	Ci	///	6.00	
61	29/07/2010	14:49	CFH, Multi-Therm, Vaisala Sci, Meisei, Graw	995.2	30.4	81	180	5.5	40	Lightning	10-/5	Cb,Cu,Ci	10-/1	Ci,Cu	///	6.01	Rig hit by lightning at 279.7 hPa all sonde stopped tx RoA 6.01
62	29/07/2010	20:02	Vaisala, Meisei, Graw, Changfeng Huayun, Sippican	996.6	27.9	92	180	2.5	20	Nil	10/10	Sc, Cu	10/10	Sc	///	6.33	
63	30/07/2010	00:50	InterMet, Modem, Sippican, Jinyang, Meteolabor, Daqiao, Vaisala	996.6	27.7	94	178	3.3	25	Nil	10-/4	Ac, Cu	10/1	Ac, Cu	///	6.80	
64	30/07/2010	08:40	Vaisala, Meisei, Graw, Changfeng, Huayun, Multi-Therm	996.8	28.8	88	254	1.2	30	Nil	10-/6	Cu, Ac	10/10	Cu	///	6.18	
65	30/07/2010	12:55	InterMet, Modem, Sippican, Jinyang, Meteolabor, Daqiao	996.7	31.9	70	204	3.5	48	Nil	10-/3	Ci, Cu, Ac	10-/5	Cu, Ci	///	6.93	

8th WMO Intercomparison of Radiosonde Systems July 2010, Yangjiang, China

Flight No.	Launch		Manufacture	15 minutes before launch											Time to cloud (s)	Rate of ascent m/s	Additional information
	Date (L)	Time (L)		Pressure hPa	Temperature °C	Humidity %	Wind		Visibility km	Significant Weather	General cloud		Local cloud				
							Direction	Speed			Amount	Type	Amount	Type			
66	30/07/2010	14:54	CFH, Multi-Therm, Vaisala Sci, Meisei Sci, Graw	995.8	31.3	76	188	4.2	40	Nil	10-/6	Cu, Ci	10-/8	Cu, Ci	///	5.39	
67	31/07/2010	00:46	Meisei, Modem, Sippican, Jinyang, Meteolabor+SW, Daqiao, Vaisala	997.5	28.2	92	213	3.6	30	Nil	10-/0	Ci	8-/0	Ci	///	6.59	
68	31/07/2010	03:05	Vaisala, InterMet, Graw, Changfeng, Huayun, Sippican	996.3	27.8	92	200	3.3	40	Nil	9/0	Ac, Ci, Fc	9/0	Ac, Ci	///	6.59	
69	31/07/2010	08:32	Vaisala, Meisei, Graw, Changfeng, Huayun	997.3	28.7	87	194	4.1	40	Nil	6/4	Cu, ci	4/2	Ci, Cu	///	5.70	
70	31/07/2010	12:47	InterMet, Modme, Sippican, Jinyang, Meteolabor, Daqiao	997.5	30.7	77	157	5.9	40	Nil	10-/7	Cu, Ci	10-/3	Ci, Cu	///	6.21	
71	01/08/2010	00:47	Meisei, Modem, Sippican, Jinyang, Meteolabor, Daqiao, Vaisala	998.6	28.4	86	153	5.3	40	Nil	4/4	Cu, Fc	2/2	Cu, Fc	///	6.40	
72	01/08/2010	02:53	Vaisala, InterMet, Graw, Changfeng, Huayun, Sippican	998.2	28.1	87	150	4.7	40	Nil	3/3	Cu	0/0	-	///	7.13	

Annex G - Radiosonde Comparison Software (RSKOMP ©) for WIN32 Platform

Expert team has used the Radiosonde Comparison Software (RSKOMP©) which has been regularly used in radiosonde intercomparisons since 1990. It implements the well established comparison methodology and provides multiple important features that make RSKOMP a powerful and complete tool for radiosonde data analysis.

In this comparison RSKOMP was used for the following tasks:
- To create a common data base of all intercomparison flights;
- To reconcile different entry data standards from different participants;
- To perform post-flight data quality analysis;
- To detect and eliminate missyncronizations;
- To hide data where measurements were judged atypical;
- To calculate and analyze statistical results;
- To produce other relevant reference materials for the report.

During its existence the RSKOMP has been thoroughly verified. History of major applications of RSKOMP includes:
- Phase 3 of WMO Radiosonde Intercomparison (1989, USSR)
- Potential Reference Radiosonde Test (1992, UK)
- Phase 4 of WMO Radiosonde Intercomparison (1993, Japan)
- WMO Intercomparison of Humidity Sensors (1995, USA)
- Flight Phase of Ozonesonde Intercomparison (1996, Switzerland)
- Phase 5 of WMO Radiosonde Intercomparison (2001, Brazil)
- WMO Intercomparison of High-Quality Radiosondes (Mauritius, 2005)
- plus many other tests / experiments of the smaller scale.

It should be noted that WRSKOMP applicability is not limited to radiosonde data neither to any particular manufacturer standard. **Practically any data that are represented in a form of vertical profiles may be analyzed with WRSKOMP**. So, the dataset may include radiosondes, ozonesondes, remote soundings data, theoretical models or combination of the above data sources.

The readers who are interested in more details may refer to the Web site: www.rskomp.net

Annex – H Estimated resources for the Intercomparison

	Costs (excl man-power costs) [Euros]	Man-power [Man-days]
Manufacturers	400’000	1925
Project Team (excl. GRUAN and CMA)		295
GRUAN Team	50’000	160
Host country general support	140’000	1200
Host country remote sensing campaign	60’750	1880
WMO	116’000	93
TOTAL	**766’750**	**5553**